DOCTOR OF SCIENCES

Design and Synthesis of Phenylguanidine-Based and Benzamidine-Based FXIIa Inhibitors

SIMON, Francois

Award date:
2020

Awarding institution:
University of Namur

University of Namur

Design and synthesis of Phenylguanidine-Based and Benzamidine-Based FXIIa inhibitors

Submitted by François Simon
for the PhD degree in Chemical Sciences

2020

JURY

Prof. Guilaume Berionni (President of the Jury, UNamur)

Prof. Steve Lanners (Promoter and Secretary, UNamur)

Dr Lionel Pochet (Co-promoter, UNamur)

Prof. Jean-Pierre Gillet (UNamur)

Prof. Raphaël Frédérick (UCLouvain)

Prof. Raphaël Robiette (UCLouvain)

Prof. Wim De Borggraeve (KU Leuven)

University of Namur
NAmur MEdicine & Drug Innovation Center (NAMEDIC)
Rue de Bruxelles, 61, 5000 Namur, Belgium

Design and synthesis of Phenylguanidine-Based and Benzamidine-Based FXIIa inhibitors

By François SIMON

The Coagulation Factor XIIa has emerged as a potential therapeutic target for a whole range of medical conditions, including thrombosis, Alzheimer's disease, sepsis, and multiple sclerosis. Despite their upsides compared to biological or biobased inhibitors, research for synthetic small inhibitors of FXIIa is scarce. Consequently, the *in vivo* non-clinical and clinical development of this category of compounds is close to non-existent compared to its alternatives. In an attempt to fill this gap, the general aim of this thesis was to design and to synthesize small, non-peptidic molecules targeting FXIIa in order to generate hit compounds that could be used to identify promising scaffolds and to yield lead compounds.

In the first part of this thesis, we focused on the structural refinement of 2,5-dichlorobenzyl triazole inhibitors. The adequacy of the envisaged modulations was first highlighted using molecular docking. The promising compounds were then synthesized and tested in vitro on FXIIf to assess their potency. The analysis of the results allowed us to further refine the structure of the potential inhibitors, using once again molecular docking, in an iterative process.

In the second part of this thesis, in an attempt to develop new tools to simplify and to increase the throughput of our syntheses, we investigated a novel methodology of early-stage amidination, leading to fully Boc-protected amidine compounds. In order to make this synthetic strategy as versatile as possible, the compatibility of such intermediates with some of the most used reactions in medicinal chemistry, namely Pd-catalyzed cross couplings and substitution reactions, was verified experimentally.

In parallel to this work, our group reviewed exhaustively the FXIIa inhibitors described in the literature and performed vHTS of existing drugs. From this work, two potent biscationic compounds were identified: nafamostat and pentamidine. In the third part of this thesis, three derivatives of these compounds will be designed using molecular docking in order to improve their potency, their selectivity and their metabolic stability, in an attempt to make them more suitable as potential lead compounds. Their synthesis will then be tackled using our improved early-stage amidination metholodogy.

Université de Namur
NAmur MEdicine & Drug Innovation Center (NAMEDIC)
Rue de Bruxelles, 61, 5000 Namur, Belgium

Conception et synthèse d'inhibiteurs du FXIIa dérivés de la phénylguanidine et de la benzamidine

Par François SIMON

Le facteur de coagulation XII (FXII) s'est révélé être une potentielle cible thérapeutique pour toute une gamme de pathologies dont la thrombose, la maladie d'Alzheimer, le sepsis et la sclérose en plaques. Malgré leurs avantages comparés aux inhibiteurs biologiques et biobasés, la recherche autour de petites molécules synthétiques inhibitrices du FXIIa reste marginale. Le développement clinique et non-clinique de cette catégorie de composés est en effet minime comparé à ses alternatives. Ce travail doctoral vise à remédier à ce manquement et à concevoir et à synthétiser des composés non-peptidiques de bas poids moléculaire inhibiteurs du FXIIa afin de générer des composés « hits », qui pourront eux-mêmes être utilisés pour identifier des structures prometteuses et mener à des composés « lead ».

Dans la première partie de cette thèse, nous nous sommes focalisés sur la modulation structurale d'inhibiteurs dérivés de triazoles 2,5-dichlorobenzylés. La pertinence des modulations envisagées a d'abord été mise en valeur par docking. Les composés prometteurs ont ensuite été synthétisés et testés in vitro sur le FXIIf pour évaluer leur activité. L'analyse des résultats nous a ensuite permis d'affiner d'autant plus les modulations structurales, dans un processus itératif, en utilisant à nouveau le docking.

Dans la deuxième partie de cette thèse, afin de de développer de nouveaux outils pour simplifier et pour raccourcir nos synthèses, nous avons étudié une nouvelle méthodologie d'amidination « early-stage ». Afin de rendre cette approche aussi générale que possible, la compatibilité des intermédiaires concernés avec les réactions les plus utilisées en chimie médicinale, notamment les couplages croisés catalysés au palladium et les réactions de substitution, a été vérifiée expérimentalement. En parallèle, notre groupe passa en revue l'ensemble des inhibiteurs de FXIIa décrits dans la littérature et effectua un vHTS de principes actifs de référence. De ce travail, deux composés bicationiques fortement inhibiteurs du FXIIa ont été identifiés : le nafamostat et la pentamidine, tous deux d'adéquats points de départ vers des candidats plus complexes. Dans la troisième partie de cette thèse, après docking, trois dérivés de ces composés ont été imaginés afin d'améliorer leur activité, leur sélectivité et leur stabilité métabolique. Leur synthèse a été initiée, en utilisant notre méthodologie d'amidination « early-stage ».

Effectuer un travail doctoral revient, pour la plupart du temps, à réaliser en marathon en solitaire. Cependant, au cours du voyage, on est amené à marcher quelques kilomètres avec des personnes qui nous donnent la motivation et les outils nécessaires pour le terminer.

Je souhaiterais remercier Steve et Lionel de m'avoir donné l'opportunité d'effectuer ce travail dans leur laboratoire. Leur accompagnement sans faille, leurs conseils avisés, les longues discussions scientifiques et les innombrables heures qu'ils m'ont consacrées sont à la base même du travail que je peux présenter aujourd'hui.

Merci à Clara, pour son travail qui a été indispensable à la bonne exécution de cette thèse, pour les nombreux débats autour du FXIIa et pour sa bonne humeur constante.

Merci aux collègues et (ex-)mémorants du COS avec lesquels j'ai pu collaborer mais surtout bien rire au cours de ces années : Loïc, Bastien, Mathilde, Oliver, le Zeta, Pierre, Steffy, Kalina, Elise et Eduardo. Ce n'aurait pas été pareil sans vous.

Je remercie également tous les doctorants de l'Unité de Chimie Organique pour avoir contribué à instaurer une ambiance de travail agréable à l'étage et pour leur bienveillance.

Je n'aurais pas pu mener ma thèse à bien sans le soutien et l'appui de ma famille. Jonathan, Clara, Maman, Papa, Mamy, Papy, Marraine, Parrain, merci pour tout ce que vous avez fait pour moi, je ne vous le rendrai jamais assez.

Fanny, je pense à toi.

Table of Contents

List of Abbreviations

2,2-DMP	2,2-Dimethoxypropane
A21	Amberlyst A21
Aβ	β-Amyloid peptide
Ac	Acetyl
AD	Alzheimer's disease
AF	Atrial fibrillation
AIBN	Azobisisobutyronitrile
Ar	Aryl
ASO	Antisense oligomer
AT	Antithrombin
BCMD	Blood-contacting medical device
BINAP	2,2′-Bis(diphenylphosphino)-1,1′-binaphthyl
BK	Bradykinin
Bn	Benzyl
Boc	*tert*-Butoxycarbonyl
Bu	Butyl
C1INH	C1 esterase inhibitor
CAS	Contact activation system
CHD	Coronary heart disease
cin	Cinnamyl
CNS	Central nervous system
conc.	Concentrated
CSA	Camphorsulfonic acid
CTI	Corn trypsin inhibitor
dba	Dibenzylideneacetone
DCC	Dicyclohexylcarbodiimide
DET	Diethyl tartrate
DIAD	Diisopropyl azodicarboxylate
DMAc	Dimethylacetamide
DMAP	Dimethylaminopyridine
DME	Dimethoxyethane
DMF	Dimethylformamide

DIC	Disseminated intravascular coagulation
DIPA	Diisopropylamine
DOAC	Direct oral anticoagulant
DNA	Desoxyribonucleic acid
DVT	Deep vein thrombosis
DXS	Dextran sulfate
ECMO	Extracorporeal membrane oxygenation
EGF	Epidermal growth factor
Et	Ethyl
FG	Functionalizable group
FnI	Fibronectin type I domain
FnII	Fibronectin type II domain
FII	Coagulation factor II
FIV	Coagulation factor IV
FV	Coagulation factor V
FVI	Coagulation factor VI
FVII	Coagulation factor VII
FVIII	Coagulation factor VIII
FIX	Coagulation factor IX
FX	Coagulation factor X
FXI	Coagulation factor XI
FXII	Coagulation factor XII
FXIIf	Coagulation factor XII fragment
FXIII	Coagulation factor XIII
HA	Human albumin
HAE	Hereditary angioedema
HMPA	Hexamethylphosphoramide
HMWK	High-molecular-weight kininogen
HPLC	High-performance liquid chromatography
IC_{50}	Half maximal inhibitory concentration
iPr	Isopropyl
LiHMDS	Lithium hexamethyldisilazide
LMWH	Low-molecular-weight heparin
MABR	Methylaluminum bis(4-substituted-2,6-di-*tert*-butylphenoxide)

MCoTI-II	*Momordica cochinchinensis* trypsin inhibitor-II
MHV	Mechanical heart valve
MP	Melting point
mRNA	Messenger ribonucleic acid
MS	Mass sclerosis
Ms	Mesyl
N.I.	Non-isolated
NBS	*N*-Bromosuccinimide
NHC	*N*-Heterocyclic carbene
NMR	Nuclear magnetic resonance
ODA	Orphan drug act
ON	Overnight
OPLS-AA	Optimized Potentials for Liquid Simulations – All Atoms
PDMS	Polydimethylsiloxane
PET	Polyethylene terephthalate
PG	Protecting group
Ph	Phenyl
Piv	Pivaloyl
PK	Plasma kallikrein
pNA	*para*-Nitroaniline
PRR	Proline-rich region
PolyP	Polyphosphate
PPK	Plasma prekallikrein
PTFE	Polytetrafluoroethylene
PTSA	*para*-Toluenesulfonic acid
PVC	Polyvinyl chloride
Py	Pyridine
QSAR	Quantitative structure-activity relationship
Quant.	Quantitative
ROS	Reactive oxygen species
RNA	Ribonucleic acid
RT	Room temperature
SAE	Serious adverse event
SDS-PAGE	Sodium dodecyl sulfate - polyacrylamide gel electrophoresis

SEM	Trimethylsilylethoxymethyl
SEMX	Subendothelial matrix
SFXIBS	Secondary FXI-binding site
SKR	Sharpless kinetic resolution
siRNA	Small interfering ribonucleic acid
S_N2	Bimolecular nucleophilic substitution
SP	Serine protease
SVT	Superficial vein thrombosis
TBAF	Tetrabutylammonium fluoride
TBAI	Tetrabutylammonium iodide
TBS	*tert*-Butyldimethylsilyl
*t*Bu	*tert*-Butyl
TF	Tissue factor
TFA	Trifluoroacetic acid
TFAA	Trifluoroacetic anhydride
THF	Tetrahydrofuran
THR	Thrombin
TIPS	Triisopropylsilyl
TLC	Thin layer chromatography
tMCAO	Transient middle cerebral artery occlusion
TMEDA	Tetramethylethylenediamine
TMS	Trimethylsilyl
Tol.	Toluene
UFH	Unfractionated heparin
vHTS	Virtual high throughput screening
VKA	Vitamin K antagonist
VTE	Venous thromboembolism
VWF	von Willebrand factor
wt	Wild-type
XP	Extra-precision
XRD	X-ray diffraction

Preface: the Heritage of John Hageman

July 1953. John Hageman, a 37-year old American brakeman, needed surgery.[1] He had had symptoms of a duodenal ulcer since 1943, which ultimately led to gastric outlet obstruction. Pre-operative testing systematically included the clotting times of the plasma, to predict any complications during the operation. Even though he had never had any signs of hemophilia, Hageman's plasma unexpectedly coagulated in glass test tubes at least 10 times slower than a reference sample.[1] In 1954, the gastrojejunostomy was performed nonetheless. No excessive bleeding occurred, and his recovery was uneventful.[2]

A man whose blood does not coagulate spontaneously in glass test tubes yet has no problems of coagulation *in vivo* encouraged further studies. His blood was proven to be deficient in a "fraction" found in normal globulin. They called this fraction after him, the Hageman factor, and the related deficiency the Hageman trait.[1] The Hageman Factor was later identified as an enzyme. It was the 12th coagulation factor identified, and nowadays is commonly called the factor XII (FXII).

Years later, March 1968. Hageman fell from the ladder of a boxcar and broke his hemipelvis. On the 12th day of bedrest, he died from pulmonary embolism,[2] which is the blockage of an artery of the lungs by a blood clot.

How could a man that had a deficiency in coagulation factor XII and whose blood toiled at coagulating in vitro die from an unwanted and uncontrolled formation of a blood clot? And how comes he was not even an exception?[2] John Hageman has left us with many questions, some of them that we can answer nowadays (and those will be addressed in this thesis), some of them that we still cannot. But more importantly, he has left us with a beautiful heritage: the hope for novel treatment against the cause of his demise, thromboembolism.

Chapter 1: Introduction

1.1. Hemostasis, Thrombosis and Thromboembolism

1.1.1. Hemostasis

Hemostasis is the physiological process that stops bleeding at the site of an injury by the formation of a thrombus (Figure 1-1).[3]

Primary hemostasis (yellow on Figure 1-1) consists in platelet aggregation and in the formation of a platelet plug.[3] Platelet adhesion is initiated by interaction of receptors present on the platelet surface and constituents of the exposed subendothelial matrix (SEMX, Figure 1-1B). These interactions may be mediated by a third constituent, for example the von Willebrand Factor (VWF). These platelets are then activated, which induces conformational change and activation of platelet-recruiting receptors and, through successive platelet-platelet interactions, the aggregation is propagated to yield a platelet plug (Figure 1-1C).

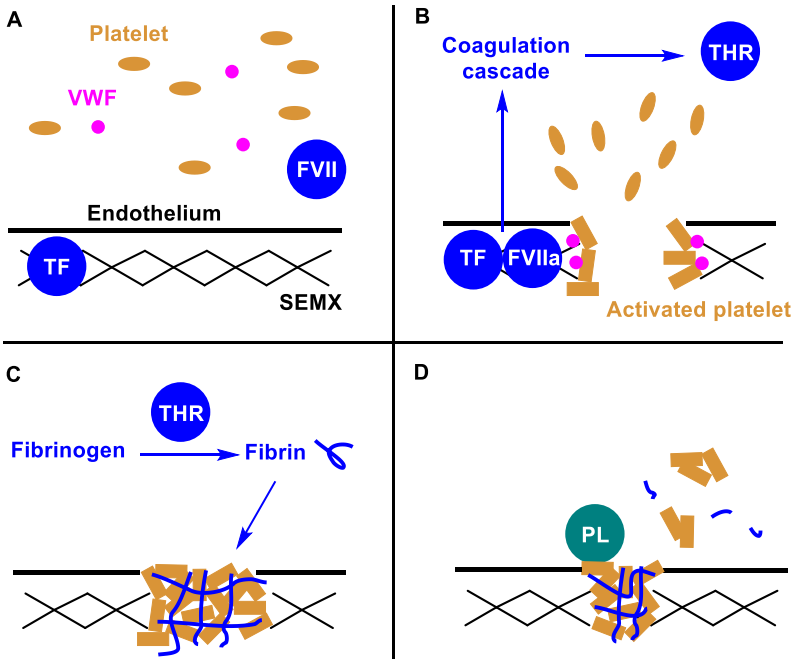

Figure 1-1. Schematic representation of the processes of hemostasis. (A) Blood vessel at rest. (B) Breached blood vessel. Platelets adhere to the SEMX via the VWF and FVII binds to TF, initiating the coagulation cascade to yield thrombin. (C) Formation of a stabilized platelet plug. Platelet-platelet interactions lead to platelet aggregation and fibrinogen is cleaved by thrombin to yield fibrin, polymerizing at the site of injury. (D) Fibrinolysis. In parallel to wound healing, plasmin cleaves the polymer of fibrin, breaking down the thrombus

Secondary hemostasis (blue on Figure 1-1) consists in the formation of an insoluble cross-linked fibrin polymer that stabilizes the platelet plug.[3] When the activated coagulation factor VII (FVIIa) binds with its cofactor, the tissue factor (TF), present in the exposed SEMX, an enzymatic cascade of coagulation factors is initiated (Figure 1-1B).

This process ultimately leads to the thrombin (THR)-mediated cleavage of fibrinogen to fibrin, which spontaneously polymerizes at the site of the injury (Figure 1-1C). Primary and secondary hemostasis cross-communicate mutually and activate each other.

Fibrinolysis (green on Figure 1-1), sometimes called tertiary hemostasis, consists in progressively dissolving the blood clot, also called thrombus, in parallel to wound healing.[3] This process is mainly mediated by plasmin, which is able to progressively cleave the polymer of fibrin (Figure 1-1D). The thrombus is then fragilized and breaks down little by little.

1.1.2. Thrombosis and Thromboembolism

Thrombosis is the obstruction of blood flow due to the formation of a thrombus.[3–5] In some cases, the thrombus can detach (embolize) partially or completely, becoming an embolus, and travel in the blood system. It further can lodge into and block a downstream blood vessel. This process is called thromboembolism. Both thrombosis and thromboembolism can occur in arteries and in veins due to different endogenous causes, leading to different consequences as well, but can also be caused exogenously by blood-contacting medical devices (BCMD).

1.1.2.1. Arterial Thrombosis and Thromboembolism

Arterial thromboses are mainly initiated by two diseases: atherosclerosis and atrial fibrillation (AF). Atherosclerosis is an asymptomatic condition that consists in the narrowing (also called stenosis) of arteries due to the presence of atheromas, which are amorphous plaques of macrophage cells and cellular debris, in the SEMX (Figure 1-2A).[3–5]

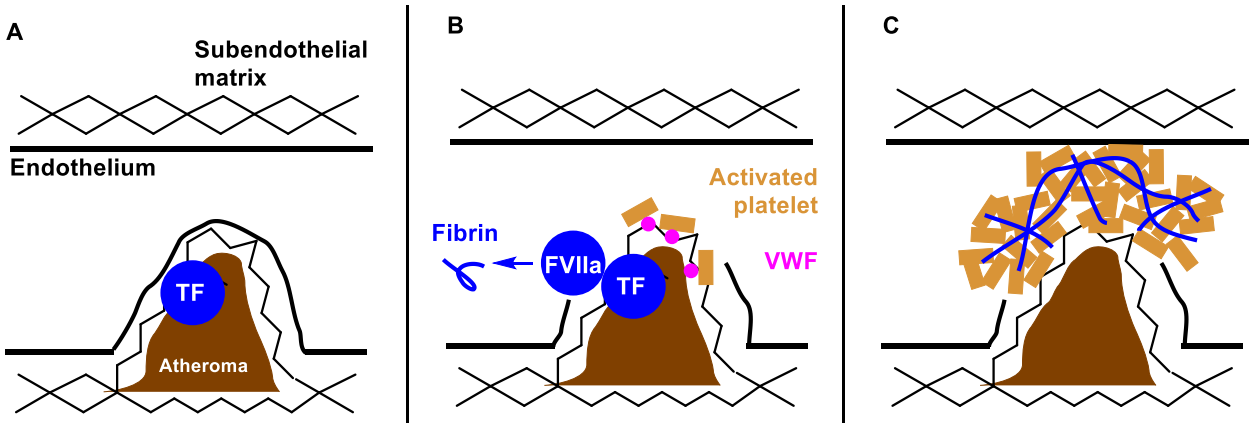

Figure 1-2. (A) Atherosclerosis in an artery. (B) Initiation of thrombosis after rupture of the endothelium covering the atheroma. Platelet activation and propagation and activation of the coagulation cascade. (C) Arterial thrombosis.

Upon high shear flow of arterial blood, the endothelial cell layer may weaken and break, exposing to the blood the surface of the atheroma, the SEMX, and the TF (Figure 1-2B). As is the case for the SEMX, atheromas are highly thrombogenic, with a high affinity toward VWF and platelets, and platelet aggregation and propagation are promptly initiated.

In parallel, the coagulation cascade is activated by TF/FVIIa. The resulting thrombus may then block the already narrowed artery and/or embolize (Figure 1-2C).

AF is a cardiac arrhythmia characterized by a rapid and irregular beating of the atrial chambers of the heart.[6] The exact mechanism by which it promotes thromboembolism is not understood, but anomalous thrombus formation and embolization tend to occur in the heart of patients suffering from AF.[7,8] An excessive production of TF in the cardiac endothelium is a possible partial cause.

In both cases, blockage of the arteries may cause shortage of oxygen to several tissues and organs (ischemia) and lead to coronary heart diseases (CHD), including myocardial infarctions, strokes, and gangrenes.[3–5] The causes for atherosclerosis and AF are not clear yet, but risk factors include older age, hypertension, obesity, smoking, and family history of similar events.[3–5,9] Prophylaxis of arterial thrombosis usually involves antiplatelet and/or anticoagulant medication.[3,10]

1.1.2.2. Venous Thrombosis and Thromboembolism

Blood pressure is much lower in veins than in arteries. Because of this, and to ensure that blood flows in the right direction, endothelial one-way two-cusp valves are found throughout venous vessels (Figure 1-3A and B).[5] However, in problematic cases, the blood flow rate is so low that the oxygen supply to the endothelial cells in the bend of the cusp can become critical (Figure 1-3C). Upon hypoxic stress, these cells tend to become adherent to TF-bearing leukocytes (L).[3–5] This important accumulation of TF initiates, *via* FVIIa, the coagulation cascade.

Because of the slow blood flow, the activated coagulation factors are not quickly cleared away and the process becomes more and more intense. Even though, through cross-communication between both processes, platelet aggregation is also initiated, it does not keep up with the burst of fibrin formation and most of the polymeric fibrin net ends up trapping red blood cells. The clot gets bigger and bigger and eventually prevents the cusp from opening and thus, the blood from flowing (Figure 1-3D). Venous thromboembolism (VTE) is prevalent in the superficial veins of the legs and is simply called superficial vein thrombosis (SVT). Moreover, the unique composition of the thrombus makes it prone to embolization. The resulting embolus is then likely to lodge into the deep vein of the leg (deep vein thrombosis, DVT) and from there, can further travel and block lung arteries, causing a life-threatening pulmonary embolism.[3–5]

Risk factors are multiple but include conditions where blood may not flow correctly such as older age, surgery, obesity and bed rest.[4,5] VTE being initiated by coagulation factors, typical therapy and prophylaxis involve anticoagulant medication.[11,12]

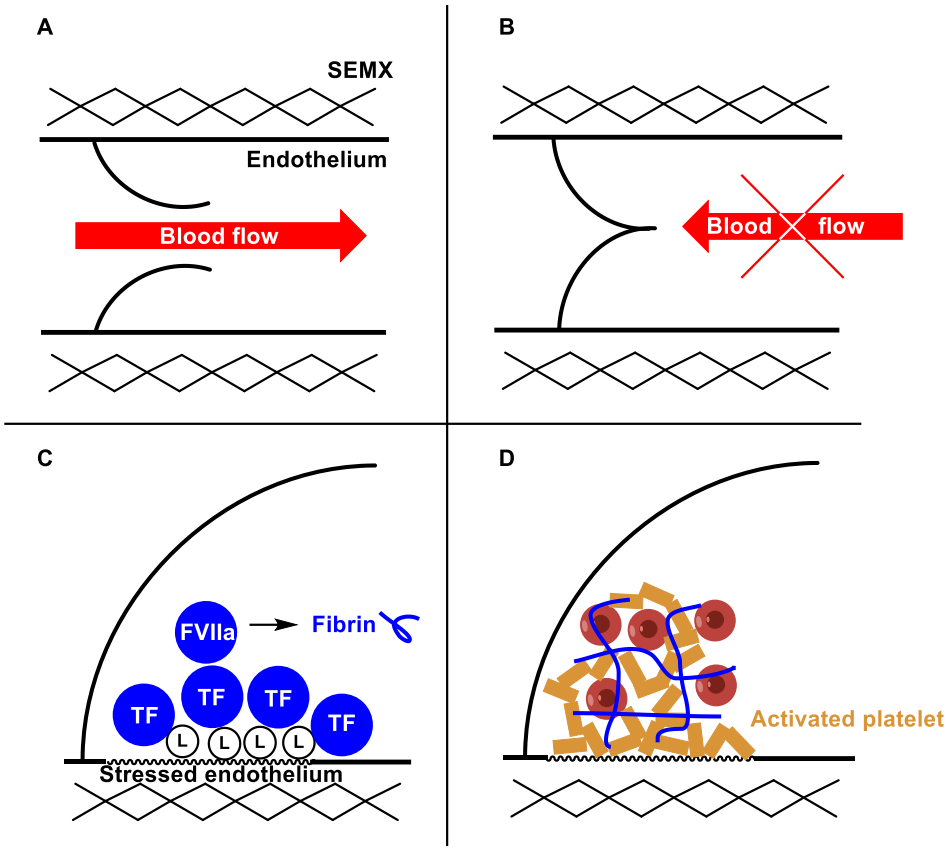

Figure 1-3. (A) Blood allowed to flow in the right direction in a vein. (B). Blood prevented from flowing in the wrong direction in a vein. (C). Zoom in the bend of a valve cusp. Adherence of TF-bearing leukocytes onto hypoxia-stressed venous endothelium and initiation of the coagulation cascade. (D) Venous thrombosis. The cusp cannot open anymore and prevent blood from flowing. The unique structure of the thrombus, rich in red blood cells, makes it prone to embolization.

1.1.2.3. Thrombosis Induced by Blood-Contacting Medical Devices

Numerous patients depend on blood-contacting medical devices (BCMDs) to live, such as mechanical heart valves (MHVs), stents and catheters. Proteins tend to absorb on artificial surfaces, including the VWF and FXII (Figure 1-4),[13] which is known in vitro to be activated by numerous surfaces.[14] The accumulation of VWF can trigger platelet activation and aggregation, while FXII auto-activates on the surface to become FXIIa and initiates the coagulation cascade, in addition to a local inflammatory response.[13,15]

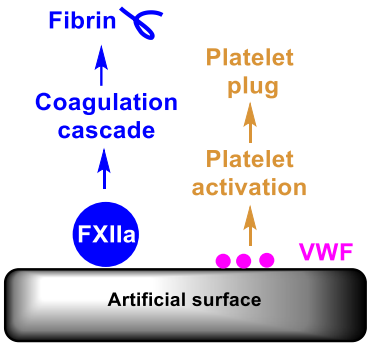

Figure 1-4. Thrombosis on BCMDs.

The resulting clot can cause failure of the device, resulting in severe complications for the patient. Typical prophylaxis involves anticoagulant medication.[16,17]

1.1.2.4. Anticoagulants: the Cornerstone of Thrombosis Therapy

Nowadays, anticoagulants are routinely administered in the framework of efficient therapy and prophylaxis against thrombosis. Unfortunately, common serious adverse events (SAEs) inseparable from currently prescribed anticoagulants are bleeding diathesis (an unusual susceptibility to bleed) and/or aggravation of major bleeding events (e.g. due to surgery, accidents, or cancers).[11,12,18–20] To understand why and how this happens, and how we could circumvent it, the coagulation cascade needs to be further detailed.

1.2. The Coagulation Cascade and Anticoagulants

1.2.1. The Coagulation Cascade upon Injury

The coagulation cascade is a series of serine proteases (SPs) that consecutively cleave and activate each other.[3,21] As described before, coagulation upon injury begins with the TF pathway (Figure 1-5). The complex of plasmatic FVIIa with TF is able to activate FX. From there, following the common pathway, FXa, with its cofactor FVa, transforms prothrombin (also called Factor II, FII) into thrombin. Finally, thrombin turns fibrinogen into fibrin, which polymerizes, and FXIII into FXIIIa, which stabilizes the newly formed network.

In parallel, the generated thrombin is involved in an important feedback loop (indicated by the circle-shaped green arrow, Figure 1-5). It can indeed initiate a new pathway, that we decided to call in this work the FXI pathway, leading to the activation of FXI into FXIa, capable of activating in return FIX into FIXa. In the presence of FVIIIa, FIXa cleaves FX into FXa. From there, it follows the common pathway (hence the name) until the polymer of fibrin.[3,21]

Theoretically, *via* the contact activation system (CAS, Figure 1-5, detailed further in this chapter), FXII could also initiate the FXI pathway and thus the coagulation cascade by interaction with collagen, a known FXII activating surface, which is exposed to blood upon injury .

However, as discussed before in the case of John Hagerman, a deficiency in FXII is not accompanied with hemophilia. Moreover, attempts at generating TF-deficient mice results in embryolethal death.[22] Similarly, human TF deficiency has not been reported. Together, these observations suggest that hemostasis *in vivo* occurs mainly, if not exclusively, by TF activation and that FXII has little to no role in the process.[23–25] This conclusion is in contrast to the fact that FXIIa is known as the primary driver of BCMD-thrombosis.

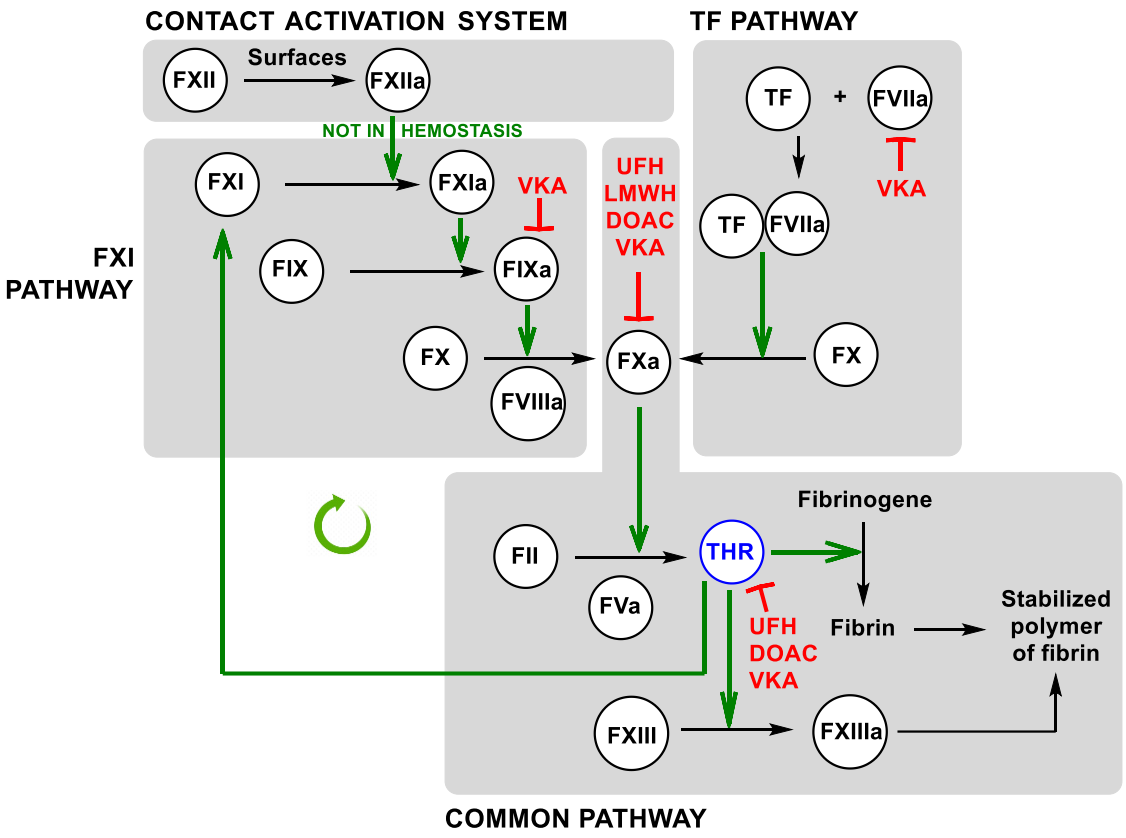

Figure 1-5. The coagulation cascade and its different exogenous direct and indirect inhibitors.

1.2.2. Anticoagulants

1.2.2.1. Characteristics of Commonly Used Anticoagulants

The names of the different families of anticoagulants and their targets are summarized (Figure 1-5) and are further detailed in the following paragraphs.

Unfractionated heparin (UFH) is a mixture of sulfated glycosaminoglycans (3 to 30 kDa), mainly isolated from porcine intestines.[26,27] The most common disaccharide unit is made up of a 2-*O*-sulfated iduronic acid and of a 6-*O*-sulfated-*N*-sulfated glucosamine (Scheme 1-1).[28] About 1/3 of these polymers can bind to antithrombin (AT), an endogenous suicide inhibitor of FXa and THR. When bonded to UFH, AT is much more reactive towards FXa and thrombin, efficiently downregulating the coagulation cascade.[26,27]

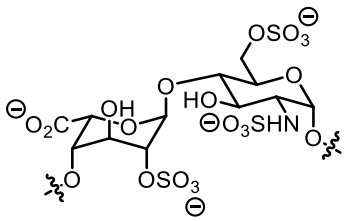

Scheme 1-1. The most common disaccharide in UFH.

As expected, bleeding is the most common serious adverse event. Pharmacological properties are unpredictable from one patient to another depending on their blood composition, as UFH tends to adsorb on multiple plasma proteins and on endothelial cells. Because of this, monitoring of patients treated with therapeutic doses is thus required. UFH is to be administered parenterally and continuously if an effect is needed over a long time, due to its very short elimination half-life (30 min to 1 h).[26,27]

Low-molecular weight heparins (LMWHs) are derived from UFH by chemical or enzymatic cleavage to yield fragments approximately 1/3 the size of UFH.[26,27] Depending on the method used, different types of LMWHs can be obtained, sold under different names but displaying similar properties. LMWHs are able to bind AT, but this interaction only makes AT more reactive towards FXa and not towards thrombin. Thus, bleeding is rarer and less important compared to UFH treatment but is still present. Because of the limited size of LMWHs, reduced adsorption on plasma proteins results in much more predictable pharmacological properties. LMWHs are administered parenterally, once to twice a day thanks to a moderate elimination half-life (4 to 5 h).[26,27]

The vitamins K (Scheme 1-2) are involved as recyclable cofactors in the post-translational modifications of FVII, FIX, FX and FII.[29,30] Vitamin K antagonists (VKAs) inhibit the recycling of vitamin K, preventing the different zymogens from being modified and thus from being functional.[27,30] The most prescribed VKA in North America is warfarin (Scheme 1-2).[27] Warfarin, and VKAs in general, have complex pharmacological properties, with several known interactions with other drugs, a dose-response relationship highly dependent on diet, alcohol consumption and vitamin K-rich aliments intake.[27,30] Because of this, patients tend to go out of their therapeutic window and bleeding (when overdosed) or thrombotic events (when underdosed) are recurrent. Careful and regular monitoring is thus needed to adjust dosage. The 36-42 h elimination half-life of warfarin allows single daily intakes.

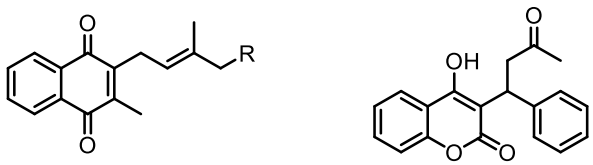

Scheme 1-2. The general structure of vitamins K (R = terpene chain) and the structure of warfarin.

Direct oral anticoagulants (DOACs) are the most recent type of authorized anticoagulants (Scheme 1-3).[27,31–33] These are small synthetic molecules that inhibit directly and selectively either thrombin (dabigatran) or FXa (rivaroxaban, apixaban, edoxaban, betrixaban). Pharmacological properties are predictable, allowing a fixed-dose regimen. Monitoring is thus not required.

The elimination half-lives are between 5 and 27 h, so only single or double daily intakes are necessary. The risks of life-threatening intracranial bleeding are significantly lowered compared to VKAs.

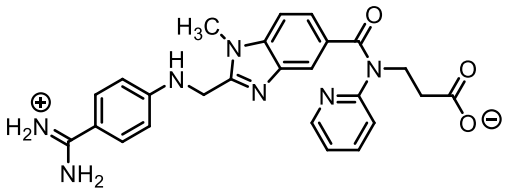

Dabigatran

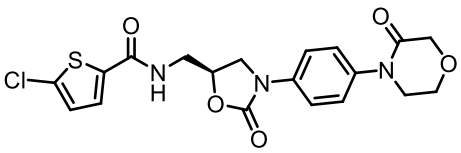

Rivaroxaban

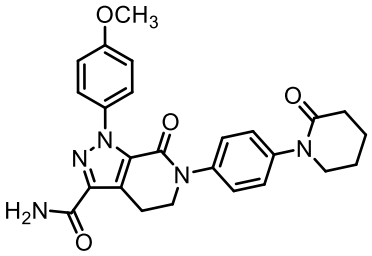

Apixaban

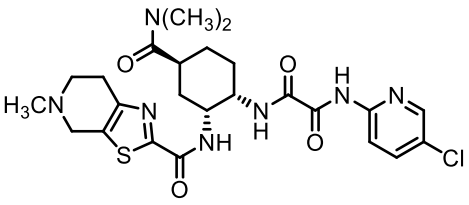

Edoxaban

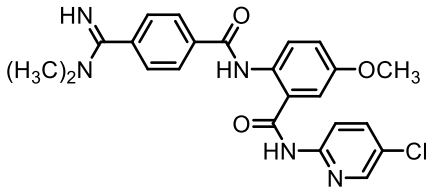

Betrixaban

Scheme 1-3. Structure of the DOACs.

1.2.3. In the Search of Non-Antihemostatic Antithrombotics

All common anticoagulants have bleeding diathesis and/or aggravation of major bleeding events as possible SAEs, even the most modern ones.[11,12,18–20] The DOACs may not require any monitoring nor cause complications in everyday life, their intake must still be adapted before surgery to avoid hemorrhagic complications.[10] Moreover, in the case of an accident, an unplanned surgical operation, or an overdose, the management of the bleeding is delicate and not well-established.[18,19] People who cannot take DOACs because of contraindication (e.g. patients with gastrointestinal cancers[11,12]) or because the indication has not been investigated yet (e.g. patients with catheter[16] or MHV[17]) must continue taking VKAs and are at even higher risk of hemorrhage.

Bleeding is a logical consequence as the enzymes inhibited by all these anticoagulants, mainly FX(a) and (pro)thrombin, are key coagulation factors in hemostasis. Thrombosis and hemostasis are often considered as two faces of the same coin:[34,35] if a drug is to be antithrombotic, it will also be inevitably antihemostatic.

This paradigm may be an oversimplification, as we know that FXIIa is involved in thrombosis caused by BCMD yet is *not* part of hemostasis. Could the inhibition of FXIIa mean reduced exogenous thrombosis without any bleeding SAEs, even if it would seem contradictory with Hageman's death? And what if FXIIa also happened to have a role in endogenous thrombosis? Could it represent a therapeutic target against a panel of thromboses?

1.3. Validation of FXIIa as a Therapeutic Target for Thrombosis

1.3.1. Preclinical Data: Observation in Animals

Inhibition of FXIIa in rabbits attenuated both cathether thrombosis and extracorporeal circulation thrombosis.[36–38] Similarly, inhibition of FXIIa in baboons provided thromboprotection from extracorporeal circulation.[39,40] These observations confirm that FXIIa initiates the coagulation cascade in thromboses caused by BCMD and suggest that FXIIa is a potential therapeutic target for BCMD-related thromboprophylaxis. However, additional experiments indicate that the interest of FXIIa may be broader than this application.

Genetically modified knockout mice, deficient with one ($FXII^{+/-}$) or both ($FXII^{-/-}$) alleles of the FXII gene, were generated.[24] Consequently, compared to the wild-type (wt) breed, $FXII^{+/-}$ mice display a halved FXIIa activity, while $FXII^{-/-}$ mice display no activity. As observed in humans, these FXII-deficient mice are completely asymptomatic.[24] Surprisingly, $FXII^{+/-}$ mice are not more protected from thrombosis than the wt breed,[41] as opposed to $FXII^{-/-}$ mice, which are more resistant to several models of thromboses: pulmonary embolism initiated by an injection of collagen,[41] artery thrombosis initiated either by exposure of the vessels to $FeCl_3$ (Figure 1-6A), ligation (Figure 1-6B),[41] or ROS generation by Rose Bengal/laser,[42] and thrombosis due to cerebral ischemia caused by transient middle cerebral artery occlusion (tMCAO).[43]

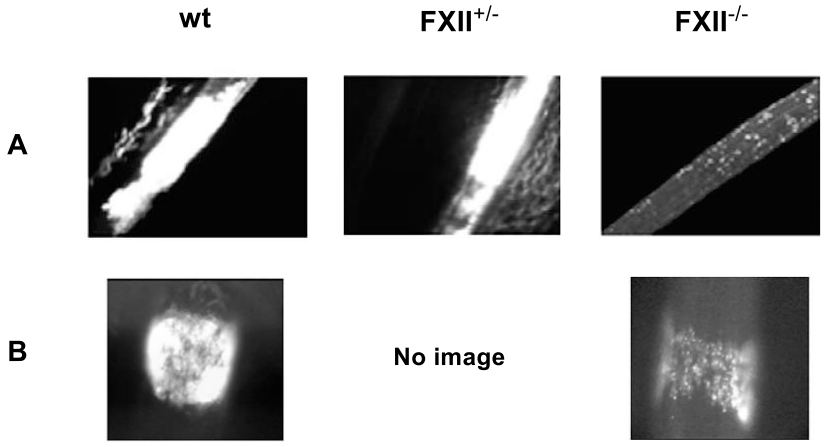

Figure 1-6. Photomicrographs of thrombosis models in mice. (A) Thrombus formation in mesenteric arterioles, 25 minutes after topical exposure to 20% $FeCl_3$. (B) Thrombus formation in the carotid artery, 8 minutes after ligation with a surgical filament. Adapted with authorization from [41].

Similar results were obtained in wt mice by inhibition of FXII expression [44] or by direct inhibition of FXIIa.[45] To our knowledge, the influence of a FXII deficiency on arterial and venous thrombosis in non-human primate models has never been described.

To summarize, together these experiments on animals strongly suggest that inhibition of FXIIa may be a therapeutic target for a variety of thromboses, and not only for BCMD-thromboses.

1.3.2. Epidemiological Data: Observations in Humans

Even though the Hagerman case taken alone does not corroborate this hypothesis, following the findings of the experiments on animals, patients with a deficiency in FXII should *statistically* be less prone to thromboembolism.

There have been debates for years about this topic: some studies conclude that FXII deficiency is actually a risk factor for thromboembolic events such as CHD,[46,47] venous thrombosis,[48,49] and ischemic stroke.[50] Others suggest that this deficiency has no influence on such events, all taken together.[51–55] We could find only one study that actually concludes that FXII deficiency is thromboprotective.[56] A recurrent problem in this field of research is that only few people get detected for FXII deficiency, and thus, studies rely on small, statistically weakly relevant pools of patients, resulting in these different conclusions.

A more representative meta-analysis was performed and studied the survival rate over 5 years of 8936 patients diagnosed with FXII deficiency, depending on the severity of their deficiency.[57] The lower the FXII plasma activity, the lower the survival rate. Very surprisingly, this tendency does not apply to patients with minimal to no plasma FXII activity (≤10%), whose survival rate is equivalent to that of the reference group, resulting in a U-shaped graph (Figure 1-7).

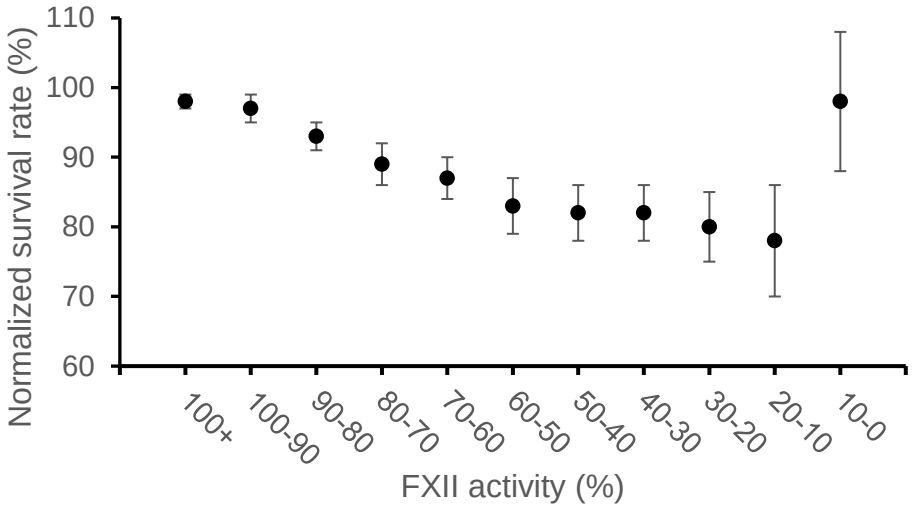

Figure 1-7. Normalized survival rate of patients according to their FXII plasma activity.

This increase in mortality, however, is most likely not due to an increase in thrombosis. Two recent small-cohort studies,[58,59] discriminating patients with a moderate FXII deficiency from patients with a severe one, showed that neither of these two groups were more susceptible to thromboembolic events compared to the reference group.

1.3.3. Conclusion

These last few years, the sheer amount of positive preclinical data made FXII one of the most promising therapeutic targets to obtain antithrombotics with no antihemostatic effects.[23,60–65] However, epidemiological data in humans is contrasted, and the most recent studies suggest that a FXII deficiency has no antithrombotic effect, hinting that FXII may not be as involved in human thrombosis as it is in murine or rat thrombosis. Although the interest of FXII inhibition in BCMD-induced thrombosis remains important, its appeal in the field of venous and arterial thromboprophylaxis is less obvious and needs to be further investigated.

1.4. Biochemical Properties of FXII and FXIIa

1.4.1. The Contact Activation System

The activation of FXII takes place *via* the contact activation system (CAS), whose name comes from its initiation by the interaction of FXII with surfaces. The initiation of the CAS is detailed below (Figure 1-8).

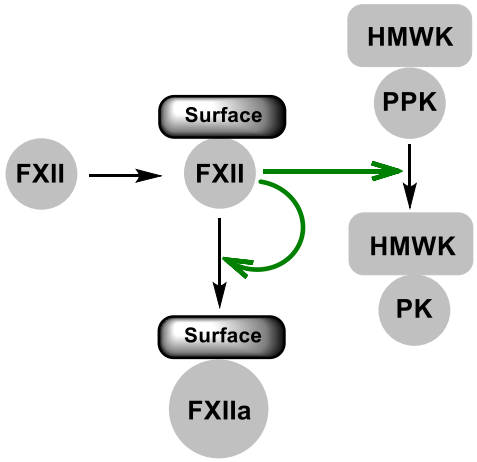

Figure 1-8. Initiation of the CAS.

Two processes happen when FXII adsorbs on a surface: it becomes susceptible to cleavage and develops a weak proteolytic activity.[66] This adsorbed FXII is thus able to cleave a small amount of other adsorbed FXII enzymes into FXIIa and/or a small amount of plasma prekallikrein (PPK), naturally complexed with high-molecular weight kininogen (HMWK), a non-enzymatic protein, into plasma kallikrein (PK).

Once initiated, the propagation of the CAS is complex (Figure 1-9). The activating surfaces play a double role: as described before, it promotes the cleavage of FXII into FXIIa, but it is also hypothesized to act as a cofactor necessary for the proteolytic activity of FXIIa towards PPK.[67] Adsorbed FXIIa and PK cross-activate each other in a positive feedback loop (Figure 1-9, pathway A).[68,69] PK can further cleave FXIIa into the Factor XII fragment (FXIIf, pathway B), which is still able in return to activate PPK into PK (pathway C).[69] The formed PK is able to cleave its partner, HMWK, and to release bradykinin (BK), a vasodilator (pathway D). CAS-induced generation of BK has no clear purpose in healthy subjects and its elusive role is most likely physiologically not primordial.[70] Indeed, as we discussed before, FXII-deficient patients, whose CAS is thus defective, do not have any relevant symptoms.

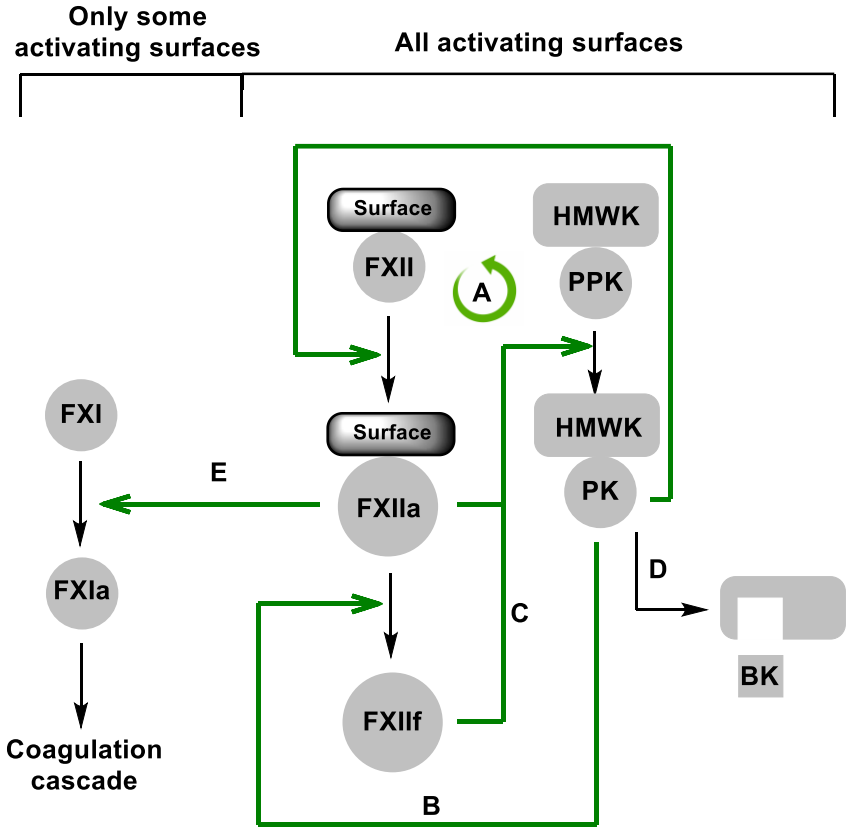

Figure 1-9. Propagation of the CAS.

If all activating surfaces induce the proteolytic activity of FXIIa towards PPK, only a selection of these surfaces allow FXIIa to cleave FXI (pathway E),[14,67] and thus to initiate the coagulation cascade. Furthermore, FXIIf has no proteolytic activity towards FXI.[69] In this work, we will call the surfaces allowing FXIIa to initiate PPK activation "proinflammatory surfaces" and the surfaces able to initiate both PPK and FXI activation "procoagulant surfaces". The dual character of FXIIa, depending on the surface that it is adsorbed on, and the inactivity of FXIIf towards FXI will both be rationalized based on the structures of these enzymes.

1.4.2. The Nature of the Activating Surfaces

Some of the activating so-called surfaces are actually soluble compounds (i.e. polyphosphates, PolyPs) but, for historical reasons, the term surface is universally used when talking about compounds activating FXII.

The requirements for being an activating surface of FXII are not well understood. They are often referred as negatively-charged in the literature because glass, kaolin (an aluminosilicate), heparin, dextran sulfate (DXS, a persulfated polymer of glucose), ellagate (Scheme 1-4Scheme 1-4. Structure of the ellagate anion.), and PolyPs, among others, are well-described activators.[14,70] However, numerous uncharged activators exist as well, including materials used in BCMD such as cuprophan (medical-grade regenerated cellulose), PET, PTFE, PVC, and PDMS.[14,62]

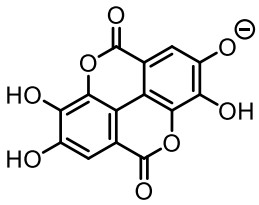

Scheme 1-4. Structure of the ellagate anion.

The differences between proinflammatory and procoagulant surfaces is even less understood and the classification is purely empiric.[14] It was hypothesized that insoluble surfaces are procoagulant while soluble surfaces are only proinflammatory.[67] However, the procoagulant or proinflammatory character of a surface seems to depend on several parameters. The medium is especially crucial: for example, DXS is procoagulant in vitro, not *in vivo*.[14,67]

1.5. Other Medical Conditions Involved with FXIIa

Even though FXII(a) inhibition has been intensively studied for its thromboprotective properties, recent developments have shown that its therapeutic potential may apply to other medical conditions, which we will discuss in this section.

1.5.1. Hereditary Angioedemas

Hereditary angioedemas (HAE) type I to III are orphan, genetic life-threatening swelling diseases, laryngeal edema and asphyxiation being the associated primary causes of mortality.[70] Even though, as discussed before, CAS-induced generation of BK has no known role in healthy patients, it is directly involved in HAE.[70] C1 esterase inhibitor (C1INH) is a serpin acting as a naturally-occurring inhibitor of PK. Patients suffering from HAE I and II display respectively a C1INH deficiency and a C1INH dysfunction, resulting in an overproduction of vasodilator BK, which was identified as the principal mediator of vascular leakage in HAE.

On the other side, patients suffering from HAE III display a mutation of the FXII gene, resulting in the translation of an overreactive FXII enzyme. Treatment involves infusion of C1INH, bradykinin-receptor antagonists, and PK inhibitors.[70] An additional promising therapeutic target is the enzyme which is responsible for the initiation of the CAS: FXII(a).[71] FXII inhibition was proven to reduce edema formation in three different mice models.[72,73]

The FDA and the EMA approved the sheer amount of 6 medicines against HAE these last 12 years, all under the Orphan Drug Designation.[74,75] The Orphan Drug Act (ODA) strongly encourages orphan drug development with numerous economic incentives including marketing exclusivity, tax credits, and research grants.[76]

The success of the orphan drugs against HAE, combined with the economic advantages offered by the ODA, has made HAE-treatment a hot research topic. These last few years, as will be detailed in section 1.7., the antithrombotic potential of certain FXII(a) inhibitors was set aside to study their potential as anti-HAE drug.

1.5.2. Sepsis

Sepsis is an exaggerated inflammatory response to an infection.[77] In the case of a blood infection by bacteria, among other processes, FXII gets activated after interaction with procoagulant surfaces present on the bacterial cell membrane, such as lipopolysaccharides and peptidoglycans, and bacteria-produced PolyPs. In parallel, neutrophils, a type of white blood cells, release their nuclear contents, including procoagulant DNA, further activating FXII. Coagulation is initiated and the resulting harmless clots are meant to trap the pathogens and to minimize host damage.[77]

At its most extreme, this process can over-activate and lead to widespread microvascular thrombosis, called disseminated intravascular coagulation (DIC), leading to numerous ischemias.[77] This formation of a large number of thrombi depletes the stocks of fibrin, platelets and coagulation factors, which is a condition known as consumptive coagulopathy. The hemostatic balance is disrupted, and bleeding occurs throughout the body. Together, generalized ischemias and bleedings are prone to lead to multiple organ failures and, ultimately, death.[77]

As FXII is considered as one of the drivers of this immune response, it represents an ideal therapeutic target in the management of sepsis complications. FXII deficiency or inhibition was proven to improve survival in a murine gram-negative pneumonia-derived sepsis model,[78] a murine polymicrobial sepsis model,[79] and a baboon *S. aureus*-induced sepsis model.[80] However, the protective effect of a FXII deficiency seems to be highly dependent on the kind of bacteria involved in the sepsis.

For example, FXII deficiency had no influence on mortality in murine gram-positive pneumonia-derived[78] and in baboon and murine *E. coli*-induced sepsis models.[81,82] Clearly, additional studies are needed to further clarify the role of FXII in sepsis, its pathogen-specific behaviors, and its extent as a therapeutic target.

1.5.3. Alzheimer's Disease

Alzheimer's disease (AD) is a life-threatening neurodegenerative disorder, characterized by the accumulation of β-amyloid peptides (Aβ) in the brain. Even though Aβ are known as the primary drivers of the disease, the exact mechanisms by which it disrupts neuronal functions is not fully understood.[83,84]

CAS-mediated inflammation was identified to be one of these mechanisms, as increased activation of CAS enzymes, including FXII, was found in the blood of AD patients and of AD mice models.[83] Specific Aβ aggregates were proven to be procoagulant surfaces, leading locally to proinflammatory and prothrombotic states, both potentially harmful to neurons.[84] The toxicity of the Aβ-mediated CAS activation was confirmed in an AD murine model, where FXII depletion provided partial protection from neurodegeneration.[85] These promising results should further stimulate research on the validation of FXII as a therapeutic target.

1.5.4. Multiple Sclerosis

Multiple sclerosis (MS) is an autoimmune disease characterized by the degradation of myelin, a substance that surrounds and protects the neurons of the central nervous system (CNS). The disruption of the transmission of nerve impulses results in numerous physical and mental symptoms.[86]

The CAS is thought to be involved in CNS autoimmunity. In a MS murine model, FXII deficiency or inhibition both limited CNS inflammation.[87] Moreover, higher FXII protein levels were found in MS patients than in healthy subjects.[88] Further studies are required to fully apprehend the role of FXII in MS.

1.6. Structure and Functioning of FXII, FXIIa and FXIIf

1.6.1. Mechanism of Serine Protease-Catalyzed Hydrolysis

As mentioned previously, both FXIIa and FXIIf are serine proteases. These enzymes catalyze the hydrolysis of peptide bonds thanks to the side-chains of three residues, referred to as the catalytic triad: an aspartate, an histidine, and a serine. The general mechanism of such a reaction is described (Scheme 1-5).[89]

The polypeptide substrate (in red) fits into the active site of the enzyme, next to the serine of the catalytic triad (A, Scheme 1-5). Through a concerted mechanism, the aspartate deprotonates the acidic hydrogen of the imidazole of the histidine, which in turn deprotonates the hydroxyl group of the serine, which itself adds onto the carbonyl moiety of the peptide bond of the substrate. The negative charge of the resulting tetrahedral intermediate is stabilized by H-bonding with the amidic hydrogen atoms of the backbone of three consecutive residues (B, Scheme 1-5). This pocket is usually called the oxyanion hole. Eventually, the tetrahedral intermediate collapses via the reverse mechanism (B, Scheme 1-5) , releasing the N-terminal part of the cleaved polypeptide and an acyl enzyme (C, Scheme 1-5). [89]

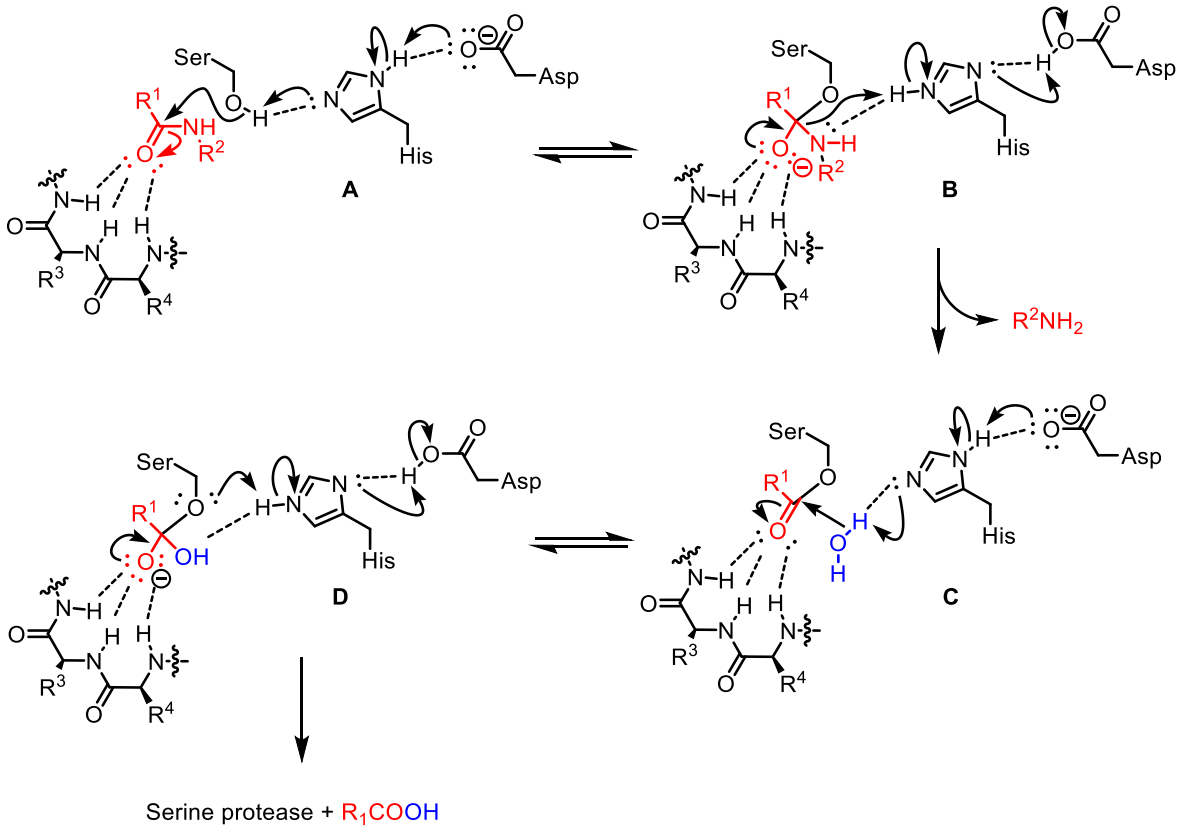

Scheme 1-5. Mechanism of serine protease-catalyzed hydrolysis

This acyl enzyme is then hydrolyzed following the same two-step process: the aspartate deprotonates the histidine, which in turn deprotonates a molecule of water, which itself adds onto the carbonyl moiety of the acyl enzyme (C, Scheme 1-5). The tetrahedral intermediate, once again stabilized in the oxyanion hole, collapses (D, Scheme 1-5), releasing the free serine protease and the C-terminal part of the cleaved polypeptide.[89] The 3D-structure of the active site of FXIIa and FXIIf as described in the following subchapters, are consistent with such a mechanism.

1.6.2. Primary Structures

Starting from the N-terminus, the primary structure of FXII (Figure 1-10) consists of a heavy chain containing mainly recognition domains (353 residues) and a light chain containing most of the protease domain (243 residues).[90,91]

The heavy chain can be further categorized into a fibronectin type II domain (FnII), a first epidermal growth factor-like domain (EGF1), a fibronectin type I domain (FnI), a second EGF domain (EGF2), a kringle domain, and a proline-rich region (PRR).[90,91]

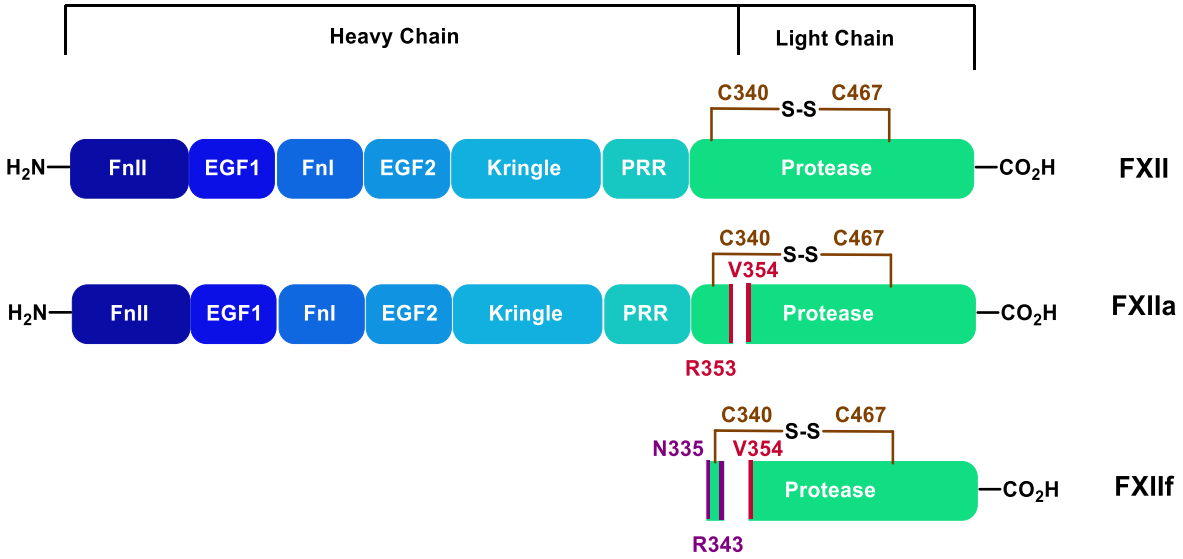

Figure 1-10. Simplified chain and domain repartition in FXII and in its activated forms. The cleavage sites which yield FXIIa and FXIIf are shown in red and purple, respectively

In FXIIa, the peptidic bond between both chains is hydrolyzed at Arg353-Val354 (simply called afterward the R353 site) and both chains are held together *via* a single disulfide bond at Cys340-Cys467.[90] In FXIIf, the peptidic bonds at Arg334-Asn335 and at Arg343-Leu344 are further hydrolyzed, discarding a major part of the heavy chain.[92]

The FnII and FnI domains (residues 1-71 and 112-154) share homology with the sequence of the type II and type I domain of fibronectin, respectively.[90,93,94] The EGF1 and the the EGF2 domains (71-112 and 154-191) each contains 6 Cys and 2 Gly spread at specific positions over 50 residues, as found in the epidermal growth factor.[90,95]. The kringle region (191-276), named after a Scandinavian pastry that possesses a similar pretzel-like structure,[96] is a common domain characterized by 3 invariant internal disulfide bonds and around 40% sequence homology from one kringle domain to another.[90,96,97] The PRR (276-330) region features 33% of Pro residues and does not have any sequence homology to other known prolin-rich protein.[90,91]

1.6.3. Functioning of the Domains of the Heavy Chain

Even though FXII has been known for years, structural data are limited. To our knowledge, only two crystal structures of a part the heavy chain have been reported: FXII-FnIE, a polypeptide corresponding to the FnI-EGF2 domains, in its native state and in a holmium-bound state.[98] Consequently, the precise role of each domain remains elusive. Moreover, research about this subject is scarce. Still, in vitro, important questions have been answered:

- The FnII domain is responsible for protecting the R353 site from cleavage in the absence of activating surfaces.[99]
- In addition to the active site of the protease domain, the FnII domain does contain a secondary FXI binding site (SFXIBS).[100] As FXIIf has lost this domain, it cannot bind efficiently to FXI anymore, and thus is not involved in the coagulation cascade.
- All domains of the heavy chain have been proven to bind activating surfaces. However, their binding does not necessarily mediate FXI activation; the binding of some of them only mediate PPK activation while the binding of PRR does not mediate any of these processes. These data are summarized (Table 1-1).

Table 1-1. Heavy chain domains in FXII and their ability to mediate, by binding, FXI activation / PK activation. Adapted from [67].

domain	mediates FXI activation?	mediates PPK activation?	refs.
FnII /EGF1	Yes	n.d.	[99,101,102]
FnI	Yes	n.d.	[103]
EGF2/Kringle	No	Yes	[102,104,105]
PRR	No	No	[102]

Using that information, a hypothetical model for FXII activation can be suggested (Figure 1-11).[67] At rest in solution, the FnII domain protects sterically the R353 site from cleavage and FXII stands still (Figure 1-11A). A minimal requirement to yield a version of FXIIa which is able to initiate PPK activation is the binding of an activating surface to the EGF2 and the kringle domains (Figure 1-11B). These interactions are sufficient to promote the shifting of the FnII domain, which exposes the R353 site to peptidic cleavage, but not strong enough to expose the SFXIBS. Finally, the requirement to yield a version of FXIIa which is able to initiate both FXI and PPK activation is the binding of the activating surfaces to the N-terminal FnII, EGF1, and FnI domains – but these surfaces also happen to bind the EGF2 and kringle domains (Figure 1-11C). These interactions both expose the R353 site to peptidic cleavage and the secondary FXI binding site.

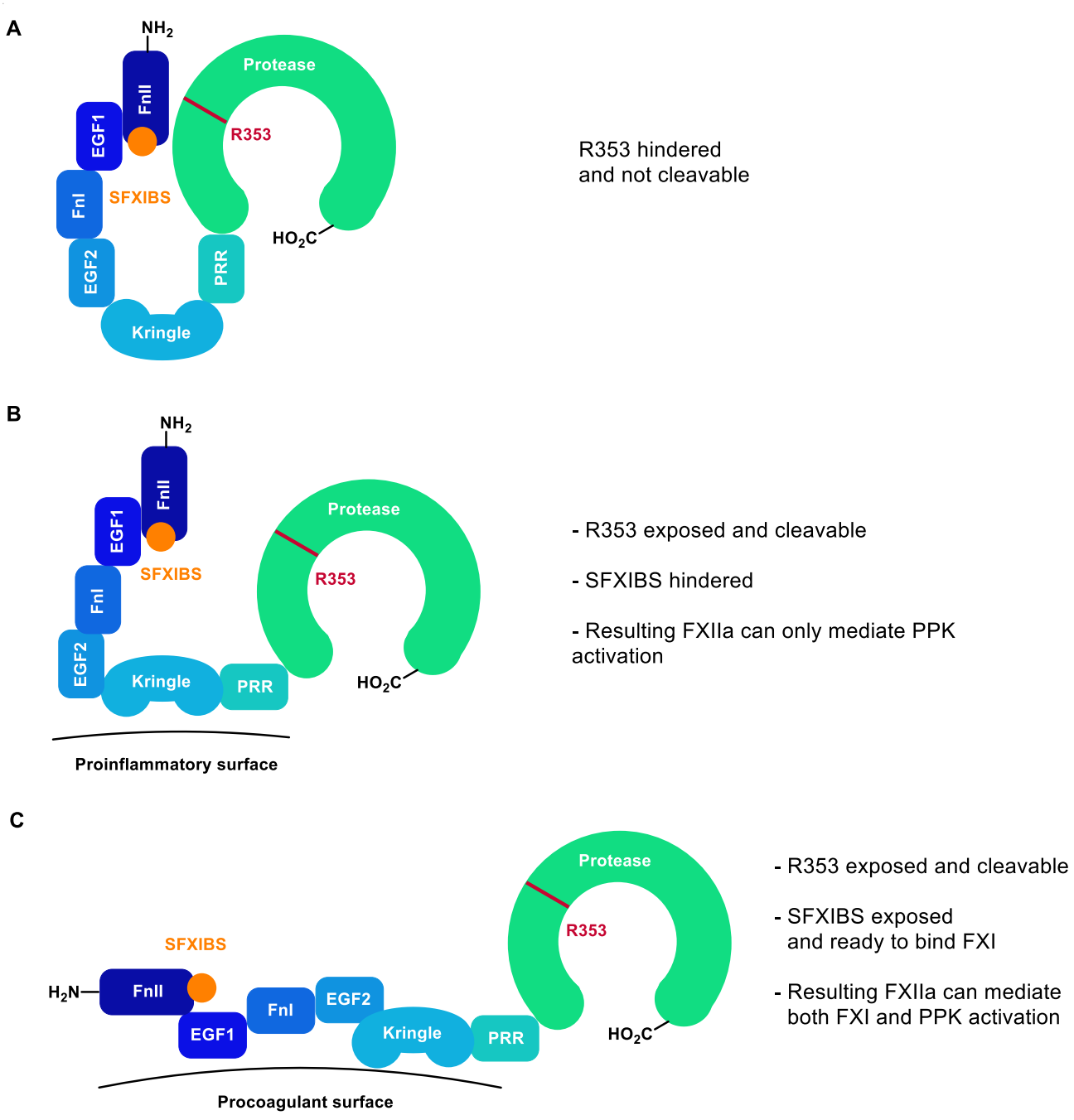

Figure 1-11. Hypothetical model of the conformations of FXII. (A) In solution. (B) Adsorbed on a surface. (C) Adsorbed on surface.

1.6.4. Functioning and 3D-Structure of the Protease Domain

Wild-type, human FXIIf and a His-tagged FXIIf recombinant were successfully crystallized, giving us the opportunity to explore the protease domain under its activated form.[106,107] For uniformity reasons, when referring to specific residues of the catalytic site, the numbering system of the chymotrypsinogen residues, one of the first SPs to have been studied, is used.

.

The protease domain of FXIIf is similar to those of other trypsin-like active SPs, the tertiary structure mainly consisting of 2 β-barrels delimitating the substrate-binding site (Figure 1-12). In addition to the catalytic triad, several pockets were identified the S1 and S3/4 pocket (S for specificity), the H1 pocket, and the oxyanion hole.[106]

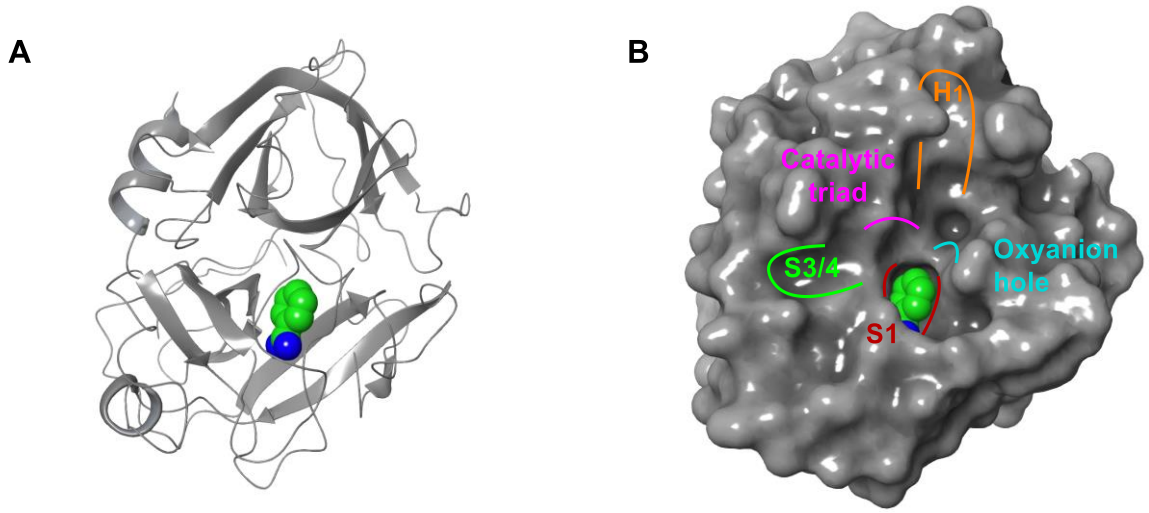

Figure 1-12. Structure of wild-type, human FXIIf cocrystallized with benzamidine as a ligand. (A) Ribbon diagram. (B) Molecular surface representation and pocket repartition. Molecules of water and inorganic ions are omitted.

The active site and the pockets are further detailed (Figure 1-13, next page). The catalytic triad , made up of Asp102, His57 and Ser195, is adequately positioned to perform its proteolytic activity. The negative charge of the tetrahedral intermediate is stabilized in the oxyanion hole by H-bonding with the backbone amidic hydrogens of Ser195, Asp194 and, Gly193.

The S1 pocket, also known as the primary specificity pocket, is characterized by Asp189 at its bottom. As in all trypsin-like SPs, this negatively-charged residue is meant to interact with a positively-charged Lys or Arg residue of the substrates.

The S3/S4 pocket is delimitated by aromatic residues Tyr99 and Trp215 and tipped by Met180. Finally, the H1 pocket is made up of aliphatic side-chain residues Leu59, Leu106, Leu54 and Leu33. Asp60A makes a small protuberance opposite to the H1 pocket. It is not really included in the H1 pocket *per se* but is worth mentioning as it will have a crucial role in our following discussions.

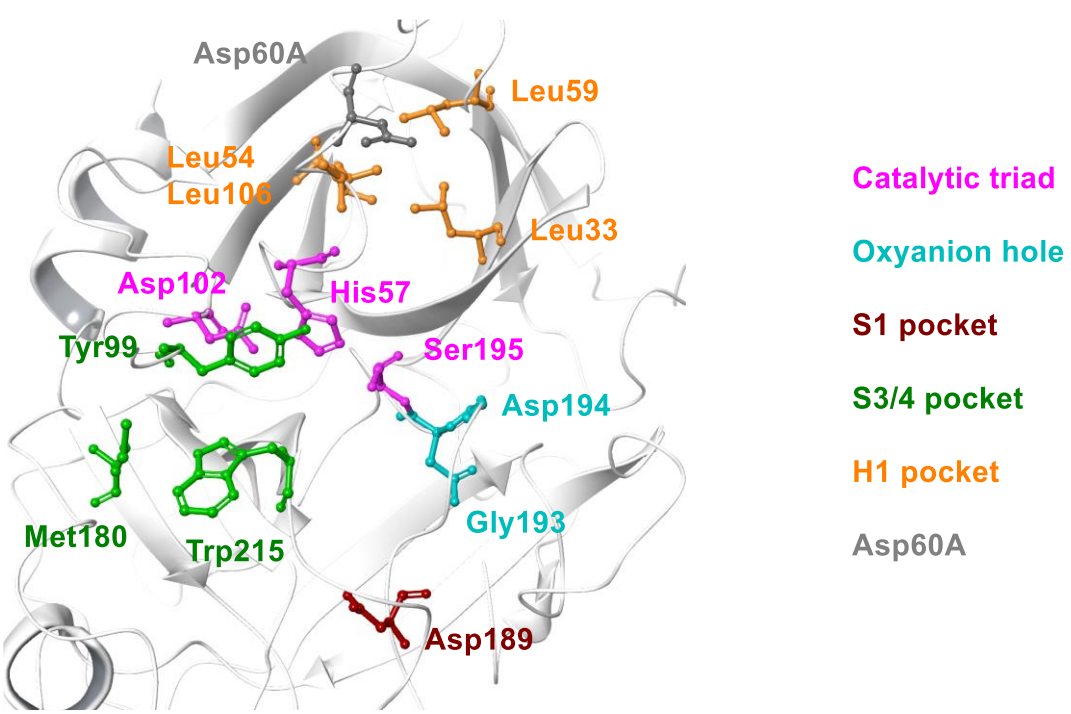

Figure 1-13. The residues of the different pockets of the substrate-binding site of FXIIf. The hydrogen atoms are omitted for clarity.

1.7. Inhibitors of FXII and FXIIa: State of The Art

1.7.1. Mechanisms of Inhibition

There are several types of possible mechanisms that have been envisaged to inhibit, directly or indirectly, the FXIIa activity. We can classify the different FXII(a) inhibitors in the following categories (Figure 1-14):

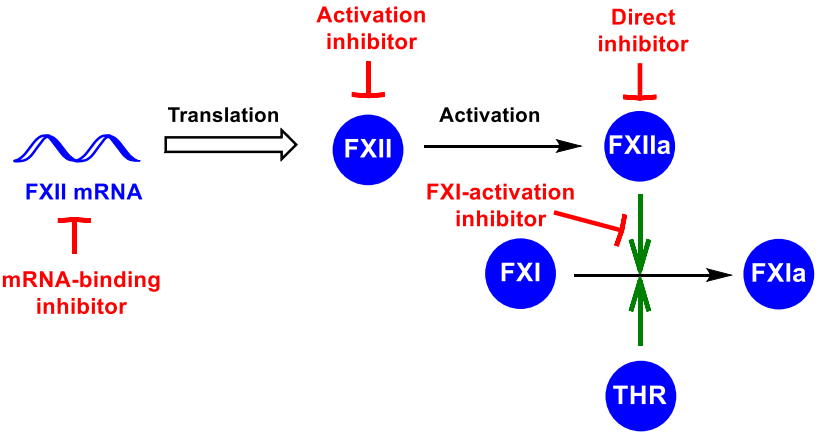

Figure 1-14. The different mechanisms of direct or indirect inhibition of FXIIa activity.

- mRNA-binding inhibitor: the compound is able to bind selectively to the mRNA coding for the expression of FXII, preventing its translation.
- Activation inhibitor: the compound inhibits the cleavage of FXII into FXIIa by binding to FXII.

- Direct inhibitor: the compound inhibits the proteolytic activity of FXIIa by binding to it.
- FXI-activation inhibitor: the compounds prevents selectively FXI from being activated by FXIIa by binding to FXI. The activation of FXI by thrombin, however, is still possible.

1.7.2. Protein-Based Inhibitors

1.7.2.1. Antibodies

There are numerous FXII(a)-inhibiting antibodies described in the literature.[20,62] We focus here on the most representative ones and those who have been the most studied

3F7 is a fully human recombinant antibody, direct inhibitor that binds selectively to the FXIIa active site. It has provided successful thromboprotection in several models, namely $FeCl_3$-induced thromboses in mice and extracorporeal membrane oxygenation (ECMO) in rabbits.[37,108] Affinity maturation of 3F7 led to the development of CSL312, which displayed a 44-fold higher affinity for FXIIa. CSL312 was not tested as an anti-thrombotic, but as an anti-inflammatory against HAE.[73] Thanks to the positive results obtained, CSL312, now called Garadacimab, is undergoing phase II clinical trials for HAE until 2021 (clinicaltrials.gov, ID: NCT03712228). Interestingly, Garadacimab was also planned to undergo phase I/II clinical trials against catheter-associated thrombosis (ID: NCT04281524) but the study was canceled for non-safety related business reasons.

The development of a second promising antibody began with 14E11, a murine antibody which acts as a FXI-activation inhibitor.[42] Administration protected from thrombosis in several models: $FeCl_3$-induced,[42] tMCAO,[109] and coronary artery ligation in mice,[110] and in an ex vivo flow model of baboon blood.[42] A humanized recombinant version of 14E11, now called AB023 or Xisomab 3G3, showed similar properties[111] and passed phase I clinical trials (ID: NCT03097341). As of November 2020, recruitment is ongoing for a phase II clinical trial evaluating the use of Xisomab 3G3 for the prevention of catheter-associated thrombosis (ID: NCT04465760). Another phase II trial, evaluating its use as an antithrombotic agent in chronic hemodialysis, was completed in June 2019 (ID: NCT03612856). The treatment is well tolerated but its efficacy has not been highlighted, probably because the trial took place on a small cohort of 24 human subjects.

Other antibodies have been developed as well. 15H8 acts as an activation inhibitor that binds selectively to the FnI and/or kringle domain.[39] It was proven to provide thromboprotection in an ex vivo flow models of human and baboon blood and in $FeCl_3$-induced thromboses in mice.

More recently, 5C12, a direct inhibitor, has displayed reduced thrombus formation in a baboon ECMO model.[40]

1.7.2.2. Proteins isolated or derived from natural sources

Ixodes ricinus contact phase inhibitor (Ir-CPI) was isolated from the castor bean tick, the most common tick in western Europe.[112] This protein is a direct inhibitor of both FXIIa and FXIa, suspected to prevent the catalytic activity because of steric hindrance due to binding to an exosite. It displayed thromboprophylactic activities in several models: Rose Bengal/laser-induced and collagen-induced thrombosis in mice,[112] cathether-induced thrombosis and arteriovenous shunt in rabbit, and cardiopulmonary bypass in sheep.[113] As of November 2020, Ir-CPI is the flagship product of the Walloon company Bioxodes and is entering phase I clinical trials.[114]

Infestin-4 is a recombinant protein based on the gene coding for infestin, a naturally-occuring thrombin inhibitor isolated from the hematophagous kissing bug *Triatoma infestans* found in South America, and was identified as a direct inhibitor of FXIIa.[115] Infestin-4 was fused with human albumin (HA) to increase its elimination half-life *in vivo* and the resulting protein, called rHA-Infestin-4, proved to be a potent inhibitor of FXIIa, selective over FXIa, FXa, FVIIa and thrombin.[116] rHA-Infestin-4 protected mice from $FeCl_3$-induced thrombus formation and tMCAO-induced stroke,[116] and reduced thrombosis due to arteriovenous shunt in rat and in rabbit.[45] It is hypothesized that rHA-Infestin-4 binds the active site of FXIIa.[45] Infestin-4 has also been further refined to yield mutants with an even better selectivity and potency toward FXIIa in vitro.[117]

Corn trypsin inhibitor (CTI) is a reversible SP inhibitor, isolated from corn and first shown to inhibit trypsin.[118] It was also proven to act as a potent direct inhibitor of FXIIa with selectivity over thrombin and FXa.[119] It is thought to bind the active pocket, mainly *via* the Arg residue of the S1 pocket. CTI can be used to shut down the CAS contribution to the coagulation cascade in ex vivo experiments.[120] Moreover, in rabbits, CTI-coated catheters were proven to be less thrombogenic than unmodified catheters.[38]

Momordica cochinchinensis trypsin inhibitor-II (MCoTI-II) is one of the two cyclotides displaying direct and reversible inhibition properties toward serine proteases and were isolated from the gac plant, a type of melon native to Southeast Asia.[121] Cyclotides are head-to-tail cyclic knotted oligopeptides characterized by the presence of three disulfide bonds (Figure 1-15).[122] The wt MCoTI-II inhibits non-selectively FXIIa and is also active on FXa, plasmin and trypsin. Optimization of the residue sequence allowed the development of a fully synthetic McoTI-II

derivative with a nanomolar inhibitory activity FXIIa, a >100-fold selectivity over other coagulation factors and 10-fold over plasmin and trypsin.[123]

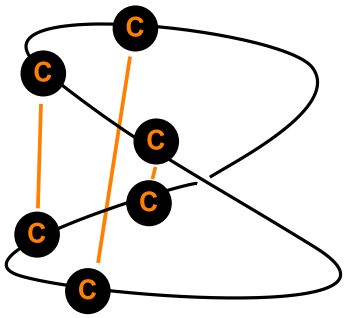

Figure 1-15. Schematic representation of a cyclotide. The knotted black line represents the backbone of the peptide and the oranges lines the disulfide bridges between cysteins.

Ecotin is a dimeric protein isolated from *Escherichia coli*, acting as a direct inhibitor of chymotrypsin-like proteases by forming a stable hetero-tetramer with the latter *via* two interfaces: the substrate-like primary binding site and the antibody-like secondary binding site.[124] Ecotin is potent but poorly selective, inhibiting PK, FXa, and FXIIa in the picomolar range.[125,126] Point mutations in both binding sites allowed the development of the variant XII-18, maintaining a picomolar activity toward FXIIa, with a 13 000-fold selectivity over FXa and 370-fold over PK.[127]

1.7.3. RNA-based inhibitors

1.7.3.1. Small-interfering RNAs

Small interfering RNAs (siRNAs) are small synthetic analogs of double-stranded RNA that associate with the RNA-induced silencing complex (RISC) found in the cell.[128] One of both strands (the passenger strand) is lost and the remaining strand (the guide strand) allows RISC to bind and then cleave the targeted mRNA, preventing the expression of the protein. An optimized siRNA, called ALN-F12, was developed to selectively interact with the FXII mRNA and was found to deplete efficiently the amount of plasmatic FXII in rats, mice and cynomolgus monkeys.[72] ALN-F12 was successfully used *in vivo* to reduce angioedema in murine models.

1.7.3.2. Antisense oligomers

Antisense oligomers (ASOs) are synthetic analogs of single-stranded RNA, complementary to the target mRNA.[128] The double-stranded complex of the ASO with the mRNA prevents its translation by steric hindrance and/or by recruitment of RNAse H, and thus prevents the expression of the protein. The selective depletion of FXII by ASO protected rabbits from $FeCl_3$-induced arterial and venous thrombosis [44] and from catheter-associated thrombosis.[36]

1.7.3.3. Aptamers

Aptamers are single-stranded RNA whose tertiary structure allows them to bind with high affinity to a target.[129] They can be seen as the RNA-analogs of antibodies. An aptamer targeting FXII(a) has been developed and acts as a direct inhibitor. It has only be tested in vitro.[130]

1.7.4. Synthetic Small Molecules

1.7.4.1. Modified oligopeptides

D-Pro-Phe-Arg chloromethyl ketone (**PCK**) is a synthetic chemically-modified tripeptide (Scheme 1-6),[131] direct inhibitor of FXIIa with moderate selectivity towards FXIIa over thrombin, FXa and FVIIa.[132] It has a prophylactic effect against tMCAO-induced stroke in mice.[43]

FXII402 was obtained as a micromolar-active, selective direct inhibitor of FXIIa after phage display experiments who generated over 4 billion bicyclic peptides (Scheme 1-6).[133] It was proven to inhibit the CAS in human plasma.

Two years later, after generation of over 8 billion candidates, the same team developed **FXII618** (Scheme 1-6), with a 60-fold improved, nanomolar inhibitory activity towards FXIIa, and a 10-fold improved selectivity.[134] Molecular docking suggests that the Phe-Arg-Leu sequence, also found in CTI, are the key residues binding the active site.

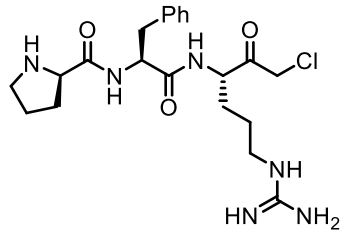

PCK

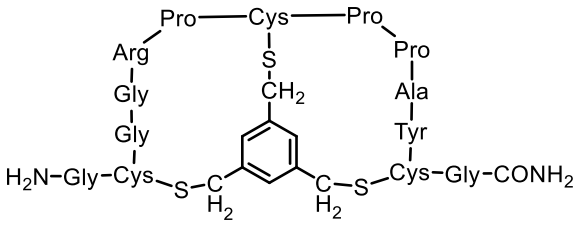

FXII402

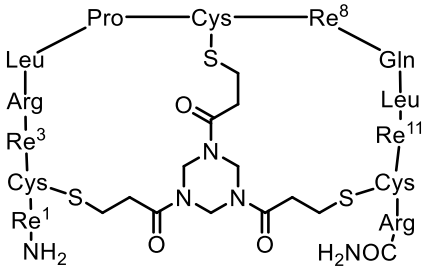

Compound	Re^1	Re^3	Re^8	Re^{11}
FXII618	Arg	Phe	Arg	Arg
FXII801	nor-Arg	Phe(4-F)	Arg	Arg
FXII900	D-Arg - D-Ser	Phe(4-F)	His	βHArg

Scheme 1-6. Structure of the synthetic oligopeptidic inhibitors of FXIIa.

Based on these observations, **FXII618** was further refined to yield **FXII801** by replacing the Phe of the key sequence by its *para*-fluoro derivative, with now a sub-nanomolar activity (Scheme 1-6). The N-terminal Arg was also replaced by a norarginine, in order to improve the

stability of the peptide in plasma.[135] **FXII801** was conjugated, thanks to a PEG linker, with a heptapeptide-palmitoyl tag displaying a binding affinity toward albumin, to further improved its metabolic stability.[136] Named tag-3xPEG24-FXIIa inhibitor, this conjugate inhibited the CAS activation in human plasma.

Another refinement of **FXII618** was performed with four changes in residues. Two D-amino acids were chosen at the N-terminus for metabolic stability; the three other changes were meant to improve potency.[137] The resulting derivative, called **FXII900** (Scheme 1-6), had a picomolar activity towards FXIIa and a day-long stability in human plasma. It was successfully used in a $FeCl_3$-induced murine thrombosis model and provided thromboprotection in a rabbit ECMO model.

1.7.4.2. *N*-Acylbenzotriazoles and *N*-acylaminotriazoles

Through virtual high throughput screening (vHTS) of the entire 72 million PubChem compound database using quantitative structure-activity relationship (QSAR) models, 17 virtual FXIIa inhibitor hits were identified and confirmed by enzymatic assays with potencies in the low micromolar – high nanomolar range.[138] Among these compounds, 6 were part of *N*-acylbenzotriazoles **A** and 6 others of the *N*-acylaminotriazoles **B** (Scheme 1-7). Their selectivity and *in/*ex vivo potency were not assessed. Further optimization using combinatorial chemistry led to the identification of compound **B'**,[139] with a potency toward FXIIa in the low nanomolar range, a >10-fold selectivity over thrombin and 200-fold over PK, FXIa and FXa. Compound B' was shown to have thrombophylactic properties both in vitro and ex vivo.

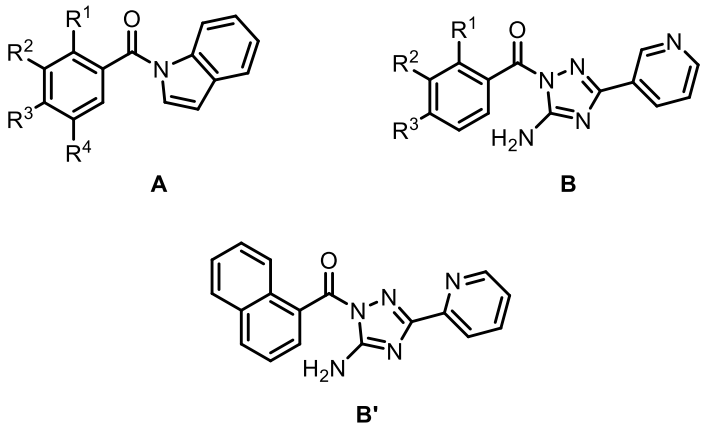

Scheme 1-7. Structure of the FXIIa-inhibiting hit compounds N-acylbenzotriazoles A and N-acylaminotriazoles B, identified by vHTS and then experimentally confirmed, and of optimized compound B', discovered by combinatorial chemistry.

1.7.4.3. Coumarins

3-Carboxyamido coumarins are known mechanism-based inhibitors of chymotrypsin-like enzymes [140] and thus represented an ideal starting scaffold against FXIIa. fter screening and

several modulations, two selective hit compounds with inhibitory activity in the low micromolar range were identified, **COU254** and **COU294** (Scheme 1-8).[132] Interestingly, **COU254** failed at prophylaxis for tMCAO-induced thrombosis in mice.[141] Unfavorable pharmacological properties and structural differences between human and murine FXIIa might be at cause.

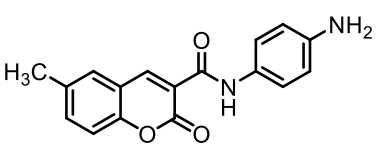

COU254: IC_{50} = 14 µM

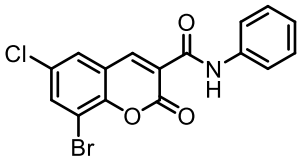

COU294: IC_{50} = 4.4 µM

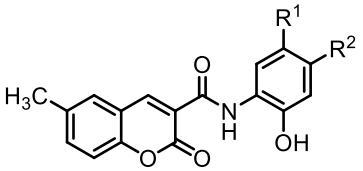

ChB05: R^1 = Cl, R^2 = H, IC_{50} = 5 µM
ChB06: R^1 = H, R^2 = Cl, IC_{50} = 8 µM
ChB10: R^1 = R^2 = H, IC_{50} = 7 µM

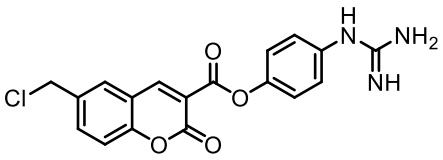

RF1: IC_{50} = 6 µM

Scheme 1-8. Structure of coumarins identified as hit compounds for the inhibition of FXIIa.

In order to improve its solubility in physiological media, the series was further modulated with hydroxyl groups. Compounds **ChB05**, **06** and **10** were identified and showed similar inhibition and selectivity profiles to those of **COU294** (Scheme 1-8), but improved pharmacological properties as determined in silico.[142] The compounds were tested ex vivo on whole human blood but, again, no inhibition of the CAS was observed. This result was attributed to the poor activity/lipophilicity ratio of the molecules.

In parallel, screening of our in-house chemolibrary yielded water-soluble hit compound **RF1** (Scheme 1-8), a micromolar-potent inhibitor of human FXIIa with medium selectivity over thrombin, FXIa and FXa.[143] Its antithrombotic activity has been highlighted in whole human blood in ex vivo models. The phenylguanidinium moiety is thought to mediate the initial interaction *via* an ionic interaction Asp189 in the S1 pocket. Attempts at optimizing the selectivity profile of this compound led to a general decrease in activity.

1.7.4.4. 2,5-Dichlorobenzyl Triazoles

2,5-Dichlorobenzyl inhibitors were confirmed by crystallography to fit the S1 pocket of thrombin, also a part of the chymotrypsin-like enzymes.[144] The 5-chloro moiety interacted with Tyr218 *via* a Cl-π interaction, an attractive interaction mainly sustained by dispersion forces

between an organic chloride and the π electron cloud of an aromatic ring.[145] The 2-chloro moiety, on the other side, acted as a conformational lock.

On the assumption that the S1 pockets of thrombin and of FXIIa were similar, our group started to develop 2,5-dichlorobenzyl inhibitors for FXIIa. The click Huisgen cycloaddition was used in order to generate as many compounds as possible in a limited time.

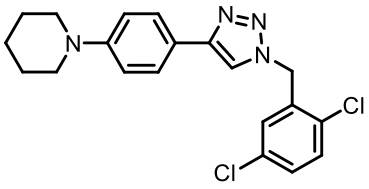

ChB49: IC_{50} = 10 µM

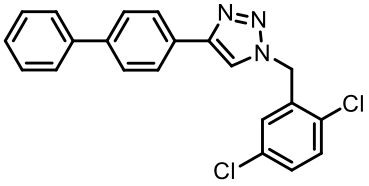

ChB50: IC_{50} = 8 µM

Scheme 1-9. Structure of triazoles identified as hit compounds for FXIIa inhibition.

Sixteen 2,5-dichlorobenzyl triazoles were successfully synthesized and two showed and inhibitory activity against FXIIa in the low micromolar range, **ChB49** and **ChB50** (Scheme 1-9).

1.7.4.5. Others

A patent of novel, structurally diverse FXIIa inhibitors has been submitted but the general strategy, the potency and the selectivity are neither discussed nor mentioned.[146]

1.7.5. Comparison of the Characteristics of the Different Inhibitors

All categories of inhibitors are potentially promising, and a summary of their distinctive characteristics is shown (Table 1-2).

Table 1-2. Characteristics of the different prophylactic and therapeutic strategies.

	ASO - siRNA	Aptamers	Antibodies	Proteins - peptides	Small, non-peptidic molecules	
					Water-soluble	Lipophilic
Delivery	Parenteral	Parenteral	Parenteral	Parenteral or oral (rare)	Parenteral	Oral
Onset of action	Delayed	Immediate	Immediate	Immediate	Immediate	Rapid
Dosing interval	Weekly - monthly	Daily	Weekly-monthly	Daily	Daily	Daily
Cost	++	++	++	++	-	-

ASOs, siRNAs and antibodies stand out by and their monthly or weekly administration, offering the promise of safe and little invasive thromboprophylactic treatment for chronic conditions.Aptamers, proteins/peptides, and water-soluble small non-peptidic molecules stand out by their immediate onset of action. They could all be potentially used both as acute thrombotherapeutic and thromboprophylaxic treatments by their parenteral administration, with a few exceptions that could be administered orally, namely cyclotides.

Lipophilic, small non-peptidic molecules stand out by their ability to be administered orally, which is the ideal mode of administration for at-home long-term medication. Moreover, the production of pharmacological-grade small molecules is overall 22 times cheaper than the production of pharmacological-grade biomacromolecules.[147,148]

Chapter 2: General Objectives and Strategies

The Factor XIIa has emerged as a potential therapeutic target for a whole range of medical conditions, including thrombosis, AD, sepsis and MS. Despite their upsides compared to biological or biobased inhibitors, namely their cost and the fact that they are potentially more easily administered orally, research for synthetic small inhibitors of FXIIa is scarce. Consequently, the *in vivo* non-clinical and clinical development of this category of compounds is close to non-existent compared to its alternatives. In an attempt to fill this gap, the general aim of this thesis is to design and to synthesize small, non-peptidic molecules targeting FXIIa to generate hit compounds that could be used to identify promising scaffolds and to yield lead compounds.

In the first part of this thesis (Scheme 2-1), we will focus on the refinement of the 2,5-dichlorobenzyl triazole inhibitors **1a**. As previously discussed, preliminary developments allowed our group to synthesize compounds potent against FXIIa in the low µM range. Our goal is to achieve even lower potencies by modulating progressively the structure of our hit compounds. The adequacy of the envisaged modulations will first be estimated based on molecular docking performed using the novel XRD structure of FXIIf. The promising compounds will be then synthesized and tested in vitro on FXIIf to assess their potency. The analysis of the results will allow us to further refine the structure of the potential inhibitors, using once again molecular docking, in an iterative process. This work will lead us to synthesize amidines as potential hit compounds but will also highlight that amidination protocols, as described in the literature, are ill-adapted to our needs.

In the second part of this thesis (Scheme 2-1), in order to develop new tools to simplify and to increase the throughput of our syntheses, we will develop a novel methodology of early-stage amidination, leading to fully protected amidine compounds **1b**. In order to make this synthetic strategy as versatile as possible, the compatibility of such intermediates with some of the most used reactions in medicinal chemistry, namely Pd-catalyzed cross couplings and substitution reactions, will be verified experimentally.

1. Refinement in order to improve potency

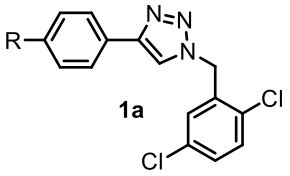

1a

Amidination protocols ill-adapted to our needs

2. Development of an amidination protocol

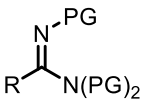

1b

Two biscationic hits identified as potent hit compounds

3. Refinement in order to improve potency, selectivity, metabolic stability

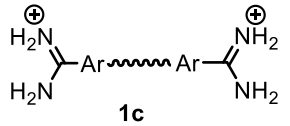

1c

Scheme 2-1. Objectives and workflow of the thesis

In parallel to this work, our group will review exhaustively the FXIIa inhibitors described in the literature and will perform vHTS of existing drugs. From this work, two potent biscationic compounds **1c** will be identified: nafamostat and pentamidine, both adequate starting points toward more complex candidates. In the third part of this thesis (Scheme 2-1), three derivatives of these compounds will be designed using molecular docking in order to improve their potency, their selectivity and their metabolic stability, in an attempt to make them more suitable as potential lead compounds. Their synthesis will then be tackled using our improved early-stage amidination metholodogy. The compounds will then be tested in vitro and ex vivo to assess these different parameters. As in the first part of this thesis, the analysis of these results will allow us to further refine the structure of the potential inhibitors, using once again molecular docking, in an iterative process.

Chapter 3: Triazole-Based Inhibitors

3.1. Objectives and Strategy

In a previous work from our group, by synthesizing a range of 2,5-dichlorobenzyltriazoles using click chemistry, compounds **ChB49** and **ChB50** were identified as micromolar potent inhibitors of FXIIa. Our goal was to further refine the structure of these compounds in order to improve their activity.

During this thesis, in 2018, the crystal structure of the active site of FXIIf was published, which allowed us to use structure-inspired ligand design. Molecular docking was used to validate the target compounds, which were then synthesized. Inhibition assays on FXIIa allowed us to evaluate the effect of our modifications and to design more refined targets, in an iterative process.

3.2. First-Generation Collection

3.2.1. Design and Retrosynthesis

As discussed before, the 2,5-dichlorophenyl moiety of micromolar potent compounds **1** is thought to fit the S1 pocket of FXIIa *via* a key Cl-π interaction. At the time, the crystal structure of the active site of FXIIf was not published and we hypothesized that replacing the 2,5-dichlorophenyl moiety with a phenylguanidine moiety, as illustrated by our first-generation collection of compounds **3**, would lead to better inhibitory activities (Scheme 3-1).

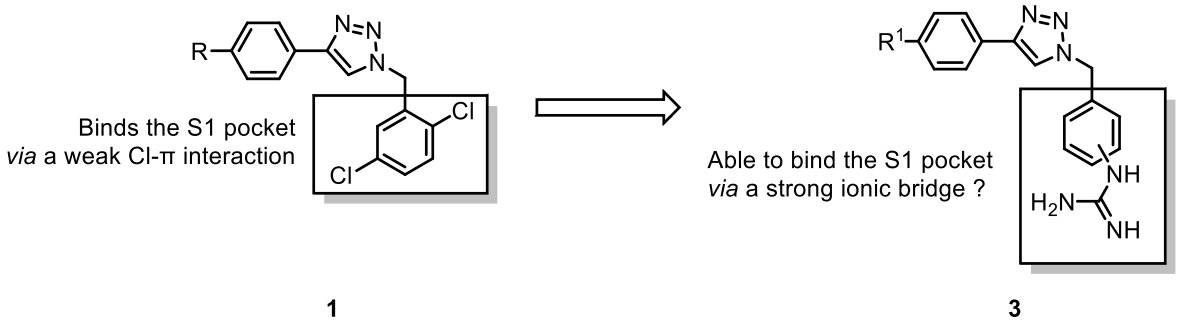

Scheme 3-1. Rational design towards first-generation collection 3 as potential inhibitors.

Indeed, the weak Cl-π interaction would be replaced by a strong H-bond-mediated, bridged ionic interaction between the guanidinium and Asp189 from the S1 pocket. The guanidinium moiety has been chosen over other cationic species, as guanidinium-bearing coumarin **RF1** has also shown an inhibitory activity on FXIIa in the low micromolar range The detailed structure of the six members that we will synthesize in this collection is represented (Scheme 3-2).

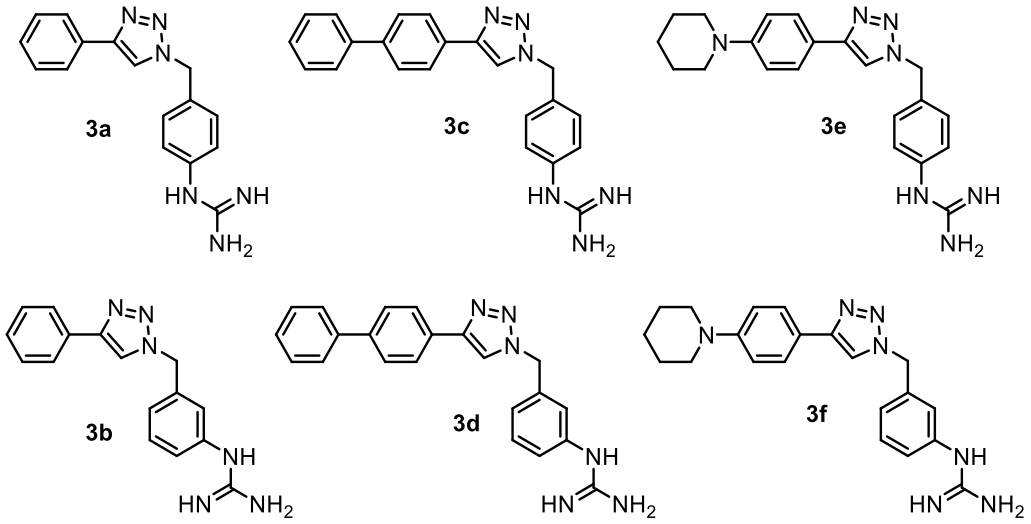

Scheme 3-2. Structure of the members of our first-generation collection 3.

The biphenyl and *N*-piperidylphenyl side-chains are taken from compounds **ChB49** and **50** and the phenyl side-chain will be used as a reference. *Para*- and *meta*-compounds will be both tested for comparison purposes.

The suggested retrosynthesis is identical for all members of this first-generation collection (Scheme 3-3). The guanidinium moiety will be synthesized *via* guanidylation of the corresponding anilines **4**. These molecules will arise from a Buchwald C-N Pd-catalyzed coupling of aromatic bromides **5**. The triazole linker will be obtained *via* a cycloaddition between alkynes **6** and azides **7**. Finally, these latter compounds will be synthesized by substitution of commercial benzyl bromides **8**.

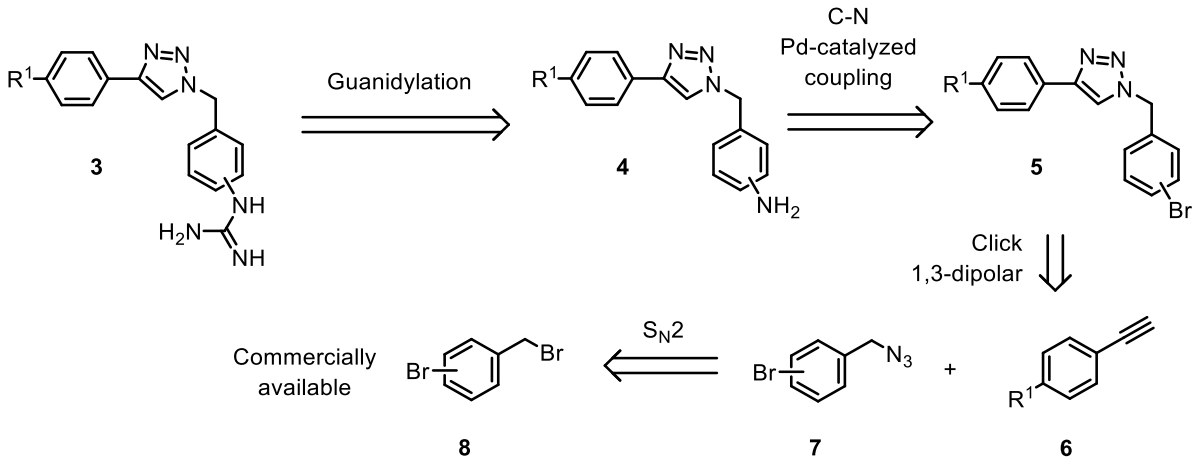

Scheme 3-3. Retrosynthesis of first-generation collection 3.

3.2.2. Synthesis

3.2.2.1. Synthesis of the Alkyne Precursors

Three alkynes will be used in this synthesis: phenylacetylene (**9**) and two direct derivatives **10** and **11**. The first two are commercially available for a reasonable price; **11** was synthesized as described (Scheme 3-4).

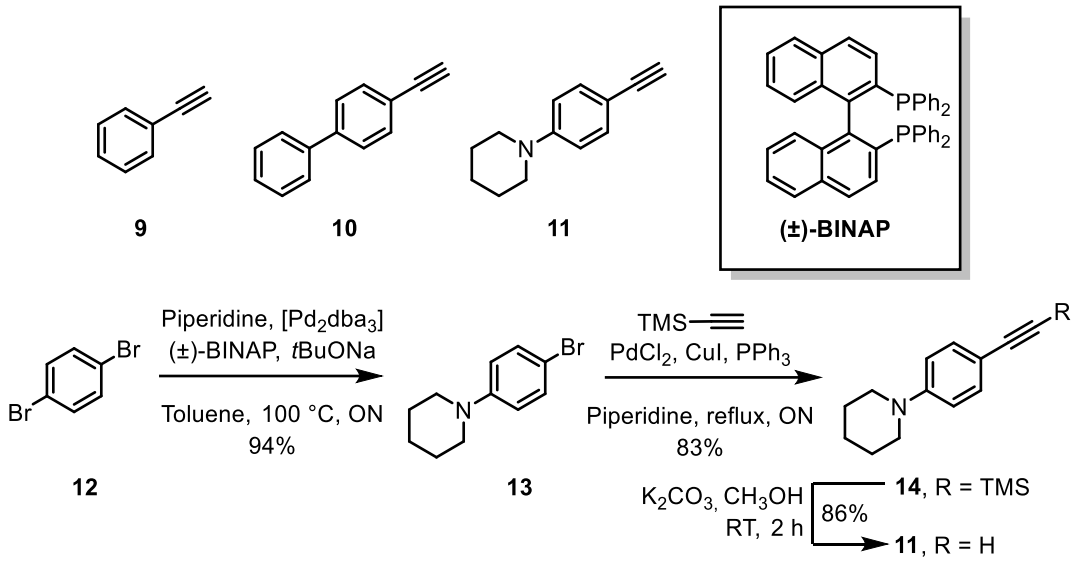

Scheme 3-4. Alkynes necessary for the synthesis of our target molecules and preparation of alkyne 11.

1,4-Dibromobenzene (**12)** underwent a Buchwald coupling with piperidine in the presence of [Pd_2dba_3], (±)-BINAP and *t*BuONa in toluene at 100 °C.[149] An excess of aryl bromide was used, yielding selectively monocoupling product **13**. Sonogashira coupling with TMS-acetylene catalyzed by $PdCl_2$, CuI and PPh_3 in refluxing piperidine afforded phenylacetylene **14**. Finally, treatment with K_2CO_3 in CH_3OH removed the TMS group to release terminal alkyne **11**.[150]

3.2.2.2. Synthesis of Guanidinium Salts

Para- and *meta*-bromobenzyl bromides (**15** and **16)** were substituted with NaN_3 in DMF at 80 °C to form the corresponding azides **17** and **18** (Scheme 3-5.[151] Warning, both inorganic and organic azides are potentially toxic and explosive, see experimental part for more details). These compounds reacted in a click [3+2] cycloaddition with acetylenes **9-11** in the presence of Amberlyst A21 impregnated with CuI (A21 · CuI), to yield to yield the six triazoles **5a-f** in good yields.[152] A21 · CuI was previously synthesized in-house by stirring CuI and Amberlyst 21 in CH_3CN.[152] When compatible, heterogeneous catalysis in the framework of click 1,3-dipolar cycloaddition is advantageous since no extraction is necessary.[152] The catalyst is simply filtered, and, in our cases, the desired products are recrystallized or precipitated directly from the crude mixture.

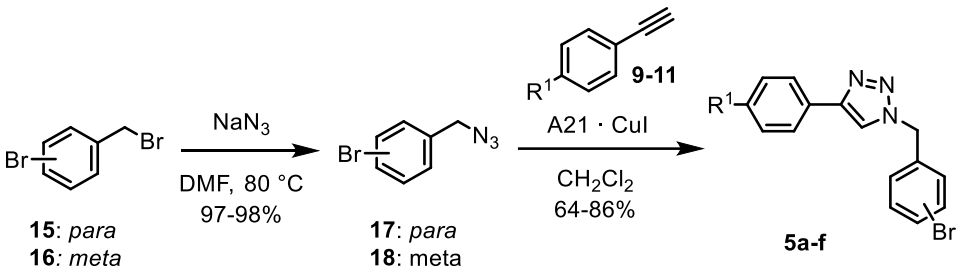

Scheme 3-5. Synthesis of triazoles 5a-f.

Compounds **5a-f** then underwent transformation into protected phenylguanidines (Scheme 3-6). Buchwald couplings were performed with acetophenone imine in the presence of [Pd_2dba_3], (±)-BINAP and *t*BuONa in toluene at 100 °C. The crude coupling products **19a-f** were not isolated but directly hydrolyzed in aqueous acidic THF to release anilines **4a-f**.[149] Guanidylation was performed with thiocarbamimidate **20** in DMF at 0 °C in the presence of $HgCl_2$ and Et_3N to yield protected guanidine **21a-f**.[153] The moderate yields for this latter reaction are explained by partial deprotection of one of the two Boc groups – probably because of the Lewis acidity of Hg^{II} –, leading to mono-Boc side-products **22a-f**.

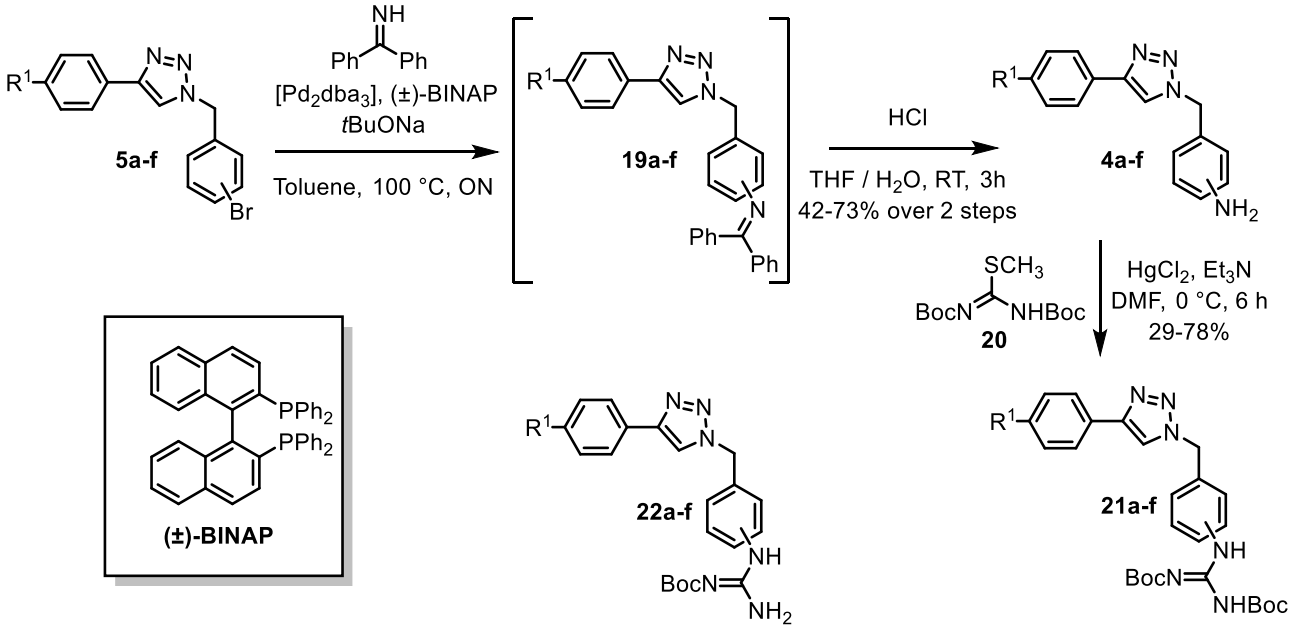

Scheme 3-6. Synthesis of protected phenylguanidines 21a-f.

Even though it is commercially available, thiocarbamimidate **20** could be obtained on a multigram scale in two steps in the laboratory (Scheme 3-7).[154] Thiourea (**23**) was methylated with CH_3I in refluxing EtOH to yield thiouronium **24**. Deprotonation with NaOH followed by treatment with Boc_2O in 1,4-dioxane and H_2O afforded thiocarbamimidate **20**.

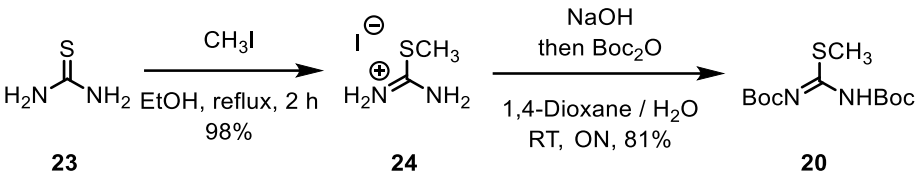

Scheme 3-7. Synthesis of thiocarbamimididate 20.

Boc groups are frequently removed using TFA / CH_2Cl_2,[155] and the deprotected guanidine is usually isolated as the TFA salt. However, the trifluoroacetate anion is known to be cytotoxic even at nanomolar concentrations and thus should be avoided in *in* and ex vivo studies.[156] Even though we will only perform in vitro studies, we first tried to obtain the HCl salt of our guanidines.

Table 3-1. Attempts at synthesizing guanidine 3a.

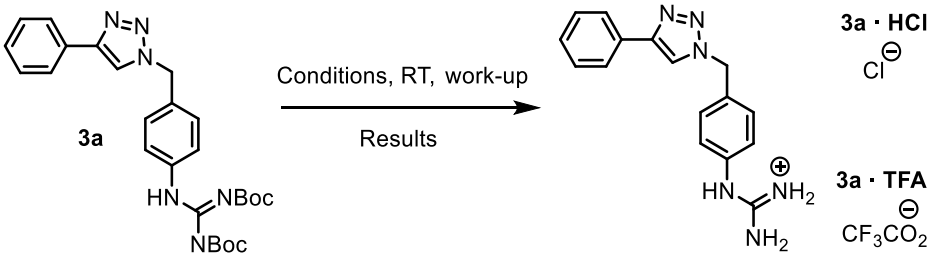

N°	Conditions	Work-up	Conv. into 3a	Arisen problem
a	$HCl_{(aq.)}$, 1,4-Dioxane, 2 d	None	Partial	Partial hydrolysis
b	$HCl_{(dry)}$, 1,4-Dioxane, ON	None	Quant.	Residual 1,4-dioxane
b	$HCl_{(dry)}$, 1,4-Dioxane, ON	Trituration with Et_2O	Quant.	Residual Et_2O
b	$SnCl_4$, AcOEt, 3 h	Precipitation in CH_3OH/Et_2O	N.A.	Complex mixture
e	TFA / CH_2Cl_2 1:1, 2 h	Trituration with Et_2O	Quant.	Residual Et_2O
f	TFA / CH_2Cl_2 1:1, 2 h	Trituration with pentane	Quant.	None.

Removal of the Boc group from protected guanidine **3a** required several attempts before obtaining cleanly the desired product (Table 3-1). The reaction in an aqueous HCl solution of 1,4-dioxane was slow and led to partial hydrolysis of the guanidine moiety (entry a). To avoid this problem, a dry solution of HCl in 1,4-dioxane was used instead and led cleanly to the desired product (entry b). However, and as determined by ^{1}H NMR, 1,4-dioxane remained in the sample event after prolonged heating under reduced pressure (< 10 mbar, 50 °C, 48h). Trituration with Et_2O removed the 1,4-dioxane and replaced it with Et_2O, which, once trapped in the sample, is surprisingly as difficult to remove as 1,4-dioxane (entry c).

The ability of guanidinium moieties to form strong H-bonds, both with 1,4-dioxane and Et_2O, may explain this apparent affinity. Other acids than HCl were then envisaged. High-yielding deprotection of Boc-guanidines is described using $SnCl_4$ in AcOEt at RT.[157] In our case, using this protocol, the reaction was sluggish, (entry d) and the crude product was complex as determined by ^1H NMR analysis.

Faced with these repeated failures, we decided to come back to the classical TFA / CH_2Cl_2 deprotection conditions. The reaction was fast and quantitative, leading however to a metastable viscous oil, difficult to weigh precisely for in vitro testing. Trituration in Et_2O solidified the oil into a white powder but led once again to trapping of the solvent into the sample. (entry e).

Trituration in pentane was slower at solidifying the sample, and cycles of evaporation of the solvent / trituration were needed to obtain a full solidification, but eventually led to the same white powder, finally free from any etherated solvent (entry f).

Eventually, all protected guanidines synthesized so far **21a-f** underwent this protocol to quantitatively yield guanidines **3a-f · TFA**. (Scheme 3-8).

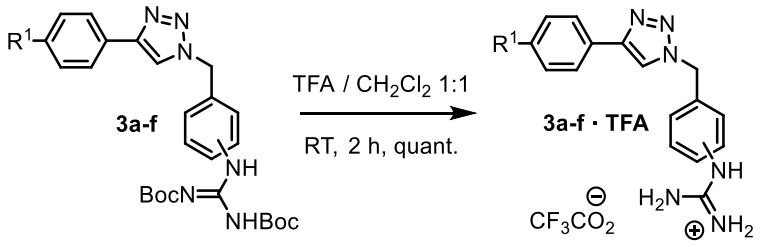

Scheme 3-8. Synthesis of guanidines 3a-f.

3.2.3. FXIIf inhibition Assays

3.2.3.1. Basics of the assay

Because of its tendency to adsorb on surfaces, FXIIa is unpractical for in vitro uses. However, our group has proven that inhibition assays on FXIIa and on FXIIf give near-identical results. For practical reasons, all inhibitions assays in this thesis were performed on FXIIf.

The inhibitory potency of our compounds on FXIIf was measured through kinetic studies. The principle of the utilized protocol is described (Scheme 3-9). The hydrolysis of commercial D-Pro-Phe-Arg-pNA · 2HCl (also referred to as **S-2302**) is catalyzed by FXIIf in an aqueous buffer stabilized at pH 7.4 to form side-product **25** and *para*-nitroaniline (pNA) **26**. The latter absorbs light in the visible spectrum and the reaction can thus be followed using spectrophotometry. The percentage of inhibition is extrapolated from the initial reaction rates, performed with and without test compound. The practical details can be found in the experimental section.

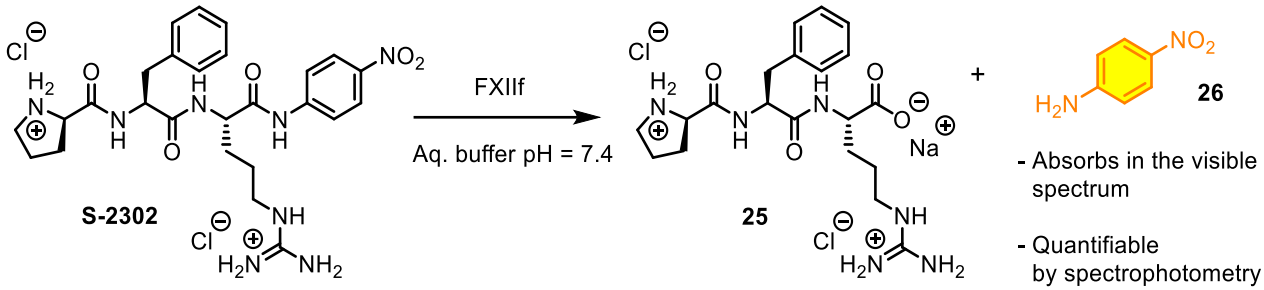

Scheme 3-9. Reaction taking place in the inhibition assay of FXIIf.

3.2.3.2. FXIIf Inhibition Assay of the First-Generation Collection

To be able to detect weak inhibitors, we set the screening concentration at 500 µM. The structure of the molecules and their inhibition percentages on FXIIf at that concentration are reported (Table 3-2). Our first-generation collection displays only weak inhibitory activity toward FXIIf. For compounds **3c**, **3d** and **3e**, precipitation occurred before any significant inhibitory activity was detected. The percentages of inhibition at 500 µM for compounds **3a**, **3d** and **3e**, soluble are very low (<50%) and similar to that of plain benzamidine (Table 3-2).

Table 3-2. FXIIf inhibition percentages at 500 µm for compounds 3a-f · TFA.

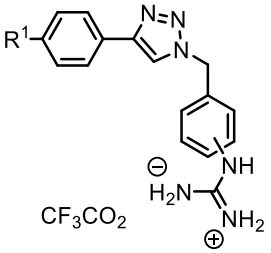

Compound	R^1	*para/meta*	% inhibition
3a		*para*	7%
3b		*meta*	21%
3c	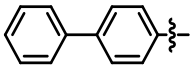	*para*	Precipitation
3d		*meta*	Precipitation
3e	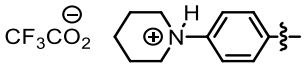	*para*	Precipitation
3f		*meta*	44%
Benzamidine · HCl	/	/	27%

These unexpected low activities and precipitations rose doubt about our hit compounds **ChB49** and **ChB50** and led us to think that their inhibitory activities were false-positive results. Moreover, the fact that plain benzamidine was almost as active as our compounds suggested that benzamidine could be a better starting scaffold than phenylguanidine. Both these hypotheses were investigated.

3.2.4. 2,5-Dichlorobenzyl Triazoles: false-positive results

The IC_{50} (µM or nM) of a compound for a specific enzyme is extrapolated from its dose-inhibition curve, which follows the Hill equation [158,159]:

$$\%inh = 100 - \frac{100}{1+\left(\frac{C_I}{IC_{50}}\right)^n}$$

where %inh is the percentage of inhibition (%), C_I the total concentration of inhibitor (µM or nM), and n is the Hill coefficient. The greater the Hill coefficient, the steeper the dose-response curve. For competitive inhibitors, the Hill coefficient is by definition equal to 1, also called a standard slope. In hit discovery programs, a Hill coefficient superior to 1.5 may suggest that the compound precipitates or forms colloids at higher concentrations, sequestrating the enzymes in a non-specific manner.[160]

For the extrapolation of the IC_{50} of the 2,5-dichlorobenzyl triazoles, which were expected to be competitive inhibitors, our group used a linear regression forcing a standard slope, potentially preventing us from detecting false-positive results due to precipitation/colloid formation. The FXIIf inhibition assay of our first-generation collection supports the fact that the activities of compounds **ChB49** and **ChB50** might be artifactual. We wanted to verify this hypothesis experimentally. The dose-response curve of **ChB49** on FXIIf as performed at the time is shown (Figure 3-1). The linear regression has a much gentler slope than what the scatter plot suggests, indicating that the forcing of a standard slope was inappropriate.

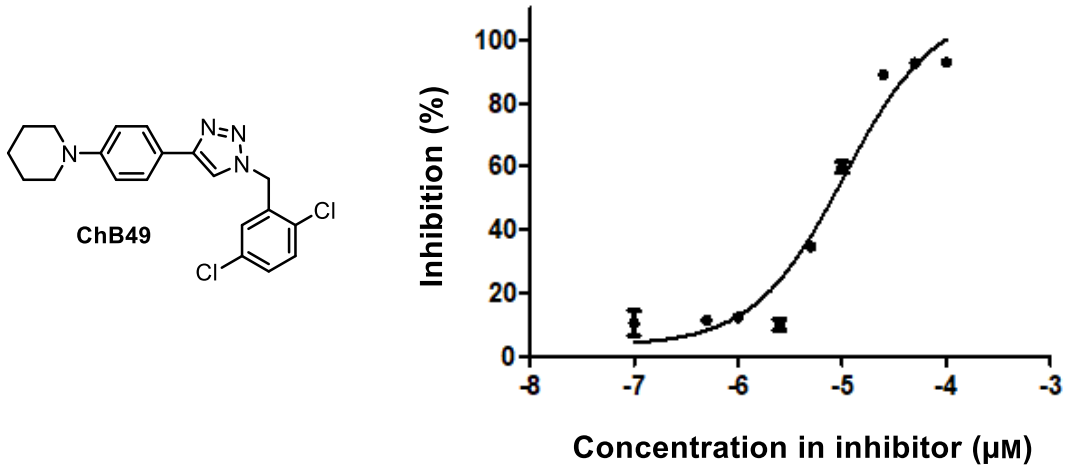

Figure 3-1. Dose-inhibition curve: compound ChB49 and FXIIf.

In parallel, we performed a dose-response experiment on the most active member of our first-generation collection, compound **3f,** which can be seen as the *meta*-amidinio derivative of compound **ChB49** (Figure 3-2).

The estimated Hill coefficient is equal to 3.054, strongly suggesting that the observed inhibition is due to colloid formation or precipitation. If compound **3f**, which is positively charged at pH 7.4, is associated to insolubility, it is highly likely that neutral compound **ChB49** is even more subject to this problem. Together, these experiments suggest that the apparent inhibitory activities of **ChB49** and **ChB50** are artifactual and are associated with colloid formation-mediated inhibition.

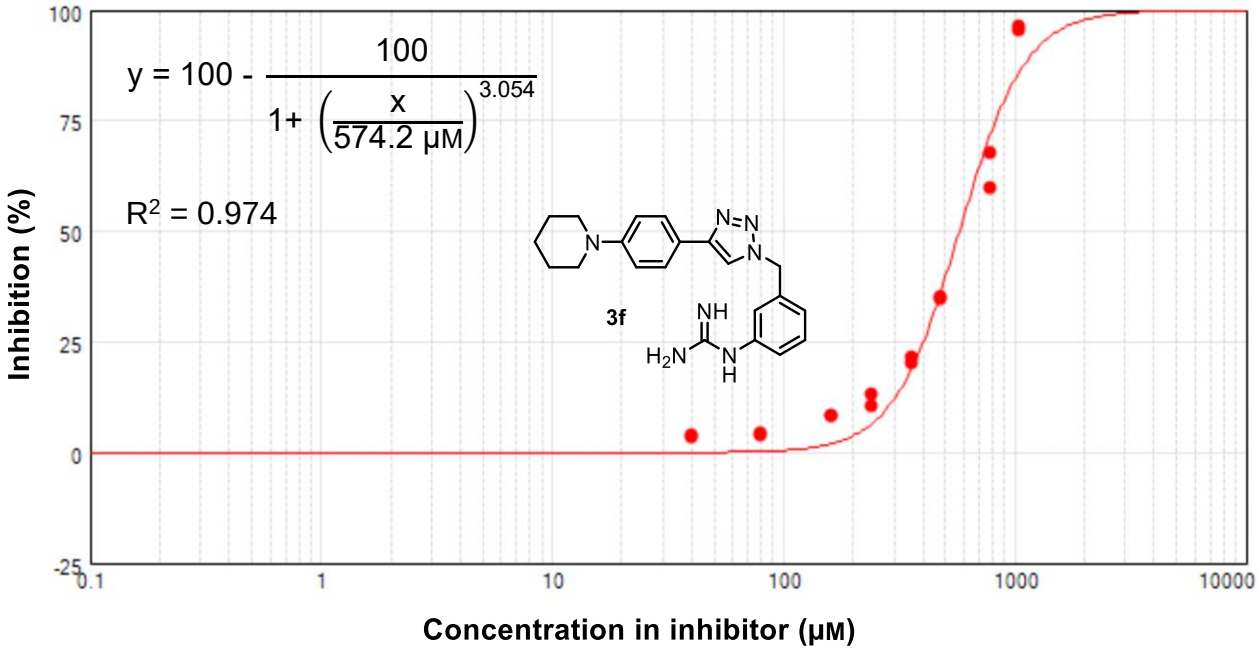

Figure 3-2. Dose-inhibition curve: compound 3f and FXIIf.

3.2.5. Amidine VS Guanidine

3.2.5.1. In vitro experiments

To check experimentally if benzamidines are better at inhibiting FXIIf, we determined the inhibitory potency of benzamidine (**2**) and 4-aminobenzamidine (**27**), and their guanidine equivalents phenylguanidine (**28**) and 4-aminophenylguanidine (**29**) (Scheme 3-10). The latter compound was synthesized in-house.

p-Phenylenediamine (**30**) reacted with $(Boc)_2O$ in the presence of K_2CO_3 in a wet mixture of THF and DMF to provide monoprotected compound **31**. The guanidylation of the remaining amine with commercial agent **32** in THF afforded protected guanidine **33**.[161] Eventually, the Boc groups were removed with TFA in CH_2Cl_2 to provide the TFA salt of 4-aminophenylguanidine (**29 · 2TFA**).

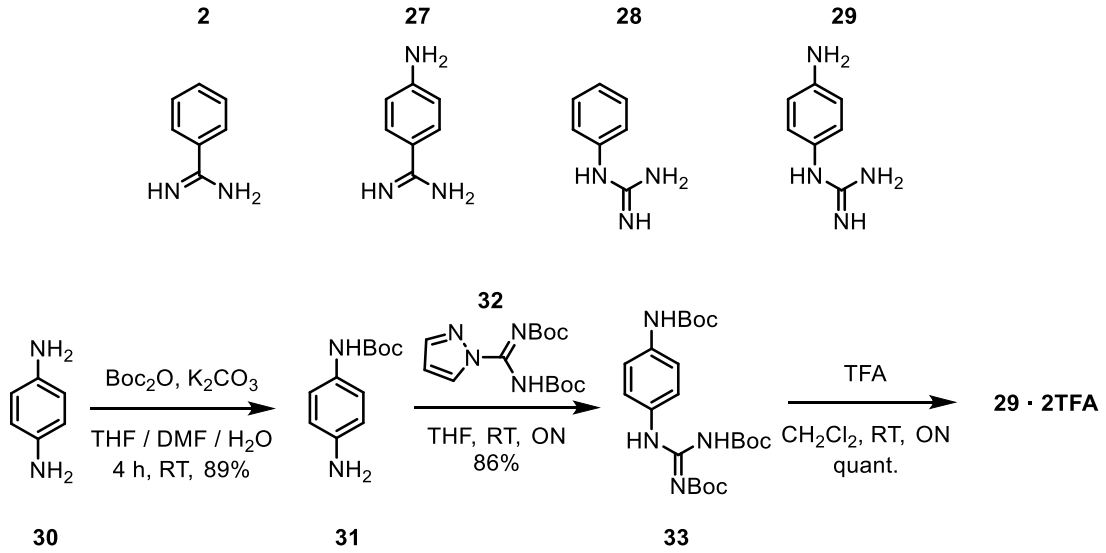

Scheme 3-10. Structure of the studied amidines and guanidines and synthesis of 4-ammoniophenylguanidinium trifluoroacetate 29.

The results of the screening performed at an inhibitor concentration of 3 mM are summarized (Table 3-3) and suggest indeed that guanidines are less potent FXIIf inhibitors than their amidine counterparts.

Table 3-3. FXIIf inhibition percentages at 3 mM for compounds 2 and 27-29.

Compound	Structure	Salt form	% inhibition
2	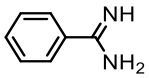	HCl	57%
27	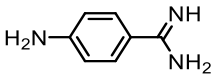	2 HCl	88%
28	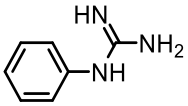	HCl	4%
29	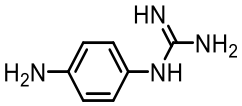	2 TFA	16%

3.2.5.2. In silico experiments

By the time we finished the synthesis of our six compounds, the crystal structure of FXIIf had been published, allowing us to further verify this hypothesis in silico using the Glide program (Grid-based Ligand Docking with Energetics).[162]

Glide generates hundreds of docking poses for a given ligand and classes them progressively by evaluating their interaction with the active site of the enzyme using hierarchical filters.[163,164]

The first filters test the spatial fit between the ligand and the enzyme and examine the ligand-receptor interactions using an empirical scoring function, ChemScore. The next filters aim at evaluating and at further minimizing the interaction energy between the ligand and the enzyme as calculated by the force field OPLS-AA (Optimized Potentials for Liquid Simulations – All Atoms). Finally, a GlideScore is assigned to the energy-minimized poses, based on the binding enthalpic parameters as calculated by OPLS-AA, with added bonuses and penalties for (un)favorable entropic parameters. The extra-precision (XP) mode uses more computational resources to generate more precise poses and was designed to screen out false positives.[165] All the docking poses discussed in this thesis were generated using the XP mode and, unless differently specified, were determined as having the lowest GlideScore.

Compounds **2** and **27-29** were docked within the active site of FXIIf using the XP mode of Glide and the poses with the lowest GlideScore are shown (Figure 3-3).

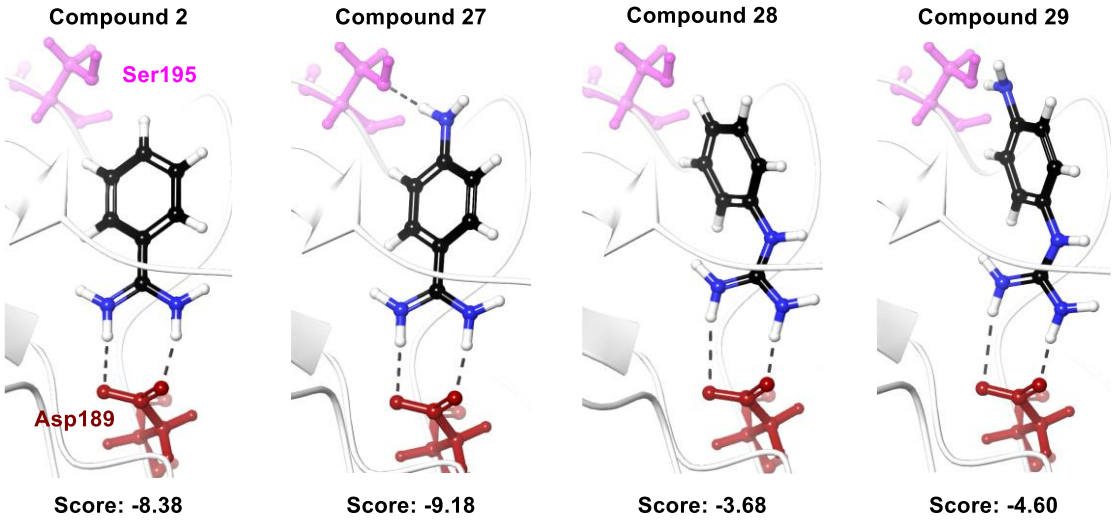

Figure 3-3. Molecular docking of compounds 2 and 27-29 in the S1 pocket of FXIIf. Black dotted lines: H-bonds.

All compounds were confirmed to fit the S1 pocket by interacting with Asp189 *via* an H-bond-mediated ionic bridge. Moreover, the amino group of compound **27** seems to interact *via* H-bonding with the hydroxyl group of Ser195. This is not the case in compound **29** because of an unfavorable orientation.

A comparison between the docking poses of compound **27** and **29** is realized (Figure 3-4). One of the two N-H···O=C bond was significantly shorter in the case of amidinium **27** than in the case of the guanidinium **29** (2.76 VS 2.11 Å). This observation suggests a stronger interaction with the enzyme and thus a stronger binding affinity.

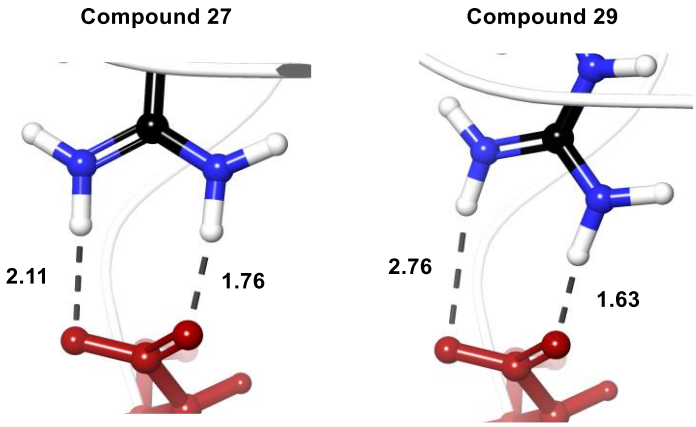

Figure 3-4. Comparison on the interaction of compounds 27 and 29 with Asp189. Distance are in Å.

Amidinium compounds are more acidic than their guanidinium counterparts and thus better H-bond donors, which could explain why it binds tighter the aspartate. Moreover, the positive charge is less delocalized in an amidinium than in a guanidinium, improving the strength of the ionic bonds.

The lesser FXIIf inhibitory activity of guanidines compared to amidines drove the development of both following subprojects, performed in parallel: the synthesis of our second-generation collection, described in the next subsection 3.3, and the synthesis of a peptidomimetic analog model, described in subsection 3.4.

3.3. Second-Generation Collection

3.3.1. Design and Retrosynthesis

Because their design was based on false-positive results, the compounds of our first-generation series were weak inhibitors and are thought to form colloids in aqueous media, probably due to their highly hydrophobic sidechains. Moreover, these compounds featured phenylguanidines, which we have proven to be poor at inhibiting FXIIa. In order to further check if the triazole scaffold was worth considering, we designed the second-generation collection, whose compounds should be more potent and more soluble (Scheme 3-11).

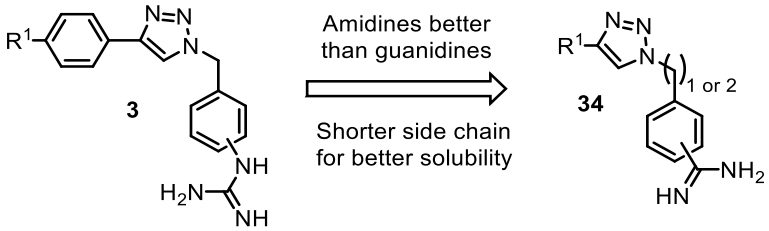

Scheme 3-11. Rationale of the evolution of our first-generation collection 3 into second-generation collection 34 as potential inhibitors of FXIIf.

The members of the second-generation collection that we intend to synthesize are represented (Scheme 3-12). Phenylguanidines are replaced by benzamidines to improve the general inhibitory activity. The polyaromatic chain is reduced to a phenyl group or completely removed, in order to avoid insolubility and formation of colloids.

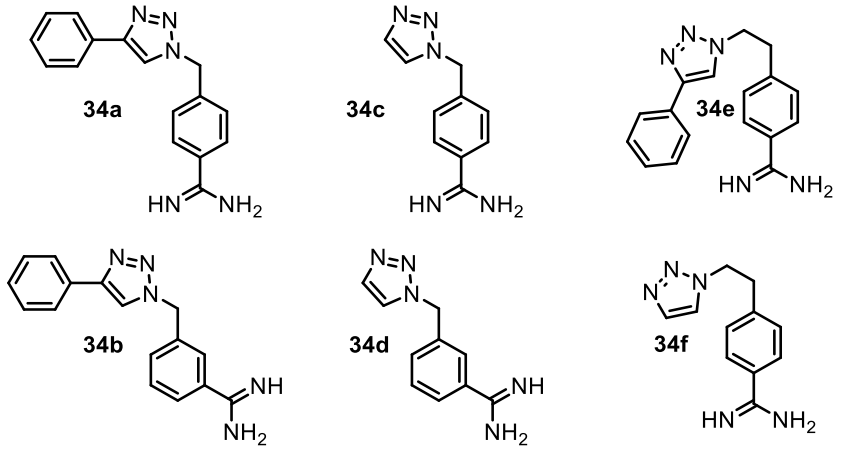

Scheme 3-12. Structure of the members of our second-generation collection.

Furthermore, in addition to methylene, ethylene linkers between the triazole and the benzamidine group are also envisaged to introduce more flexibility and adaptability. *Para*- and *meta*-benzamidines are both considered for comparison purposes.

The target compounds were docked within the active site of FXIIf using the XP mode of Glide and the poses with the lowest GlideScore are shown (Figure 3-5). As expected, all benzamidine moieties dock within the S1 pocket by interacting with Asp189. However, the overall docking positions and scores vary greatly depending on the benzamidine substitution pattern and on the sidechain.

The phenyl group of compound **34a** is ideally positioned to form a parallel-displaced π-π stacking with His57, which can explain its promising docking score, the second-lowest of the collection. In contrast, the *meta* counterpart, compound **34b**, does not have the right geometry and is only able to form a weak H-bond between the benzylic hydrogen and the oxygen of Ser195.

Without the phenyl, compounds do not seem to interact much with the enzyme. Methylene compounds **34c**-**d** interact mainly *via* their amidinium moiety and, even though compound 34C is involved in two weak π-π stackings, they have a docking score similar to that of plain benzamidine (-8.38). On the other side, compound **34f** is involved in a H-bond between an aromatic CH and the oxygen of Ser195. This stabilizing interaction is largely counterbalanced by a steric clash between the triazole core and Tyr99, resulting in a high docking score.

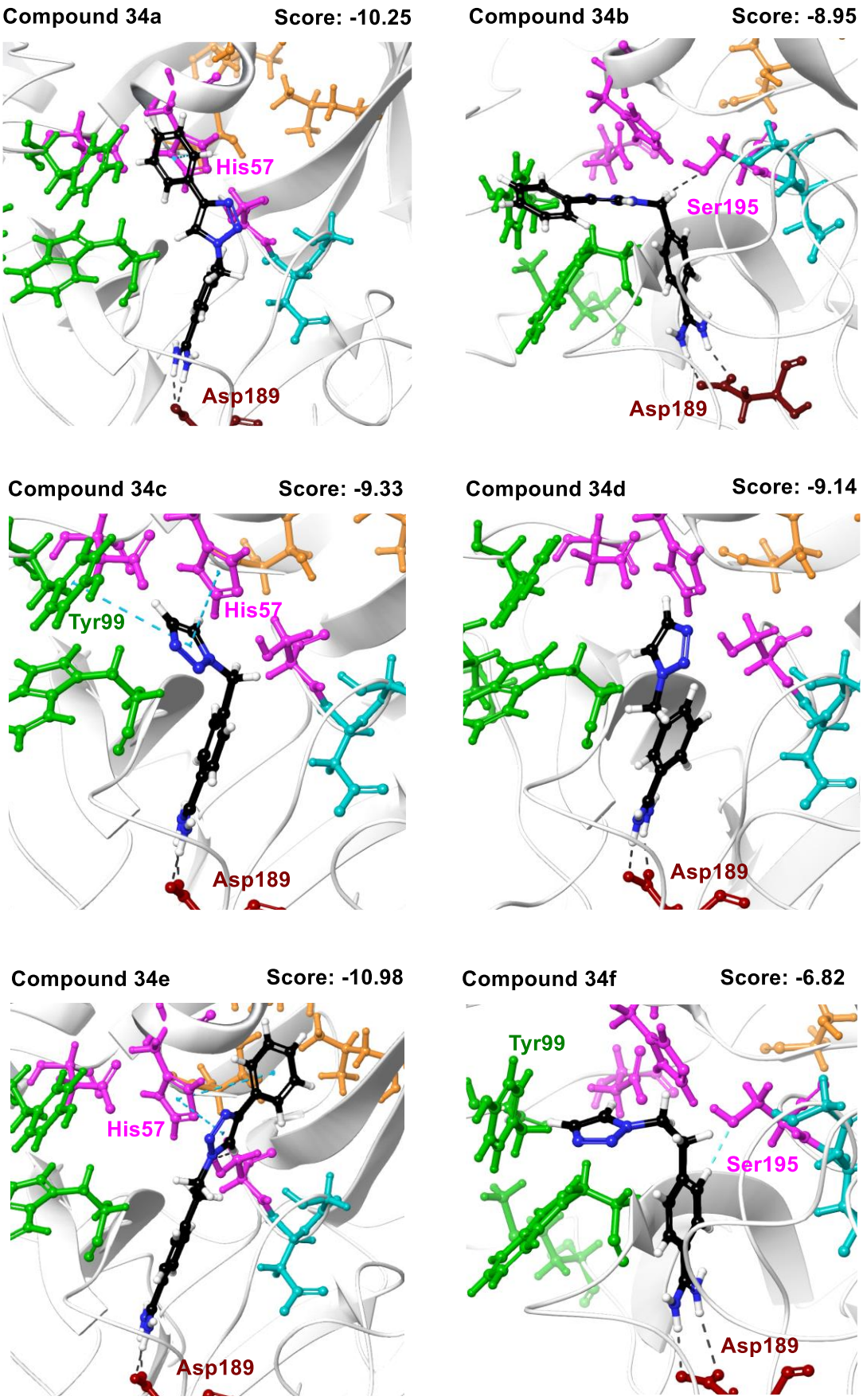

Figure 3-5. Molecular docking of compounds 34a-f in the binding site of FXIIf. Brown: S1 pocket. Pink: catalytic triad. Turquoise: oxyanion hole. Green: S3/4 pocket. Orange: H1 pocket. Black dotted lines: H-bonds. Blue dotted lines: π-π stackings.

Finally, compound **34e**, featuring the lowest docking score of the collection, stands out as the best candidate: it is involved in two π-π stackings with His57 and stacks its phenyl moiety within the apolar pocket H1. Overall, the results of the molecular docking study are encouraging, as most compounds scored better than plain benzamidine.

The suggested retrosynthesis is discussed below (Scheme 3-13). For all members of this second-generation, the amidine moiety will be synthesized *via* a Pinner-like reaction of the corresponding nitriles **35**.

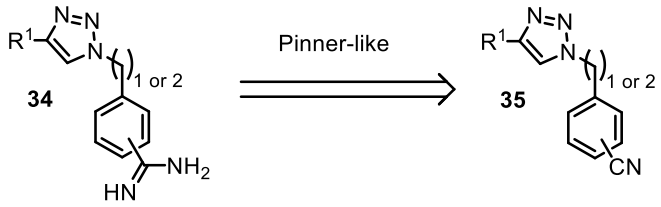

Scheme 3-13. Retrosynthesis of our second-generation collection.

The retrosynthesis of these nitriles differs according to the availability of the starting materials. Benzonitriles **35a-b** and **e-f** will be obtained from a C-CN coupling from the corresponding bromides **36a-b** and **e-f** (Scheme 3-14).

As was the case for the first-generation collection, the triazole linker of such compounds will be obtained *via* a cycloaddition between alkynes **38** and azides **37**. Finally, these latter compounds will be synthesized by substitution of commercial bromides **39**.

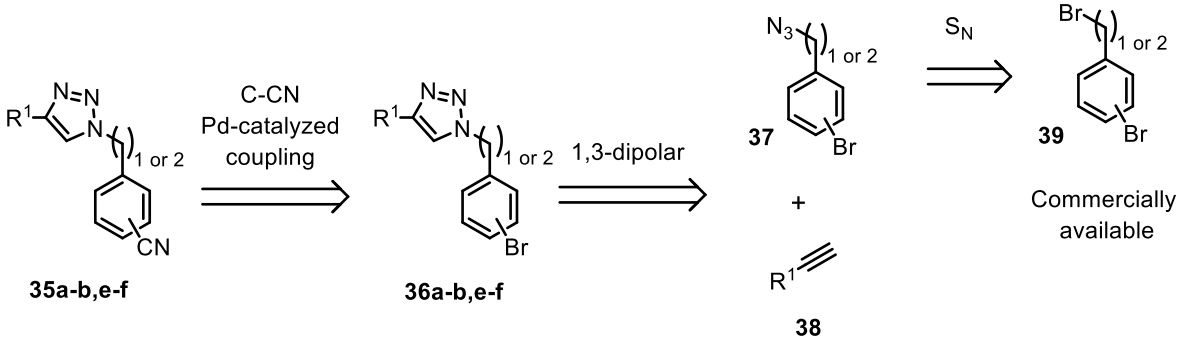

Scheme 3-14. Retrosynthesis of *para*-substituted benzonitriles 35a-b and e-f

On the other side, benzonitriles **35c-d** will be obtained directly *via* a cycloaddition between alkynes **38** and cyanobenzyl azides **40** (Scheme 3-15). The latter compound will be synthesized by substitution of commercial cyanobenzyl bromides **41**.

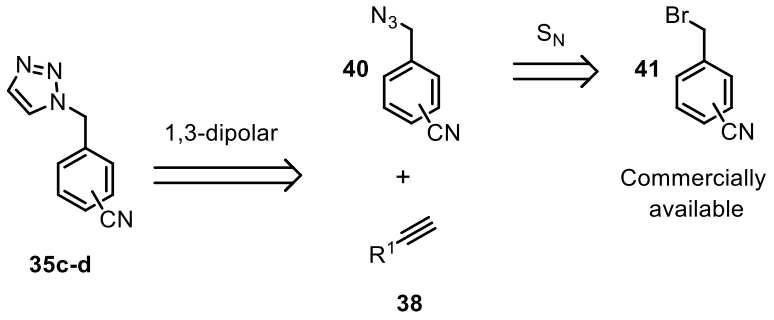

Scheme 3-15. Retrosynthesis of meta-substituted benzonitriles 35c-d.

3.3.2. Synthesis

3.3.2.1. Synthesis of the Benzonitriles 35a-b and e-f

The synthesis of the needed benzonitriles was performed. Bromides **15**, **16** and **42** were substituted with NaN_3 in DMF at 80 °C to form the corresponding azides **17** and **43** (Scheme 3-16.[151] Warning, both inorganic and organic azides are potentially toxic and explosive, see experimental part for more details). These compounds reacted in a click 1,3-dipolar cycloaddition with phenylacetylene to yield triazoles **36a**, **b** and **e**. In parallel, azide **43** reacted in the same conditions with TMS-acetylene yield silane **44**.[152] The TMS group was then removed by TBAF in THF to afford triazole **36f** .

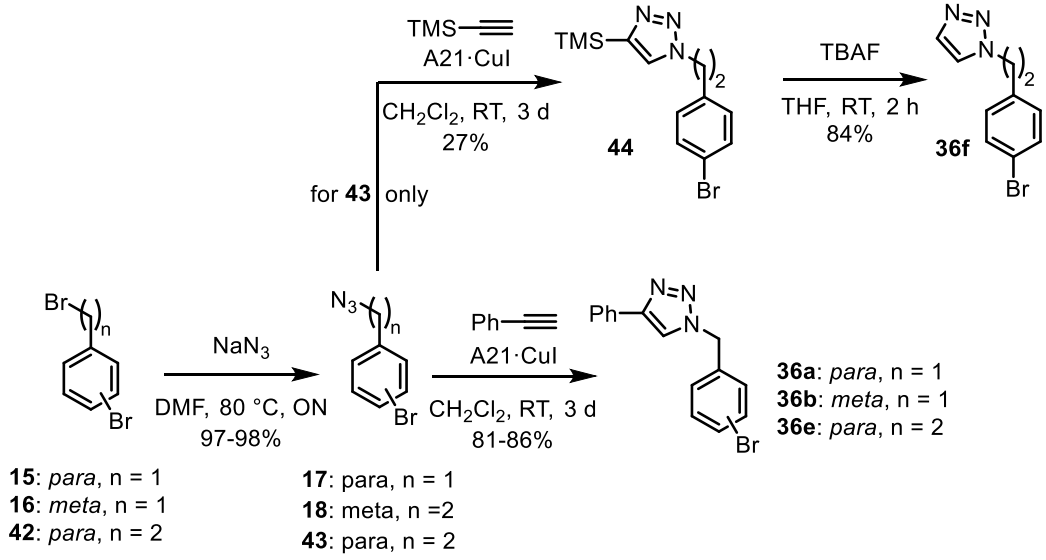

Scheme 3-16. Synthesis of *para*-substituted bromobenzenes 36a-b and e-f.

Finally, the four aryl bromides **36a-b** and **e-f** underwent cyanation with $K_4[Fe(CN)_6]$ in DMAc at 120 °C in the presence of $Pd(OAc)_2$ and Na_2CO_3 to yield nitriles **35a-b** and **e-f** (Scheme 3-17).[166]

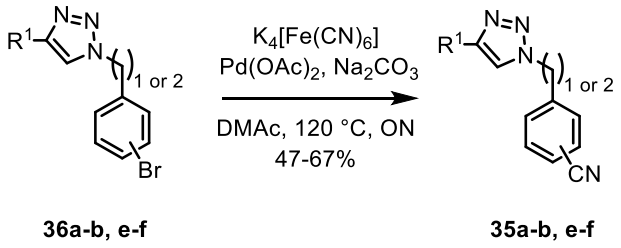

36a-b, e-f **35a-b, e-f**

Scheme 3-17. Synthesis of substituted benzonitriles 35a-b and e-f.

3.3.2.2. Synthesis of the Benzonitriles 35c-d

The synthesis of the other needed benzonitriles was performed (Scheme 3-18). Cyanobenzyl bromides **41c-d** were substituted with NaN_3 in a mixture of water and acetone at RT to form the corresponding azides **40c-d**.[167]

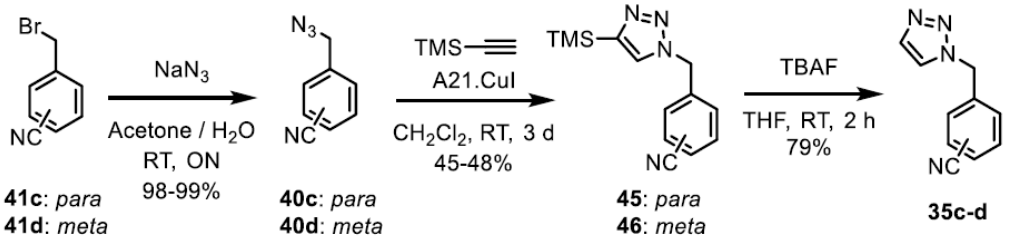

Scheme 3-18. Synthesis of benzonitriles 35c-d

These compounds reacted in a click 1,3-dipolar cycloaddition with TMS acetylene in the presence of A21·CuI to yield silanes **45** and **46**.[152] The TMS group was then removed by TBAF in THF to lead to triazoles **35c-d.**

3.3.2.3. Synthesis of the Target Benzamidines

The protocol for amidine formation was first tested on previously synthesized molecule **35a** (Scheme 3-19). The nucleophilic addition of NH_2OH onto the cyano moiety in refluxing EtOH afforded hydroxyamidine **47**.[168,169] The acetylation of the hydroxyl group was achieved with Ac_2O in AcOH to yield compound **48**. The cleavage of the N-O bond by hydrogenation with H_2 in the presence of $Pd(OH)_2$ in AcOH led to amidinium acetate **34a · AcOH**.[168,169]

None of these intermediates could be purified properly, whether by column chromatography or recrystallization, because of their low solubility in common organic solvents. A reaction with $(Boc)_2O$ in the presence of Et_3N in CH_3OH at 50 °C afforded derivative **49** (Scheme 3-19),[170] much more soluble and suitable for isolation by column chromatography. The Boc group can then be removed using TFA / CH_2Cl_2 to obtain pure amidine **34a · TFA** (Scheme 3-19).

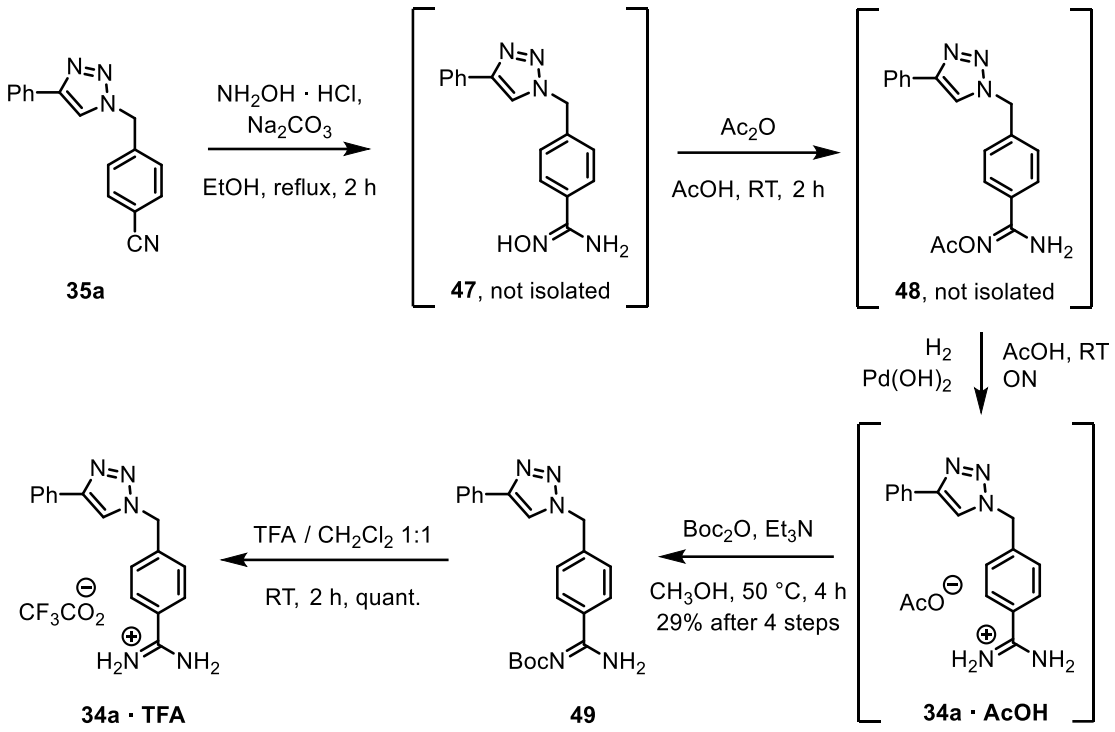

Scheme 3-19. Synthesis of amidinium trifluoroacetate 34a · TFA.

Even though this synthetic pathway works, its lengthiness and its practical tediousness, i.e. the insolubility of most reagents and products, inspired us to explore improved conditions which were used to perform these reactions routinely for the synthesis of our collection of six amidines.

The nucleophilic addition of hydroxylamine, generated in situ from its HCl salt and Et_3N, onto the cyano moiety in refluxing ethanol to afford the corresponding hydroxyamidines (Scheme 3-20Scheme 3-20. Synthesis of amidines 34e-f · PivOH.).[168,169] We used Et_3N instead of Na_2CO_3 because it is liquid and soluble in EtOH even when protonated. When possible, the insoluble hydroxyamidines are then more easily isolated by filtration, and not contaminated by carbonate salts.

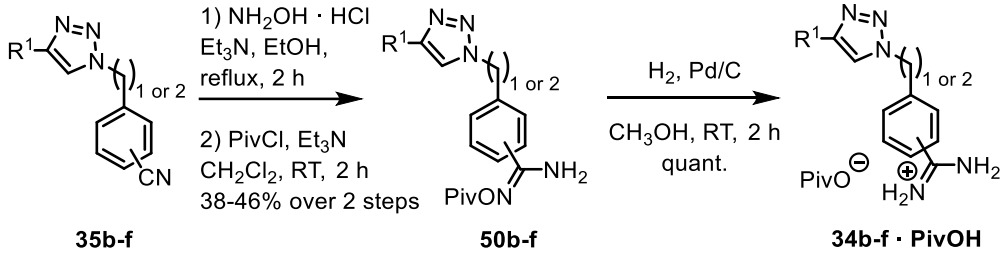

Scheme 3-20. Synthesis of amidines 34e-f · PivOH.

Pivaloylation of the hydroxyl group was achieved with PivCl and Et_3N in CH_2Cl_2 (Scheme 3-20).[171] The Piv group was selected in order to improve the solubility of the resulting acyloxyamidines **50e-f**. All derivatives were freely soluble in CH_3OH and could be purified by column chromatography.

Hydrogenation catalyzed by Pd/C in CH_3OH quantitatively afforded the desired amidinium pivalates **34e-f · PivOH**. Acid and the more active catalyst $Pd(OH)_2$ are actually not necessary in our case for this transformation.

3.3.3. FXIIf Inhibition Assays

The compounds were tested using the previously described inhibition assay. No precipitation was observed and the experimental Hill coefficient of the dose-response curve of our most potent compound, **34e**, was equal to 1.284, suggesting that we do not have solid- or colloid-mediated inhibition (Figure 3-6)

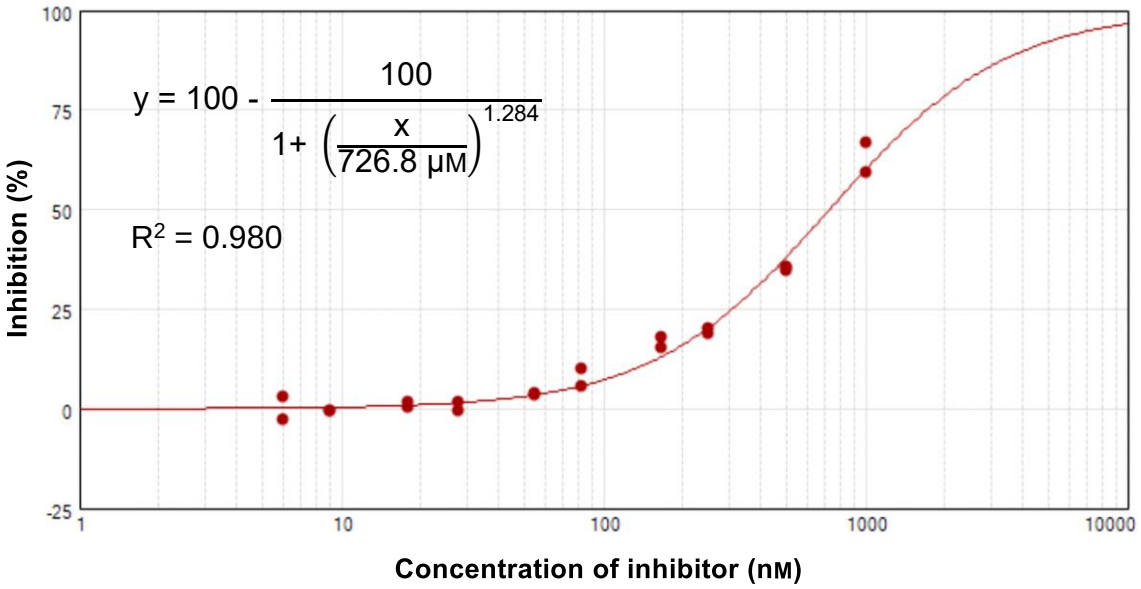

Figure 3-6. Dose-inhibition curve: compound 34f and FXIIf.

The structure of the molecules and their inhibition percentage on FXIIf at 500 µM are reported (Table 3-4, next page). The *para/meta*-orientation of the benzamidine has no influence on the intensity of the inhibition. As expected by molecular docking, compounds **34a-b** are better inhibitors than their phenyl-free counterparts and compound **34f** is the most potent compound of the collection. However, our compounds are similar in potency to plain benzamidine **2**, suggesting that the triazole-based side chain in these molecules is non-essential for inhibition.

3.4. Synthesis of a Peptidomimetic Inhibitor Model

3.4.1. Design and Retrosynthesis

In parallel to the synthesis of our second-generation collection and in the framework of a Master thesis in our group, we designed *de novo* a potential collection of inhibitors based exclusively on the 3D-structure of FXIIf.

Table 3-4. FXIIf inhibition percentages at 500 µm for compounds 34a-f.

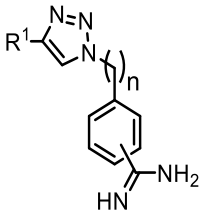

Compound	Salt form	n	R^1	*para/meta*	% inhibition
34a	TFA	1	Ph	*para*	18%
34b	PivOH			*meta*	19%
34c	PivOH	1	H	*para*	10%
34d				*meta*	11%
34e	PivOH	2	Ph	*para*	35%
34f			H		24%
Benzamidine	HCl	/	/	/	27%

The active site of FXIIf is surrounded by three pockets and we wanted to design ligands which would interact with each of these pockets. The collection of compounds **51** (Scheme 3-21), whose simplest member is compound **51a**, was hypothesized to be adequate, based on the XP Glide molecular docking of the latter. This collection is a bioisosteric replacement of tetrahedral intermediate **52** (Scheme 3-21), present in the active site of FXIIf during the proteolysis of FXI, and can thus be considered as peptidomimetic.

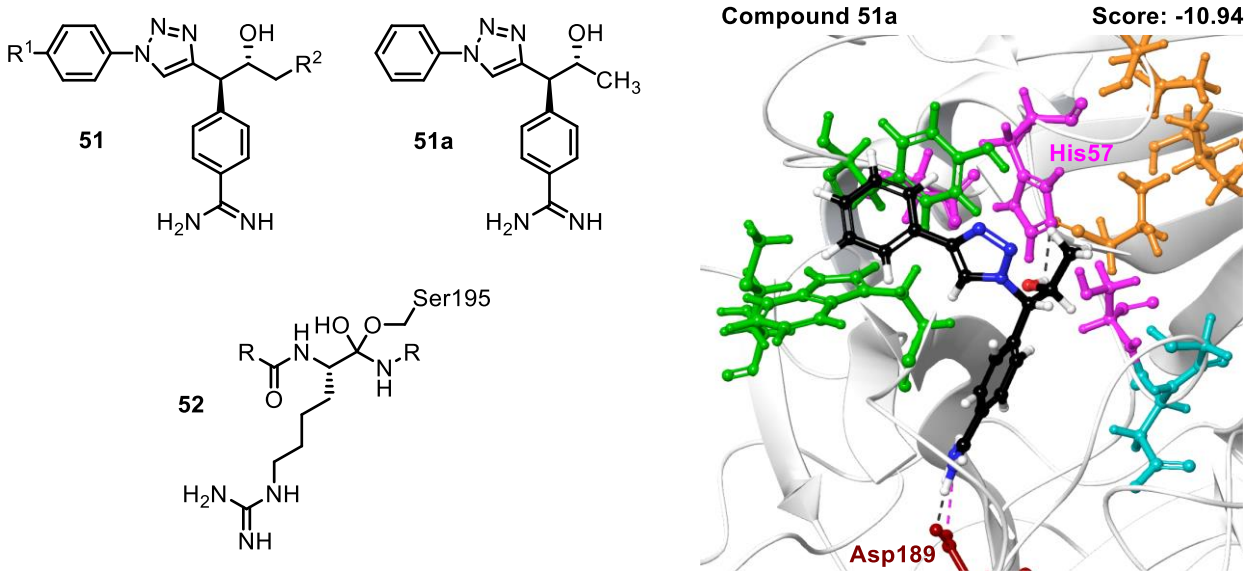

Scheme 3-21. Structure of collection 51 and of its simplest member 51a, of the tetrahedral intermediate 52 involved in the active site of FXIIa, and docking of compound 51a within the binding site of FXIIf. Brown: S1 pocket. Pink: catalytic triad. Turquoise: oxyanion hole. Green: S3/4 pocket. Orange: H1 pocket. Black dotted lines: H-bonds. Pink dotted lines: ionic bridges.

The benzamidine moiety is a bioisostere of the lateral chain of arginine and binds the S1 pocket by interaction of the amidinium with Asp189 (Scheme 3-21). The phenyl group stacks onto apolar pocket S3/4. The triazole linker is a known bioisostere of amidic bonds. The polar hydroxyl group, meant to mimic the hemiacetal of compound **52**, forms a H-bond with His57. The methyl group is strategically oriented towards the apolar H1 pocket, suggesting that aliphatic R^2 groups would fit adequately.

We first focused on the synthesis of model compound **53** without the amidine moiety, to verify if this particular scaffold is obtainable with currently available methodologies. The suggested retrosynthesis is described (Scheme 3-22). The triazole moiety of target compound **53** will be obtained *via* a click cycloaddition between easily accessible phenyl azide **54** and alkyne **55**.

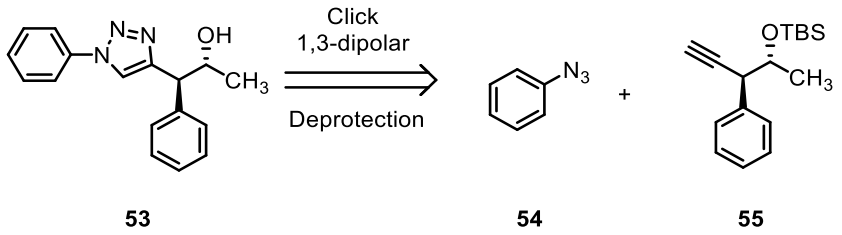

53 **54** **55**

Scheme 3-22. Retrosynthesis of model compound 53.

The latter alkyne will come from a Seyferth-Gilbert homologation of aldehyde **56** (Scheme 3-23). The peculiar *anti* scaffold of compound **56** can be selectively formed by rearrangement of 1,2-epoxy ether **57**. Such a molecule can be classically obtained *via* a Sharpless kinetic resolution (SKR) of corresponding racemic allylic alcohol **58**. Finally, this allylic alcohol will be obtained *via* a 1,2-reduction of easily accessible α,β-unsaturated ketone **59**.

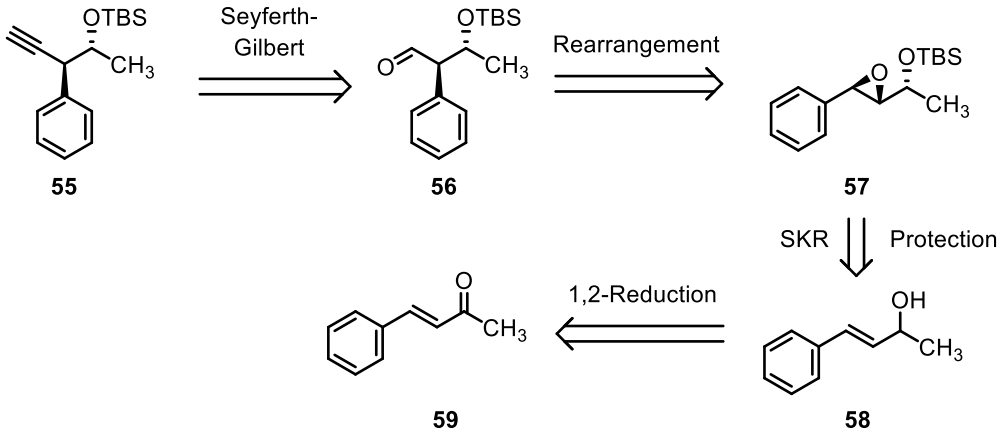

55 **56** **57** **59** **58**

Scheme 3-23. Retrosynthesis of alkyne 55.

3.4.2. Synthesis

The following synthetic work was performed by Steffy Pierard, a master student who worked under my supervision. α,β-Unsaturated ketone **59** was selectively 1,2-reduced with $NaBH_4$ in a

mixture of THF and CH_3OH to yield allylic alcohol **58** (Scheme 3-24).[172] Sharpless kinetic resolution with *t*BuOOH in the presence of $Ti(OiPr)_4$ and (-)-DET in CH_2Cl_2 at -20 °C afforded enantio-enriched epoxide **60**.[173,174] The enantiomeric excess of this compound has still to be determined by chiral HPLC. The alcohol moiety was then protected with TBSCl in the presence of imidazole in DMF to form silyl ether **57**.[175]

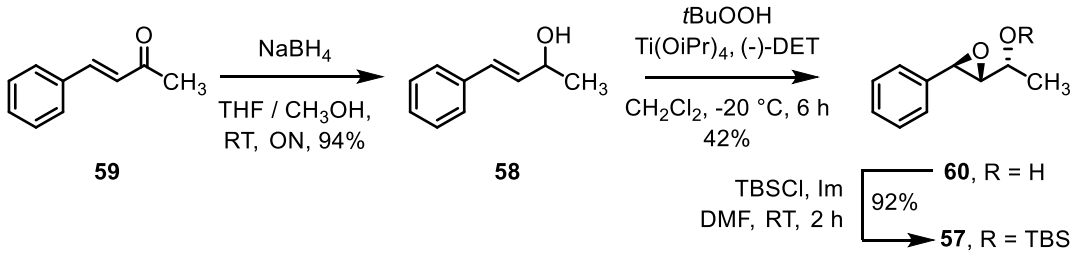

Scheme 3-24. Synthesis of protected 1,2-epoxy alcohol 57.

Epoxide **57** then underwent stereospecific rearrangement in the presence of MABR, a Lewis acid, in CH_2Cl_2 at -78 °C to form *anti* aldehyde **56** (Scheme 3-25).[176]

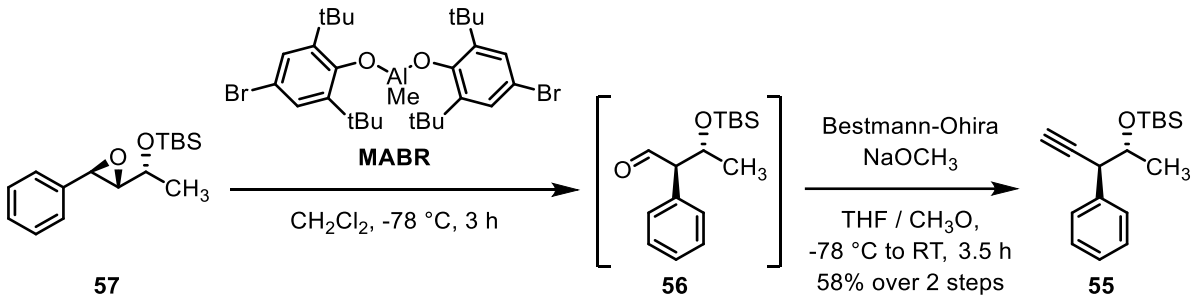

Scheme 3-25. Synthesis of alkyne 55.

This compound could not be isolated by column chromatography and was directly treated with the Bestmann-Ohira reagent in the presence of $NaOCH_3$ in mixture of THF and CH_3OH to yield terminal alkyne **55**.[177,178] The stereospecificity of the rearrangement can be rationalized by two different mechanisms. In the first hypothetical mechanism (Scheme 3-26), the complexation of MABR with the epoxide moiety fragilizes the C-O bond α to the phenyl moiety, as the partial positive charge is best stabilized next to an aromatic group.

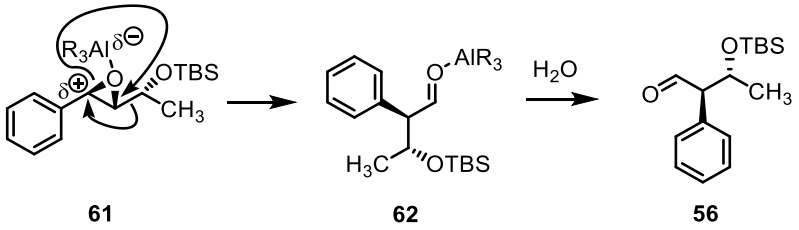

Scheme 3-26. First hypothetical mechanism of the MABR-promoted rearrangement of epoxide 57 into aldehyde 56.

This process promotes the stereospecific migration of the TBS oxyethyl group, in concert with the collapse of the epoxide into an aldehyde, resulting in complex **62**.[176] Finally, an aqueous quench, releases *anti* product **56** from the Lewis acid.

In a second hypothetical mechanism, the interaction with MABR makes complex **61** prone to epoxide migration, yielding silyloxiranium **61'** (Scheme 3-27). The aluminum alkoxide then collapses, promoting the migration of the phenyl which opens the silyloxiranium moiety, ultimately yielding the same complex **62**.

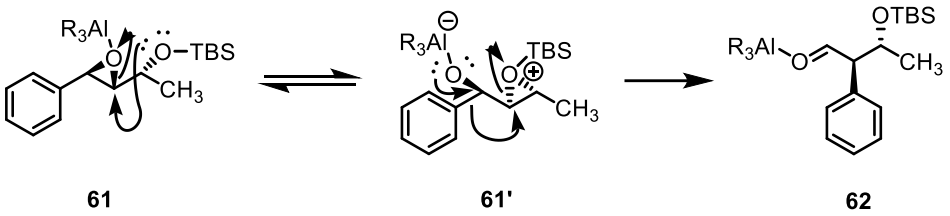

Scheme 3-27. Second hypothetical mechanism of the MABR-promoted rearrangement of epoxide 57 into complex 62.

Even though aldehyde **56** was confirmed as the sole product of the MABR-catalyzed rearrangement by ^{1}H NMR, attempts at isolation by column chromatography led either to complete epimerization (when performed on untreated silica gel or Et_3N-neutralized silica gel) or to degradation (Florisil gel).

Our hypothesis was that minute amounts of Brønsted acid, naturally occurring in the stationary phases, are able to promote the tautomerization equilibrium of aldehyde **56** into resonance-stabilized enol **63** (Scheme 3-28). This process involves the loss of the stereogenic information present on the carbon α to the aldehyde, resulting eventually in a 50:50 mixture of *syn*/*anti* diastereoisomers **64**. In Florisil, enol **63** is thought to eliminate via a E1cb-like mechanism the TBS siloxide, resulting in highly reactive phenylbutenal **65** and eventually degradation (Scheme 3-28).

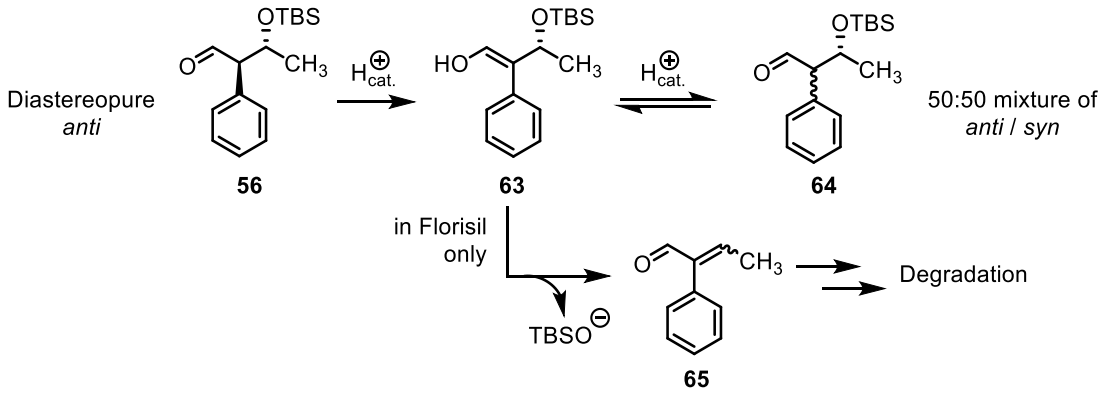

Scheme 3-28. Hypothetical mechanisms of the epimerization of the degradation of aldehyde 56 on different stationary phases.

In an attempt to unambiguously prove the *anti* relative configuration by NOESY experiments, the synthesis of a conformation-locked derivative of aldehyde **56** was envisaged. Freshly synthesized crude aldehyde **56** was directly reduced with $NaBH_4$ in CH_3OH at 0°C to yield alcohol **66** (Scheme 3-29).[176]

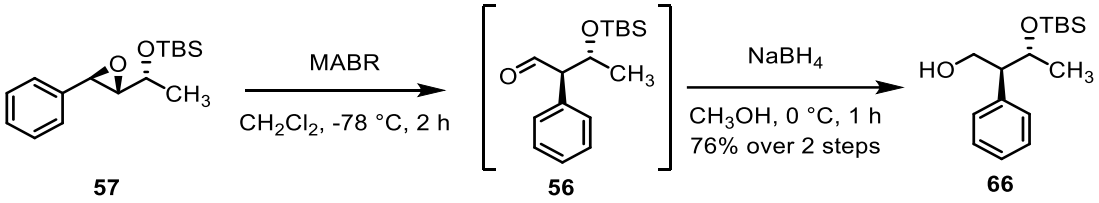

Scheme 3-29. Synthesis of alcohol 66.

Removal of the TBS group was performed with TBAF in THF at 0 °C to provide diol **67** (Scheme 3-30). Unfortunately, the attempt to yield conformation-locked dioxane **68** by treatment in 2,2-dimethoxypropane in the presence of CSA failed. Even though only one product was detected by revelation with UV-254 nm irradiation and by *p*-anisaldehyde staining, degradation occurred upon treatment with aqueous $NaHCO_3$, with disappearance of our only spot on TLC at the profit of numerous others. The absence of the desired product in the crude mixture was confirmed by ^{1}H-NMR analysis.

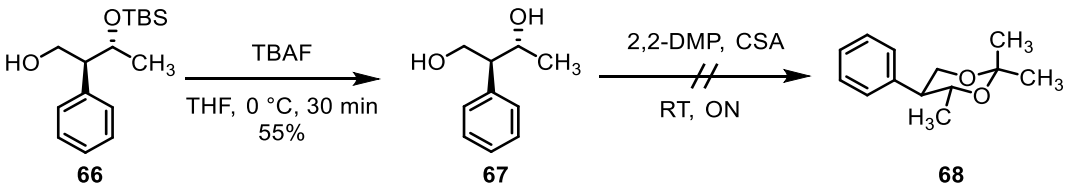

Scheme 3-30 Attempt at synthesis of dioxane 68.

Even though we were not able to obtain decisive evidence of the relative configuration in our case, it is described in the literature that only the *anti* compound is obtained via this transformation.[176] Further experiments are needed to remove any ambiguity.

Finally, alkyne **55** reacted with phenyl azide (Warning, both inorganic and organic azides are potentially toxic and explosive, see experimental part for more details) in the presence of the A21 · CuI in CH_2Cl_2 to form triazole **69** (Scheme 3-31).[152] The TBS group was removed using TBAF in THF at 0 °C, releasing target compound **53**, proving eventually that such a complex and highly epimerizable scaffold can be obtained with reasonable difficulty. In parallel to this synthetic work, our group reviewed exhaustively FXIIa inhibitors described in literature[179] and performed a vHTS of referenced drug compounds.[180] The results that we obtained were promising and encouraged to put on hold for the time being this peptidomimetic approach and to orient our efforts towards third-generation inhibitors based on these new discoveries.

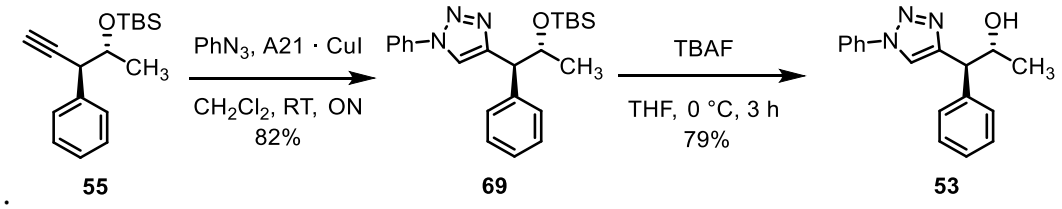

Scheme 3-31. Synthesis of target model compound 53.

3.5. Third-Generation Inhibitors

3.5.1. Towards Bis-Cationic Compounds

Two potent inhibitors of FXIIf, namely pentamidine (**70**) [181,182] and nafamostat (**71**) [183], were identified and are active in the micromolar and nanomolar ranges, respectively (Scheme 3-32). Nafamostat was identified by literature review[179] and has been little studied to date as a FXIIa inhibitor. Pentamidine obtained the lowest GlideScore of a vHTS of 2858 referenced drug compounds using the standard precision mode of Glide.[180] Interestingly, both compounds are characterized by two strongly basic groups at their extremities: two amidines for pentamidine, and one amidine and one guanidine for nafamostat.

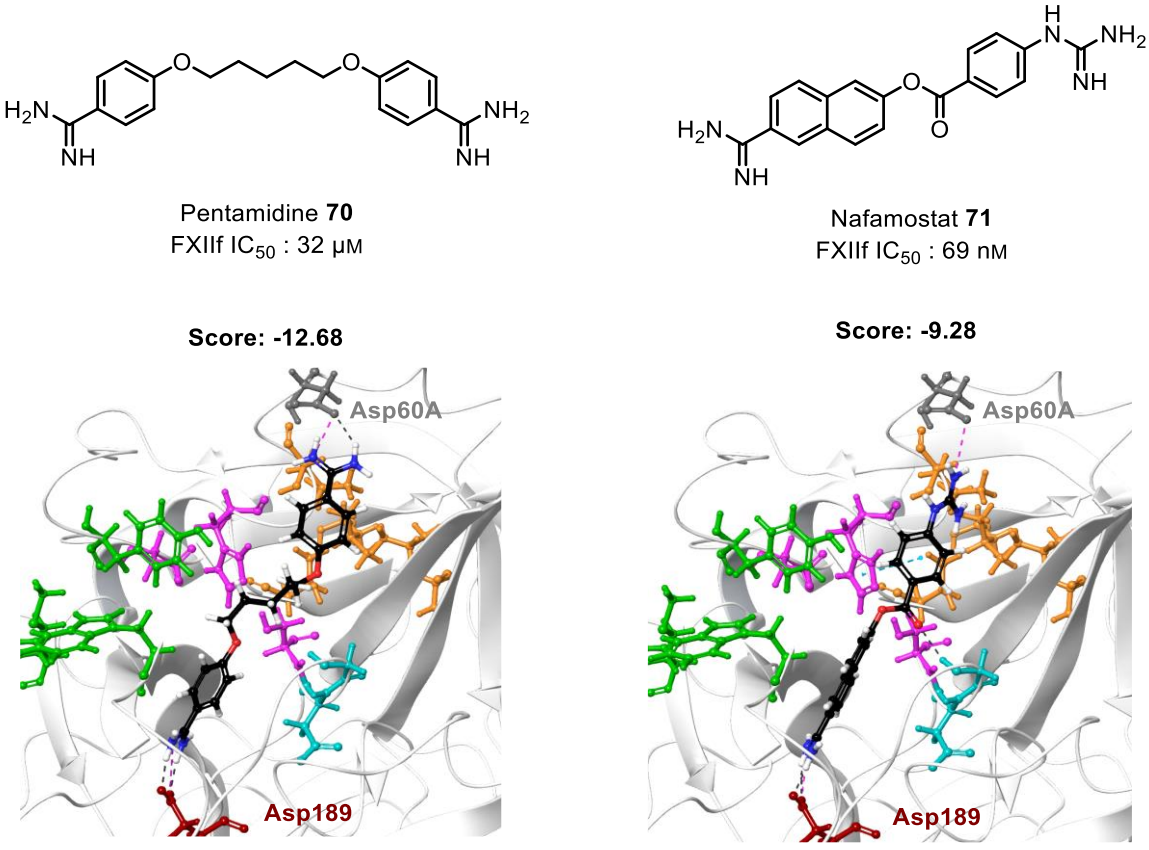

Scheme 3-32. Structures of pentamidines and of nafamostat and their IC_{50} on FXIIf.

Nafamostat is a known broad-spectrum inhibitor of serine proteases, active against FXIIa but mainly against thrombin and FXa[184], and is approved as an anticoagulant for hemodialysis in Japan. It is safer than UFH and LMWH for patients at high bleeding risk [185,186] With an elimination half-life of 5-8 minutes,[184,185] nafamostat requires hourly parenteral administrations.

Docking experiments using the XP mode the Glide program allowed to rationalize these activities (Figure 3-7). In their lowest-scoring docking poses, both compounds stand a linear conformation, forming ionic bridges *via* their amidinium/guanidinium with Asp189 within the S1 pocket and Asp60A. Nafamostat forms a π-π stacking with His57 and a H-bond *via* its carbonyl with the backbone amidic hydrogen of Gly194.

Despite these additional interactions, nafamostat scored lower than pentamidine (-9.28 VS -12.68). Indeed, while pentamidine is longer and thus able to interact with Asp60A with both the NH_2 groups of its amidinium, nafamostat can only interact *via* one the two NH_2 of its guanidinium.

Surprisingly, nafamostat is actually a better inhibitor than pentamidine. It is thought to act as a covalent inhibitor thanks to its ester functional group, which would then explain its superior activity. Together, these observations encouraged us to adapt our compounds in order to resemble these bis-cationic species

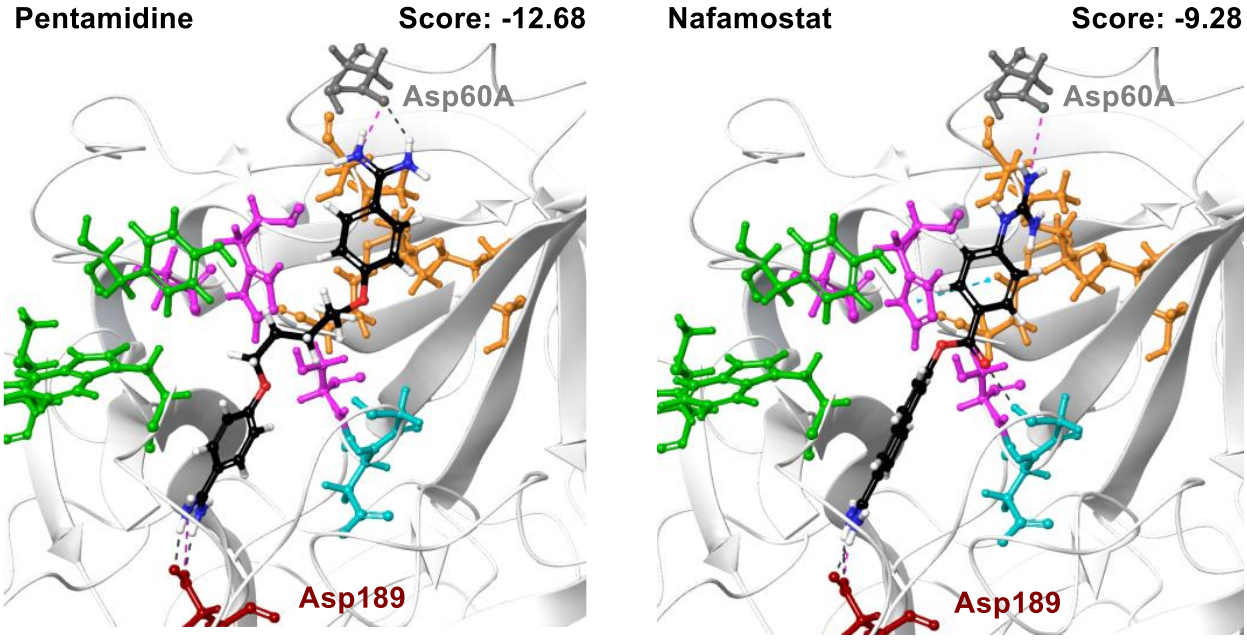

Figure 3-7. Molecular docking of pentamidine and nafamostat in the binding site of FXIIf. Brown: S1 pocket. Pink: catalytic triad. Turquoise: oxyanion hole. Green: S3/4 pocket. Orange: H1 pocket. Black: Asp60A. Black dotted lines: H-bonds. Blue dotted lines: π-π stackings. Pink dotted lines: ionic bridges.

3.5.2. Design and Retrosynthesis

Compound **34e**, the most potent candidate of our second-generation collection, had the required size to adapt to our bis-cationic strategy.

By adding a second amidine at its extremity, we identified our new targets: compound **72a** and its analog **72b**, with a 3-membered aliphatic chain instead of a 2-membered one (Scheme 3-33).

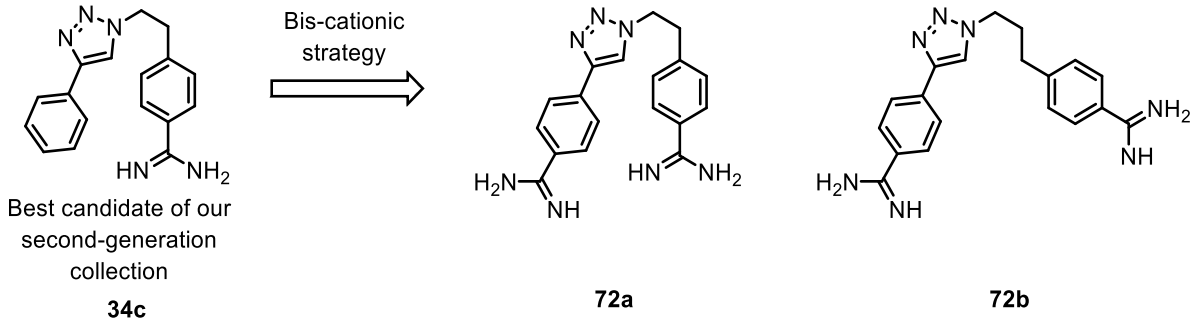

Scheme 3-33. Rationale of the design of our third-generation compounds as potential inhibitors of FXIIf based on the most potent candidate in the second-generation collection.

Compounds **72a** was docked within the active site of FXIIf using the XP mode of Glide and the pose with the lowest GlideScore is shown (Figure 3-8). The molecule stands in a linear conformation within the binding site. One of the two amidinium moieties interacts with Asp189 but the other one is too far away from Asp60A and is involved in H-bonding with Ser40 and Cy58.

We designed analog **72b** with a longer aliphatic chain to remedy this problem. Surprisingly, the lowest-scoring docking pose (1st pose, Figure 3-8) of compound **72b** is twisted and interacts ionically with Asp189 from the S1 pocket, with Asp102 from the catalytic triad, and *via* π-π stacking with His57

The second lowest-scoring docking pose is very similar but the third one (3rd pose, Figure 3-8) is linear as we first expected. The amidinium moieties interact with Asp189 and Asp60A and one of them is further involved in H-bonding with His57 and Ser40. The score of this linear docking pose is much lower than the score of the twisted docking pose. Overall, the docking experiments suggest that the two amidinium moieties in compounds **72a** and **72b** are involved in strong interactions with the enzyme and may improve the inhibitory activity toward FXIIf.

The suggested retrosynthesis is discussed below and is identical for both target compounds (Scheme 3-34). Both amidine moieties will be obtained *via* an addition reaction on corresponding bis-nitriles **73**. One of these two cyano group of will come from a C-CN coupling with aryl bromides **74**. The triazole linker of such compounds will be obtained *via* a cycloaddition between easily accessible azides **75** and alkyne **76**. 4-Cyanophenylacetylene is a direct Sonogashira derivative of commercially available 4-iodobenzonitrile **77**.

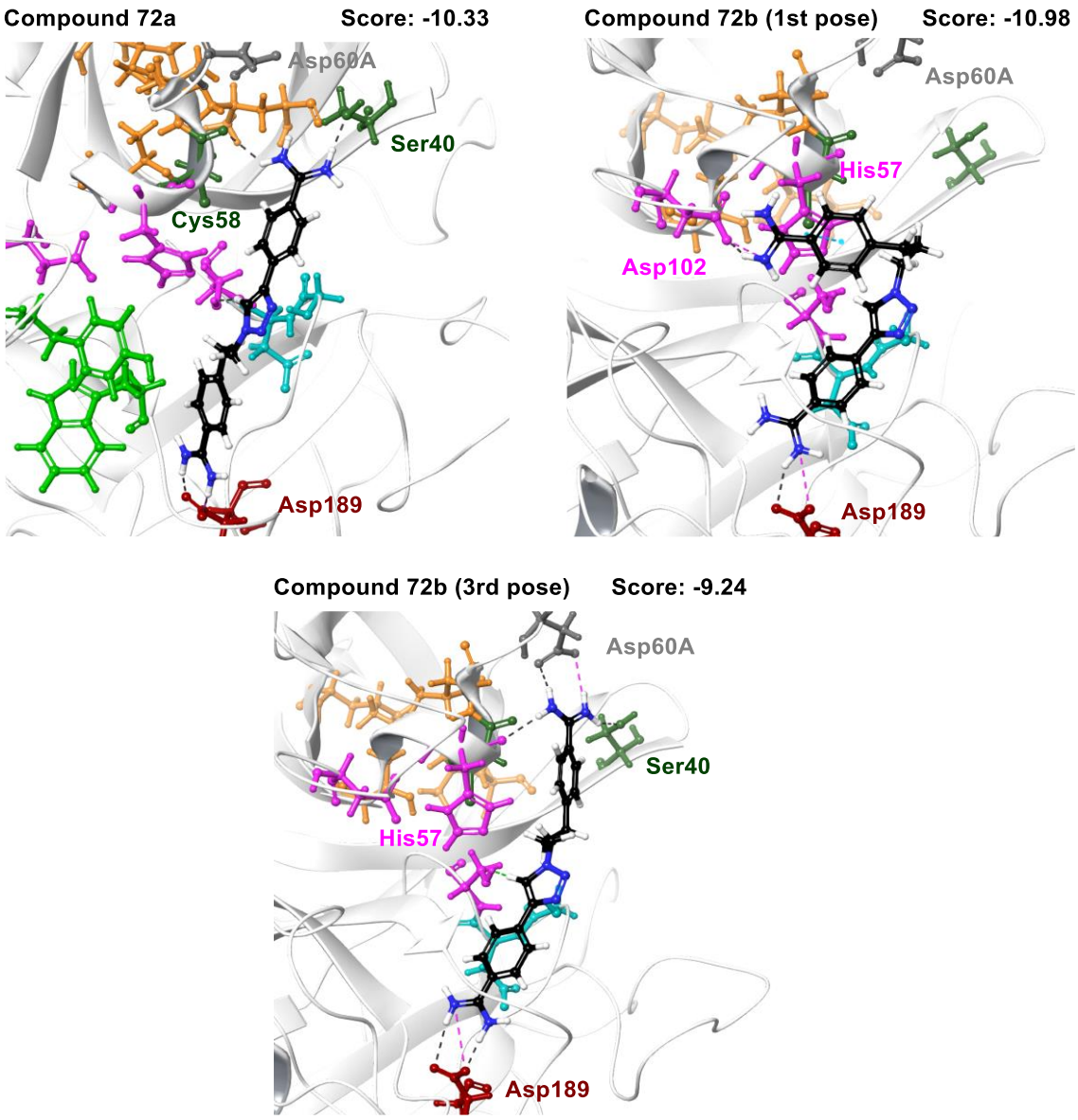

Figure 3-8. Molecular docking of compounds 72a and 72b in the binding site of FXIIf. Brown: S1 pocket. Pink: catalytic triad. Turquoise: oxyanion hole. Green: S3/4 pocket. Orange: H1 pocket. Grey: Asp60A. Black dotted lines: H-bonds. Blue dotted lines: π-π stackings. Pink dotted lines: ionic bridges.

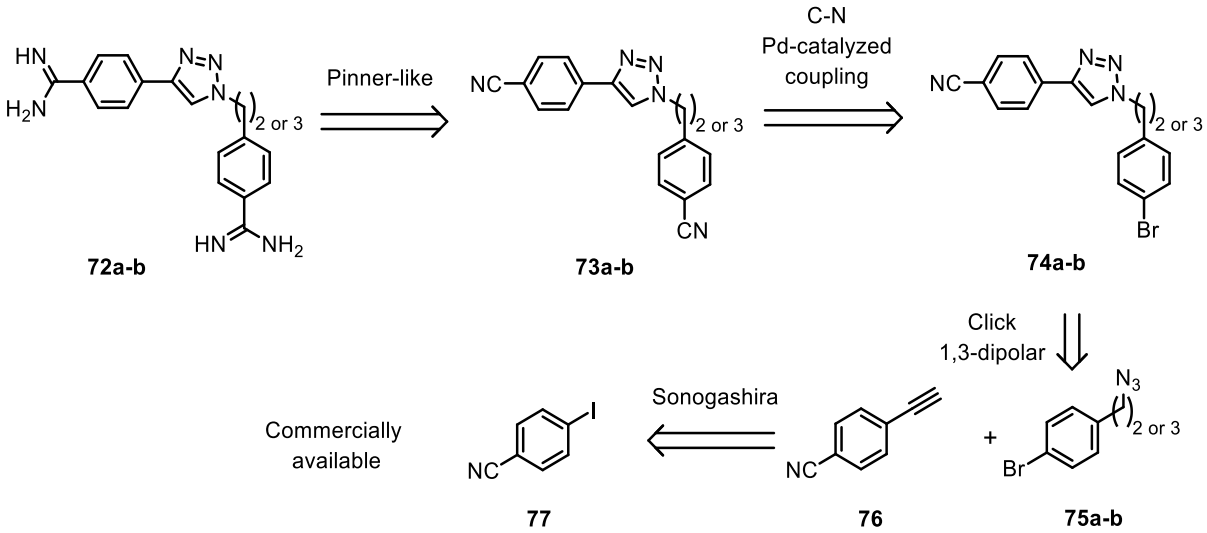

Scheme 3-34. Retrosynthesis of our third-generation molecules.

3.5.3. Synthesis

4-Bromophenethyl bromide **78** was substituted with NaN_3 in DMF at 70 °C to yield azide 75a (Scheme 3-35).[151] In a similar way, 4-bromohydrocinnamyl alcohol **79** reacted with MsCl in the presence of Et_3N in CH_2Cl_2 to form mesylate **80**, which was directly used in a NaN_3 substitution using the same conditions as previously to yield azide **75b** (Scheme 3-35).[187] Warning, both inorganic and organic azides are potentially toxic and explosive, see experimental part for more details.

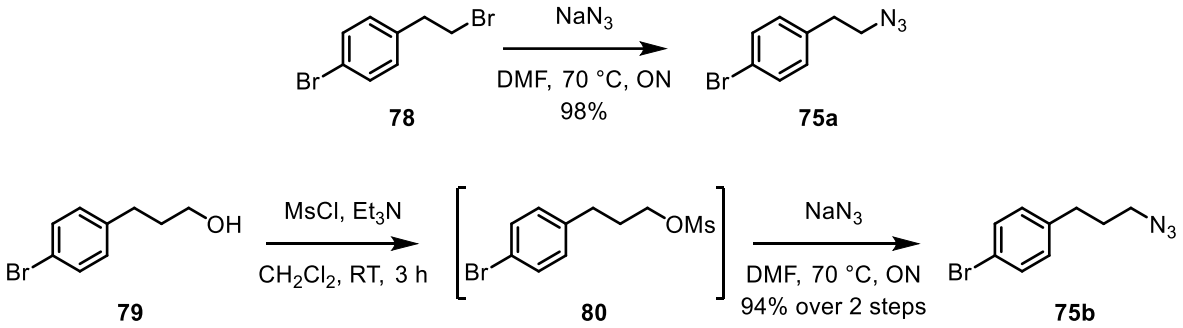

Scheme 3-35. Synthesis of azides 75a-b.

In parallel, 4-iodobenzonitrile **77** underwent a Sonogashira coupling with TMS-acetylene in the presence of $[Pd(PPh_3)_2Cl_2]$ and CuI in DIPA to form protected alkyne **81**,[188] which was directly treated with K_2CO_3 in CH_3OH leading to terminal alkyne **76** (Scheme 3-36).[150]

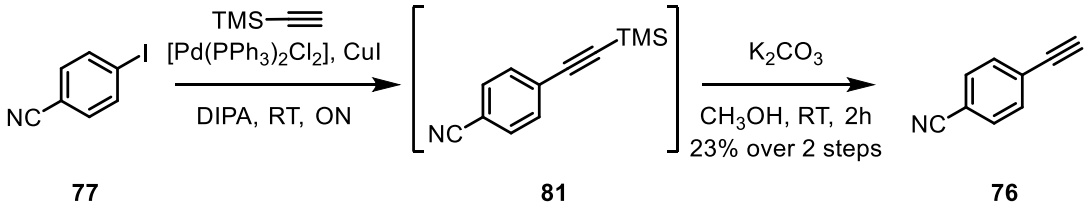

Scheme 3-36. Synthesis of 4-cyanophenylacetylene 76.

Both previously obtained azides **75a-b** reacted with this alkyne in a click cycloaddition in the presence of A21 · CuI in CH_2Cl_2 to yield triazoles **74a-b** (Scheme 3-37).[152] Cyanation of the bromophenyl moiety with $K_4[Fe(CN)_6]$ in the presence of $Pd(OAc)_2$ and Na_2CO_3 in DMAc at 120 °C allowed the formation of dicyanides **73a-b**.[166]

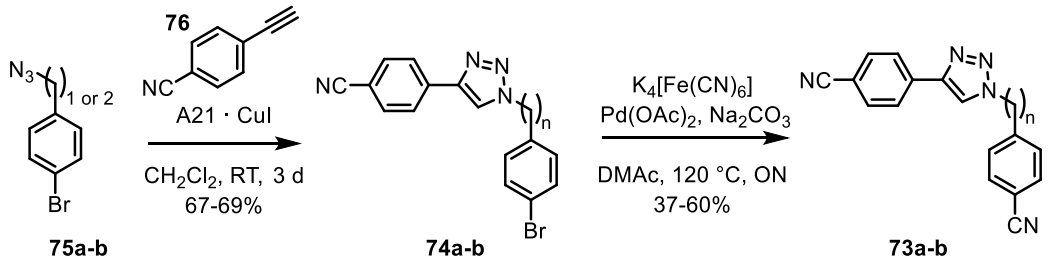

Scheme 3-37. Synthesis of dicyanides 73a-b.

The double amidination was performed as previously improved (Scheme 3-38). The nucleophilic addition of hydroxylamine, generated in situ from its HCl salt and Et_3N and the subsequent acylation with PivCl and Et_3N in CH_2Cl_2 were carried out to form compounds **82a-b**. Finally, hydrogenation catalyzed by Pd/C in CH_3OH gave quantitatively the desired amidinium pivalates **72a-b · 2PivOH**.

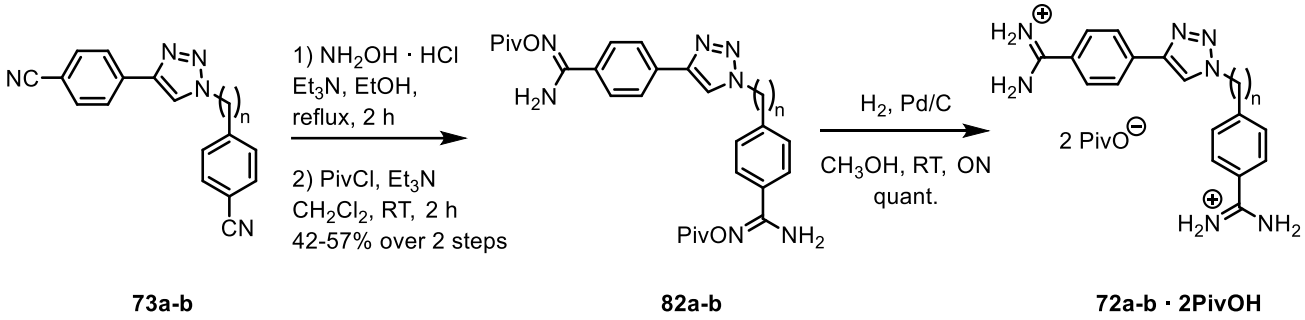

Scheme 3-38. Synthesis of diamidinium salts 72a-b · 2PivOH.

3.5.4. FXIIf Inhibition Assays

The compounds were tested using the previously described inhibition assay. The dose-inhibition curves of compounds **72a** and **72b** are shown (Figure 3-9). The Hill coefficients are equal to 1.047 and 1.069, respectively, suggesting that the observed inhibition is not due to precipitation or colloid formation.

The IC_{50} on FXIIf are estimated from the fitted equations (Table 3-5). Compound **72a** has a similar potency to that of pentamidine **70** but the fact that is not actually *more* potent suggests once again that the triazole moiety does not contribute to the inhibition. Surprisingly, longer compound **72b**, which scored better in the docking study and was estimated as more promising according to docking poses, is one order of magnitude less potent than its shorter analog **72a**.

3.6. Conclusion and Outlooks

In this first chapter, we have used structure-inspired ligand design to evaluate the potency of compounds by molecular docking and to decide which ones were worth synthesizing. All 15 target compounds were successfully obtained by organic chemical synthesis and tested on FXIIf. The synthesized molecules were equally or less potent than our references inhibitors. Analysis of these results led us to four main conclusions: the inhibitory activity of compounds **ChB49** and **ChB50** were false-positive results, benzamidines are better at inhibiting FXIIf than phenylguanidines, the triazole moiety does not add any potency to the compounds, and bis-cationic compounds are better hit compounds than mono-cationic compounds.

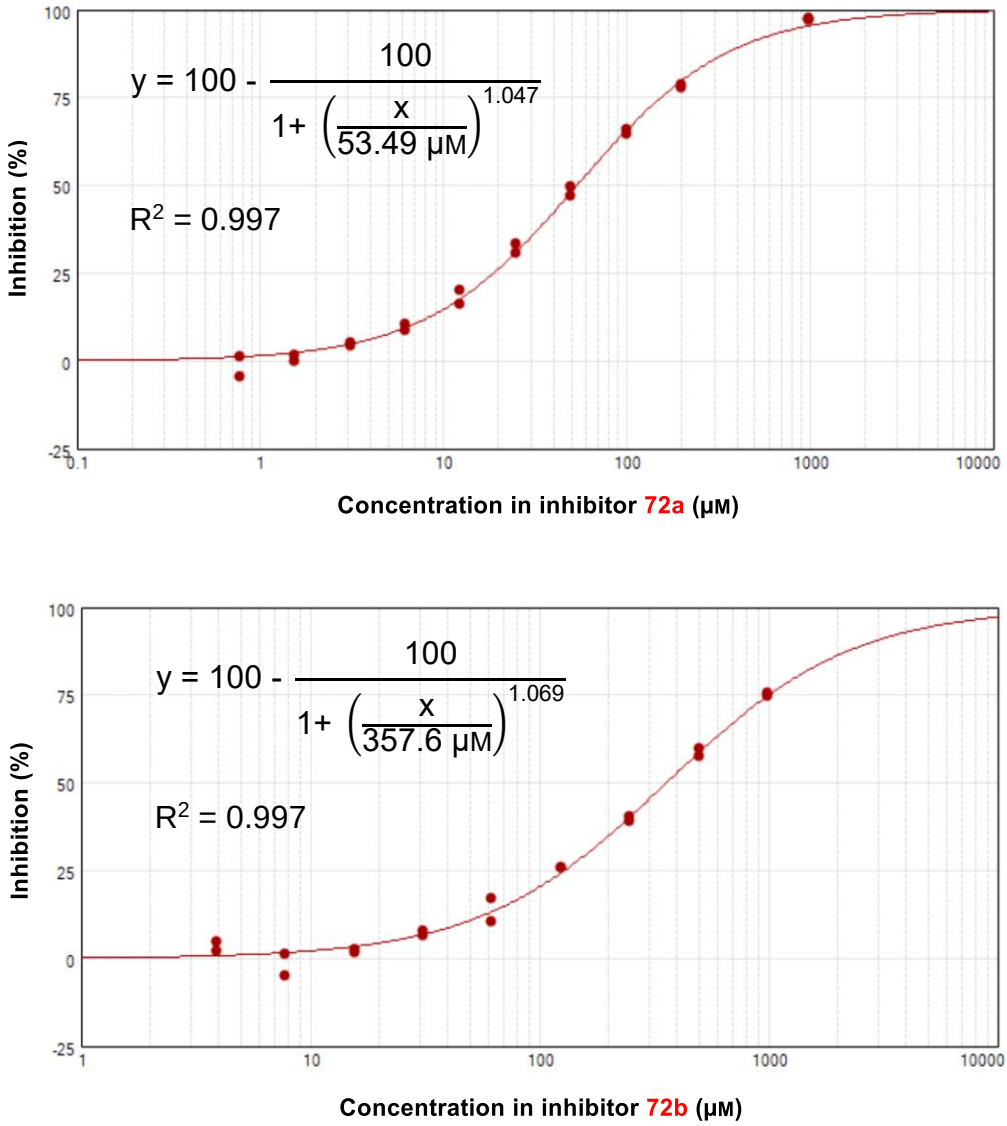

Figure 3-9. Dose-inhibition curve: compounds 72a-b and FXIIf.

Table 3-5. IC_{50} of compounds 72a-b on FXIIf.

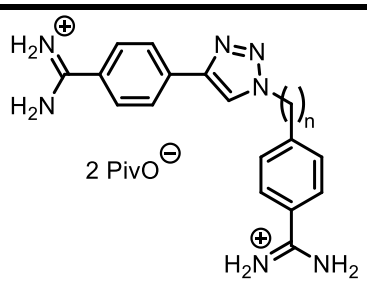

Compound	n	IC_{50} (µM)
72a	2	54
72b	3	358
Pentamidine · 2HCl	/	32

At this stage, we decide to explore more into details the bis-benzamidine strategy and to put hold the triazole moiety strategy, which led to mitigated results in our three collections. Synthesizing more benzamidines meant performing more late-stage benzamidination, and the process that we had been using so far, despite having been improved in-house, was inherently flawed and ill-adapted to the medicinal chemist's needs. The exact nature of these flaws, and how we tried to remedy them, is described in the next chapter

Chapter 4: Early-Stage Amidination

4.1. Preliminary Considerations

In the literature, amidination is typically the final reaction leading to the target molecule.[39,189–194] Indeed, amidines are protic, basic, chelating, and polar compounds, incompatible with important categories of reagents including basic organometallics, inorganic metal catalysts and electrophiles. To avoid these restrictions, their late-stage integration to the molecule is the usual strategy in organic synthesis, but little suitable for synthetic medicinal chemistry.

4.1.1. First Flaw: Amidination is Weakly Adapted to Late-stage, Complex Substrates

Typical conditions leading to benzamidines are weakly compatible with polyfunctional late-stage substrates and tedious to perform or to work up. The three most common ways to synthesize benzamidines are represented, and all three use aryl nitriles as starting material (Scheme 4-1).

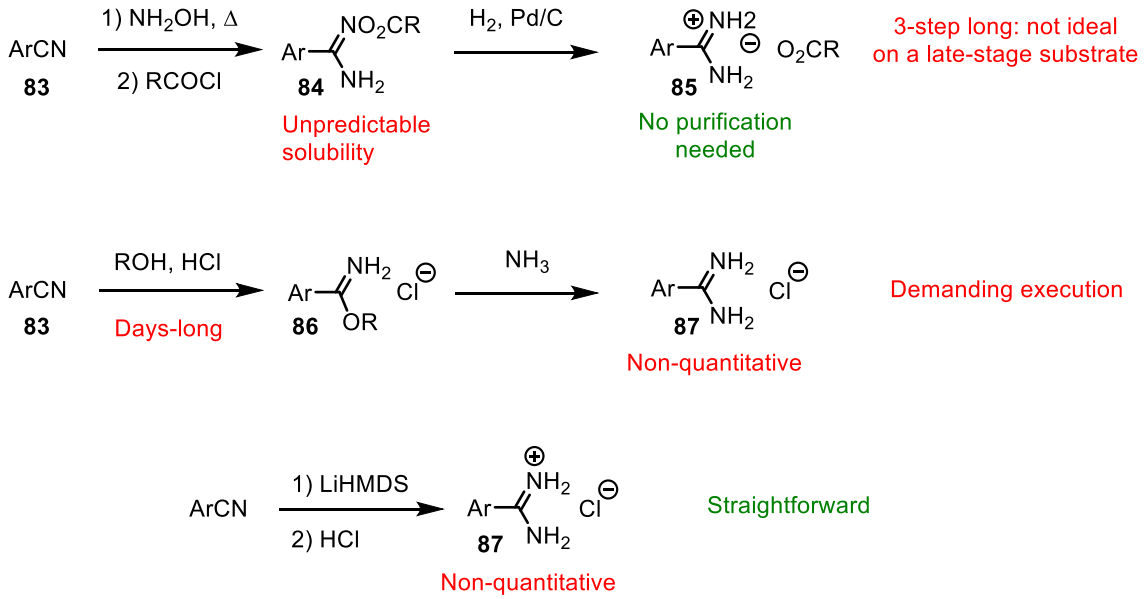

Scheme 4-1. Pros and cons of the three most common amidination protocols.

The first one[169] is the method that we used in the previous chapter and that we adapted to our substrates (Scheme 4-1). Addition of NH_2OH onto nitrile **83** followed by acylation of the resulting hydroxyamidine provides acyloxyamidine **84**, which can be purified by classical normal-phase column chromatography. Hydrogenation of the N-O bond is then quantitative and yields directly amidinium carboxylate **85** as a pure compound.

The main problem encountered in our case was the low and/or unpredictable solubility of the hydroxy- and acyloxyamidine, making each work-up unique, as well as the relative high number of necessary steps for such a transformation. Moreover, treatment with NH_2OH in refluxing ethanol is arguably not compatible with amides, esters, ketones, and electrophiles in general.

The second one[195] is the classical Pinner reaction and accounts for 1/3 of all published benzamidines in the literature (Scheme 4-1).[196] An alcohol (usually EtOH) adds onto nitrile **83** in the presence of HCl forming imidate hydrochloride **86**, not purified, then NH_3 is substituted to the alcohol to form the HCl salt of amidine **87**. Three problems are recurrent: the reaction is not quantitative and requires purification of the amidinium chloride salt, the reaction takes days until completion, and its execution is demanding. Indeed, despite several attempts during this thesis, we never managed to get any conversion using this reaction.

The third one[197] is the addition of LiHMDS on nitrile **83**, followed by HCl-catalyzed hydrolysis, in a one-pot reaction, yielding directly amidine salt **87** (Scheme 4-1). The process is straightforward but is usually not quantitative and leads to ammonium salts as side-products, which requires purification.

4.1.2. Second Flaw: Late-Stage is Equal to More Work

Ideally, in synthetic medical chemistry, all steps should be planned before the derivatization step as it will limit the number of reactions to be performed (Scheme 4-2). Every reaction before the derivatization step is to be performed only once, while every reaction after is to be performed n times, n being the number of target compounds.

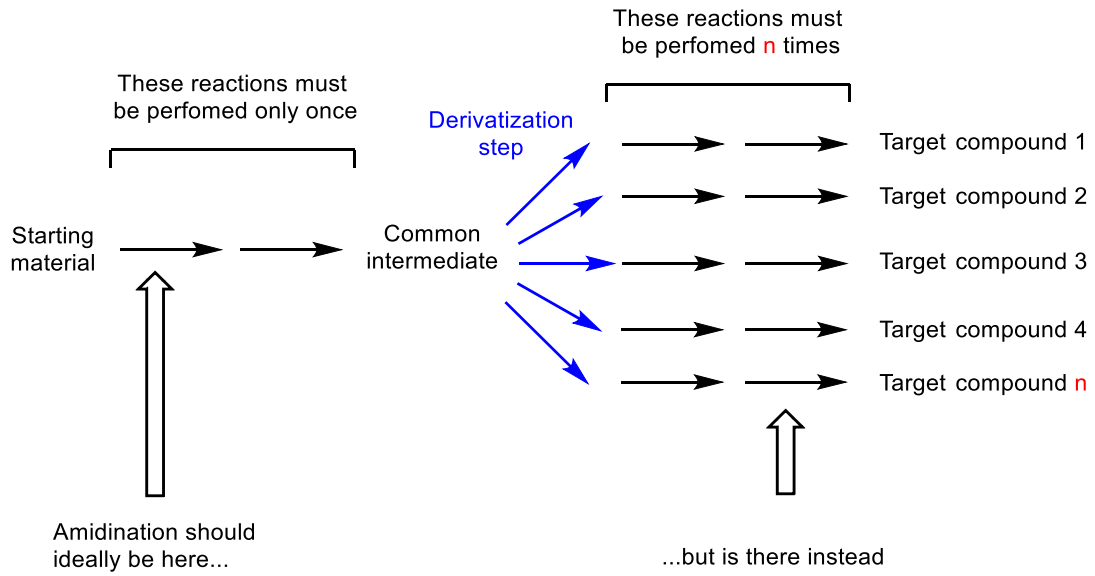

Scheme 4-2. General synthetic pathway toward a large variety of compounds in medicinal chemistry: early- VS late-stage amidination.

As discussed before, amidination is performed late-stage, often as the last reaction, thus necessarily after the derivatization step, giving much more work to the synthetic chemist. Put together, these two flaws encouraged us to use an early-stage benzamidination protocol.

4.1.3. The Choice for a Protecting Group

Inevitably, if we want the amidination to be early-stage and compatible with a range of reagents as wide as possible, including organolithium reagents, the benzamidine moiety must be fully protected to remove any acidic hydrogen. To our knowledge, such compounds are sparsely described and only three examples of fully protected arylamidines are mentioned in the literature: benzyloxyoxadiazoles **88**,[198] SEM-di-Boc-protected amidines **89**,[199] and tris-Boc-protected amidines **90** (Scheme 4-3).[200]

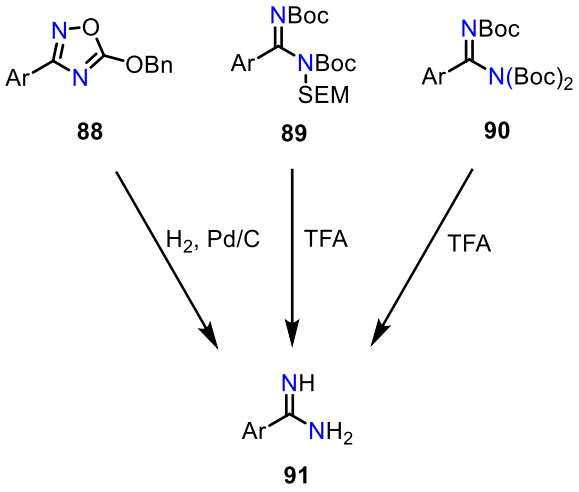

Scheme 4-3. Triprotected benzamidines and how to remove their protecting groups.

Oxadiazoles **88** are biaryl compounds, known for their limited solubility in organic solvents, a problem that we want to avoid. On the contrary, Boc groups are known for their capacity at enhancing the solubility. To avoid orthogonality problems, limiting the number of different protecting groups should be prioritized. Tris-Boc-protected amidines **90** are thus suggested to be user-friendlier than their mixed SEM/Boc-protected counterparts **89** and will be used in this thesis.

4.2. Objectives and Strategy

Based on the literature, we suggest, when possible, the replacement of traditional late-stage benzamidination with the following early-stage protocol (Scheme 4-4).

An aryl nitrile attached to a functionalizable group (FG in Scheme 4-4) will be transformed straightforwardly into benzamidine **93** using the LiHMDS/HCl reaction (previously described in section 5.1.1). The purity of the resulting benzamidine is not crucial, as it will be directly transformed into tris-Boc protected derivative **94**, easily purified by column chromatography.

The functionalizable group will then react in the derivatization step to form compound **95**. Finally, as we already performed in the case of of the guanidine synthesis, the Boc group will be quantitatively removed in the presence of TFA yielding amidine **96**. As summarized in green, this pathway solves every problem that we highlighted.

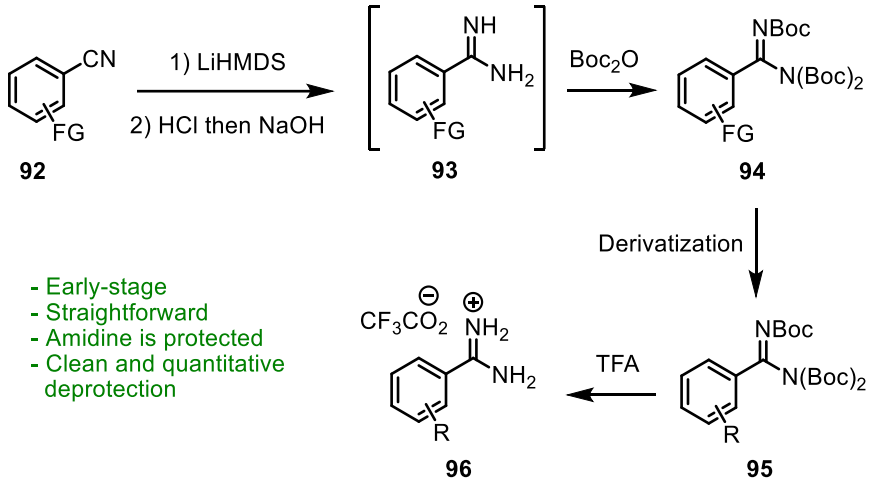

Scheme 4-4. Suggested synthesis of benzamidines 96 using an early-stage amidination.

The major uncertainty in this hypothetical synthetic pathway is the orthogonality of the Boc groups to the derivatization step. In our case, we will study two derivatization reactions largely used in the generation of potential hit compounds in medicinal chemistry:[201] substitutions and Pd-catalyzed cross-couplings. Even though the tolerance of the Boc group to such reactions is common knowledge, we will see that tris-Boc protected amidines display an unexpected behavior in some of these reactions.

4.3. Synthesis

4.3.1. Synthesis of the Common Intermediates

4-Substituted benzonitriles **97a-b** were treated with LiHMDS in THF / Et_2O and subsequently with concentrated aqueous HCl then NaOH to yield amidines **98a-b** (Scheme 4-5).[197]

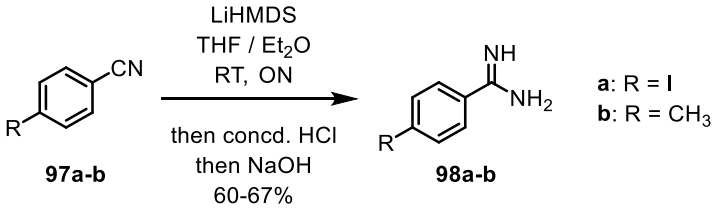

Scheme 4-5. Synthesis of amidines 98a-b.

To our knowledge, no mechanistic studies were performed to understand this peculiar reaction. However, indirect evidence suggests the following, non-trivial mechanism (Scheme 4-6).

The first step is the addition of the silylamide onto the Li-activated nitrile **99** to form lithiated compound **100**.[202] This activation is supported by the fact that LiHMDS is known to make Li-mediated complexes with nitriles, as proven by XRD.[202,203]

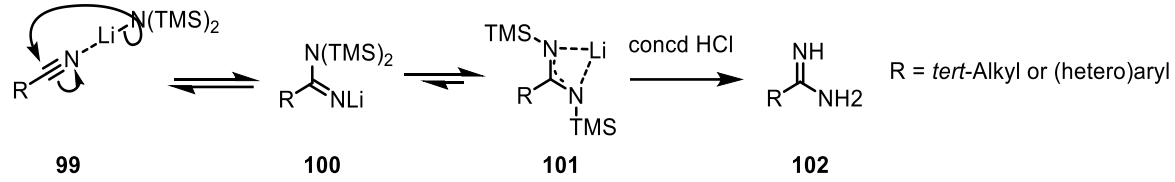

Scheme 4-6. Mechanism of formation of amidines from benzonitriles with LiHMDS.

The second step is the isomerization of compound **100** into more stable amidinate **101**, where the negative charge is now delocalized between both nitrogen atoms. The existence of such an anion in this reaction has been proven : numerous derivatives have been isolated, including vanadium and TMEDA-lithium complexes,[202,204] and their structures have been confirmed by XRD. However, how this isomerization takes place has not been determined yet. A [1,3]-sigmatropic rearrangement has been hypothesized.[203] In our case, amidinate **101** is then protonated and the TMS are hydrolyzed in acidic conditions to yield corresponding amidine **102**.

Amidines **98a-b** then underwent monoprotection using $(Boc)_2O$ in acetone to yield compounds **103a-b** (Scheme 4-7), which was then further protected twice using $(Boc)_2O$ in THF in the presence of Et_3N and DMAP to lead to tris-Boc amidines **104a-b**.[205]

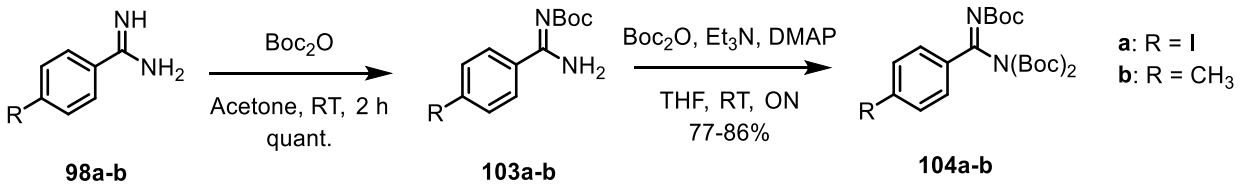

Scheme 4-7. Synthesis of tri-Boc protected benzamidines 104a-b.

Finally, toluyl derivative **104b** was halogenated *via* a radical reaction with NBS initiated by AIBN in refluxing $CHCl_3$ to yield benzyl bromide **105** (Scheme 4-8).[206]

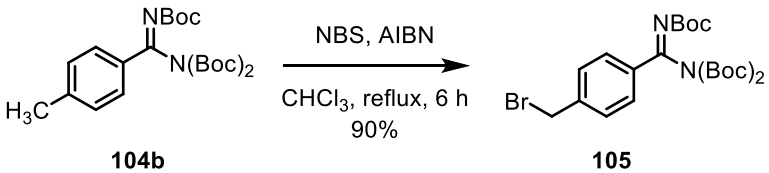

Scheme 4-8. Synthesis of benzyl bromide 105.

4.3.2. Orthogonality of Pd-Catalyzed Cross-Couplings with tris-Boc Protected Amidines

The ability of iodo derivative **104a** to undergo the most used Pd-catalyzed cross-couplings in medicinal chemistry was then investigated at RT, in order to limit Boc removal . A Suzuki coupling with phenylboronic acid in THF in the presence of $[Pd_2dba_3]$, P(*t*Bu)$_3$, and KF yielded uneventfully biphenyl **106** (Scheme 4-9).[207] Similarly, a Sonogashira coupling with phenylacetylene in DIPA in the presence of $[Pd(PPh_3)_2Cl_2]$ and CuI led to alkyne **107**. [188]

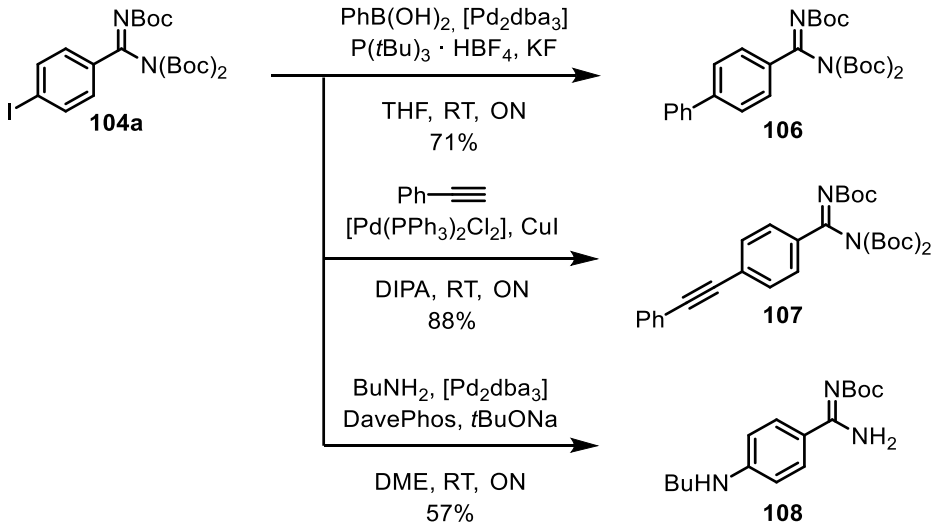

Scheme 4-9. Examples of Suzuki, Sonogashira, and Buchwald coupling involving aryl iodide 104a.

A Buchwald coupling with $BuNH_2$ in DME in the presence of $[Pd_2dba_3]$, DavePhos, and *t*BuONa [208] was successful but these conditions also deprotected two of the three Boc groups, leading to monoprotected benzamidine **108** (Scheme 4-9). We hypothesized that, in those conditions, the Pd^{II} ion plays a dual role: it acts as an intermediate in the coupling catalytic cycle, but also as a Lewis acid, which promotes the removal of the Boc groups. This dual behavior of a single Pd-complex in a one-pot transformation has already been described.[209]

4.3.3. Orthogonality of Substitution Reactions with Tris-Boc-Protected Amidines

Benzylic bromide **105** seems to be compatible with S_N2 reactions and reacted with sodium catecholate in CH_3OH at 50 °C to yield monoether **109** (Scheme 4-10). Due to health and safety concerns raised for laboratory work in 2020, we could not test this reaction with other substrates.

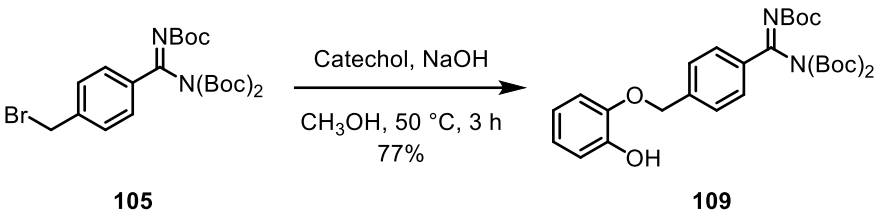

105 **109**

Scheme 4-10. Example of substitution reaction involving benzyl bromide 105.

4.4. Conclusion and Outlooks

In this chapter, we have successfully synthesized iodo- and bromomethyl-tris(Boc)-benzamidines and experiments suggest that they are compatible respectively with Sonogashira, Suzuki and Buchwald couplings, and substitution reactions. The late-stage amidination should not be considered as a necessary evil, as this preliminary work shows that it could be circumvented with early-stage amidination in at least 4 cases – and probably more that we have not investigated.

Thanks to these results, we opened new retrosynthetic opportunities involving early-stage amidination and are able to avoid the typical problems of purification involved with late-stage amidination.

Chapter 5: Pentamidine and Nafamostat

5.1. Objectives and Strategy

New information and insights for future developments emerged during the course of this thesis. Among those, our group found that nafamostat and pentamidine were both promising hit compounds, and that early-stage amidination could be envisaged to simplify syntheses and to improve their throughput. By using molecular docking-mediated ligand design, we decided to synthesize and to test analogs of nafamostat and of pentamidine in an attempt to improve either their inhibitory potency or their selectivity towards FXIIf.

From this approach, we designed three potentially promising analogues, each detailed in the following subchapters.

5.2. A Keto-Analog of Nafamostat

5.2.1. Design and Retrosynthesis

Nafamostat would represent a convenient lead compound thanks to its high potency towards FXIIf. As discussed previously, this potency is partially due to covalent inhibition, namely by acylation of hydroxyl group of Ser195. The presence of the highly reactive ester group explains its short elimination half-life and makes nafamostat weakly adapted for at-home treatments.

Our strategy to increase the metabolic stability of nafamostat *in vivo* is to replace the ester group with a non-cleavable ketomethylene group, leading to compound **113** (Scheme 5-1). Covalent inhibition would still be possible by formation of a hemiacetal between the keto group and Ser195.

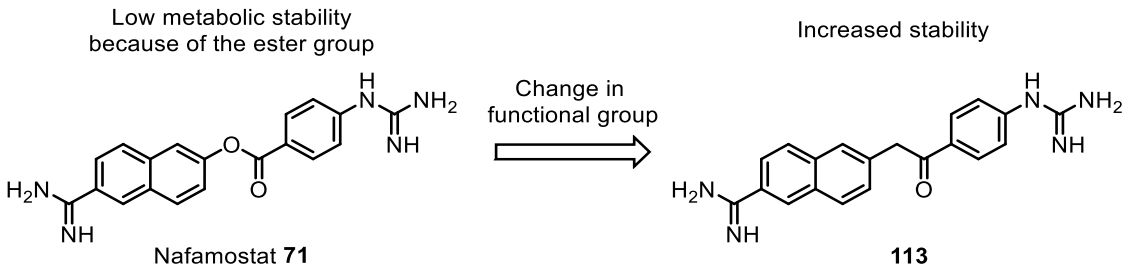

Scheme 5-1. Rationale of the design of compound 113

Compound **113** was docked within the active site of FXIIf using the XP mode of Glide. The pose with the lowest GlideScore is shown and can be compared to that of plain nafamostat (Figure 5-1).

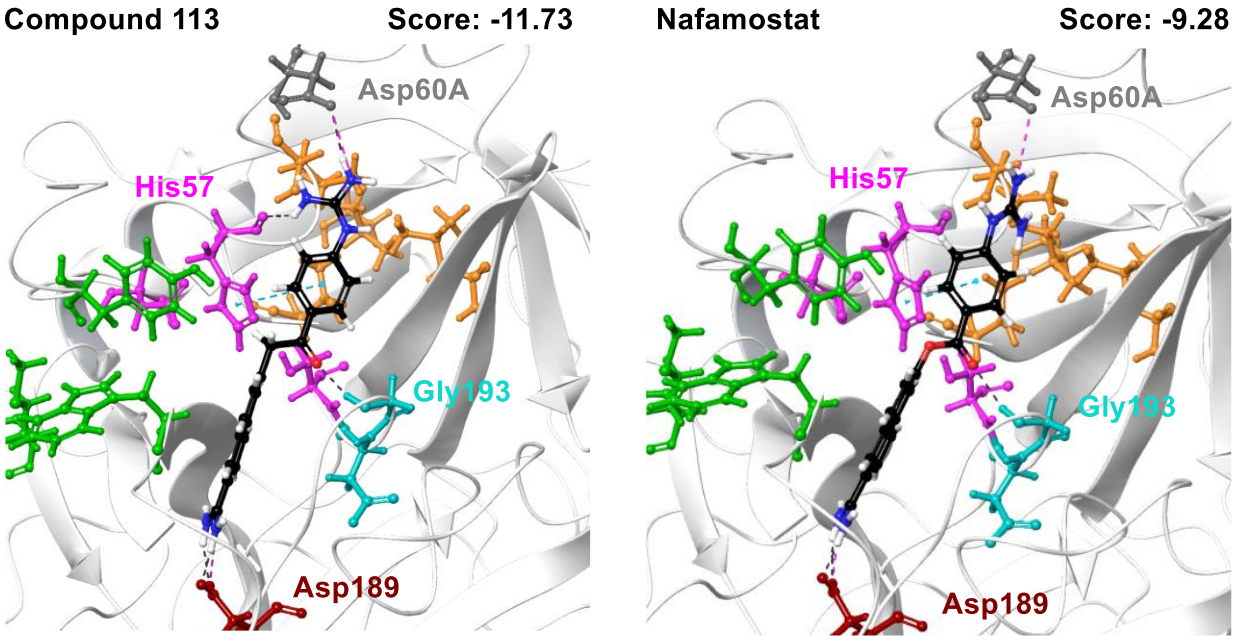

Figure 5-1. Molecular docking of compound 113 and of nafamostat in the binding site of FXIIf. Brown: S1 pocket. Pink: catalytic triad. Turquoise: oxyanion hole. Green: S3/4 pocket. Orange: H1 pocket. Grey: Asp60A. Black dotted lines: H-bonds. Blue dotted lines: π-π stackings. Pink dotted lines: ionic bridges.

The amidine of compound **113** is oriented in another direction than in nafamostat and is now able to form H-bonding with the carboxylate of Asp60A and the backbone amidic hydrogen of His57, resulting in a significantly lower docking score. The replacement of an sp^2 oxygen by an sp^3 methylene has an influence on the bonding angle (120.7° VS 114.4°), and this change in molecular geometry gives more place for the guanidinium moiety to rotate, yielding a more favorable docking pose.

The first suggested retrosynthesis is straightforward (Scheme 5-2). The C-C bond between the naphthyl moiety and the ketone moiety can be formed *via* a Pd-catalyzed arylation, and the guanidine via a classical guanidylation, simplifying the structure into commercially available 4-aminoacetophenone **114** and protected naphthamidine **115**.

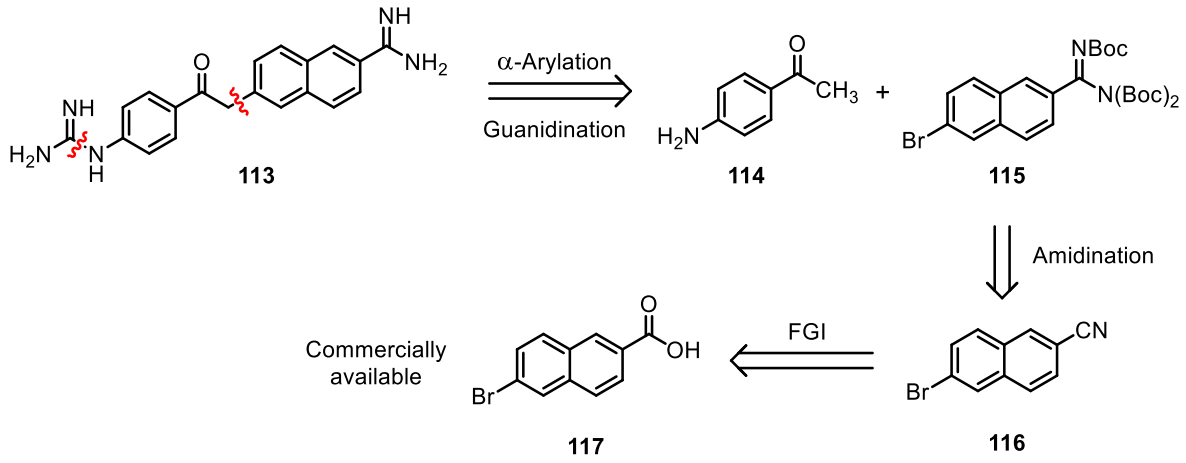

Scheme 5-2. First retrosynthesis of compound 113.

The latter is a direct amidinated derivative of nitrile **116**, which, by FGI, can be further simplified into commercially available 6-bromo-2-naphthoic acid **117**.

5.2.2. First Attempt at Synthesis

5.2.2.1. Synthesis of the bromonaphthyl precursor

The synthesis of bromonaphtyl precursor **115** was performed (Scheme 5-3). 6-Bromo-2-naphthoic acid **117** reacted with $(COCl)_2$ in CH_2Cl_2 in the presence of catalytic DMF, and the freshly synthesized acyl chloride was quenched with NH_3 to yield amide **118**.[210] The latter compound was dehydrated using TFAA in the presence of pyridine in 1,4-dioxane to form nitrile **116**.[210] Treatment with LiHMDS in THF at reflux, then sequentially with concentrated HCl and aqueous NaOH afforded amidine **119**. Monoprotection using $(Boc)_2O$ in acetone yielded compound **120**, which is then further diprotected using $(Boc)_2O$ in THF in the presence of Et_3N and DMAP to lead to tris-Boc protected naphthamidines **115**.[205]

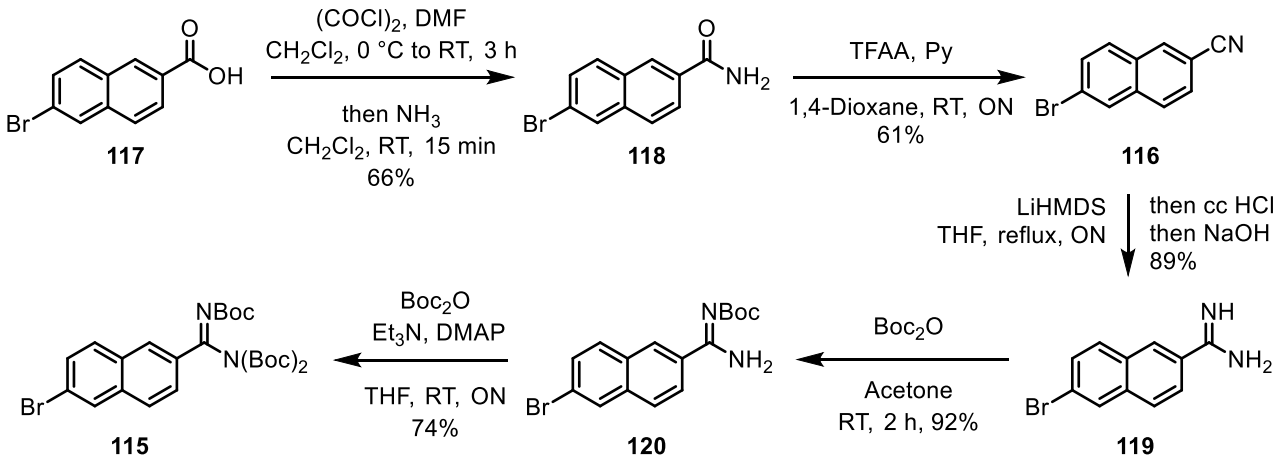

Scheme 5-3. Synthesis of bromonaphtyl precursor 115.

5.2.2.2. Pd-catalyzed arylation

α-Arylation of 4-aminoacetophenone **114** with naphthyl bromide **115** was attempted in the presence of $Pd(OAc)_2$, $P(t\text{Bu})_3$ and *t*BuONa in THF at RT, the standard conditions described by S. Buchwald's group for this transformation (Scheme 5-4).[211]

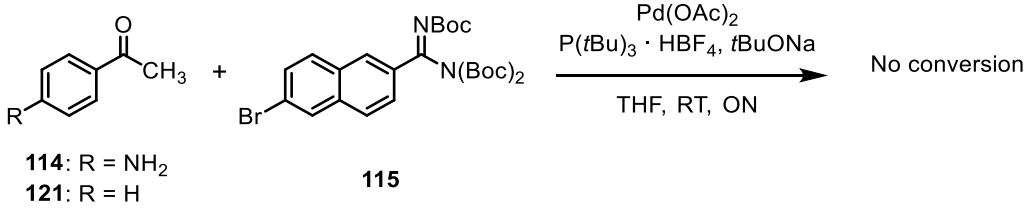

Scheme 5-4. Attempt at arylation of acetophenones 114 and 121.

However, no reaction occurred and the starting materials were recovered. We hypothesized that the anilino group might poison the Pd catalyst, so the reaction was performed with simple acetophenone **121**, yet no reaction took place. These conditions are seemingly incompatible with naphthyl substrate **115**, so we looked for other catalytic systems and found the second-generation conditions, still described by Buchwald, using biaryl phosphine ligands.[212] We decided to test them on several substrates to check simultaneously which functional groups were problematic and if the reaction was reproducible in our hands.

The reaction of 4-aminoacetophenone **114** and bromobenzene **122** in the presence of [Pd_2dba_3], JohnPhos and *t*BuONa in toluene at RT yielded exclusively undesired amine arylation product **123** (Scheme 5-5). The C_{Ar}-N coupling seems to be faster than the C_{Ar}-enolate coupling. Unprotected anilines are thus incompatible with ketone α-arylation in these conditions.

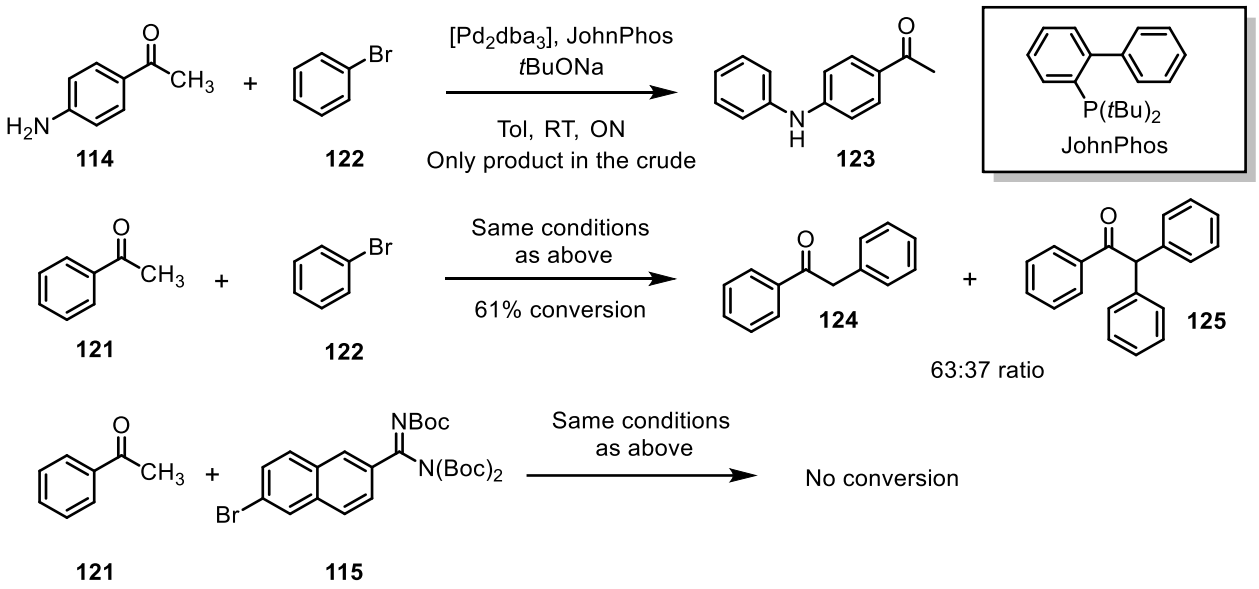

Scheme 5-5. Different attempts at arylation of acetophenones.

The reaction between acetophenone **121** and bromobenzene **122** in the same conditions yielded a 63:37 mixture of monoarylated compounds **124** and diarylated compound **125** (Scheme 5-5). Even though this success was rewarded with moderate conversion, reproducibility was compromised as this problem of mono- vs bis-arylation is neither described nor observed in the literature.[211,212]

Faced with these partially positive results, the coupling was then tried between acetophenone and naphthyl bromide **115**, once again in the same conditions (Scheme 5-5). No conversion occurred. Compared with the previous reaction, it then seemed clear that the tris(Boc) amidine was poisoning the catalytic system.

As also described in the literature, JohnPhos was replaced by other Buchwald's ligands, such as BINAP, XPhos, or Xantphos,[212] or by Nolan's NHC-based ligands,[213] to try to make this last reaction work, using higher temperatures as well, but to no avail (Scheme 5-6).

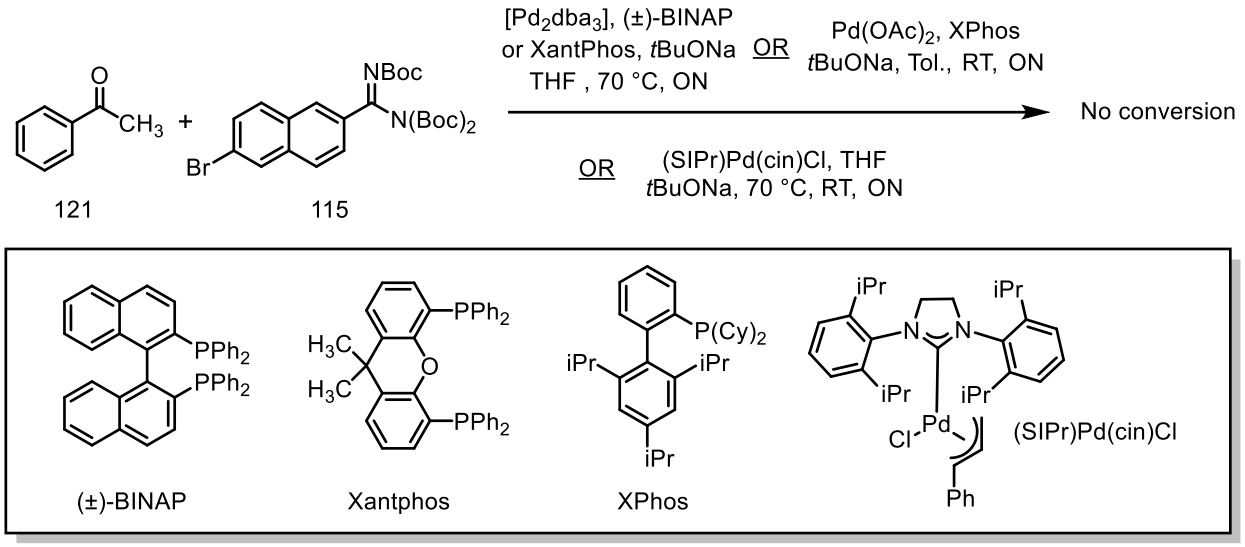

Scheme 5-6. Several attempts at coupling acetophone 121 and naphthyl bromide 115.

Apart from minimal, slow removal of the Boc groups from the amidine, no reaction occurred. This complete lack of reactivity towards coupling reaction was so curious that we even doubted the quality of naphthyl bromide **115**. A Sonogashira coupling was attempted with 4-aminophenylacetylene **126** in the presence of $[Pd(PPh_3)_2Cl_2]$ and CuI in DIPA and successfully yielded push-pull alkyne **127** (Scheme 5-7),[188] suggesting that naphthyl bromide **115** is indeed not the limiting factor in the coupling reaction.

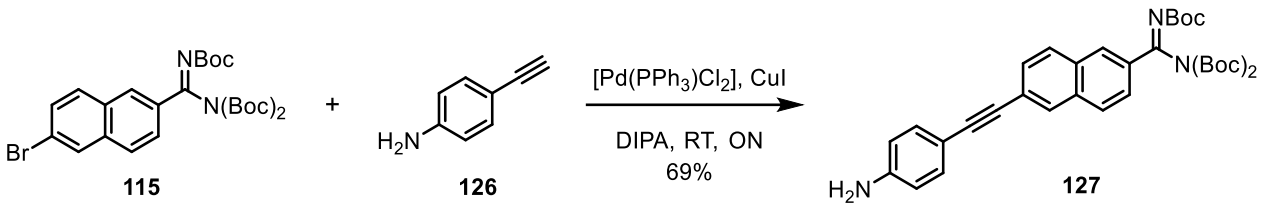

Scheme 5-7. Sonogashira coupling between aryl bromide 115 and phenyacetylene 126.

At this point, it seemed clear that the α-arylation of acetophenone by naphthyl bromide **115** would require optimizing. Heating up our experiments at more than 70 °C should be avoided as it would greatly accelerate the Boc removal and as it would favor the undesired bis-arylation. The main parameter to be optimized was thus the ligand. However, we had already used all potential commercial ligands at our disposal at that time. Instead of buying overly expensive, modern ligands or of synthesizing them, we decided to adapt our retrosynthesis

5.2.3. Second Retrosynthesis

The second retrosynthesis of compound **113** is described (Scheme 5-8). The C-C bond between the naphthylmethyl moiety and the phenylcarbonyl moiety can be formed *via* an addition mediated by *Umpolung*, and the guanidine *via* a classical guanidylation, simplifying the structure into dithiane **128** and protected naphthamidine **129.**

The C-N bond of aniline **130** can be synthesized with a Buchwald-type coupling from bromide **130**, a direct derivative of commercially available 4-bromobenzaldehyde **131**. In parallel, benzylic bromide **129** is simplified into methylnaphthalene **132**. As usual, the amidine moiety is derived from corresponding nitrile **133**, itself a product by FGI of commercially available 6'-methyl-4'-acetonaphthone **134**.

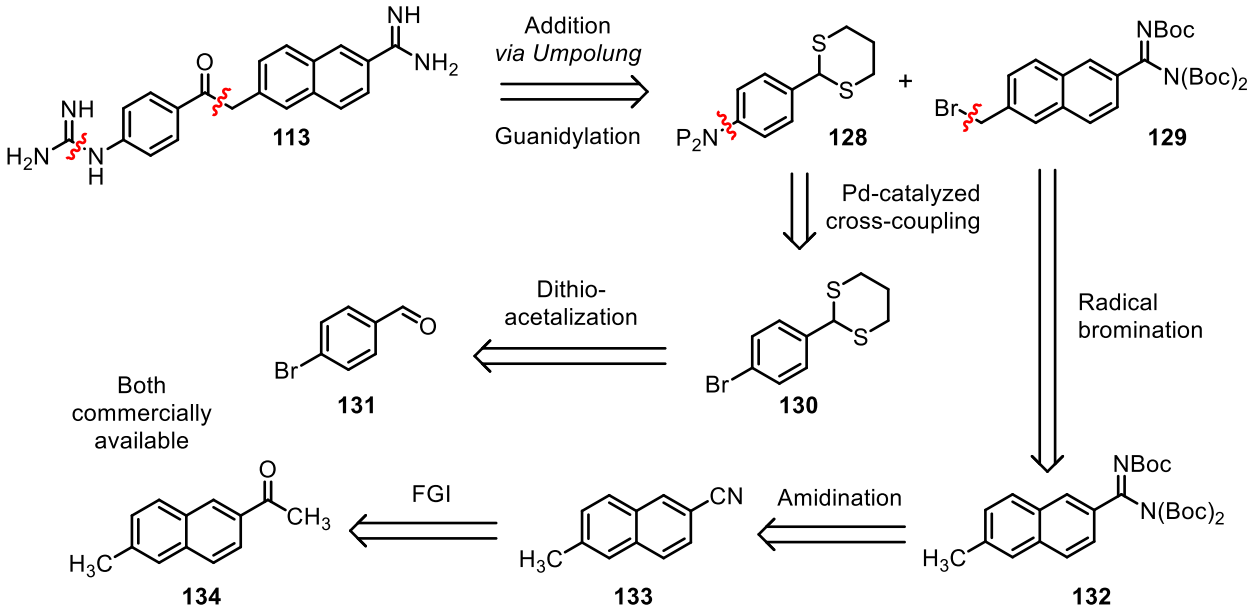

Scheme 5-8. Second retrosynthesis of compound 113.

The key step will be in the addition *via Umpolung* of the benzylic dithianyl anion derived from compound **128** on benzylic bromide **129**. In order to check the feasibility of this reaction on our substrates, we will first develop this process for the synthesis of model molecule **135**, whose retrosynthesis (and thus synthesis) is much shorter, which will then allow us to detect early on if the reaction is possible (Scheme 5-9). The dithianyl-benzyl bond should be formed *via* our key addition *via Umpolung*, starting from dithiane **136** and benzyl bromide **137**.

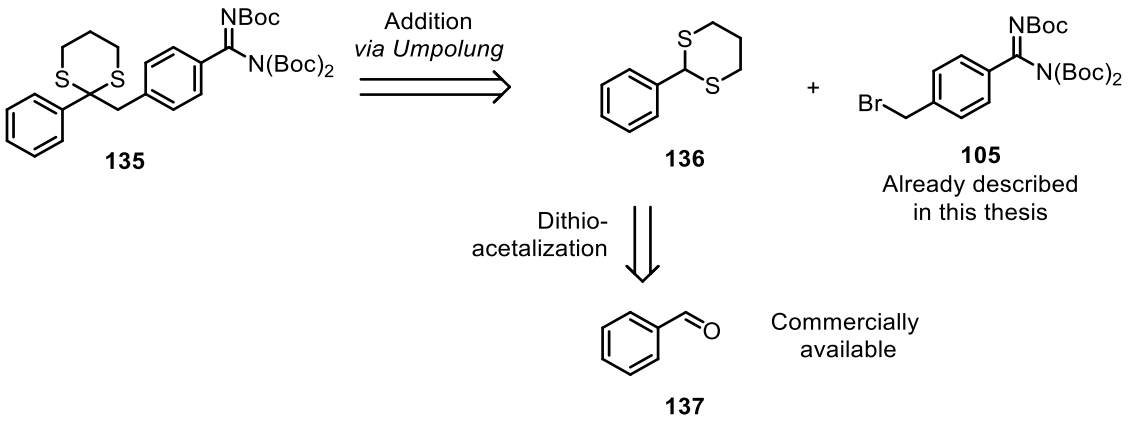

Scheme 5-9. Retrosynthesis of model compound 135.

Dithiane **136** is directly derived from benzaldehyde while benzyl bromide **105** is a compound that we already obtained on a gram-scale in this thesis.

5.2.4. Second Attempt at Synthesis

Benzaldehyde **137** readily reacted with 1,3-propanedithiol in the presence of I_2 in CH_2Cl_2 to quantitatively yield phenyldithiane **136** (Scheme 5-10).[214] Lithiation of the dithiane at the 2 position was performed with BuLi at -45°C in THF, and then the resulting phenyldithiathyl lithium adds onto benzyl bromide **105** to provide model compound **135** in 3% yield.[215] The reaction was also attempted in Et_2O and in a mixture of THF and HMPA, in order to influence the Li coordination sphere and to make the dithianyl anion more reactive, but, similarly, only traces of the product were detected by ^{1}H NMR.

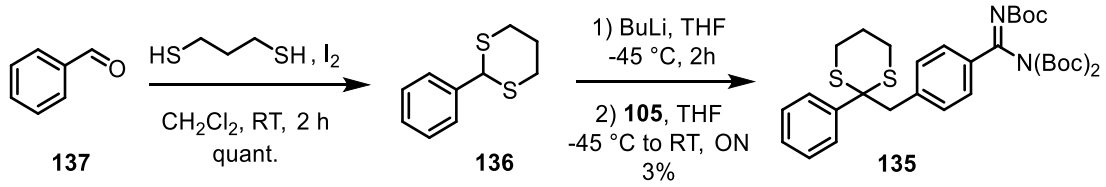

Scheme 5-10. Synthesis of phenylbenzyldithiane 135.

Our hypothesis to explain this failure at reacting is threefold. First, the dithianyl anion is resonance-stabilized, which makes it less nucleophile. Second this reaction may not be suitable for amidinic, electron-poor benzylic bromide. In the literature, the addition of phenyldithianyl lithium was never described with electron-poor benzylic bromides, only with electron-neutral or electron-rich ones.[216–220] On the other hand, two patents describe this reaction with electron-poor benzylic bromides,[221,222] but only one of them specified the yield, a low 30%.[221] Third, the $N(Boc)_2$ present in our electrophile represents a suitable bidentate ligand that could bind the Li ion (Scheme 5-11). The nucleophile would then be placed opposite to the benzylic bromide moiety which it is meant to substitute.

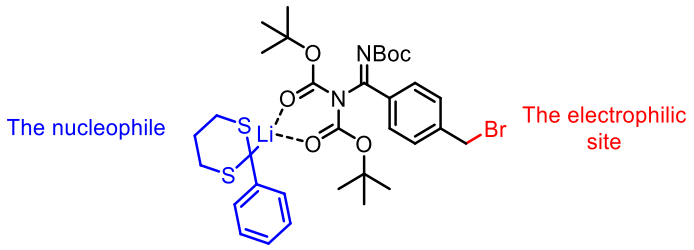

Scheme 5-11. Potential complex forming in the reaction, placing the nucleophile at the opposite of the electrophilic site.

5.2.5. Third Retrosynthesis

A third retrosynthesis of compound **113** is described (Scheme 5-12). Once again, the guanidine will come from the guanidylation of aniline **138**. The ketone will be synthesized by hydration of alkyne **127**, which is actually a molecule that we already obtained earlier in this thesis. If successful, the synthesis should then be straightforward

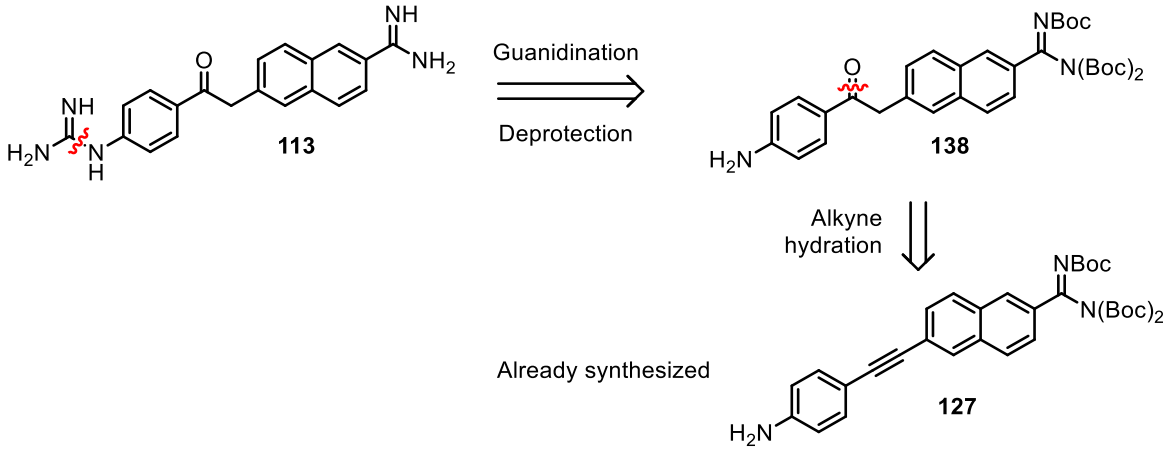

Scheme 5-12. Third retrosynthesis of compound 113.

5.2.6. Third Attempt at Synthesis

The hydration of alkyne **127** (Scheme 5-13) was attempted. The first trial to perform this reaction in EtOH in the presence of a catalytic amount of PTSA at reflux in the presence of PtO_2, as described in the literature for similar substrates [223]. However, as expected in strong acidic conditions, we only observed Boc removal. Lowering the temperature to 50 °C or to RT only slowed down the deprotection, but did not yield the desired product.

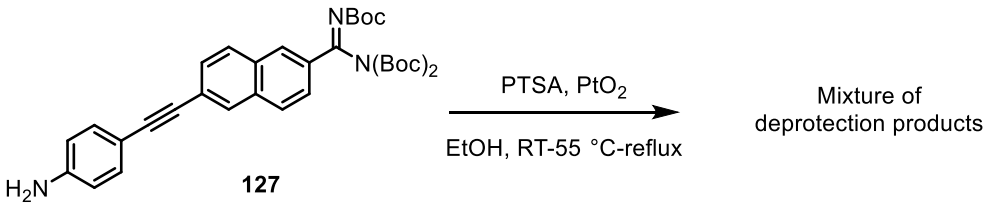

Scheme 5-13. Attempt at hydrating alkyne 127.

This lack of success suggests that Bronsted acid-catalyzed hydration is probably not adapted to our substrate, so we directly decided to change our approach toward a Lewis acid-catalyzed version instead. We had planned to test the hydration1in the presence of an NHC-gold chloride complex and $AgSbF_6$ in aqueous 1,4-dioxane at 60-70 °C.[224] Unfortunately, restricted access to the laboratory was implemented at this period due to health safety concerns, and we could not perform it.

5.3. A Sulfonamide Derivative of Nafamostat

5.3.1. A secondary pocket, the S1* pocket

The ideal FXIIf inhibitor should not only be potent, but also selective. In this context, we looked for specific structural features in FXIIf binding sites that would not be present in other key activated coagulation factors, namely thrombin, FXa, FVIIa and FXIa.

The S1 pockets of these different enzymes, as imaged by XRD analysis of co-crystals with non-covalent inhibitors, are shown (Figure 5-2). The S1 pockets of thrombin,[225] FXa,[226] FVIIa,[227] and FXIa[228] are well-defined holes. In contrast, that of FXIIf is more of a shallow ridge, which is almost fused to what could be considered as a side-pocket, absent from the other coagulation factors, containing a sulfate as a co-ligand. We decided to call this side-pocket the S1* pocket.

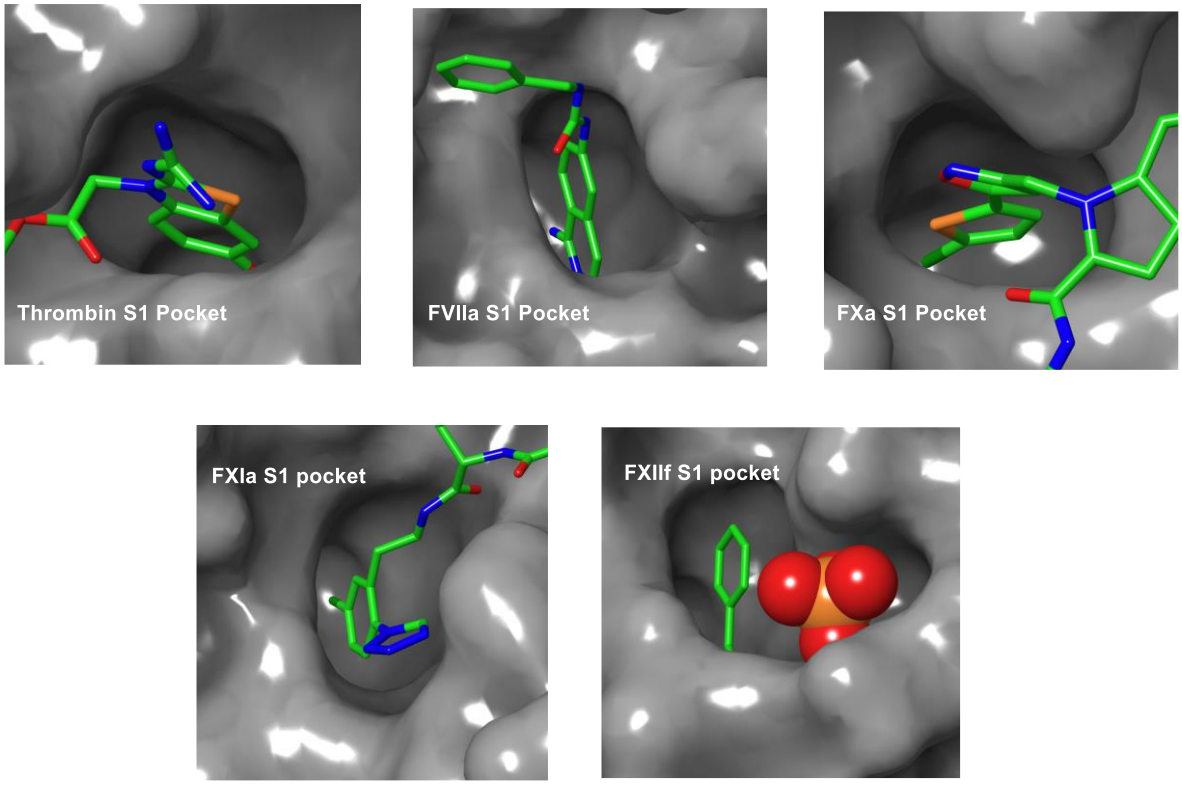

Figure 5-2. The S1 pocket in different coagulation factors.

A reorientation of the S1* pocket allowed us to determine the residues constituting it (Figure 5-3). The pocket is delimited by Gln192, His143 and Gly220 and tipped by a disulfide bond between Cys191 and Cys219. The sulfate interacts *via* hydrogen bonding with the polar hydrogens of sidechains of Gln192 and His143 and with the backbone amidic hydrogens of Gln192 and Gly220.

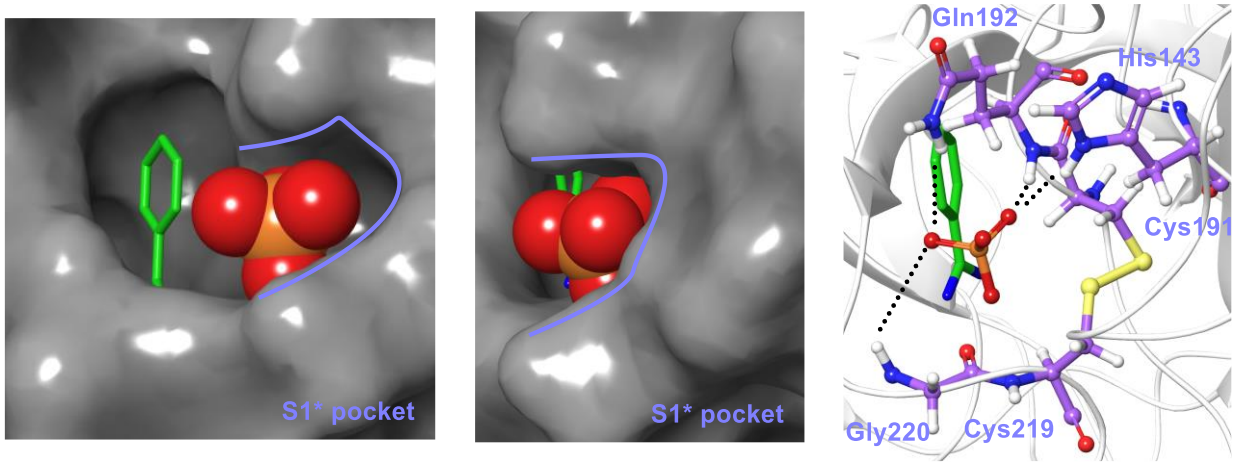

Figure 5-3. Two views of the S1* pocket of FXIIf and residues delimiting it. Black dotted lines: H-bonds.

5.3.2. Design and Retrosynthesis

Our idea was to synthesize an analog of our most potent identified inhibitor, nafamostat, that would also bind to the S1* pocket in order to potentially improve its potency and its selectivity toward FXIIf. Mimicking the sulfate present in the crystal structure of FXIIf seemed promising and we thus decided to add to nafamostat a sulfonamide moiety, which would play the role of a sulfate surrogate, resulting in compound **139** (Scheme 5-14).

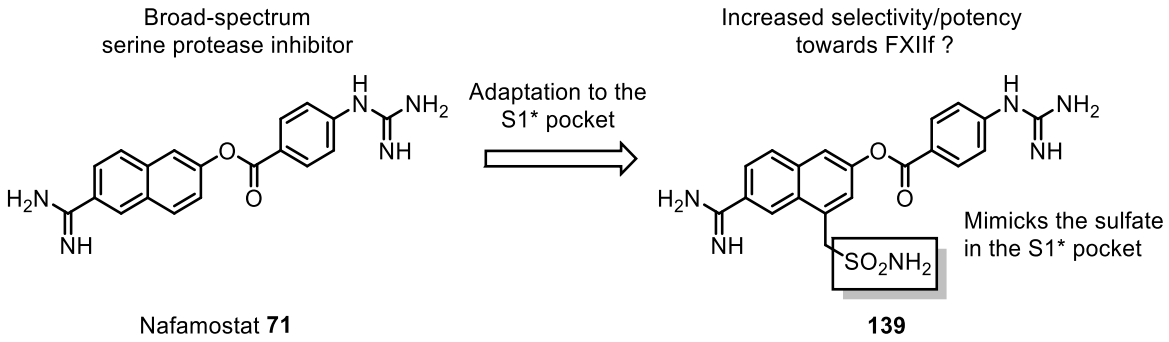

Scheme 5-14. Rationale of the design of compound 139.

Compound **139** was docked within the active site of FXIIf using the XP mode of Glide and the pose with the lowest GlideScore is shown (Figure 5-4). As usual, the amidinium interacts *via* an H-bond-mediated ionic bridge with Asp189. The carbonyl of the ester group interacts with the backbone amidic hydrogen of Gly193 and the phenyl group forms π-π stacking with His57.

The guanidinium, however, is positioned too far from Asp60A and is not involved in any interaction with the enzyme. The sulfonamide moiety binds the S1* pocket, but in a slightly different way than the sulfate group (zoom in Figure 5-4). The oxygen atoms of the sulfonamide are involved as H-bond acceptors with the amidic hydrogens of the side-chain of Gln192 and with the backbone amidic hydrogens of Gly220. One hydrogen atom of the sulfonamide moiety is involved in H-bonding with the backbone carbonyl moiety of Gly220.

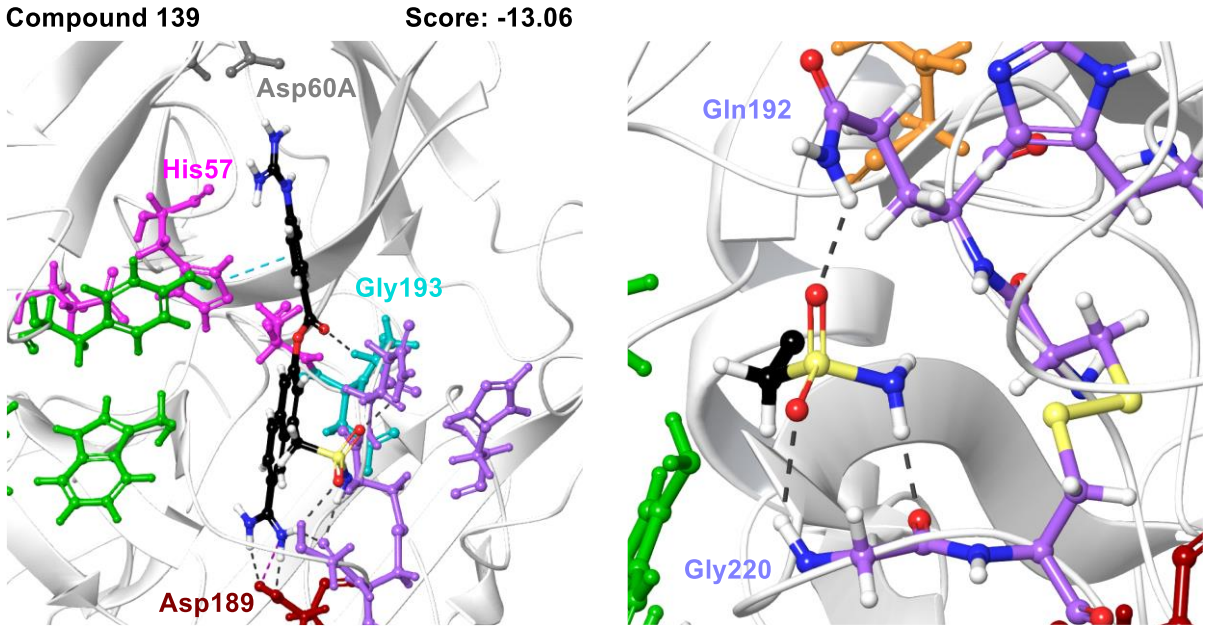

Figure 5-4. Molecular docking of compound 139 in the binding site of FXIIf and zoom on the S1* pocket. In th right picture, the rest of compound 139 is omitted for clarity.Brown: S1 pocket. Pink: catalytic triad. Turquoise: oxyanion hole. Green: S3/4 pocket. Orange: H1 pocket. Grey: Asp60A. Violet: S1* pocket. Black dotted lines: H-bonds. Blue dotted lines: π-π stackings. Pink dotted lines: ionic bridges.

Overall and although the guanidinium does not interact anymore with Asp60A, the additional interactions caused by the addition of this sulfonamide moiety seem favorable, as indicated by the -13.06 docking score, the lowest reported in this thesis so far.

The retrosynthesis of compound **139** is described (Scheme 5-15). Target ester **139** can be fragmented into commercially available carboxylic acid **140** and naphthol **141**. The benzyl sulfonamide moiety can be converted from the corresponding benzyl bromide **142**, arising itself from the radical bromination of methylnaphthalene **143**. The protected amidine moiety can be simplified into a nitrile group, leading to compound **144**. As previously in this work, the cyano group can be integrated from the corresponding naphthyl halide **145**, accessible by aromatic halogenation of compound **146**. Eventually, naphthyl ether **146** can be seen as the formal condensation of plain benzyne **147** and of dienol **148**, a tautomer of ketone **149**, previously described in the literature.

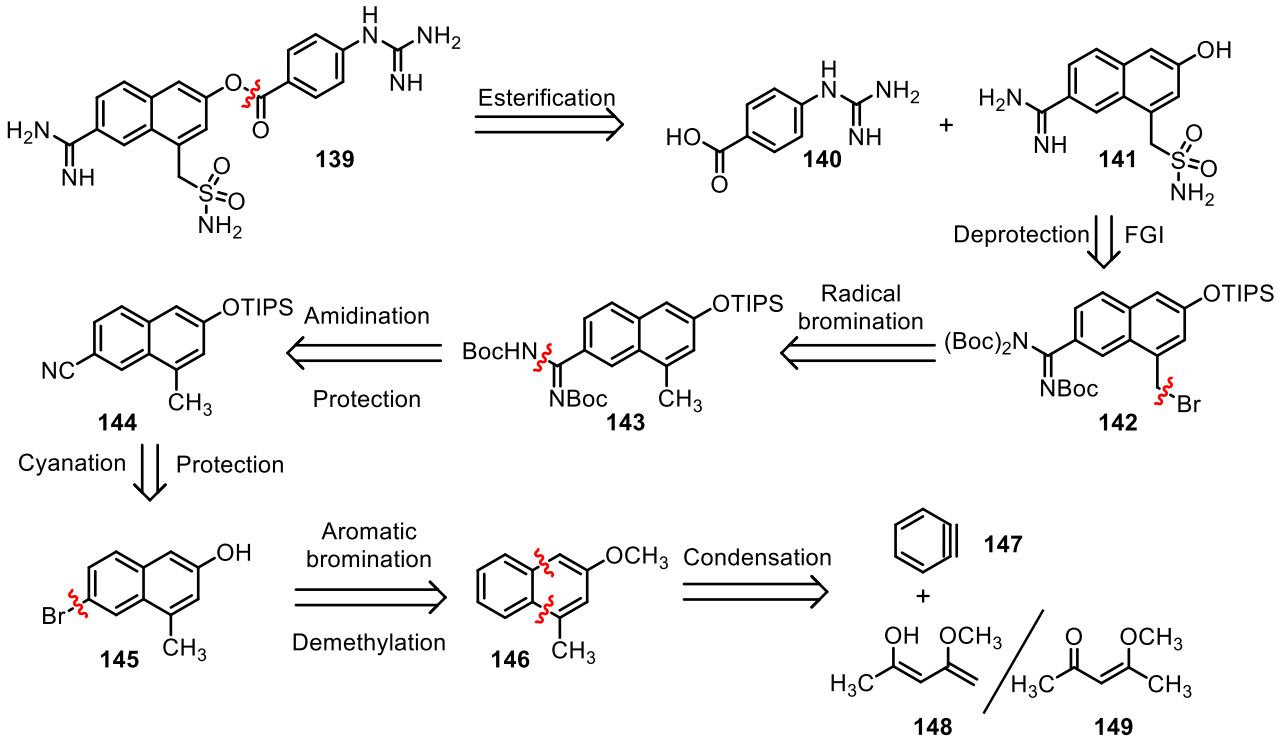

Scheme 5-15. Retrosynthesis of the sulfonamide derivative 139.

5.3.3. Synthesis

The following synthetic work was performed by Oliver Garot, a master student who worked under my supervision. Treatment of acetylacetone with CH_3OH in the presence of $HC(OCH_3)_3$ and PTSA yielded methyl enol ether **149** (Scheme 5-16).[229] The reaction between this compound and bromobenzene in the presence of $NaNH_2$ and *t*BuONa in THF at 55 °C, followed by an acidic work-up, afforded methoxynaphthalene **146**.[230]

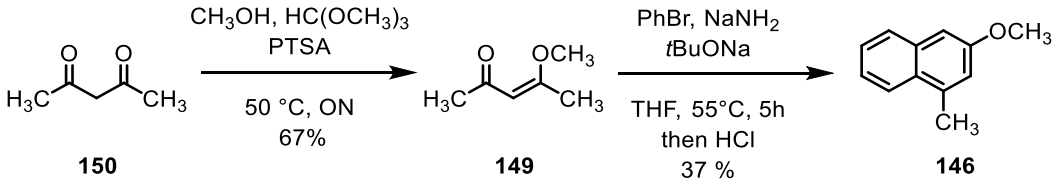

Scheme 5-16. Synthesis of naphthol ether 146.

Two general mechanisms can be suggested for this last reaction.[231,232] $NaNH_2$ is poorly soluble in THF, but it forms soluble complexes with *t*BuONa, improving its reactivity.[233] In a first possible mechanism (Scheme 5-17), the resulting complex base generates benzyne **147** from bromobenzene **122** and vinylogous enolate **152** from α,β-unsaturated ketone **151**, respectively. α-Addition of enolate **152** onto benzyne **147** leads to the formation of compound **153**, which undergoes a 4-*exo*-trig cyclization to form 4-membered ring **154**. This alkoxide collapses into a resonance-stabilized anion **155**, which then undergoes a a 6-*exo*-trig cyclization to form 6-membered ring **156**.

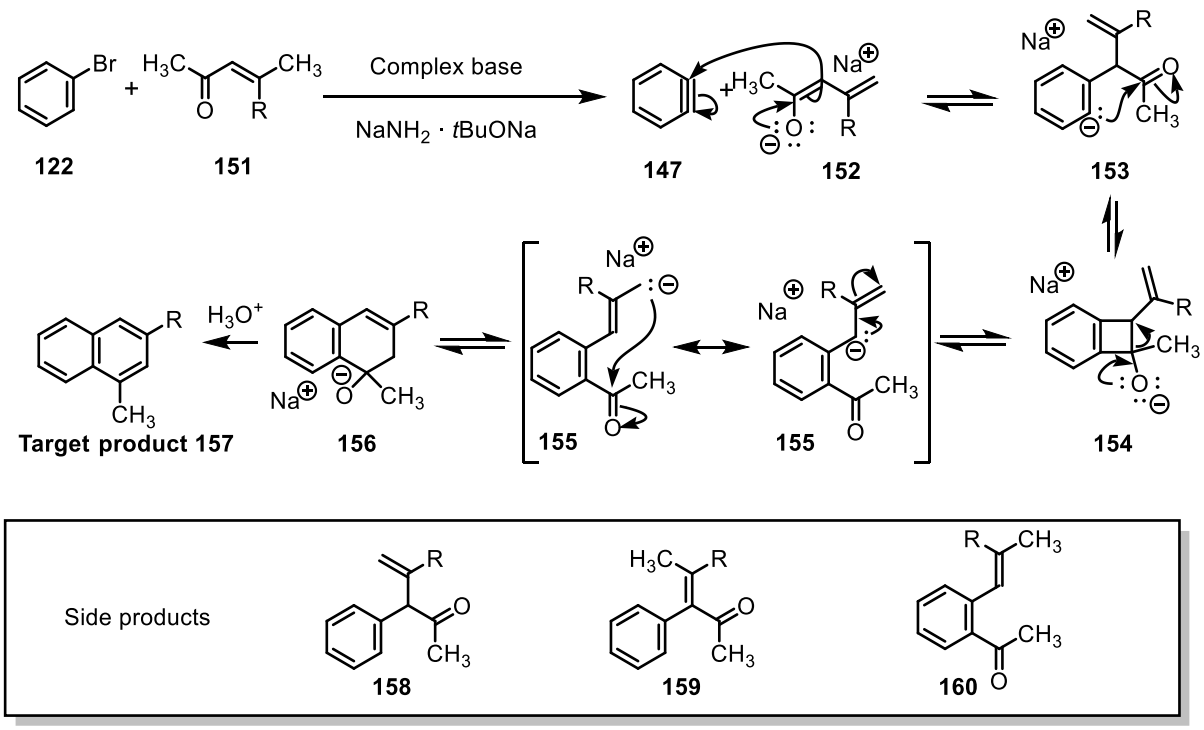

Scheme 5-17. First possible mechanism of formation of naphthalene 157 from bromobenzene 122 and α,β-unsaturated ketone 151.

Treatment in an aqueous acidic medium allows elimination of water and rearomatization, yielding target product **157**. This mechanism accounts for the formation of side products **158**, **159**, and **160** which are respectively trapped forms of intermediates **153** and **155a-b**.[231]

In a second possible mechanism, γ-addition of enolate **152** onto benzyne **147** leads to the formation of compound **153'** (Scheme 5-18). The resulting phenyl anion then adds onto the ketone moiety, form 6-membered ring **156'.** Once again, Treatment in an aqueous acidic medium allows once again elimination of water and rearomatization, yielding target product **157**.

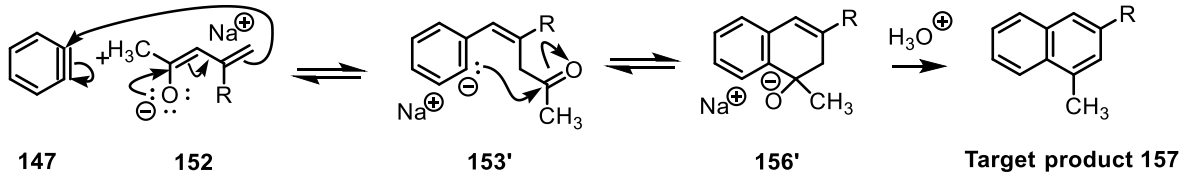

Scheme 5-18. Second possible mechanism of formation of naphthalene 157.

Next, methoxynaphthalene **146** was demethylated in the presence of BCl_3 and TBAI in CH_2Cl_2 at -84 °C to yield naphthol **161** (Scheme 5-19).[230]

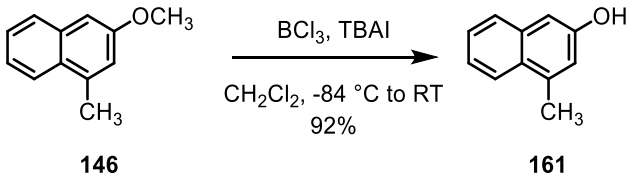

Scheme 5-19. Demethylation of naphthol ether 146.

The selective 6-bromination of naphthol **146** is to be performed in a multi-step process, based on the literature (Scheme 5-20).[234] First, the naphthol should be dibrominated with Br_2 at the 1- and 6-positions to form aryl dibromide **162**. Second, treatment of this species with tin will selectively reduce the bromo at the 1-position, yielding 6-bromonaphtol **145**.

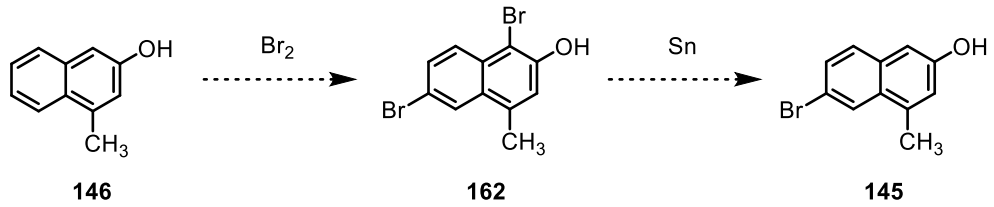

146 **162** **145**

Scheme 5-20. Synthetic plan towards naphthol 145.

We first investigated the right conditions for the dibromination step and found that treatment with 2 equivalents of Br_2 in AcOH at 70 °C successfully afforded 1,6-dibromo-2-naphthol **162** (Table 5-1, entry 1).

The temperature is a decisive parameter for the outcome of the reaction. At 60 °C, only a monobromination occurs and 1-bromo-2-naphthol **163** is the only product detected by ^{1}H NMR (entry 2). On the contrary, at reflux, radical bromination is initiated and overbrominated naphthol **164** is formed as a side-product (entry 3).

Table 5-1. Dibromination of naphthol 146. N.I. = Non isolated

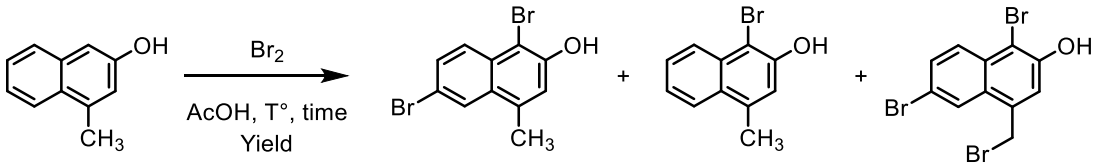

146 **162** **163** **164**

entry	T°	time	**162** yield	**163** yield	**164** yield
1	70 °C	3 h	56 %	0 %	0 %
2	60 °C	0.5 h	0%	Only product, N.I.	0%
3	Reflux	3 h	0%	Ratio **163**/**164** : 6:1. N.I.	

We then tried to perform the dibromination followed directly by the selective monoreduction, in a one-pot process (Table 5-2). Naphthol **146** reacted according to our optimized dibromination conditions, before the direct addition of tin to the reaction medium. Debromination was incomplete after 3 h in the case of our first trial (entry 1). Following the advice of the original publication,[234] we added water to the medium and observed complete conversion after the same amount of time (entry 2). We hypothesized that water acts as an efficient HBr trap, and that the latter reacts with metallic tin to form $SnBr_2$, the effective reducing agent in this reaction.

Table 5-2. Selective monobromination of naphthol 146. N.I. = Non isolated

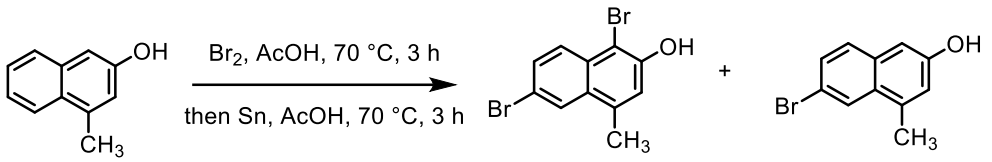

146 **162** **145**

entry	presence of water	**162** yield	**145** yield
1	No	25 %	67 %
2	Yes	0 %	61 %

Compound **145** then reacted with TIPSCl in the presence of imidazole in DMF to form protected naphthol **145a** (Scheme 5-21). Cyanation was then attempted using the same conditions we have previously used in this thesis for this transformation : $K_4[Fe(CN)_6]$ in DMAc at 120 °C in the presence of $Pd(OAc)_2$ and Na_2CO_3.[166] However, using ^{13}C NMR, nitrile **144** was not detected in the crude product, and the conditions led to the deprotection of the TIPS, yielding compound **145** as the sole product. This is where our synthetic efforts stand as of October 2020.

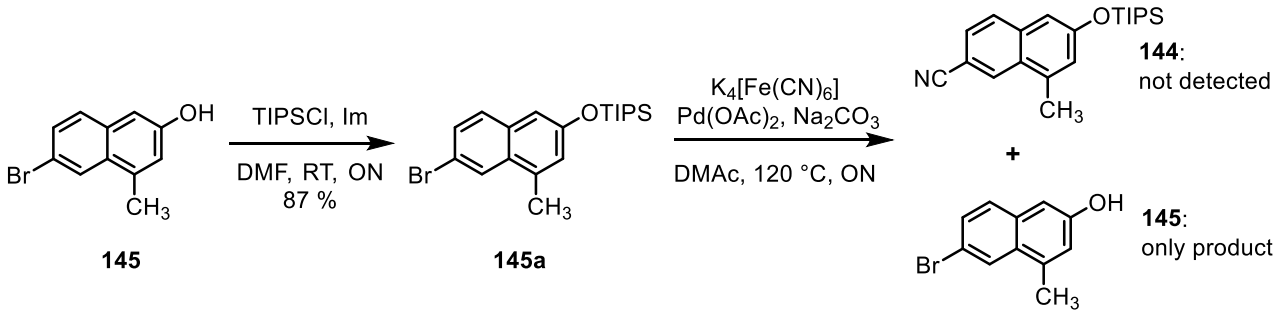

145 **145a**

Scheme 5-21. Attempts at synthesizing compound 144.

In the next few weeks, our group will change its approach toward compound **144**. Modern cyanation protocols are compatible with electron-rich substrates and tolerate free hydroxyl groups.[235–237] Compound **145** will first react with $K_4[Fe(CN)_6]$ in DMAc at 140 °C in the presence of $PdCl_2$, $P(tBu)_3$ and Na_2CO_3 (Scheme 5-22).[235] Resulting cyanonaphthol **145b** will then be protected with a TIPS using the same conditions as previously, yielding compound **144**.

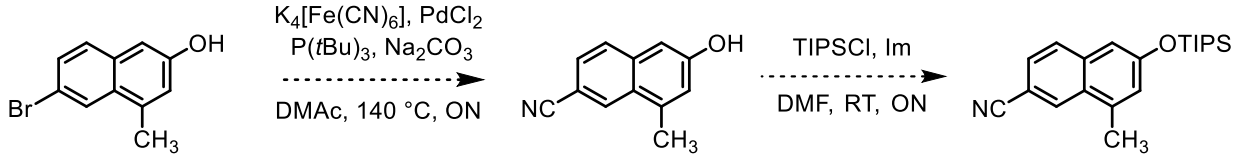

146 **145b** **144**

Scheme 5-22. Synthetic plan toward compound 144.

Next, the following transformations will be performed (Scheme 5-23). Nitrile **144** will be transformed into protected amidine **143** using the LiHMDS / $(Boc)_2O$ protocols used in this thesis. The bromination of the benzylic methyl group will take place in the presence of NBS and AIBN. Substitution of the benzylic bromide with Na_2SO_3, followed by transformation of the sulfonate into sufonamide and TIPS deprotection will yield compound **141**. A reaction between phenol **141** and acid **140a** in the presence of DCC and pyridine will lead to ester **139a**, and all Boc groups will be removed in TFA to yield target compound **139** (Warning, DCC is skin-irritant and potentially carcinogenic, work with caution if used). FXIIf inhibition assays will then be performed.

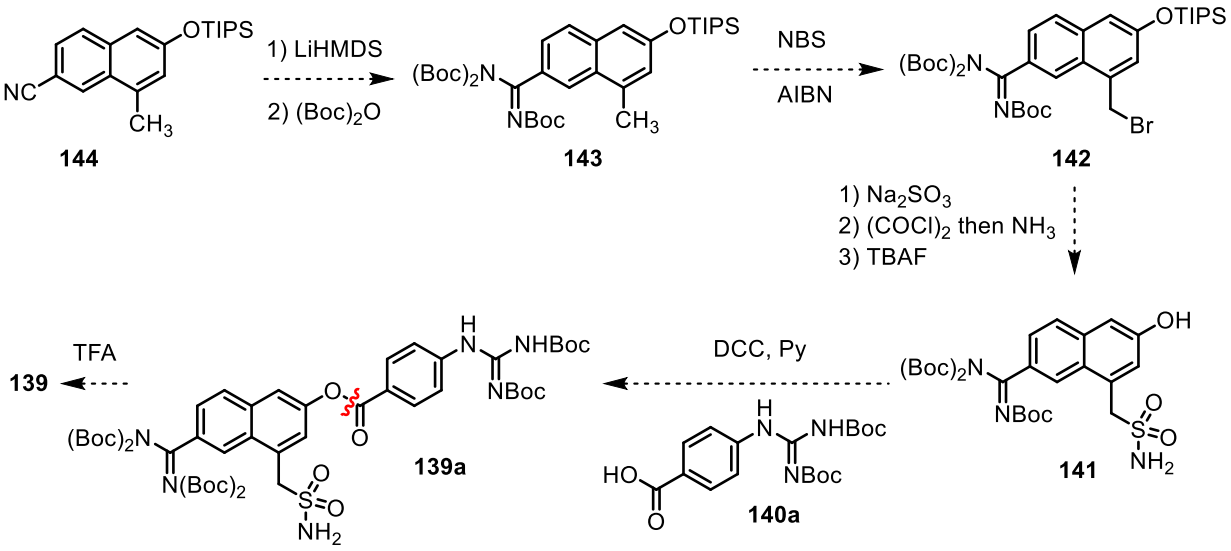

Scheme 5-23. Synthetic plan toward target compound 139.

5.4. An Indole Derivative of Pentamidine

5.4.1. Design

Pentamidine (**70**) represents a promising hit compound thanks to its 32 µM IC_{50} on FXIIf. However, as it contains numerous rotatable bonds, its binding entropy to FXIIf is likely highly unfavorable. To limit this adverse contribution, rigidifying the structure is a viable strategy. Moreover, experimental screening of our in-house library showed that bicylic polyaromatic amidines are more potent than plain benzamidines.

Thus, we suggested indole **165** as a more rigid – and hopefully more potent – pentamidine analog (Scheme 5-24). The indole core was chosen as a rigidifying group based on the fact that 4-aminobenzamidine **27** is a more potent FXIIf inhibitor than benzamidine, thanks to its ability to form H-bonds via its amino moiety.

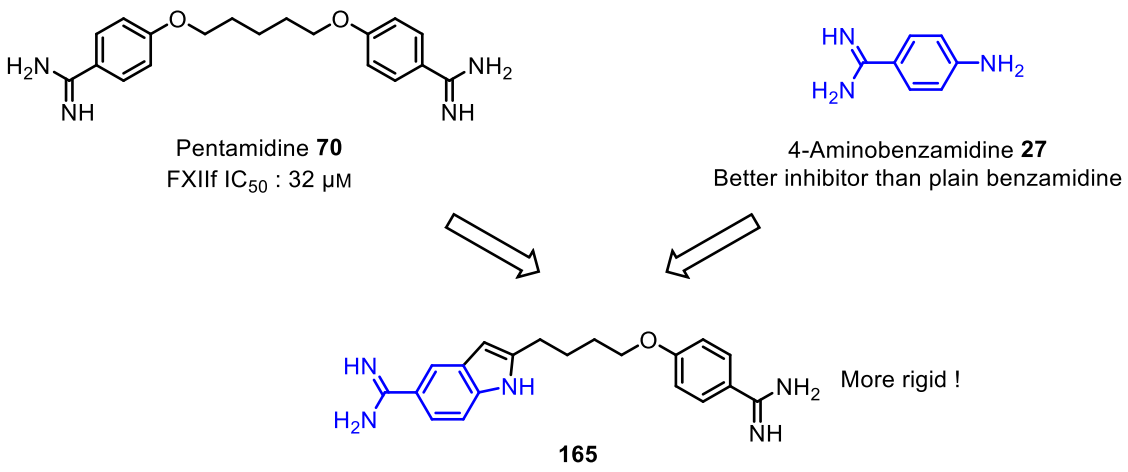

Scheme 5-24. Rationale of the design of compound 165.

Compound **165** was docked within the active site of FXIIf using the XP mode of Glide. The pose with the lowest GlideScore is shown and can be compared to that of plain pentamidine (Figure 5-5). The amidinium moieties interact with Asp189 and Asp60A *via* H-bond-mediated ionic bridges. The indole core is able to form T-shaped π-π stacking with His57. Surprisingly, the indolic hydrogen is not involved in any interaction with the enzyme. These additional interactions encouraged us to synthesize compound **165**.

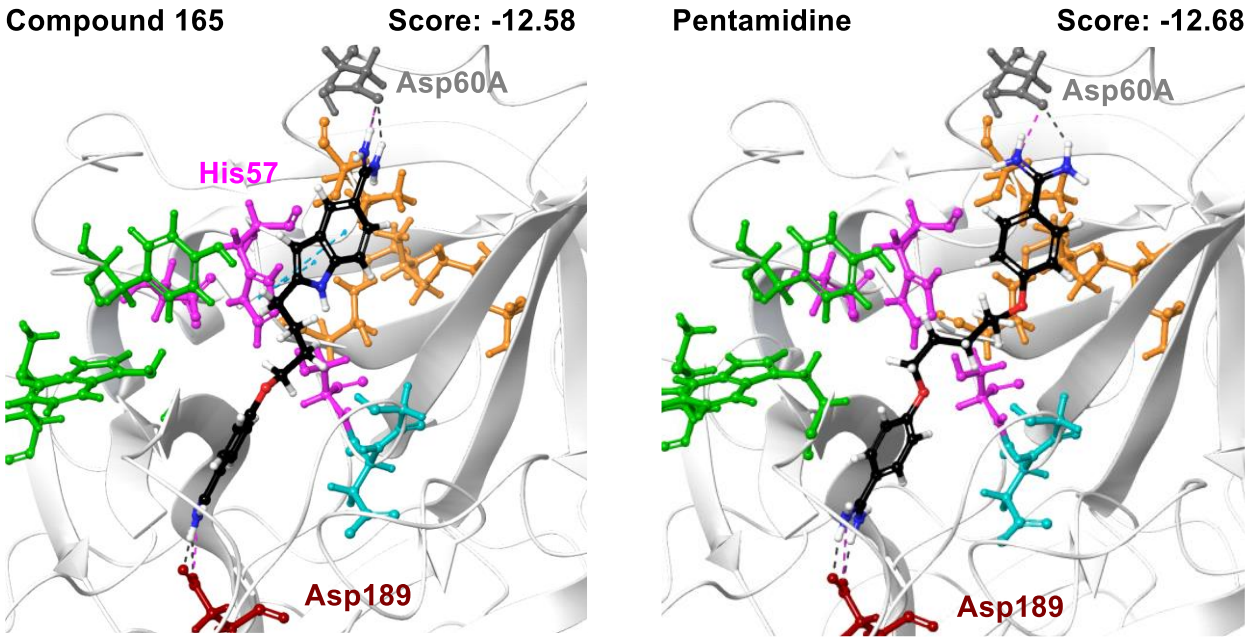

Figure 5-5. Molecular docking of compound 165 and of pentamidine in the binding site of FXIIf. Brown: S1 pocket. Pink: catalytic triad. Turquoise: oxyanion hole. Green: S3/4 pocket. Orange: H1 pocket. Grey: Asp60A. Black dotted lines: H-bonds. Blue dotted lines: π-π stackings. Pink dotted lines: ionic bridges.

5.4.2. First retrosynthesis

The retrosynthesis of target molecule **165** is the following (Scheme 5-25, next page). The alkane chain will be derived from the hydrogenation of alkyne **166**. The aryl-alkyne bond can be obtained *via* a Sonogashira coupling between terminal alkyne **167** and indolyl iodide **168**.

The ether bond in compound **167** can be obtained from a Mitsunobu reaction between homopropargylic alcohol **169** and the deprotected form of compound **170**. Compound 1**70** will come from the LiHMDS amidination of commercially available 4-cyanophenol **171**. In parallel, the amidine moiety of compound **168** can arise from the LiHMDS amidination of nitrile **172**, and the iodide can be easily incorporated from commercially available indole **173**.

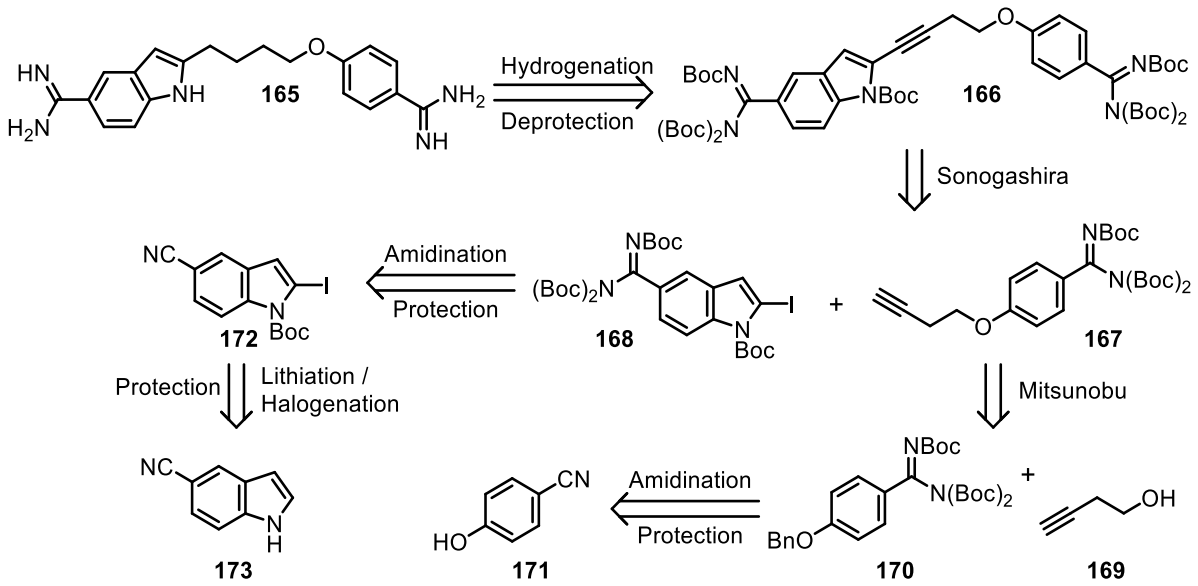

Scheme 5-25. Retrosynthesis of compound 165.

5.4.3. First attempt at synthesis

4-Cyanophenol **171** reacted with BnBr in the presence of NaH in DMF at 60 °C to yield protected alcohol **174** (Scheme 5-26).[238] Treatment with LiHMDS in THF at reflux, followed by hydrolysis in concd. aqueous HCl then rebasicification allowed the isolation of amidine **175**.[197]

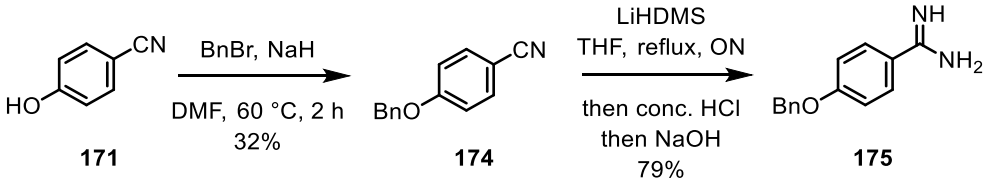

Scheme 5-26. Synthesis of benzamidine 175.

Earlier in this thesis, we described several examples of monoprotection of benzamidines with $(Boc)_2O$ in acetone, yielding quantitatively the desired product. In the case of amidine **175**, this reaction was reproducibly sluggish, leading to a complex mixture and yielding at best a mere 9% of contaminated monoprotected compound **176** (Scheme 5-27).

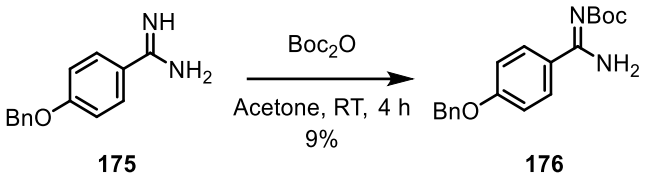

Scheme 5-27. Synthesis of mono-Boc protected amidine 176.

Since we were at the very beginning of the synthesis and for pragmatic reasons, we decided to switch retrosynthesis. In the absence of evidence, a plausible hypothesis for the failure of the reaction is that product **176** is unstable and spontaneously eliminates *tert*-butoxide thanks to the electron-donating effect of the benzyloxy group leading to isocyanate **177**, further leading to degradation products (Scheme 5-28).

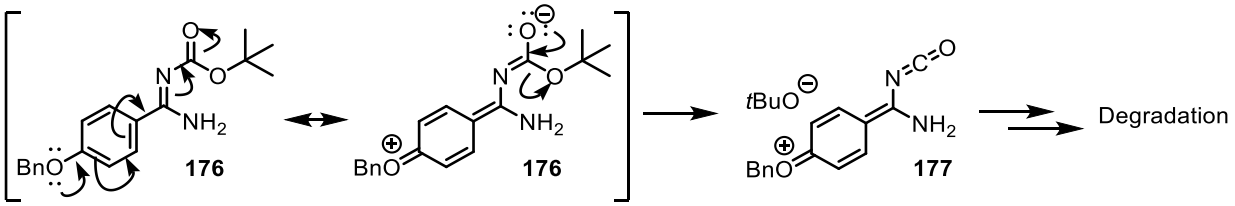

Scheme 5-28. Hypothetical mechanisms of spontaneous degradation of compound 176.

A similar reaction, the one-pot transformation of anilines into phenyl isocyanates in the presence of Boc_2O, was already described in the literature[239] and is indeed favored by electron-donating groups on the phenyl moiety.[240]

5.4.4. Second retrosynthesis

The second retrosynthesis of target molecule **165** is similar to the previous one but the amidination is performed late-stage (Scheme 5-29). Target compound **165** will come from the hydrogenation of alkyne **178**. The resulting bis-acyloxyamidine will be synthesized from bis-nitrile **179**. The aryl-alkyne bond can be obtained via a Sonogashira coupling between indolyl iodide **172** and terminal alkyne **180**. The iodide in compound **172** can be easily incorporated from commercially available indole **173**. On the other hand, the ether bond in compound **180** can be obtained from a Mitsunobu reaction between commercially available homopropargylic alcohol **169** and 4-cyanophenol **171.**

5.4.5. Second attempt at synthesis

5-Cyanoindole **173** reacted with $(Boc)_2O$ in the presence of DMAP in CH_2Cl_2 to yield protected indole **181** (Scheme 5-30).[241] A selective lithiation at the 2-position with LDA in THF at -84 °C, followed by oxidative quench with I_2 afforded indolyl iodide **172.**[242]

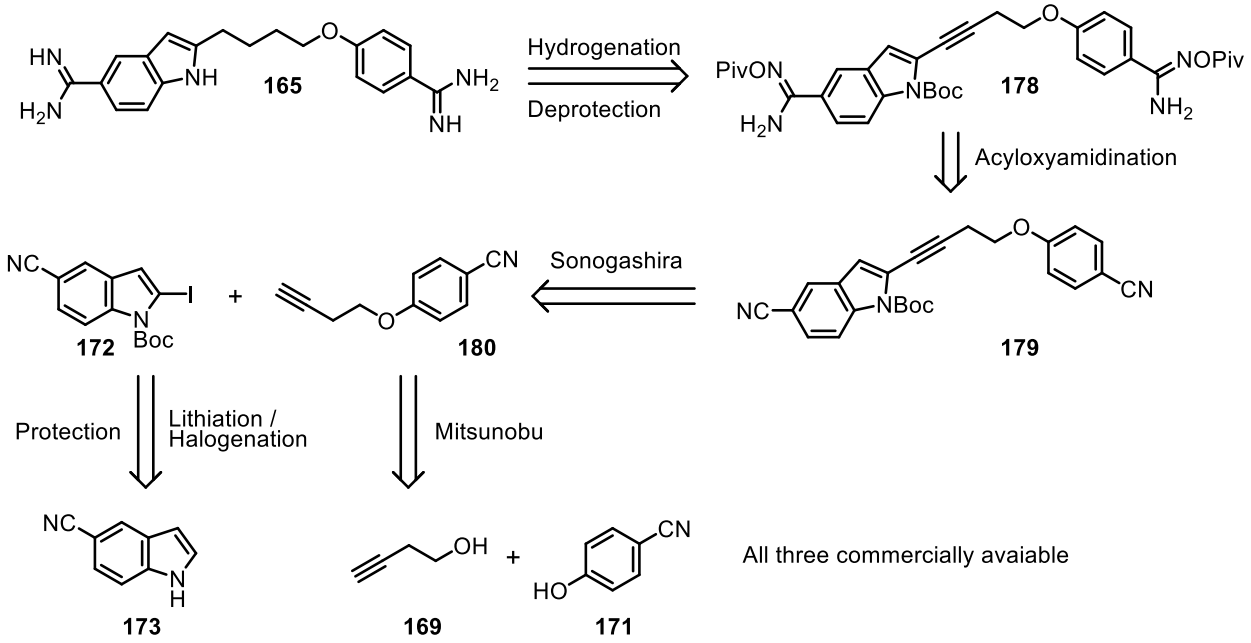

Scheme 5-29. Second retrosynthesis of compound 165.

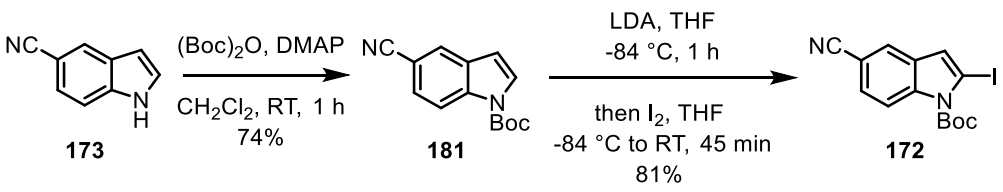

Scheme 5-30. Formation of indoyl iodide 172.

In parallel, homopropargylic alcohol **169** and 4-cyanophenol **171** were coupled *via* a Mitsunobu reaction in the presence of DIAD, PPh_3, and Et_3N in THF to yield ether **180** (Scheme 5-31).[243]

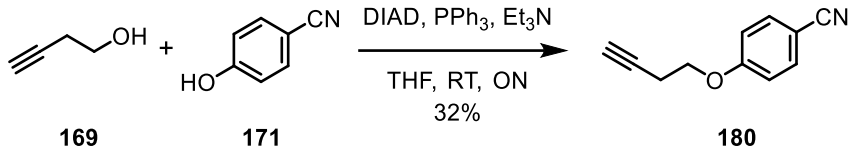

Scheme 5-31. Formation of ether 180 *via* a Mitsunobu reaction

Both synthesized indoyl iodide **172** and terminal alkyne **180** reacted in a Sonogashira coupling in the presence of $[Pd(PPh_3)_2Cl_2]$ and CuI in DIPA, leading to internal alkyne **179** (Scheme 5-32).[188] This is where our synthetic efforts stand as of October 2020.

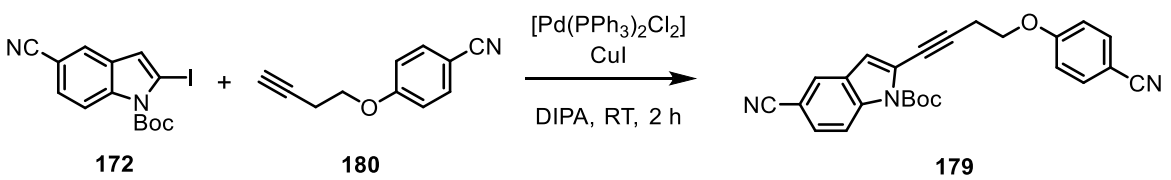

Scheme 5-32. Formation of internal alkyne 179 via a Sonogashira coupling.

In the next few weeks, our group will finish the synthesis. Using our improved protocol, dicyanide **179** will react with NH_2OH then PivCl to yield pivaloxyamidine **178,** and subsequent hydrogenation will lead to target compound **165** (Scheme 5-33).

5.5. Conclusions

In this chapter, with the help of molecular docking, we have envisaged the synthesis of three potential inhibitors of FXIIf, based either on nafamostat or on pentamidine

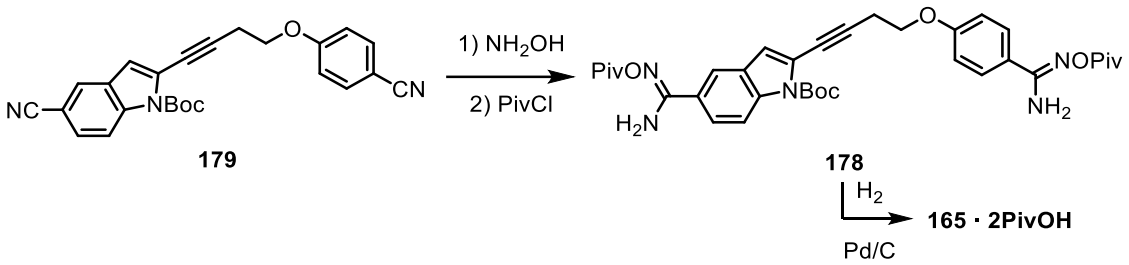

Scheme 5-33. Synthetic plan toward 165

A non-transesterifiable keto-analog of nafamostat was designed in order to improve its metabolic stability, using early-stage amidination in our retrosyntheses. Two of our resulting syntheses failed, probably because of the Boc groups present on the amidine. A third synthesis was initiated and is to be continued. When obtained, the compound will be tested on FXIIf and, if active, its elimination half-life could be evaluated in mice.

A sulfonamide analogue of nafamostat was designed in order to to mimic a sulfate group present in a pocket exclusive to FXIIf, in order to improve the selectivity of the inhibition. We once again envisaged early-stage in our retrosynthesis. Up to now, the synthesis was performed uneventfully and is to be continued. The compound will be tested on FXIIf and, if active, on FXa, FVIIa and thrombin in order to evaluate its selectivity.

Finally, an indole analogue of pentamidine was designed in order to rigidify the structure and to improve the potency of the inhibition. The synthesis using early-stage amidination failed, probably because of the electronic properties of our substrate. Traditional late-stage amidination was then envisaged and the synthesis is currently ongoing. The compound will be tested on FXIIf and, if more active than pentamidine, further refined.

Chapter 6: Conclusions and Outlooks

6.1. General Conclusions

In this thesis, we first got interested in triazole-, phenylguanidine- and benzamidine-based potential inhibitors FXIIf, using structure-inspired ligand design. We successfully managed to synthesize three generations of compounds and one model of a peptidomimetic collection. All compounds were tested for inhibition on FXIIf. By analyzing the dose-inhibition curves, we suggested that some of our key hit compounds forms colloids at higher concentrations, sequestrating the enzymes in a non-specific manner. The results related to the soluble compounds allowed us to draw three important conclusions: benzamidines are better at inhibiting FXIIf than phenylguanidines, the triazole moiety does not add any potency to the compounds, and bis-cationic compounds are better hit compounds than mono-cationic compounds. We then logically wanted to synthesize more bis-amidines and chose to favor early-stage over late-stage amidination

Indeed, late-stage amidination is poorly compatible with complex substrates with divergent syntheses as used in medicinal chemistry. Based on the literature, we successfully synthesized small Boc-protected benzamidines and showed that they were compatible with classical Pd-catalyzed cross-coupling and with substitution reactions. This practical addition to the organic toolbox opened the door for more expedient and more complex synthesis.

Thanks to this, we tackled the synthesis of three bisamidines compounds, based on the structure of two hit compounds identified by literature review and by vHTS of existing drugs: nafamostat and pentamidine. Each of these compound aims at improving a pharmacological parameter. The keto derivative of nafamostat is meant to improve the metabolic stability of the compound. Its sulfonomadive derivative will improve its selectivity toward FXIIf. Finally, an indole derivative of pentamidine is meant to improve its potency. All syntheses have been successfully initiated using early-stage amidination, and are to be continued.

6.2. Outlooks

The potential future tasks that we suggest here have the same goal as the one mentioned in the beginning of this thesis: generating hit compounds that could be used as numerous starting points toward lead compounds (Scheme 6-1).

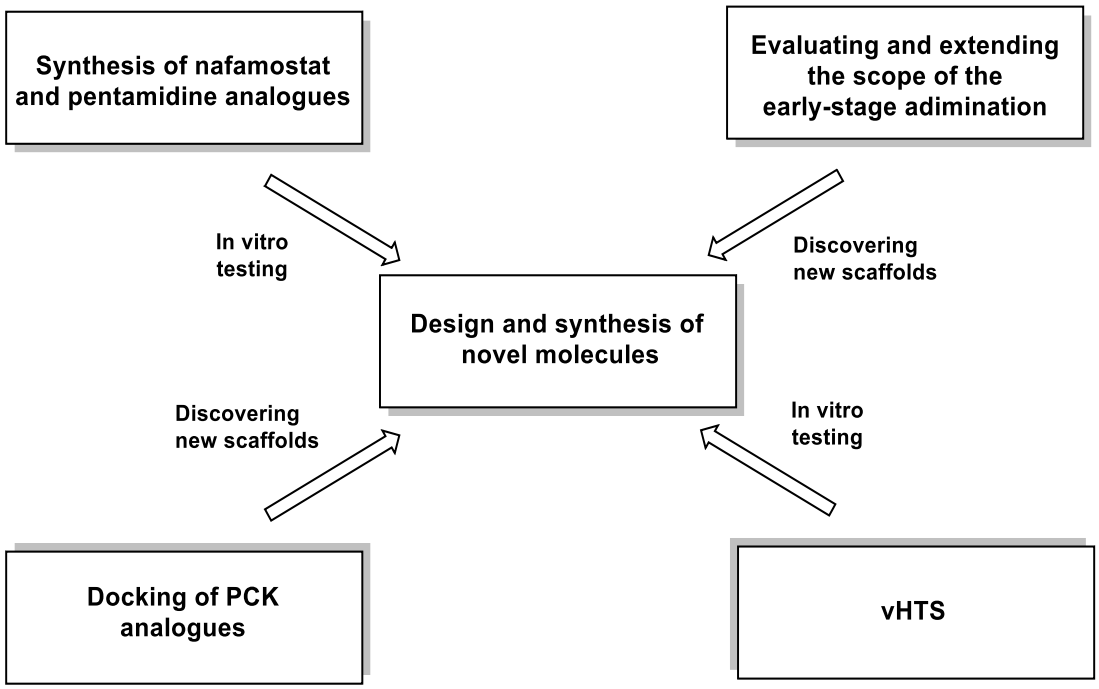

Scheme 6-1. Possible outlooks to pursue the work of this thesis.

First, the synthesis of our pentamidine and nafamostat analogs, currently ongoing in our groupn should be finished. Their potency will be evaluated in vitro by performing the same assay used throughout this thesis. Their selectivity will be assessed by comparing their potency against several other key serine proteases, namely thrombin, FXa and FVIIa. Finally, their metabolic stability will be estimated using the microsomal stability assay. The results of the different compounds in these assays will allow us to further refine the design of novel molecules.

Second, as amidines represent an ideal starting point to synthesize hit compounds, an early convenient, versatile synthetic method, adapted to medicinal chemistry, should be readily available. Our newly developed early-stage amidination, involving a tris-Boc protection of the amidine, could fill this gap. Methodology experiments could be carried out to evaluate if this strategy can be extrapolated to other aromatic cores than a plain phenyl, such as heteroaromatics and biaromatics, in order to introduce more structural diversity (Scheme 6-2). Similar experiments could be performed to check if the tris-Boc protected amidine core in compatible with other types of reactions than those tested in the thesis, namely amide formation, nucleophilic aromatic substitution and electrophilic reaction with amine (Scheme 6-2), all three in the top five most used transformations in medicinal chemistry.[201] Together, these experiments will allow us to evaluate the full scope of our early-stage amidination protocol and help us further to synthesize in an efficient way specific potential hit compounds.

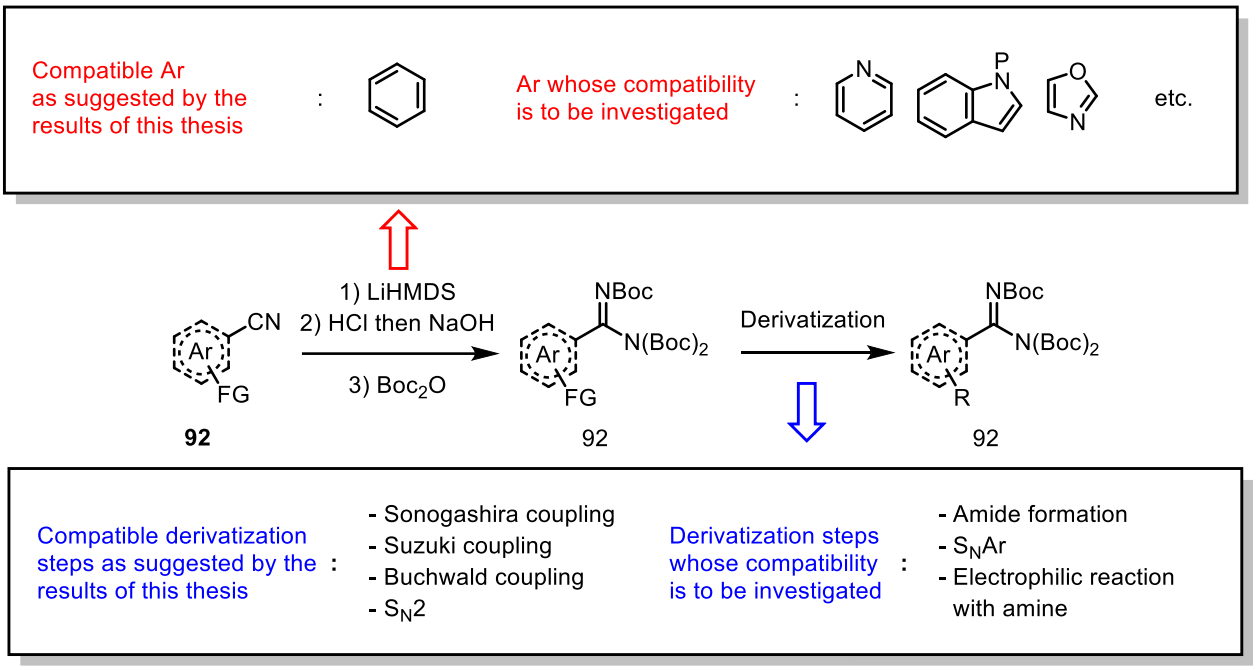

Scheme 6-2. Early-stage amidination: what is known to be compatible and what could be further investigated.

Third, with the help of the new FXIIa structural data, promising scaffolds discovered years ago could be revisited via molecular docking. For example, the D-Pro-Phe-Arg sequence (Scheme 6-3) is present both in both inhibitor PCK and in substrate S-2302, suggesting a potent interaction with FXIIa. Dozens of bioisosteric derivatives could be easily generated in silico and docked into FXIIa, which would give insights on how to further improve the potency and the selectivity of such a sequence. Because of its synthetic feasibility, an a *priori* promising candidate to be docked is compound **182** (Scheme 6-3).

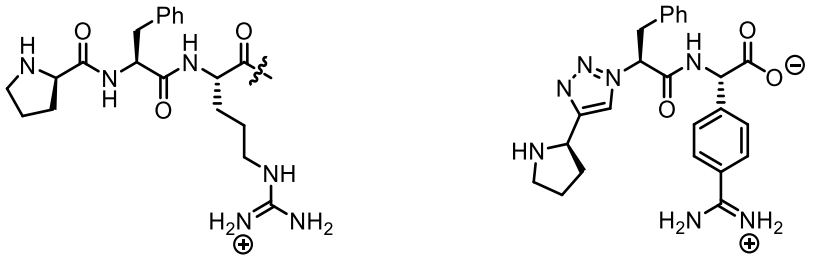

D-Pro-Phe-Arg **182**

Scheme 6-3. Structures of the D-Pro-Phe-Arg sequence and of compound 182.

The triazole group would act as an isostere of the N-terminal peptide bond. This modulation would improve the overall metabolic stability of the compound by suppressing the risk of N-terminal degradation. The benzamidinium group would act as a more rigid isostere of the amidine side-chain, improving binding by decreasing unfavorable entopic effects. Finally, the carboxylate would mimic the tetrahedral oxyanion and might be able to perform charge-mediated H-bonds with

the oxyanion hole and Ser195. Trifluoromethylketone or ketoamide warheads can also be envisaged instead of a carboxylate.[244]

The retrosynthesis of such as scaffold would indeed be straightforward and involves a triazole and an amide disconnection leading to the three fragments **183-185.** Alkyne **183** and azide **184** are both already described in the literature [245,246] and are directly derived from two amino acids, D-proline and L-phenylalanine. 4-L-Bromophenylglycine (**185**) is commercially available.

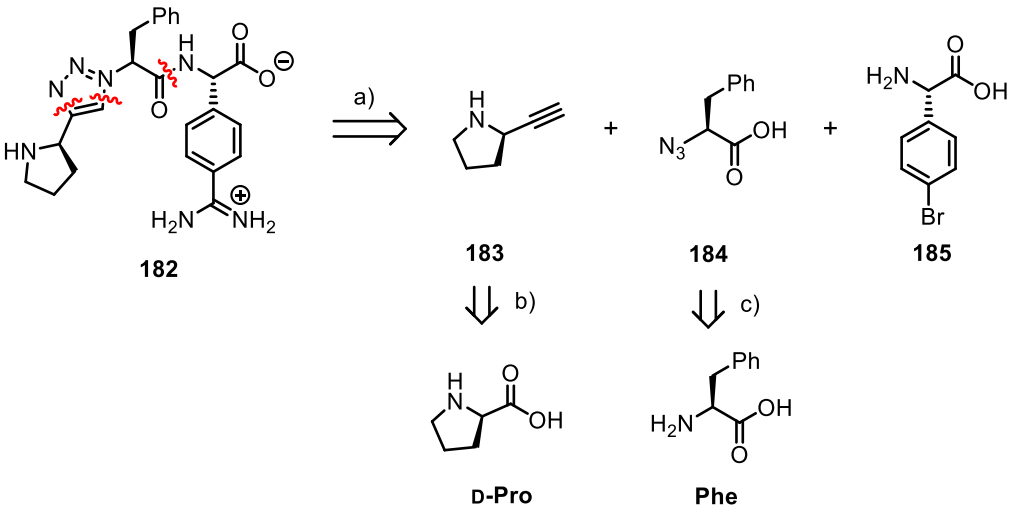

Scheme 6-4. Retrosynthesis of compound 182. a) 1,3 Dipolar cycloaddition and amide formation. b) Seyferth-Gilbert homologation and reduction. c) Azidation.

Finally, a vHTS using Glide and the MolPort virtual chemolibrary, containing more than 7 million commercial available compounds, was initiated to identify which entities could potentially be potent towards FXIIf. The virtual hit compounds will be ordered and tested on FXIIf. If active, those entities could be integrated, for example, in the scaffold of pentamidine or nafamostat to lead to novel molecules with better potency and selectivity.

Thanks to the combined efforts of medicinal chemists and biologists all over the world, the way toward small non-peptidic inhibitors of FXIIa, and commercial inhibitors of FXIIa in general, is now more accessible than ever. From a curious coagulation factor to a key enzyme involved in numerous metabolic pathways, the Factor XII emerged as a promising therapeutic target for a whole range of medical conditions, and we may be close to uncover the true potential of the heritage of John Hageman.

Chapter 7: Experimental part

7.1. Instrumentation

Thin layer chromatography (TLC) was performed using Merck aluminum silica gel TLC plates and monitored by UV light at 254 nm, *p*-anisaldehyde or $KMnO_4$.

Purifications through **adsorption silica chromatography columns** were performed using *Merck Gerduran* silica gel 60 (40-63 μm). **Flash chromatography** refers to the use of an automated *Büchi* Sepacore device.

Melting points (MP) were measured in a *Büchi* Melting Point B-545 in open capillaries, without post-correction.

Nuclear Magnetic Resonance spectra (^1H, ^{13}C NMR) were acquired on a *Jeol* JNM EX-400 (^1H 400 MHz, ^{13}C 100 MHz) or EX-500 (^1H 500 MHz, ^{13}C 125 MHz). Chemical shifts are reported in ppm downfield, from tetramethylsilane using the residual solvent signals as an internal reference ($CDCl_3$ δ_H = 7.26 ppm, δ_C = 77.16 ppm ; CD_3OD δ_H = 3.31 ppm, δ_C = 49.15 ppm ; DMSO-*d6* δ_H = 2.54 ppm δ_C = 39.52 ppm ; acetone-*d6* δ_H = 2.05 ppm, δ_C = 29.84 ppm). The resonance multiplicity is described as s singlet, d doublet, t triplet, q quartet, dd doublet of doublet, m multiplet and br broadened signal. All spectra were recorded at RT unless specified otherwise.

Infrared absorption spectra (IR) were acquired on a *Perkin-Elmer* Spectrum Two FT-IR System UATR mounted with a diamond crystal on neat compounds unless otherwise stated. Selected absorption bands are reported by wavenumber (cm^{-1}). The spectra were measured between wavenumbers of 600-4000 cm^{-1}.

All activity assays were performed on a multi-mode microplate reader SpectraMax iD3 (Molecular Devices, San Jose, CA, USA) operated by SoftMax Pro version 7.0.3 (Molecular Devices, San Jose, CA, USA). The instrument was equipped with plate shaking, injectors and temperature control system (5 °C above the ambient temperature to 66 °C ± 1.0 °C).

7.2. Materials and Methods

Reagents were purchased reagent-grade from *Acros Organic*s, *Fluorochem, Fischer,* or *Sigma-Aldrich* and used without further purification unless otherwise stated. Deuterated solvents ($CDCl_3$, CD_3OD, DMSO-*d6*, and acetone-*d6*) were purchased from *Euriso-top*.

All reactions were performed under argon in dried solvents unless otherwise stated. Dry conditioning of the glassware was realized manually by heating the glassware with a heat gun under a flux of argon for 2 minutes. CH_2Cl_2, Et_2O, THF, and toluene were dried over a Pure Solv solvent purification system. Degassed solvents were obtained using three freeze-pump-thaw cycles.

Baths for low-temperature experiments were prepared as followed: ice / water (0 °C), CH_3CN / liquid N_2 (-46 °C), acetone / dry ice (-78 °C), EtOAc / liquid N_2 (-84 °C).

Evaporation and concentration under reduced pressure were performed at 40 °C unless otherwise stated and compounds were dried at a maximum pressure of 10 mbar. Column chromatography was performed using distilled technical grade solvents.

Transparent 96-well flat-bottom polystyrene NBS microplate were provided by Corning. Human plasma FXIIf was purchased from Molecular Innovations and was supplied as a 1.12 mg/mL solution. The buffer consisted of 4 mM NaOAc, 0.15 M NaCl at pH 5.3. Reported purity was > 95% by SDS-PAGE.

7.3. Synthetic Procedures

7.3.1. General Procedures

7.3.1.1. General procedures A and B: synthesis of aliphatic azides from aliphatic bromides

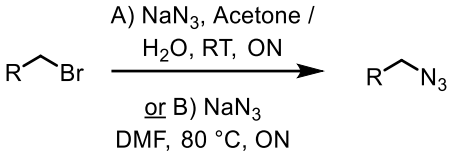

WARNING: Both organic and inorganic azides are potentially toxic and explosive.

- Personal protective equipment must be worn, including a laboratory coat, safety goggles, and gloves with adequate chemical resistance.
- Carry out the experiment in a fumehood with the sash positioned as low as possible.
- Do not concentrate azide-containing solutions using rotary evaporation above 40 °C.
- Do not expose azides to friction between two ground glass joints.
- Do not expose azides to acidic conditions to avoid the formation of toxic gaseous HN_3.
- Do not use metal spatulas for weighing or transferring azides to avoid the formation of explosive metal azides.
- With inorganic azides, do not use CH_2Cl_2 or $CHCl_3$ to avoid the formation of explosive di- or triazidomethane.

General procedure A. Protocol adapted from the literature.[167] A solution of NaN_3 (1.50 eq.) in water (0.22 mL/mmol of NaN_3) was added dropwise to a solution of the bromide (1.00 eq.) in acetone (0.83 mL/mmol of bromide). The reaction mixture was stirred ON at RT. Et_2O was added

and the organic layer was washed with water (3 ×) and dried over $MgSO_4$. The solvent was evaporated under reduced pressure to yield the desired *azide*.

General procedure B. Protocol adapted from the literature.[151] NaN_3 (1.50 eq.) was added to a solution of the bromide (1.00 eq.) in DMF (5 mL/mmol of bromide). The reaction mixture was stirred ON at 80 °C. After cooling down to rt, Et_2O was added and the organic layer was washed with brine (3 ×), water (1 ×), and brine again (1 ×) and dried over $MgSO_4$. The solvent was evaporated under reduced pressure to yield the desired *azide*.

7.3.1.2. General procedure C: synthesis of triazoles *via* click chemistry

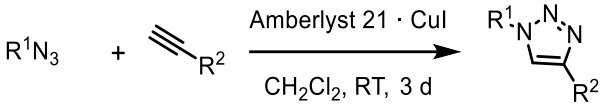

WARNING: Organic azides are potentially toxic and explosive.

- Personal protective equipment must be worn at all times, including a laboratory coat, safety goggles, and gloves with adequate chemical resistance.
- Carry out the experiment in a fume hood with the sash positioned as low as possible.
- Do not concentrate azide-containing solutions using rotary evaporation above 40 °C.
- Do not expose azides to friction between two ground glass joints.
- Do not expose azides to acidic conditions to avoid the formation of toxic gaseous HN_3.
- Do not use metal spatulas for weighing or transferring azides to avoid the formation of explosive metal azides.
- With inorganic azides, do not use CH_2Cl_2 or $CHCl_3$ to avoid the formation of explosive di- or triazidomethane.

The heterogeneous catalyst, Amberlyst A21 · CuI, was prepared by according to strictly the literature.[152]

Protocol adapted from the literature.[152] The azide (1.00 eq.) was added to a suspension of the alkyne (1.00 eq.) and Amberlyst A21 · CuI (62 mg/mmol) in CH_2Cl_2 (4 mL/mmol of azide). The reaction mixture was orbitally shaken at RT for 3 d. In the optional presence of a solid at the end of the reaction, CH_2Cl_2 was added until complete dissolution. The catalyst was removed by filtration and the solvent was evaporated under reduced pressure. The crude product was purified by recrystallization, trituration or column chromatography to afford the desired *triazole*.

7.3.1.3. General procedure D: synthesis of primary anilines from aromatic bromides

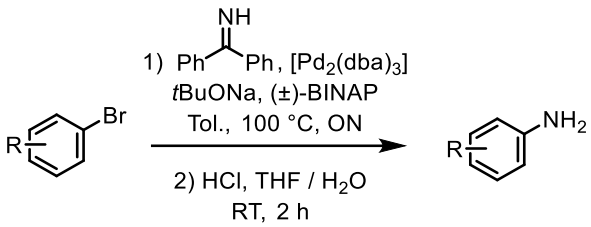

Protocol adapted from the literature.[149] *t*BuOH (1.40 eq.) was added to a suspension of NaH (60% in paraffin oil, 1.40 eq.) in toluene (4 mL/mmol of aryl bromide). The reaction mixture was stirred for 1 h. The aryl bromide (1.00 eq.), (±)-BINAP (0.03 eq.), and $[Pd_2dba_3] \cdot CHCl_3$ (0.01 eq.) were then added. The solution was degassed and benzophenone imine (1.20 eq.) was added. The reaction was stirred ON at 100 °C. After cooling down to RT, EtOAc was added and the organic layer was washed with water (3 ×) and dried over $MgSO_4$. The solvent was evaporated under reduced pressure and the residue was dissolved in THF (6 mL / mmol of aryl bromide). 2 M HCl (1.5 mL/mmol of aryl bromide) was added and the reaction mixture was stirred for 3 h. The reaction was quenched with aqueous saturated $NaHCO_3$ and CH_2Cl_2 was added. The organic layer was separated and dried over $MgSO_4$. The solvent was evaporated under reduced pressure and the residue was purified by column chromatography to afford the desired *aniline*.

7.3.1.4. General procedures E and F: synthesis of Boc-protected guanidines from anilines

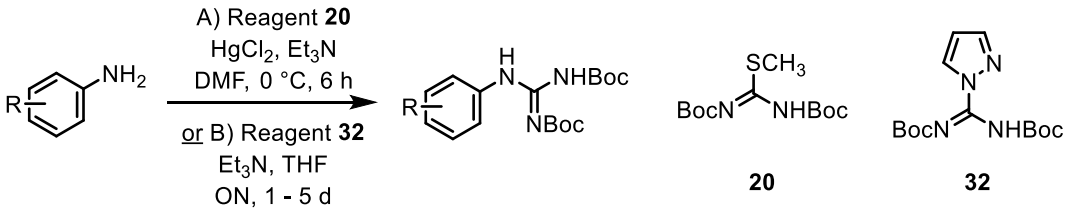

Protocol adapted from the literature.[153] $HgCl_2$ (1.10 eq.) was added at 0 °C to a solution of aniline (1.00 eq.), reagent **20** (1.05 eq.) and Et_3N (2.20 eq.) in DMF (6 mL/mmol of amine). The reaction mixture was stirred at 0 °C for 6 h. EtOAc was added and the suspension was filtered over Celite. The filtrate was washed with brine (3 ×), water (1 ×), and brine again (1 ×), and dried over $MgSO_4$. The solvent was evaporated under reduced pressure and the crude product was purified by column chromatography to afford the desired *protected guanidine*.

Protocol adapted from the literature.[161] Reagent **32** (1.00 eq.) was added to a solution of amine (1.00 eq.) and Et_3N (0.10 eq.) in THF or DMF (2 mL/mmol). The reaction mixture was stirred 1 to

5 d at RT. The solvent was evaporated under reduced pressure and the crude product was purified by column chromatography to yield the desired *protected guanidine.*

7.3.1.5. General procedure G: deprotection of Boc-protected guanidines into guanidinium salts

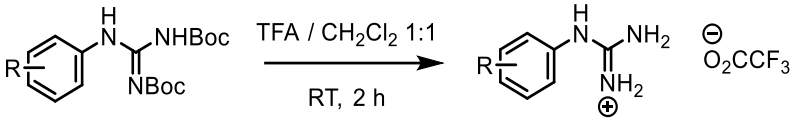

TFA (2 mL/mmol) was added to a solution of protected guanidine (1.00 eq.) in CH_2Cl_2 (2 mL/mmol). The reaction mixture was stirred at RT for 3 h and the solvent was evaporated. The oily residue was triturated with pentane, the solvent was evaporated, and the sample was dried over high vacuum. If the compound was still oily afterwards, the whole trituration process was repeated, until obtention of the *guanidinium salt* as a white powder or as a sticky reddish solid.

7.3.1.6. General procedure H: synthesis of benzonitriles from aryl bromides

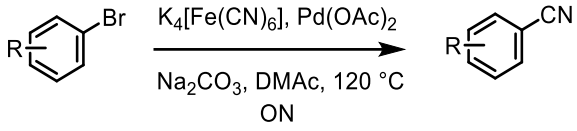

Protocol adapted from the literature.[166] A solution of aryl bromide (1.00 eq.), $K_4[Fe(CN)_6] \cdot 3H_2O$ (0.22 eq.), $Pd(OAc)_2$ (0.01 eq.), and Na_2CO_3 (1.00 eq.) in DMAc was degassed. The mixture was stirred ON at 120 °C. After cooling down to RT, EtOAc was added and the suspension was filtered over Celite. The filtrate was washed with water (3 ×) and dried over $MgSO_4$. The solvent was evaporated under reduced pressure and the crude product was purified by column chromatography to yield the *nitrile.*

7.3.1.7. General procedure I: synthesis of pivaloyloxybenzamidines from aromatic nitriles

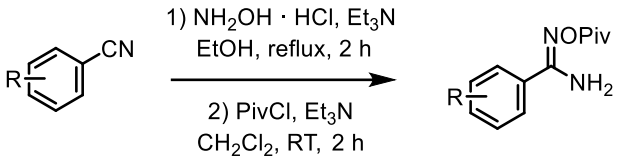

Protocol adapted from the literature.[169,171] Et_3N (1.10 eq.) was added to a solution of benzonitrile (1.00 eq.) and $NH_2OH \cdot HCl$ (1.05 eq.) in EtOH (3 mL / mmol of benzonitrile). The mixture was stirred at reflux for 2 h. After cooling down to RT, the solvent was evaporated under reduced pressure. The residue was dissolved in CH_2Cl_2 (3 mL / mmol of initial benzonitrile) then Et_3N (1.00 eq.) and PivCl (1.00 eq.) were added. The reaction mixture was stirred at RT for 2 h. The

solvent was evaporated under reduced pressure and the crude product was purified by column chromatography to yield the desired *acyloxyamidine.*

7.3.1.8. General procedure J: reduction of the N-O bond in pivaloyloxybenzamidines

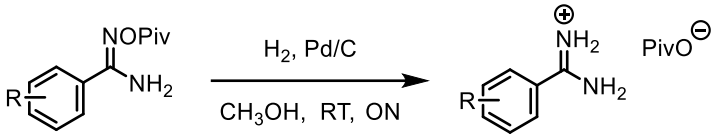

The pivaloyloxyamidine (1.00 eq.) was added to a suspension of Pd (5% on activated charcoal, 0.10 eq.) in CH_3OH (3 mL/mmol of pivaloyoxyamidine). The mixture was stirred ON at RT. The suspension was filtered over Celite and the solvent was evaporated under reduced pressure to yield the desired *amidinium pivalate.*

7.3.1.9. General procedure K: synthesis of benzamidines from benzonitriles by addition of LiHMDS

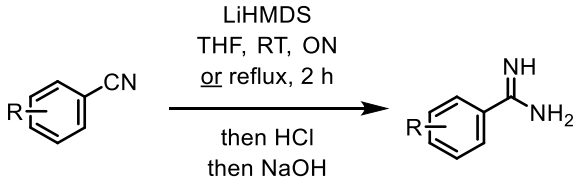

Protocol adapted from the literature.[197] The benzonitrile (1.00 eq.) was covered with a solution of LiHMDS (1 M in THF, 1.05 to 2.50 eq.). The resulting reaction mixture was stirred ON at RT or 2 h at reflux. After cooling down to 0 °C, concd. HCl (10.00 eq.) was added dropwise and the suspension was stirred for 15 min. The precipitate was filtered, washed with Et_2O (3 ×) and suspended in a biphasic mixture of water and AcOEt. Solid NaOH was added until pH 14, when complete dissolution of the solid was observed. The organic phase was separated, washed with 1 M NaOH (3 ×) and dried over Na_2SO_4. The solvent was evaporated under reduced pressure to afford the desired *benzamidine.*

7.3.1.10. General procedure L: mono Boc protection of benzamidines

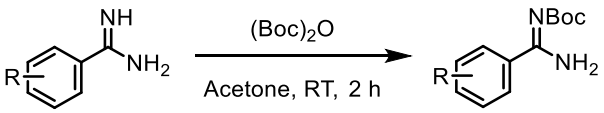

Protocol adapted from the literature.[205] The benzamidine (1.00 eq.) was added to a solution of $(Boc)_2O$ (1.00 eq.) in acetone (0.75 mL/mmol of benzamidine). The resulting reaction mixture was stirred 2 h at RT. Imidazole (0.10 eq.) then DMAP (0.10 eq.) were then added to eventually trap

the unreacted $(Boc)_2O$ and the mixture was stirred for 5 min. EtOAc was added and the solution was washed with water (3 ×) and sat. NH_4Cl (3 ×). The organic phase was separated and dried over Na_2SO_4. The solvent was evaporated under reduced to afford the desired *Boc-protected benzamidine*.

7.3.1.11. General procedure M: double Boc protection of mono Boc protected benzamidines

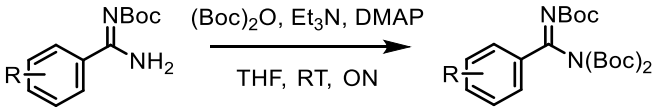

Protocol adapted from the literature.[205] A solution of $(Boc)_2O$ (2.50 eq.) in THF (0.25 mL/mmol of $(Boc)_2O$) was added over 5 h to a solution of the benzamidine (1.00 eq.) and DMAP (0.10 eq.) in THF (2.5 mL/mmol of benzamidine). The reaction mixture was stirred ON at RT. Imidazole (0.70 eq.) was then added to eventually trap the unreacted $(Boc)_2O$ and the mixture was stirred for 5 min. EtOAc was added and the solution was washed with AcOH 1% (3 ×) and sat. $NaHCO_3$ (3 ×). The organic phase was separated and dried over Na_2SO_4. The solvent was evaporated under reduced pressure to afford the desired *tris Boc-protected benzamidine*.

7.3.2. Compounds Synthesized: Protocols and Characterization.

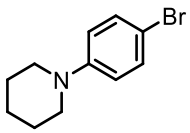

1-(4-Bromophenyl)piperidine 13. Protocol adapted from the literature.[149] *t*BuOH (1.40 eq., 1.57 mL, 16.4 mmol) was added to a suspension of NaH (60% in mineral oil, 1.40 eq., 655 mg, 16.4 mmol) in toluene (40 mL). The reaction mixture was stirred for 1 h. 1,4-Dibromobenzene **12** (5.00 eq., 13.8 g, 58.5 mmol), (±)-BINAP (0.03 eq., 218 mg, 0.35 mmol), and $[Pd_2dba_3] \cdot CHCl_3$ (0.01 eq., 124 mg, 0.12 mmol) were added. The solution was degassed and piperidine (1.00 eq., 1.16 mL, 11.7 mmol) was added. The mixture was heated up and stirred ON at 100 °C. After cooling down to RT, EtOAc was added and the organic layer was washed with water (3 ×) and dried over $MgSO_4$. The solvent was evaporated under reduced pressure and the crude product was purified by column chromatography (cyclohexane / EtOAc, from 100:0 to 90:10) to yield *aniline* **13** as a yellow powder. (2.65 g, 94%). **MP**: 74 °C. **^{1}H NMR** ($CDCl_3$, 400 MHz): δ 7.32 (d, *J* = 8.7 Hz, 2H), 6.82 (d, *J* = 8.8 Hz, 2H), 3.12 (t, *J* = 5.4 Hz, 4H), 1.78 – 1.46 (m, 6H) ppm. **^{13}C NMR** ($CDCl_3$, 100 MHz): δ 151.09, 131.90, 118.25, 111.35, 50.72, 25.72, 24.24 ppm. **FTIR:** 636.3, 686.6, 736.6, 803.5, 857.7, 916.3, 991.1, 1023.9, 1052.2, 1080.5, 1125.4, 1162.1, 1217.7, 1279.0, 1365.2, 1443.2, 1492.2, 1588.8, 1738.5, 2850.1, 2940.9 cm^{-1}. The data are consistent with the literature values.[247]

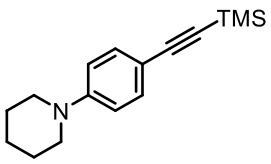

1-(4-((Trimethylsilyl)ethynyl)phenyl)piperidine 14. A solution of bromide **13** (1.00 eq., 2.60 g, 10.8 mmol), PPh_3 (0.20 eq., 566 mg, 2.16 mmol), CuI (0.10 eq., 206 mg, 1.08 mmol), and $PdCl_2$ (0.02 eq., 40 mg, 0.22 mmol) in piperidine (40 mL) was degassed and TMS-acetylene (3.00 eq., 4.60 mL, 32.4 mmol) was then added. The reaction was heated up and stirred ON at reflux. After cooling down to RT, EtOAc was added and the organic layer was washed with water (3 ×) and dried over $MgSO_4$. The solvent was evaporated under reduced pressure and the crude product was purified by column chromatography (cyclohexane / Et_2O, from 100:0 to 95:5) to yield *acetylene* **14** as a yellow powder. (2.31 g, 83%). **MP**: 112 °C. **^{1}H NMR** ($CDCl_3$, 400 MHz): δ 7.33 (d, *J* = 8.9 Hz, 2H), 6.82 (d, *J* = 7.8 Hz, 2H), 3.20 (t, *J* = 5.4 Hz, 4H), 1.85-1.45 (m, 6H), 0.22 (s, 9H) ppm. **^{13}C NMR** ($CDCl_3$, 100 MHz): δ 151.69, 133.18, 115.25, 112.54, 106.18, 91.91, 49.90, 25.60, 24.36, 0.29 ppm. **FTIR**: 637.9, 696.9, 712.8, 758.9, 812.0, 833.7, 915.6, 1025.1, 1124.1, 1191.7, 1223.1, 1245.4, 1272.0, 1346.0, 1386.9, 1444.7, 1464.6, 1508.5, 1603.5, 2146.4, 2826.2, 2853.9, 2926.5, 2942.6 cm^{-1}.

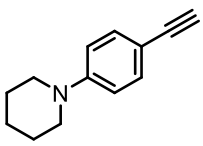

1-(4-((Trimethylsilyl)ethynyl)phenyl)piperidine 11. K_2CO_3 (8.00 eq., 9.75 g, 70.5 mmol) was added to a solution of silane **14** (1.00 eq., 2.27 g, 8.82 mmol) in a mixture of CH_3OH / THF (260 mL / 90 mL). The suspension was stirred at RT for 2 h. The inorganic salts were removed by filtration and the solvent was evaporated under reduced pressure. The residue was dissolved in Et_2O, and the solution was washed with water (3 ×) and dried over $MgSO_4$. The solvent was evaporated under reduced pressure and the crude product was purified by column chromatography (cyclohexane / EtOAc, from 100:0 to 95:5) to yield *acetylene* **11** as a pinkish powder. (1.40 g, 86%). **MP**: 68 °C. **^{1}H NMR** ($CDCl_3$, 400 MHz): δ 7.36 (d, *J* = 8.7 Hz, 2H) 6.82 (d, *J* = 8.8 Hz, 2H) 3.21 (t, *J* = 5.2 Hz, 4H), 2.98 (s, 1H), 1.81 – 1.45 (m, 6H) ppm. **^{13}C NMR** ($CDCl_3$, 100 MHz): δ 151.96, 133.26, 115.26, 111.19, 84.63, 75.24, 49.66, 25.65, 24.41 ppm. **FTIR**: 635.2, 674.0, 717.3, 780.7, 809.8, 856.9, 916.2, 957.9, 1025.1, 1066.0, 1123.5, 1164.3, 1222.4, 1246.8, 1272.0, 1349.9, 1385.9, 1447.9, 1464.3, 1508.6, 1546.7, 1604.3, 1703.3, 1881.5, 2096.6, 2187.6, 2563.5, 2824.6, 2854.0, 2941.6, 3039.4, 3296.3 cm^{-1}.

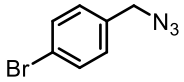

1-(Azidomethyl)-4-bromobenzene 17. 4-Bromobenzyl bromide **15** (2.00 g, 8.00 mmol) reacted according to general procedure B to yield *azide* **17** as a colorless liquid (1.65 g, 97%). **^{1}H NMR** ($CDCl_3$, 500 MHz): δ 7.52 (d, *J* = 8.4 Hz, 2H), 7.20 (d, *J* = 8.5 Hz, 2H), 4.31 (s, 2H) ppm. **^{13}C NMR** ($CDCl_3$, 125 MHz): δ 134.52, 132.15, 129.95, 122.49, 54.24 ppm. **FTIR**: 601.1, 668.6, 724.1, 791.0, 834.8, 880.5, 963.3, 1011.7, 1070.18, 1107.0, 1196.4, 1245.5, 1282.1, 1341.3, 1405.7, 1488.0, 1592.0, 2091.3, 2930.6 cm^{-1}. The data are consistent with the literature values.[248]

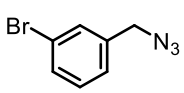

1-(Azidomethyl)-3-bromobenzene 18. 3-Bromobenzyl bromide (3.00 g, 12.0 mmol) reacted according to general procedure B to yield *azide* **18** as a pale-yellow oil (2.49 g, 98%). **^{1}H NMR** ($CDCl_3$, 500 MHz): δ 7.47 – 7.43 (m, 2H), 7.25 – 7.21 (m, 2H), 4.31 (s, 2H) ppm. **^{13}C NMR** ($CDCl_3$, 125 MHz): δ 137.81, 131.55, 131.26, 130.53, 126.77, 123.00, 54.13 ppm. **FTIR**: 664.6, 679.0, 709.5, 774.8, 838.0, 878.4, 997.1, 1070.8, 1091.5, 1166.6, 1203.0, 1217.0, 1282.6, 1339.9, 1427.5, 1473.6, 1571.0, 1598.0, 2092.3, 2939.9 cm^{-1}. The data are consistent with the literature values.[248]

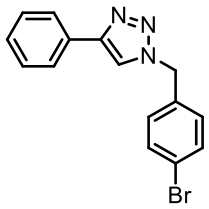

1-(4-Bromobenzyl)-4-phenyl-1*H*-1,2,3-triazole 5a. Azide **17** (1.00 g, 4.72 mmol) reacted with phenylacetylene (518 µL, 4.72 mmol) according to general procedure C. The residue was recrystallized from EtOH to yield *triazole* **5a** as white needles (1.28 g, 86%). **MP**: 157 °C. **^{1}H NMR** (DMSO-d_6, 400 MHz): δ 8.64 (s, 1H), 7.85 (d, *J* = 7.2 Hz, 2H), 7.59 (d, *J* = 8.4 Hz, 2H), 7.44 (t, *J* = 7.6 Hz, 2H), 7.36 – 7.29 (m, 3H), 5.64 (s, 2H) ppm. **^{13}C NMR** (DMSO-d_6, 100 MHz): δ 146.69, 135.39, 131.72, 130.60, 130.16, 128.89, 127.92, 125.16, 121.61, 121.43, 52.27 ppm. **FTIR**: 625.5, 693.8, 709.9, 757.0, 766.4, 804.6, 848.1, 915.0, 976.9, 1012.3, 1049.7, 1072.0, 1139.0, 1353.2, 1409.7, 1443.3, 1461.7, 1483.0, 1591.1, 2970.3, 3027.8 cm^{-1}. The data are consistent with the literature values.[249]

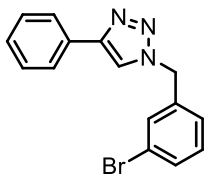

1-(3-Bromobenzyl)-4-phenyl-1*H*-1,2,3-triazole 5b. Azide **18** (600 mg, 2.83 mmol) reacted with phenylacetylene (310 µL, 2.83 mmol) according to general procedure C. The residue was recrystallized from cyclohexane to yield *triazole* **5b** as thin white needles (720 mg, 81%). **MP**: 109 °C. **^{1}H NMR** ($CDCl_3$, 400 MHz): δ 8.67 (s, 1H), 7.85 (d, *J* = 7.1 Hz, 2H), 7.60 (m, 1H), 7.55 (m, 1H), 7.48 – 7.41 (m, 2H), 7.39 – 7.30 (m, 3H), 5.67 (s, 2H) ppm. **^{13}C NMR** ($CDCl_3$, 100 MHz): δ 146.70, 138.60, 131.07, 131.02, 130.72, 130.57, 128.90, 127.94, 127.04, 125.18, 121.88, 121.71, 52.17 ppm. **FTIR**: 666.6, 679.2, 693.1, 708.0, 763.5, 782.8, 833.9, 874.3, 915.9, 960.4, 974.9, 999.6, 1025.4, 1051.6, 1073.5, 1157.1, 1207.4, 1226.7, 1347.2, 1425.7, 1463.0, 1571.7, 1597.1, 3129.4 cm^{-1}. The data are consistent with the literature values.[250]

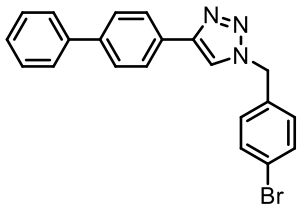

4-([1,1'-Biphenyl]-4-yl)-1-(4-bromobenzyl)-1*H*-1,2,3-triazole 5c. Azide **17** (1.00 g, 4.72 mmol) reacted with acetylene **10** (840 mg, 4.72 mmol) according to general procedure C. The residue was triturated in EtOH and filtered to yield *triazole* **5c** as a white powder (1.32 g, 72%). **MP**: 224 °C. **^{1}H NMR** (DMSO-d_6, 400 MHz): δ 8.70 (s, 1H), 7.94 (d, *J* = 8.3 Hz, 2H), 7.76 (d, *J* = 8.3 Hz, 2H), 7.71 (d, *J* = 7.5 Hz, 2H), 7.61 (d, *J* = 8.3 Hz, 2H), 7.47 (t, *J* = 7.6 Hz, 2H), 7.41–7.28 (m, 3H), 5.66 (s, 2H) ppm. **^{13}C NMR** (DMSO-d_6, 100 MHz): δ 146.35, 139.54, 139.49, 135.36, 131.73, 130.17, 129.70, 128.96, 127.55, 127.11, 126.50, 125.71, 121.72, 121.45, 52.30

ppm. **FTIR**: 636.1 , 659.4, 687.1, 723.1, 746.7, 762.0, 799.8, 812.5, 842.0, 947.6, 973.4, 1005.2, 1014.2, 1042.9, 1071.7, 1099.5, 1158.9, 1181.8, 1216.1, 1346.2, 1406.1, 1433.6, 1457.6, 1481.7, 1594.8, 3035.5 cm^{-1}.

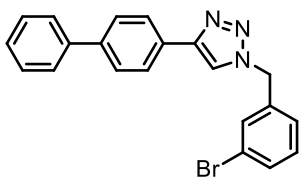

4-([1,1'-Biphenyl]-4-yl)-1-(3-bromobenzyl)-1*H*-1,2,3-triazole 5d. Azide **18** (384 mg, 1.80 mmol) reacted with acetylene **10** (323 mg, 1.80 mmol) according to general procedure C. The residue was triturated in Et_2O and filtered to yield *triazole* **5d** as off-white platelets (555 mg, 79%). **MP**: 173 °C. **^{1}H NMR** (DMSO-d_6, 400 MHz): δ 8.73 (s, 1H), 7.95 (d, *J* = 8.2 Hz, 2H), 7.76 (d, *J* = 8.2 Hz, 2H), 7.71 (d, *J* = 7.2 Hz, 2H), 7.62 (m, 1H), 7.59 – 7.53 (m, 1H), 7.48 (t, *J* = 7.8, Hz, 2H), 7.41 – 7.33 (m, 3H), 5.69 (s, 2H) ppm. **^{13}C NMR** (DMSO-d_6, 100 MHz): δ 146.38, 139.54, 139.52, 138.57, 131.10, 131.04, 130.76, 129.68, 128.97, 127.56, 127.13, 127.08, 126.51, 124.73, 121.90, 122.82, 52.22 ppm. **FTIR**: 604.6, 641.4, 670.0, 685.8, 724.1, 761.1, 801.0, 820.1, 841.8, 888.8, 911.1, 975.2, 997.6, 1006.0, 1041.5, 1072.8, 1092.0, 1120.6, 1217.0, 1407.0, 1427.5, 1474.2, 1482.8, 1571.7, 1595.8, 1738.5, 2161.6, 3031.1 cm^{-1}

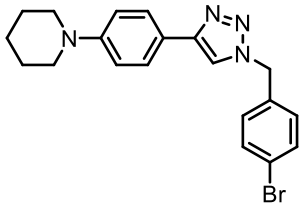

1-(4-(1-(4-Bromobenzyl)-1*H*-1,2,3-triazol-4-yl)phenyl)piperidine 5e. Azide **17** (606 mg, 2.86 mmol) reacted with acetylene **11** (529 mg, 2.86 mmol) according to general procedure C. The residue was triturated in EtOH and filtered to yield *triazole* **5e** as a white powder (728 mg, 64%). **MP**: 207 °C. **^{1}H NMR** (DMSO-d_6, 400 MHz): δ 8.49 (s, 1H), 7.69 (d, *J* = 8.8 Hz, 2H), 7.64 (d, *J* = 8.5 Hz, 2H), 7.34 (d, *J* = 8.5 Hz, 2H), 7.01 (d, *J* = 8.9 Hz, 2H), 5.64 (s, 2H), 3.22 (t, *J* = 5.2 Hz, 3H), 1.71 – 1.53 (m, 6H) ppm. **^{13}C NMR** (DMSO-d_6, 100 MHz, 40 °C): δ 151.01, 146.98, 135.41, 131.56, 129.99, 125.94, 121.22, 120.44, 119.91, 115.42, 52.08, 49.03, 25.00, 23.79 ppm. **FTIR**: 627.1, 644.3, 667.0, 696.5, 741.9, 770.8, 802.8, 817.4, 837.7, 860.4, 915.4, 933.9, 958.4, 973.5, 1012.7, 1024.3 1043.3, 1070.8, 1124.8, 1204.9, 1223.1, 1240.8, 1267.0, 1281.8, 1334.2, 1353.8, 1389.4, 1410.6, 1420.3, 1448.8, 1487.6, 1502.0, 1557.4, 1617.2, 2834.0, 2923.5, 3095.5 cm^{-1}.

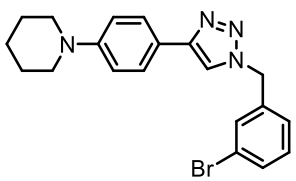

1-(4-(1-(3-Bromobenzyl)-1*H*-1,2,3-triazol-4-yl)phenyl)piperidine 5f. Azide **18** (410 mg, 1.93 mmol) reacted with acetylene **11** (358 mg, 1.93 mmol) according to general procedure C. The residue was triturated in Et_2O and filtered to yield *triazole* **5f** as light brown flakes. (565 mg, 74%). **MP**: 164 °C. **^{1}H NMR** (DMSO-d_6, 400 MHz): δ 8.47 (s, 1H), 7.66 (d, *J* = 8.5 Hz, 2H), 7.60 – 7.51 (m, 2H), 7.39 – 7.28 (m, 2H), 6.97 (d, *J* = 8.6 Hz, 2H), 5.62 (s, 2H), 3.17 (t, *J* = 5.2 Hz, 4H), 1.66 – 1.45 (m, 6H) ppm. **^{13}C NMR** (DMSO-d_6, 100 MHz): δ 151.12, 147.10, 138.76, 131.01, 130.99, 130.65, 126.99, 126.03, 121.85, 120.46, 120.16, 115.56, 52.07, 49.12, 25.10, 23.90 ppm. **FTIR**: 641.2, 658.4, 669.0, 686.9, 738.4, 757.8, 796.5, 817.3, 860.9, 889.5, 921.4, 973.5, 997.3, 1029.6,

1048.0, 1070.9, 1127.7, 1159.0, 1206.4, 1218., 1235.8, 1343.4, 1382.5, 1417.7, 1431.3, 1449.5, 1470.6, 1497.8, 1568.2, 1615.5, 2823.8, 2941.7 cm^{-1}.

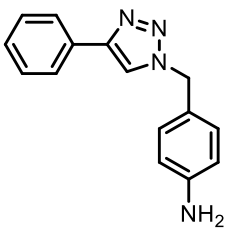

4-((4-Phenyl-1*H*-1,2,3-triazol-1-yl)methyl)aniline 4a. Aryl bromide **5a** (600 mg, 1.90 mmol) reacted according to general procedure D. The residue was purified by column chromatography (cyclohexane / EtOAc, 50:50) to yield *aniline* **4a** as an off-white powder (347 mg, 73%). **MP**: 174 °C. **^{1}H NMR** (DMSO-d_6, 400 MHz): δ 8.51 (s, 1H), 7.84 (d, *J* = 7.1 Hz, 2H), 7.42 (t, *J* = 7.6 Hz, 2H), 7.31 (t, *J* = 7.4 Hz, 1H), 7.08 (d, *J* = 8.4 Hz, 2H), 6.56 (d, *J* = 8.4 Hz, 2H), 5.40 (s, 2H), 5.19 (s, 2H) ppm. **^{13}C NMR** (DMSO-d_6, 100 MHz): δ 148.82, 146.52, 130.81, 129.24, 128.85, 127.77, 125.11, 122.49, 120.91, 113.78, 53.13 ppm. **FTIR**: 693.2, 765.7, 811.3, 826.2, 922.9, 974.2, 1049.9, 1076.7, 1147.5, 1175.2, 1221.5, 1251.9, 1280.3, 1298.1, 1324.1, 1354.5, 1449.6, 1470.7, 1518.3, 1611.9, 1641.7, 2923.9, 3137.9, 3231.9, 3340.4, 3450.8 cm^{-1}.

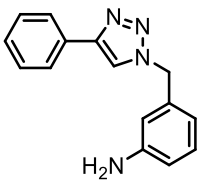

3-((4-Phenyl-1*H*-1,2,3-triazol-1-yl)methyl)aniline 4b. Aryl bromide **5b** (628 mg, 2.00 mmol) reacted according to general procedure D. The crude product was purified by column chromatography (cyclohexane / EtOAc, 50:50) to yield *aniline* **4b** as an off-white powder (211 mg, 42%). **MP**: 160 °C. **^{1}H NMR** (DMSO-d_6, 400 MHz): δ 8.58 (s, 1H), 7.86 (d, *J* = 7.2 Hz, 2H), 7.44 (t, *J* = 7.6 Hz, 2H), 7.33 (t, *J* = 7.4 Hz, 1H), 7.01 (t, *J* = 7.7 Hz, 1H), 6.58 – 6.38 (m, 3H), 5.47 (s, 2H), 5.18 (s, 2H) ppm. **^{13}C NMR** (DMSO-d_6, 100 MHz): δ 149.09, 146.55, 136.55, 130.75, 129.25, 128.87, 127.83, 125.13, 121.51, 114.89, 113.58, 112.65, 53.33 pppm. **FTIR**: 682.7, 691.1, 710.2, 748.0, 765.7, 792.3, 837.7, 873.4, 916.4, 938.4, 977.7, 994.4, 1027.2, 1050.6, 1077.9, 1144.0, 1168.7, 1199.2, 1220.3, 1286.5, 1310.6, 1355.2, 1427.7, 1442.8, 1464.6, 1484.0, 1491.9, 1604.1, 1626.2, 3091.3, 3352.9, 3433.72 cm^{-1}.

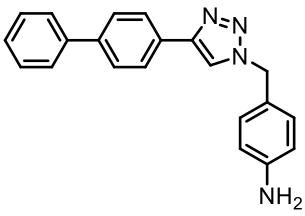

4-((4-([1,1'-Biphenyl]-4-yl)-1*H*-1,2,3-triazol-1-yl)methyl)aniline 4c. Aryl bromide **5c** (816 mg, 2.09 mmol) reacted according to general procedure D. The residue was purified by column chromatography (CH_2Cl_2 / CH_3OH, 100:0 to 99:1) to yield *aniline* **4c** as an off-white powder (370 mg, 54%). **MP**: 225 °C. **^{1}H NMR** (DMSO-d_6, 400 MHz): δ 7.93 (d, *J* = 8.2 Hz, 2H), 7.80 – 7.65 (m, 4H), 7.47 (t, *J* = 7.7 Hz, 2H), 7.37 (t, *J* = 7.3 Hz, 1H), 7.09 (d, *J* = 8.3 Hz, 2H), 6.55 (d, *J* = 8.3 Hz, 2H), 5.41 (s, 2H), 5.19 (s, 2H) ppm. **^{13}C NMR** (DMSO-d_6, 100 MHz): δ 148.84, 146.16, 139.58, 139.35, 129.92, 129.28, 128.96, 127.53, 127.08, 126.50, 125.65, 122.46, 121.04, 113.77, 53.17 ppm. **FTIR**: 634.8, 644.3, 655.2, 690.4, 699.8, 727.3, 747.1, 768.5, 786.2, 807.7, 826.4, 847.8, 917.1, 954.0, 976.0, 1004.5, 1051.6, 1071.0, 1127.4, 1149.2, 1161.1, 1175.5, 1196.5,

1222.4, 1248.9, 1267.3, 1295.9, 1324.6, 1354.6, 1409.2, 1434.4, 1467.2, 1483.7, 1518.8, 1578.9, 1611.1, 1642.8, 3138.5, 3231.7, 3340.2, 3452.7 cm^{-1}.

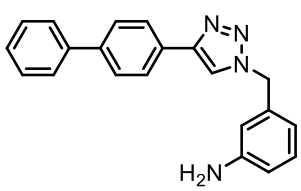

3-((4-([1,1'-Biphenyl]-4-yl)-1*H*-1,2,3-triazol-1-yl)methyl)aniline 4d. Aryl bromide **5d** (508 mg, 1.31 mmol) reacted according to general procedure D. The residue was purified by column chromatography (CH_2Cl_2 / EtOAc, 80:20) to yield *aniline* **4d** as an off-white powder (267 mg, 62 %). **MP**: 245 °C (decomposition). **^{1}H NMR** (DMSO-d_6, 400 MHz): δ 8.64 (s, 1H), 7.96 (d, *J* = 7.9 Hz, 2H), 7.76 (d, *J* = 7.9 Hz, 2H), 7.71 (d, *J* = 8.3 Hz, 2H), 7.47 (t, *J* = 7.6 Hz, 2H), 7.37 (t, *J* = 7.3 Hz, 1H), 7.03 (t, *J* = 7.6 Hz, 1H), 6.59 – 6.41 (m, 3H), 5.49 (s, 2H), 5.20 (s, 2H) ppm. **^{13}C NMR** (DMSO-d_6, 100 MHz): δ 149.67, 146.77, 140.10, 139.95, 137.09, 130.41, 129.83, 129.51, 128.09, 127.65, 127.05, 126.23, 122.17, 115.47, 114.15, 113.24, 53.93 ppm. **FTIR**: 613.8, 643.0, 660.5, 689.7, 727.5, 743.5, 766.3, 794.3, 805.6, 848.4, 917.5, 974.3, 994.9, 1005.0, 1053.5, 1074.2, 1146.5, 1161.6, 1217.5, 1314.3, 1431.4, 1463.2, 1493.4, 1604.8, 1631.3, 2942.4, 3351.7, 3455.0 cm^{-1}.

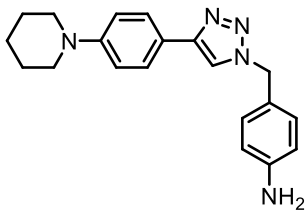

4-((4-(4-(Piperidin-1-yl)phenyl)-1*H*-1,2,3-triazol-1-yl)methyl) aniline 4e. Aryl bromide **5e** (647 mg, 1.63 mmol) reacted according to general procedure D. The crude product was purified by column chromatography (CH_2Cl_2 / EtOAc, 100:0 to 50:50) to yield *aniline* **4e** as an off-white powder (241 mg, 44%). **MP**: 187 °C. **^{1}H NMR** (DMSO-d_6, 400 MHz): δ 8.31 (s, 1H), 7.64 (d, *J* = 8.2 Hz, 2H), 7.06 (d, *J* = 8.0 Hz, 2H), 6.95 (d, *J* = 8.4 Hz, 2H), 6.54 (d, J = 7.8 Hz, 2H), 5.35 (s, 2H), 5.17 (s, 2H), 3.16 (m, 4H), 1.73 – 1.41 (m, 6H) ppm. **^{13}C NMR** (DMSO-d_6, 100 MHz): δ 151.03, 148.76, 146.86, 129.19, 125.94, 122.63, 120.78, 119.39, 115.57, 113.73, 53.00, 49.16, 25.12, 23.90 ppm. **FTIR:** 613.6, 641.8, 695.9, 772.0, 799.9, 819.3, 916.1, 975.5, 1026.1, 1050.0, 1070.8, 1127.8, 1182.4, 1232.0, 1280.1, 1448.2, 1498.3, 1519.1, 1559.1, 1615.5, 2812.5, 2936.5, 3333.9, 3474.5 cm^{-1}.

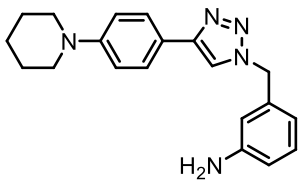

4-((4-(4-(Piperidin-1-yl)phenyl)-1*H*-1,2,3-triazol-1-yl)methyl) aniline 4f. Aryl bromide **5f** (546 mg, 1.38 mmol) reacted according to general procedure D. The crude product was purified by column chromatography (CH_2Cl_2 / EtOAc, 80:20 to 70:30) to yield *aniline* **5f** as a yellow powder (254 mg, 55 %). **MP**: 191 °C. **^{1}H NMR** (DMSO-d_6, 400 MHz): δ 8.37 (s, 1H), 7.67 (d, *J* = 8.8 Hz, 2H), 7.10 – 6.89 (m, 3H), 6.57 – 6.37 (m, 3H), 5.43 (s, 2H), 5.18 (s, 2H), 3.16 (t, *J* = 5.3 Hz, 4H), 1.66 – 1.42 (m, 6H) ppm. **^{13}C NMR** (DMSO-d_6, 100 MHz): δ 151.07, 149.07, 146.94, 136.70, 129.23, 126.00, 120.72, 119.98, 115.58, 114.90, 113.55, 112.68, 53.24, 49.16, 25.13, 23.91 ppm. **FTIR**: 606.4, 643.9, 665.1, 691.5, 737.1, 757.5, 810.7, 856.9, 915.0, 974.7,

994.8, 1025.3, 1051.6, 1071.1, 1126.0, 1169.1, 1217.9, 1238.7, 1279.0, 1300.3, 1332.3, 1385.8, 1418.2, 1449.0, 1468.7, 1500.1, 1557.7, 1589.5, 1619.3, 2820.2, 2943.2, 3358.9, 3461.5 cm^{-1}.

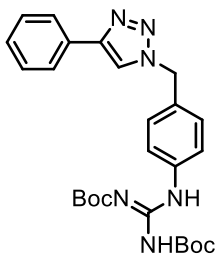

1,2-Bis(*tert*-butoxycarbonyl)-3-(4-((4-phenyl-1*H*-1,2,3-triazol-1-yl) methyl)phenyl)guanidine 21a. Aniline **4a** (1.11 g, 4.43 mmol) reacted according to general procedure E. The crude product was purified by column chromatography (cyclohexane / EtOAc, 100:0 to 80:20) to yield *Boc-protected guanidine* **21a** as snow white flakes (884 mg, 41%). **MP**: 150 °C (decomposition). **^{1}H NMR** ($CDCl_3$, 400 MHz): δ 11.62 (br, 1H), 10.40 (br, 1H), 7.79 (d, *J* = 7.2 Hz, 2H), 7.68 – 7.56 (m, 3H), 7.39 (t, *J* = 7.7 Hz, 2H), 7.35 – 7.20 (m, 3H), 5.52 (s, 2H), 1.53 (s, 9H), 1.49 (s, 9H) ppm. **^{13}C NMR** ($CDCl_3$, 100 MHz): δ 163.02, 153.62, 153.39, 148.34, 137.48, 130.93, 130.66, 129.05, 128.93, 128.27, 125.85, 122.87, 119.61, 84.282. 80.23, 53.93, 28.24, 28.20 ppm. **FTIR**: 631.9, 648.3, 695.8, 742.2, 766.1, 807.8, 846.0, 880.1, 919.7, 974.4, 1028.6, 1046.1, 1058.1, 1076.0, 1100.2, 1128.1, 1149.2, 1231.0, 1279.3, 1306.0, 1323.7, 1342.0, 1400.4, 1451.5, 1474.6, 1519.7, 1564.6, 1603.2, 1633.7, 1737.8, 2985.5 cm^{-1}.

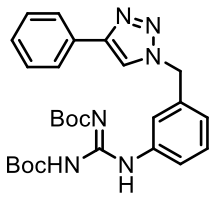

1,2-Bis(tert-butoxycarbonyl)-3-(3-((4-phenyl-1*H*-1,2,3-triazol-1-yl)methyl) phenyl)guanidine 21b. Aniline **4b** (195 mg, 0.78 mmol) reacted according to general procedure E. The crude product was purified by column chromatography (cyclohexane / EtOAc, 100:0 to 90:10) to yield *Boc-protected guanidine* **21b** as a white powder (212 mg, 55%). **MP**: 146 °C (decomposition). **^{1}H NMR** ($CDCl_3$, 500 MHz): δ 11.64 (br, 1H), 10.42 (br, 1H), 7.82 – 7.78 (m, 2H), 7.70 (s, 1H), 7.67 (s, 1H), 7.61 – 7.55 (m, 1H), 7.43 – 7.29 (m, 4H), 7.07 – 7.00 (m, 1H), 5.53 (s, 2H), 1.53 (s, 9H), 1.49 (s, 9H) ppm. **^{13}C NMR** ($CDCl_3$, 100 MHz): δ 163.51, 153.66, 153.39, 148.33, 137.71, 135.47, 130.70, 129.87, 128.88, 128.23, 125.85, 124.38, 122.58, 121.95, 119.66, 84.09, 79.95, 54.22, 28.25, 28.19 ppm. **FTIR:** 605.9, 651.9, 659.0, 679.3, 693.9, 724.3, 750.4, 766.8, 811.7, 860.0, 876.1, 887.7, 899.7, 912.0, 974.6, 1003.7, 1028.7, 1056.6, 1076.5, 1085.3, 1114.9, 1145.7, 1246.2, 1266.3, 1302.0, 1323.4, 1344.6, 1387.6, 1405.4, 1443.2, 1492.5, 1571.6, 1607.6, 1632.33, 1720.2, 2931.7, 2979.1 cm^{-1}.

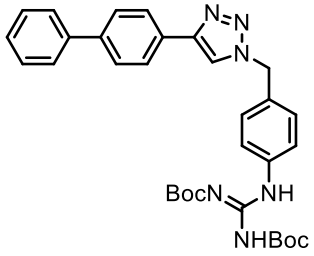

1-(4-((4-([1,1'-Biphenyl]-4-yl)-1*H*-1,2,3-triazol-1-yl)methyl) phenyl)-2,3-bis(*tert*-butoxycarbonyl)guanidine 21c. Aniline **4c** (325 mg, 1.00 mmol) reacted according to general procedure E. The residue was purified by column chromatography (cyclohexane / EtOAc, 100:0 to 70:30) to yield *Boc-protected guanidine* **21c** as an off-white powder (442 mg, 78%). **MP**: No transformation up to 250 °C. **^{1}H NMR** ($CDCl_3$, 400 MHz): δ 11.64 (br, 1H), 10.41 (br, 1H), 7.88 (d, *J* = 8.6 Hz, 2H), 7.72 – 7.58 (m, 7H), 7.44 (t, *J* = 7.5 Hz, 2H), 7.38 – 7.31 (m, 1H), 7.29 (d, *J* = 8.7 Hz, 2H), 5.53 (s, 2H), 1.53 (s, 9H), 1.50 (s, 9H) ppm. **^{13}C NMR**

($CDCl_3$, 100 MHz): δ 163.28, 153.62, 153.39, 147.97, 140.94, 140.70, 137.50, 130.80, 129.64, 129.02, 128.91, 127.58, 127.51, 127.08, 126.21, 122.84, 119.66, 84.15, 80.08, 53.92, 28.25, 28.18 ppm. **FTIR**: 641.6, 694.0, 726.1, 763.9, 777.9, 807.2, 841.8, 882.2, 975.4, 1007.2, 1028.6, 1056.8, 1097.6, 1111.0, 1126.1, 1148.7, 1232.3, 1306.4, 1342.3, 1409.2,1518.8, 1560.3, 1603.9, 1633.6, 1718.4, 2931.2, 3133.5 cm^{-1}.

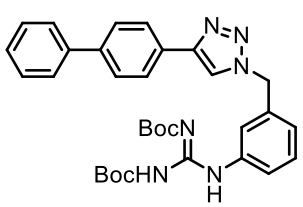

1-(4-((4-([1,1'-Biphenyl]-4-yl)-1*H*-1,2,3-triazol-1-yl)methyl) phenyl)-2,3-bis(*tert*-butoxycarbonyl)guanidine 21d. Aryl bromide **4d** (508 mg, 1.56 mmol) reacted according to general procedure F. The residue was purified by column chromatography (cyclohexane / EtOAc, 100:0 to 70:30) to yield *Boc-protected guanidine* **21d** as an off-white powder (427 mg, 48%). **MP**: 226 °C (decomposition). **^{1}H NMR** ($CDCl_3$, 400 MHz): δ 11.63 (br, 1H), 10.41 (br, 1H), 7.88 (d, J = 8.8, 2H), 7.73 (s, 1H), 7.68 – 7.60 (m, 6H), 7.44 (t, J = 7.6, 2H), 7.35 (t, J = 8.0, 2H), 7.03 (d, J = 7.6), 5.57 (s, 2H), 1.53 (s, 9H), 1.50 (s, 9H) ppm. **^{13}C NMR** ($CDCl_3$, 100 MHz): δ 163.53, 153.69, 153.40, 148.05, 140.99, 140.74, 137.52, 135.46, 129.92, 129.70, 128.93, 127.59, 127.54, 127.10, 126.26, 124.42, 122.64, 122.011, 119.68, 84.13, 80.00, 54.29, 28.26, 28.15 ppm. **FTIR**: 603.6, 650.1, 667.0, 680.0, 692.2, 728.3, 744.7, 764.6, 782.4, 800.9, 824.1, 842.3, 874.8, 892.9, 915.9, 974.8, 1004.4, 1028.0, 1052.4, 1074.2, 1084.3, 1115.0, 1148.6, 1208.6, 1228.0, 1246.6, 1304.9, 1346.4, 1365.0, 1403.6, 1426.1, 1463.0, 1481.9, 1572.8, 1609.8, 1630.1, 1726.6, 2977.0, 3129.9 cm^{-1}.

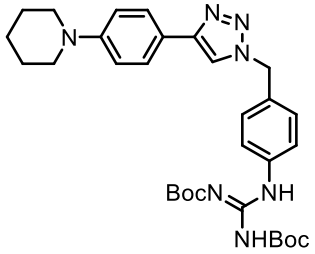

1,2-Bis(*tert*-butoxycarbonyl)-3-(4-((4-(4-(piperidin-1-yl)phenyl)-1*H*-1,2,3-triazol-1-yl)methyl)phenyl)guanidine 21e. Aniline **4e** (217 mg, 0.65 mmol) reacted according to general procedure E. The crude product was purified by column chromatography (cyclohexane / EtOAc, 100:0 to 50:50) to yield *Boc-protected guanidine* **21e** as an off-white powder (109 mg, 29%). **MP**: 150 °C (slow decomposition). **^{1}H NMR** ($CDCl_3$, 400 MHz): δ 11.62 (br, 1H), 10.36 (s, 1H), 7.65 (d, *J* = 9.2 Hz, 2H), 7.59 (d, *J* = 8.4 Hz, 2H), 7.52 (s, 1H), 7.20 (d, *J* = 9.6 Hz, 2H), 6.91 (d, *J* = 9.2 Hz, 2H), 5.44 (s, 2H), 3.16 (t, *J* = 5.4 Hz, 4H), 1.71 – 1.63 (m, 4H), 1.59 – 1.43 (m, 20H) ppm. **^{13}C NMR** ($CDCl_3$, 100 MHz): δ 163.41, 153.51, 153.27, 151.87, 148.38, 137.23, 130.99, 128.72, 126.54, 122.61, 121.18, 118.45, 116.17, 83.90, 79.77, 53.60, 50.20, 28.12 (br, 2C), 25.70, 24.31 ppm. **FTIR:** 643.5, 696.0, 731.8, 768.5, 808.5, 882.0, 913.2, 974.9, 1027.3, 1057.0, 1099.3, 1121.6, 1149.4,1230.9, 1311.1, 1414.9, 1451.1, 1501.3, 1560.2, 1604.7, 1627.7, 1722.1, 2933.6 cm^{-1}.

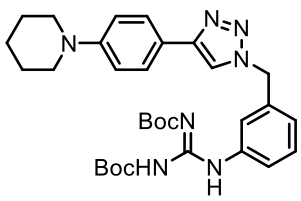

1,2-Bis(*tert*-butoxycarbonyl)-3-(4-((4-(4-(piperidin-1-yl)phenyl)-1*H*-1,2,3-triazol-1-yl)methyl)phenyl)guanidine 21f. Aniline **4f** (224 mg, 0.67 mmol) reacted according to general procedure E. The crude product was purified by column chromatography (cyclohexane / EtOAc, 100:0 to 80:20) to yield *Boc-protected amidine* **21f** as a white powder (156 mg, 40%). **MP**: 237 °C (degradation). **^{1}H NMR** ($CDCl_3$, 400 MHz): δ 11.64 (br, 1H), 10.37 (br, 1H), 7.68 – 7.58 (m, 5H), 7.34 – 7.25 (m, 1H), 7.03 – 6.87 (m, 3H), 5.49 (s, 2H), 3.18 (m, 4H), 1.71 – 1.38 (m, 24H) ppm. **^{13}C NMR** ($CDCl_3$, 100 MHz): δ 163.38, 153.54, 153.24, 151.88, 148.41, 137.50, 135.66, 129.66, 129.56, 124.23, 122.40, 121.75, 121.19, 118.49, 116.16, 83.90, 79.75, 53.92, 50.21, 28.10 (br, 2C), 25.68, 24.30 ppm. **FTIR**: 647.0, 687.3, 726.8, 768.0, 812.3, 855.4, 873.9, 912.7, 975.9, 1026.8, 1057.9, 1108.8, 1147.6, 1236.6, 1290.0, 1335.2, 1410.4, 1452.5, 1503.2, 1579.1, 1594.9, 1637.9, 1714.6, 2245.6, 2934.5, 2979.1 cm^{-1}.

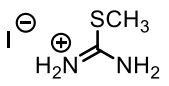

2-Methylisothiouronium iodide 24. Protocol adapted from the literature.[154] CH_3I (1.20 eq., 2.37 mL, 39.7 mmol) was added to a solution of thiourea **23** (1.00 eq., 2.50 g, 32.8 mmol) in EtOH (5 mL). The mixture was stirred at reflux for 2 h and was then cooled at 0 °C. Et_2O (5 mL) was added and the suspension was stirred for 10 min. The precipitate was collected, rinsed with Et_2O (3 ×), and the resulting residue was dried, affording *thiouronium iodide* **24** as a white powder (7.00 g, 98%). **MP**: 125 °C. **^{1}H NMR** (DMSO-d_6, 400 MHz): δ 8.78 (s, 4H), 2.50 (s, 3H) ppm. **^{13}C NMR** (DMSO-d_6, 100 MHz): δ 171.14, 13.29 ppm. The data are consistent with the literature values.[154]

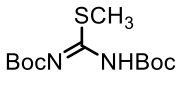

Methyl *N*,*N'*-bis(*tert*-butoxycarbonyl)carbamimidothioate 20. Protocol adapted from the literature.[154] A solution of NaOH (1.00 eq., 460 mg, 11.5 mmol) in water (5mL) was added to a solution of thiouronium iodide **24** (1.00 eq, 2.50 g, 11.5 mmol) in a mixture of water / 1,4-dioxane (25 mL : 25 mL). After 5 min, $(Boc)_2O$ (2.50 eq., 6.20 g, 28.5 mmol) was added. The reaction mixture was stirred ON at RT. The precipitate was collected. The filtrate was concentrated under reduced pressure to approximately half the volume, and the precipitate was collected again. The precipitates were combined, suspended in water at 50 °C, and filtered. The resulting solid was dried to afford *thiocarbamimidate* **20** as an off-white powder (2.71 g, 81%). **MP:** 117 °C. **^{1}H NMR** ($CDCl_3$, 400 MHz): δ 11.60 (br, 1H), 2.40 (s, 3H), 1.53 (s, 18H) ppm. **^{13}C NMR** ($CDCl_3$, 100 MHz): δ 171.43, 146.89 (br, 2C), 85.12, 81.99, 28.14, 27.40, 14.28 ppm. The data are consistent with the literature values.[154]

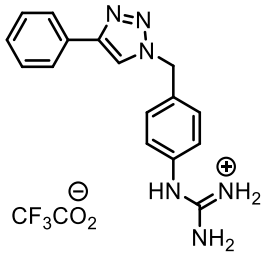

Amino((4-((4-phenyl-1*H*-1,2,3-triazol-1-yl)methyl)phenyl)amino) methaniminium trifluoroacetate 3a · TFA. Boc-protected guanidine **21a** (300 mg, 0.60 mmol) reacted according to general procedure G to afford *guanidinium salt* **3a · TFA** as a white powder (247 mg, quant.). **MP**: 184 °C. **^{1}H NMR** (CD_3OD, 500 MHz): δ 8.35 (s, 1H), 7.81 – 7.77 (m, 2H), 7.52 – 7.48 (m, 2H), 7.45 – 7.39 (m, 2H), 7.36 – 7.29 (m, 3H), 5.67 (s, 2H) ppm. **^{13}C NMR** (CD_3OD, 125 MHz): δ 158.07, 149.29, 136.57, 136.18, 131.56, 130.95, 130.00, 129.47, 126.92, 126.66, 122.37, 54.39 ppm. **FTIR**: 3329.4, 3028.2, 2970.4, 1654.9, 1609.5, 1581.0, 1519.4, 1485.0, 1464.9, 1364.8, 1312.9, 1216.8, 1202.4, 1170.4, 1136.1, 1081.9, 1058.5, 1023.1, 980.2, 834.4, 803.5, 765.6, 721.4, 697.0, 611.1 cm^{-1}. **HRMS**: m/z calcd for $[M]^+$ 293.1509, found 293.1512.

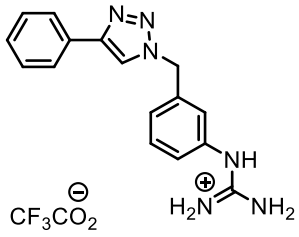

Amino((3-((4-phenyl-1*H*-1,2,3-triazol-1-yl)methyl)phenyl)amino) methaniminium trifluoroacetate 3b · TFA. Boc-protected guanidine **21b** (62 mg, 0.13 mmol) reacted according to general procedure G to afford *guanidinium salt* **3b · TFA** as a yellowish solid (54 mg, quant.). **MP:** 173 °C. **^{1}H NMR** (CD_3OD, 500 MHz): δ 8.38 (s, 2H), 7.81 (d, *J* = 7.5 Hz, 2H), 7.52 (t, *J* = 8.5 Hz, 1H), 7.43 – 7.27 (m, 4H), 5.69 (s, 3H) ppm. **^{13}C NMR** (CD_3OD, 125 MHz): δ 158.07, 149.33, 139.01, 136.93, 131.77, 131.55, 130.02, 129.49, 128.22, 126.67, 126.46, 126.02, 122.54, 54.40 ppm. **FTIR**: 3332.1, 3091.7, 1671.2, 1591.7, 1485.0, 1467.0, 1343.0, 1288.2, 1234.4, 1187.9, 1126.7, 1089.7, 1062.1, 1001.7, 980.7, 916.2, 803.4, 761.5, 720.0, 691.1, 648.3 cm^{-1}. **HRMS**: m/z calcd for $[M]^+$ 293.1509, found 293.1509.

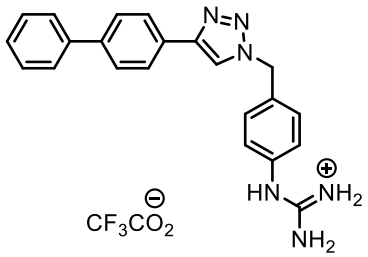

((4-((4-([1,1'-Biphenyl]-4-yl)-1*H*-1,2,3-triazol-1-yl)methyl) phenyl)amino)(amino)methaniminium trifluoroacetate 3c · TFA. Boc-protected guanidine **21c** (135 mg, 0.24 mmol) reacted according to general procedure F to afford *guanidinium salt* **3c · TFA** as a fluffy white powder (118 mg, quant.). **MP**: 224 °C. **^{1}H NMR** (CD_3OD, 400 MHz): δ 8.40 (s, 1H), 7.88 (d, *J* = 6.8 Hz, 2H), 7.70 (d, *J* = 6.8 Hz, 2H), 7.64 (d, *J* = 5.6 Hz, 2H), 7.53 (d, *J* = 6.8 Hz, 2H), 7.45 (t, *J* = 6.2 Hz, 2H), 7.37 – 7.30 (m, 3H). 5.69 (s, 2H) ppm. **^{13}C NMR** (CD_3OD, 100 MHz): δ 158.06, 148.96, 142.50, 141.70, 136.58, 136.21, 130.98, 130.52, 129.96, 128.62, 128.52, 127.84, 127.11, 126.93, 122.42, 54.41 ppm. **FTIR**: 3321.9, 3087.1, 2970.4, 1664.6, 1626.4, 1581.9, 1518.1, 1486.2, 1365.5, 1202.5, 1175.7, 1137.8, 1051.5, 838.7, 800.8, 789.8, 766.2, 720.9, 702.6, 688.3, 640.1 cm^{-1}. **HRMS**: m/z calcd for $[M]^+$: 369.1822, found 369.1831.

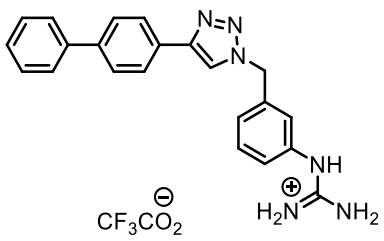

((3-((4-([1,1'-Biphenyl]-4-yl)-1*H*-1,2,3-triazol-1-yl)methyl) phenyl)amino)(amino)methaniminium trifluoroacetate 3d · TFA. Boc-protected guanidine **21d** (135 mg, 0.24 mmol) reacted according to general procedure G to afford *guanidinium salt* **3d · TFA** as an oily yellowish solid (119 mg, quant.). **^{1}H NMR** (CD_3OD, 400 MHz): δ 8.42 (s, 1H), 7.89 (d, *J* = 7.2 Hz, 2H), 7.71 (d, *J* = 8.4 Hz, 2H), 7.68 – 7.60 (m, 2H), 7.52 (t, *J* = 8.0 Hz, 1H), 7.48 – 7.26 (m, 4H), 5.71 (s, 2H) ppm. **^{13}C NMR** (CD_3OD, 100 MHz): δ 158.07, 149.00, 142.51, 141.68, 138.98, 136.94, 131.77, 130.50, 129.96, 128.63, 128.52, 128.22, 127.84, 127.13, 126.46, 126.03, 122.59, 54.44 ppm. **FTIR**: 687.9, 720.8, 763.2, 803.2, 838.3, 978.4, 1006.8, 1050.9, 1131.9, 1186.5, 1348.1, 1432.4, 1459.8, 1484.1, 1588.4, 1670.8, 3134.0 cm^{-1}. **HRMS**: m/z calcd for $[M]^+$: 369.1822, found 369.1840.

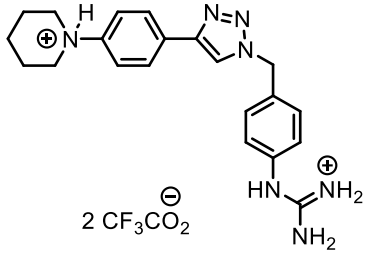

1-(4-(1-(4-((Amino(iminio)methyl)amino)benzyl)-1*H*-1,2,3-triazol-4-yl)phenyl)piperidin-1-ium trifluoroacetate 3e · 2TFA. Boc-protected guanidine **21e** (100 mg, 0.17 mmol) reacted according to general procedure G to afford *guanidinium salt* **3e · 2TFA** as an oily reddish solid (104 mg, quant.). **^{1}H NMR** (CD_3OD, 400 MHz): δ 8.51 (s, 1H), 8.03 (d, *J* = 9.2 Hz, 2H), 7.75 (d, *J* = 9.2 Hz, 2H), 7.51 (d, *J* = 8.4 Hz, 2H), 7.31 (d, *J* = 8.4 Hz, 2H), 5.69 (s, 2H), 3.66 (t, *J* = 5.8 Hz, 2H), 2.09 – 2.02 (m, 4H), 1.83 – 1.76 (m, 2H) ppm. **^{13}C NMR** (CD_3OD, 100 MHz): δ 158.08, 147.321, 143.31, 136.64, 135.87, 133.81, 130.98, 128.48, 126.86, 123.37, 122.94, 58.25, 54.49, 24.83, 22.09 ppm. **FTIR**: 613.3, 720.2, 765.7, 778.3, 799.2, 834.4, 868.7, 977.6, 1012.1, 1050.9, 1127.2, 1179.3, 1356.7, 1430.7, 1456.4, 1496.8, 1517.0, 1579.1, 1666.2, 2954.6, 3135.5, 3336.6 cm^{-1}. **HRMS**: m/z calcd for $[M]^{2+}$: 188.6158, found 188.6163.

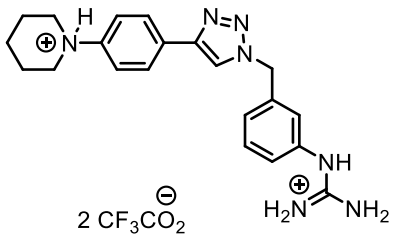

1-(4-(1-(3-((Amino(iminio)methyl)amino)benzyl)-1*H*-1,2,3-triazol-4-yl)phenyl)piperidin-1-ium trifluoroacetate 3f · 2TFA. Boc-protected guanidine **21f** (103 mg, 0.18 mmol) reacted according to general procedure G to afford *guanidinium salt* **3f · 2TFA** as an oily reddish solid (110 mg, quant.). **^{1}H NMR** (CD_3OD, 500 MHz): δ 8.53 (s, 1H), 8.04 (d, *J* = 8.5 Hz, 2H), 7.75 (d, *J* = 8.5 Hz, 2H), 7.50 (t, *J* = 7.8 Hz, 1H), 7.50 – 7.26 (m, 3H), 5.71 (s, 2H), 3.66 (t, *J* = 5.5 Hz, 4H), 2.10 – 2.04 (m, 4H), 1.83 – 1.80 (m, 2H) ppm. **^{13}C NMR** (CD_3OD, 125 MHz): δ 158.08, 147.36, 143.33, 138.73, 136.96, 133.80, 131.76, 128.51, 128.18, 126.47, 126.10, 123.54, 122.94, 58.25, 54.52, 24.85, 22.10 ppm. **FTIR**: 652.2, 695.0, 720.1, 755.7, 777.4, 799.5, 834.2, 868.5, 886.7, 977.1, 1011.9, 1050.3, 1126.8,

1179.4, 1196.9, 1354.2, 1429.2, 1455.8, 1493.3, 1586.1, 1666.5, 2953.5, 3135.5 cm^{-1}. **HRMS**: m/z calcd for $[M]^{2+}$: 188.6158, found 188.6162.

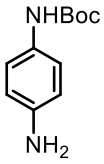

***tert*-Butyl (4-aminophenyl)carbamate 31**. Protocol adapted from the literature.[251] A solution of K_3CO_3 (1.10 eq, 1.52 g, 11.0 mmol) in water (5 mL) was added to a solution of *p*-phenylenediamine **30** (3.00 eq, 3.34 g, 30 mmol) in a mixture of THF / DMF (30 mL : 10 mL). After 5 min, a solution of $(Boc)_2O$ (1.00 eq., 2.18 g, 10.0 mmol) was added. The reaction mixture was stirred at RT for 4 h. THF was evaporated under reduced pressure and CH_2Cl_2 was added. The organic layer was washed with brine (3 ×), water (1 ×) and brine again (1 ×) and was dried over Na_2SO_4. The solvent was evaporated under reduced pressure The crude product was purified by column chromatography (CH_2Cl_2 / AcOEt 100:0 to 80:20) to yield *protected aniline* **31** as a reddish crust (1.85 g, 89% yield). **MP**: 116 °C. **^{1}H NMR** ($CDCl_3$, 400 MHz): δ 7.11 (d, *J* = 7.6 Hz, 2H), 6.61 (d, *J* = 7.2 Hz, 2H), 6.40 (br, 1H), 3.54 (br, 2H), 1.49 (s, 9H) ppm. **^{13}C NMR** ($CDCl_3$, 100 MHz): δ 153.45, 142.48, 129.79, 121.04, 115.67, 80.03, 24.47 ppm. **FTIR**: 556.7, 578.8, 618.6, 641.2, 699.6, 726.9, 761.1, 772.6, 822.0, 905.5, 928.3, 953.6, 1013.7, 1027.9, 1055.3, 1157.4, 1233.3, 1309.7, 1366.0, 1391.1, 1427.7, 1443.3, 1458.8, 1512.3, 1595.2, 1625.8, 1691.8, 2935.9, 2985.0, 3184.8, 3363.1, 3395.1 cm^{-1}. The data are consistent with the literature values.[252]

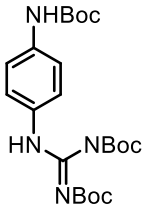

1,2-Bis(*tert*-butoxycarbonyl)-3-(4-((*tert*-butoxycarbonyl)amino)phenyl) guanidine 32. Aniline **31** (91 mg, 0.44 mmol) reacted according to general procedure F. The crude product was purified by column chromatography (cyclohexane / EtOAc, 100:0 to 90:10) to afford *protected guanidine* **32** as an off-white solid (140 mg, 70%). **MP:** 203 °C (slow decomposition). **^{1}H NMR** ($CDCl_3$, 400 MHz): δ 11.61 (br, 1H), 10.13 (br, 1.08), 7.36 (d, *J* = 9.2 Hz, 2H), 7.25 (d, *J* = 8.8 Hz, 2H), 6.96 (br, 1H), 1.52 (s, 9H), 1.48 (s, 9H), 1.47 (s, 9H) ppm. **^{13}C NMR** ($CDCl_3$, 100 MHz): δ 163.62, 154.14, 153.44, 152.88, 136.00, 131.27, 123.74, 118,89, 83.74, 80.10, 79.60, 28.48, 28.30, 28.21 ppm. **FTIR**: 554.8, 577.1, 601.0, 631.4, 640.2, 713.0, 760.7, 808.0, 851.6, 883.6, 905.9, 958.7, 1018.3, 1028.1, 1051.3, 1107.0, 1149.3, 1234.6, 1284.4, 1314.9, 1367.1, 1393.1, 1408.1, 1453.8, 1477.0, 1532.8, 1601.9, 1623.1, 1644.8, 1718.0, 2934.2, 2980.7, 3264.8 cm^{-1}.

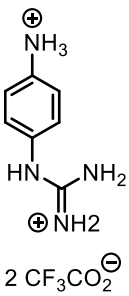

4-((Amino(iminio)methyl)amino)benzenaminium trifluoroacetate 29 · 2TFA. Protected guanidine **32** (100 mg, 0.22 mmol) reacted according to general procedure G to afford *guanidinium salt* **32** as an oily reddish solid (84 mg, quant.). **MP:** 203 °C (slow decomposition). **^{1}H NMR** (CD_3OD, 500 MHz): δ 7.29 – 7.26 (m, 2H), 7.22 – 7.19 (m, 2H) ppm **^{13}C NMR** (CD_3OD, 125 MHz): δ 158.33, 138.38, 132.31, 128.16,

122.24 ppm. **FTIR**: 563.2, 575.6, 597.0, 641.0, 721.9, 798.9, 838.5, 1022.2, 1127.4, 1183.4, 1260.8, 1432.9, 1514.8, 1662.5, 2627.3, 3161.1, 3344.2 cm^{-1}.

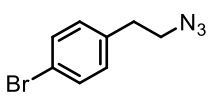

1-(2-Azidoethyl)-4-bromobenzene 43. 4-Bromophenethyl bromide **42** (1.74 mL, 11.4 mmol) reacted according to general procedure B to yield *azide* **43** as a pale yellow oil (2.52 g, 98%).**^{1}H NMR** ($CDCl_3$, 400 MHz): δ 7.63 – 732 (m, 2H), 7.19 – 6.98 (m, 2H), 3.49 (t, *J* = 7.1 Hz, 2H), 2.84 (t, *J* = 7.1 Hz, 2H) ppm. **^{13}C NMR** ($CDCl_3$, 100 MHz): δ 137.17, 131.90, 130.64, 120.86, 52.33, 34.93 ppm. **FTIR**: 540.5, 554.7, 597.5, 634.9, 711.5, 771.4, 802.4, 829.9, 909.2, 929.6, 1011.1, 1072.1, 1104.2, 1201.7, 1251.1, 1347.1, 1404.9, 1458.3, 1488.4, 1592.0, 1736.6, 2090.3, 2870.4, 2930.8 cm^{-1}.

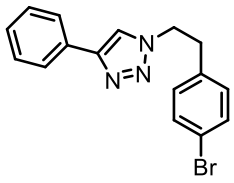

1-(4-Bromophenethyl)-4-phenyl-1*H*-1,2,3-triazole 36e. Azide **43** (1.10 g, 4.87 mmol) reacted with phenylacetylene (497 mg, 4.87 mmol) according to general procedure C. The residue was recrystallized from EtOH to yield *triazole* **36e** as fluffy white crystals (1.29 g, 81 %). **MP**: 182 °C. **^{1}H NMR** (DMSO-d_6, 400 MHz): δ 8.53 (s, 1H), 7.85 – 7.78 (m, 2H), 7.51 – 7.40 (m, 4H), 7.35 – 7.29 (m, 1H), 7.21 – 7.14 (m, 2H), 4.65 (t, *J* = 7.1 Hz, 2H), 3.20 (t, *J* = 7.1 Hz, 2H) ppm. **^{13}C NMR** (DMSO-d_6, 100 MHz): δ 146.19, 137.11, 131.28, 131.00, 130.79, 128.91, 127.82, 125.09, 121.32, 119.78, 50.34, 34.84 ppm. **FTIR:** 535.2, 546.1, 564.8, 619.3, 692.0, 710.8, 764.2, 808.1, 844.7, 911.9, 976.3, 1011.6, 1026.2, 1050.6, 1072.1, 1103.1, 1190.8, 1349.7, 1434.3, 1462.3, 1487.6, 1592.3, 3084.5 cm^{-1}.

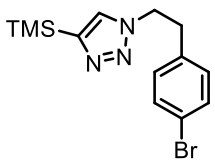

1-(4-Bromophenethyl)-4-(trimethylsilyl)-1*H*-1,2,3-triazole 44. Azide **43** (1.10 g, 4.87 mmol) reacted with TMS-acetylene (690 µL, 4.87 mmol) according to general procedure C. The crude product was purified by column chromatography (cyclohexane / EtOAc, 100:0 to 50:50) to yield *triazole* **44** as a white powder (431 mg, 27%). **MP**: 109 °C. **^{1}H NMR** ($CDCl_3$, 400 MHz): δ 7.43 – 7.36 (m, 2H), 7.28 (s, 1H), 6.97 – 6.90 (m, 2H), 4.59 (t, *J* = 7.3 Hz, 2H), 3.18 (t, *J* = 7.3 Hz, 2H), 0.31 (s, 9H).**^{13}C NMR** ($CDCl_3$, 125 MHz): δ 146.57, 136.35, 131.99, 130.59, 129.43, 121.12, 50.88, 36.50, -0.99. **FTIR**: 531.3, 541.0, 547.2, 554.2, 568.1, 577.7, 618.9, 634.1, 656.4, 710.8, 748.8, 805.7, 834.1, 999.2, 1012.0, 1052.3, 1072.2, 1106.8, 1149.0, 1194.9, 1244.1, 1407.7, 1451.9, 1488.8, 2961.4 cm^{-1}

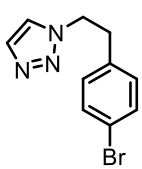

1-(4-Bromophenethyl)-1*H*-1,2,3-triazole 36f. TBAF (1 M in THF, 1.50 eq., 2.00 mL, 2.00 mmol) was added dropwise at 0 °C to a solution of silane **44** (1.00 eq., 433 mg, 1.34 mmol) in THF (3 mL). The reaction mixture was stirred ON at RT and quenched with sat. NH_4Cl. CH_2Cl_2 was added and the organic layer was washed with water (3 ×) and dried over $MgSO_4$. The solvent was evaporated under reduced pressure and the

crude product was purified by column chromatography (CH_2Cl_2 / EtOAc, 80:20) to yield *triazole* **36f** as a white powder (283 mg, 84%). **MP**: 92 °C **^{1}H NMR** ($CDCl_3$, 400 MHz): δ 7.62 (s, 1H), 7.47 – 7.31 (m, 2H), 7.27 (s, 1H), 7.00 – 6.79 (m, 2H), 4.59 (t, *J* = 7.0 Hz, 2H), 3.18 (t, J = 7.1 Hz, 2H) ppm. **^{13}C NMR** ($CDCl_3$, 100 MHz): δ 136.11, 133.73, 132.05, 130.52, 123.86, 121.19, 51.31, 36.33 ppm.

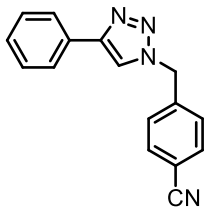

4-((4-Phenyl-1*H*-1,2,3-triazol-1-yl)methyl)benzonitrile 35a. Bromide **5a** (400 mg, 1.27 mmol) reacted according to general procedure H. The crude product was purified by column chromatography (toluene / EtOAc 80:20) to yield *nitrile* **35a** as a yellow powder (169 mg, 51 %). **MP**: 135 °C. **^{1}H NMR** ($CDCl_3$, 400 MHz): δ 7.88 – 7.76 (m, 2H), 7.73 (s, 1H), 7.71 – 7.64 (m, 2H), 7.48 – 7.30 (m, 5H), 5.66 (s, 2H) ppm. **^{13}C NMR** ($CDCl_3$, 100 MHz): δ 148.75, 140.03, 133.00, 130.25, 129.01, 128.56, 128.46, 125.83, 119.81, 118.24, 112.89, 53.54 ppm. **FTIR**: 554.0, 583.1, 676.7, 697.9, 709.7, 730.6, 764.2, 809.6, 825.0, 860.9, 923.1, 972.4, 1044.3, 1076.2, 1188.2, 1289.0, 1433.3, 1444.2, 1464.6, 1483.4, 1505.4, 1609.3, 2228.3, , 3136.7 cm^{-1}. The data are consistent with the literature values.[253]

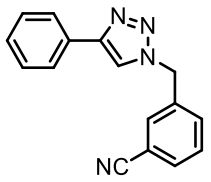

3-((4-Phenyl-1*H*-1,2,3-triazol-1-yl)methyl)benzonitrile 35b. Bromide **5b** (1.19 g, 3.79 mmol) reacted according to general procedure H. The crude product was purified by column chromatography (cyclohexane / EtOAc 70:30) to yield *nitrile* **35b** as a yellow powder (466 mg, 47%). **MP**: 141 °C. **^{1}H NMR** ($CDCl_3$, 400 MHz): δ 7.85 – 7.79 (m, 2H), 7.73 (s, 1H), 7.70 – 7.64 (m, 1H), 7.63 – 7.59 (m, 1H), 7.55 – 7.48 (m, 2H), 7.46 – 7.39 (m, 2H), 7.38 – 7.31 (m, 1H), 5.63 (s, 2H). **^{13}C NMR** ($CDCl_3$, 400 MHz): δ 148.78, 136.54, 132.54, 132.27, 131.36, 130.28, 130.22, 129.02, 128.57, 125.87, 119.73, 118.14, 113.52. **FTIR:** 547.2, 554.0, 563.6, 608.5, 677.6, 687.6, 708.5, 726.0, 754.0, 818.0, 847.9, 907.3, 941.0, 977.3, 1001.7, 1027.3, 1047.2, 1079.5, 1139.2, 1197.8, 1438.3, 1461.9, 1482.5, 1584.2 , 2229.8, 3061.3, 3081.0 cm^{-1}. The data are consistent with the literature values.[254]

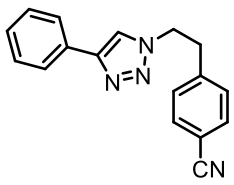

4-(2-(4-Phenyl-1*H*-1,2,3-triazol-1-yl)ethyl)benzonitrile 35e. Bromide **36e** (800 mg, 2.44 mmol) reacted according to the general procedure H. The residue was purified by column chromatography (cyclohexane / EtOAc 70:30) to yield *nitrile* **35e** as a white powder (435 mg, 65%). **MP**: 177 °C. **^{1}H NMR** ($CDCl_3$, 400 MHz): δ 7.80 – 7.73 (m, 2H), 7.59 (d, *J* = 8.1 Hz, 2H), 7.45 – 7.38 (m, 2H) 7.53 (s, 1H), 7.37 – 7.30 (m, 1H), 7.25 – 7.20 (m, 2H), 4.66 (t, *J* = 7.1 Hz, 2H), 3.35 (t, *J* = 7.1 Hz, 2H) ppm. **^{13}C NMR** (DMSO-d_6, 100 MHz): δ 146.19, 137.11, 131.28, 131.00, 130.79, 128.91, 127.82, 125.09, 121.32, 119.78, 50.34, 34.84 ppm. **FTIR**: 555.6, 582.9, 694.4, 710.5, 767.9, 825.1, 854.2, 911.4, 980.0, 1027.1, 1051.3, 1080.6, 1110.7, 1177.0, 1365.7, 1458.1, 1484.5, 1505.0, 1608.7, 2223.3, 2970.2, 3086.2 cm^{-1}.

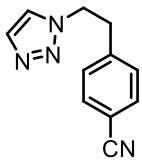

4-(2-(1*H*-1,2,3-Triazol-1-yl)ethyl)benzonitrile 35f. Bromide **36f** (230 mg, 0.91 mmol) reacted according to general procedure H. The crude product was purified by column chromatography (CH_2Cl_2 / AcOEt 100:0 to 60:40) to yield nitrile **35f** as a white powder (120 mg, 67%). **MP**: 107 °C. **^{1}H NMR** ($CDCl_3$, 400 MHz): δ 7.64 (s, 1H), 7.57 (d, *J* = 8.1 Hz, 2H), 7.30 (s, 1H), 7.18 (d, *J* = 8.1 Hz, 2H), 4.64 (t, *J* = 7.0 Hz, 2H), 3.31 (t, *J* = 7.0 Hz, 2H) ppm. **^{13}C NMR** ($CDCl_3$, 100 MHz): δ 142.61, 133.89, 132.71, 129.64, 123.83, 118.64, 111.37, 50.81, 36.82 ppm. **FTIR**: 556.8, 599.5, 638.6, 698.9, 769.6, 789.4, 826.9, 859.5, 877.0, 950.3, 1029.6, 1079.8, 1117.3, 1180.9, 1238.7, 1283.6, 1376.2, 1456.2, 1505.7, 1608.1, 2228.0, 2922.4 cm^{-1}.

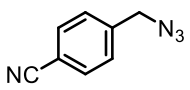

4-(Azidomethyl)benzonitrile 40c. 4-Cyanobenzyl bromide **41c** (2.50 g, 12.8 mmol) reacted according to general procedure A to yield *azide* **40c** as a pale yellow oil which crystallized into white needles upon standing (2.00 g, 99%). **^{1}H NMR** ($CDCl_3$, 400 MHz): δ 7.73 – 7.62 (m, 2H), 7.47 – 7.40 (m, 2H), 4.45 (s, 2H) ppm. **^{13}C NMR** ($CDCl_3$, 100 MHz): δ 140.90, 132.78, 128.63, 118.56, 112.35, 54.18 ppm. **FTIR**: 547.2, 617.8, 659.0, 695.3, 751.0, 814.2, 846.9, 914.6, 1020.8, 1116.9, 1177.1, 1204.7, 1255.0, 1290.8, 1345.7, 1414.3, 1439.0, 1505.9, 1609.7, 2094.7, 2229.1, 2932.2 cm^{-1}. The data are consistent with the literature values.[255]

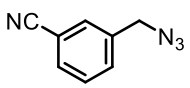

3-(Azidomethyl)benzonitrile 40d. 3-Cyanobenzyl bromide **41d** (6.94 g, 35.6 mmol) reacted according to the general procedure A to yield *azide* **40d** as a pale-yellow oil which crystallized into white needles upon standing (5.49 g, 98%). **^{1}H NMR** ($CDCl_3$, 400 MHz): 7.65 – 7.59 (m, 2H), 7.59 – 7.53 (m, 1H), 7.53 – 7.47 (m, 1H), 4.42 (s, 2H) ppm. **^{13}C NMR** ($CDCl_3$, 125 MHz): δ 137.16, 132.35, 131.91, 131.42, 129.75, 118.43, 113.02, 53.74 ppm. **FTIR:** 545.0, 562.7, 604.2, 649.9, 686.5, 730.0, 792.6, 866.3, 920.5, 1000.5, 1096.5, 1149.5, 1173.9, 1231.7, 1254.5, 1431.8, 1483.7, 1584.6, 1604.0, 2095.1, 2231.1, 2939.7 cm^{-1}. The data are consistent with the literature values.[167]

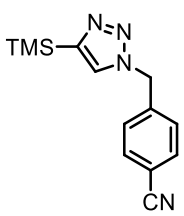

4-((4-(Trimethylsilyl)-1*H*-1,2,3-triazol-1-yl)methyl)benzonitrile 45. Azide **40c** (1.00 eq., 800 mg, 5.05 mmol) reacted with TMS-acetylene (1.50 eq., 1.1 mL, 7.58 mmol) according to general procedure C. The crude product was purified by column chromatography (cyclohexane / AcOEt 90:10 to 50:50) to yield *triazole* **45** as a yellow crust (577 mg, 45% yield). **^{1}H NMR** ($CDCl_3$, 400 MHz): δ 7.71 – 7.63 (m, 2H), 7.48 (s, 1H), 7.37 – 7.31 (m, 2H), 5.63 (s, 1H), 0.31 (s, 9H) ppm. **^{13}C NMR** ($CDCl_3$, 100 MHz): δ 147.78, 140.35, 132.91, 129.15, 128.47, 118.30, 112.65, 52.80, -1.07 ppm. **FTIR**: 548.2, 630.6, 639.5, 689.6, 724.5, 758.9, 837.3, 938.9, 1000.9, 1021.3, 1047.0, 1102.5, 1192.8, 1249.2, 1488.5, 1506.6, 1611.5, 2230.1, 2957.5, 3124.7 cm^{-1}.

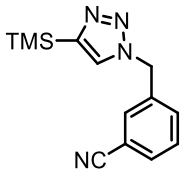

3-((4-(Trimethylsilyl)-1*H*-1,2,3-triazol-1-yl)methyl)benzonitrile 46. Azide **40d** (1.02 g, 6.45 mmol) reacted with TMS-acetylene (900 µL, 6.45 mmol) according to general procedure C. The crude product was purified by column chromatography (cyclohexane / AcOEt 90:10 to 50:50) to yield *triazole* **46** as a white powder (798 mg, 48%). **MP**: 69 °C. **^{1}H NMR** ($CDCl_3$, 400 MHz): δ 7.92 – 7.31 (m, 5H), 5.60 (s, 2H), 0.31 (s, 9H) ppm. **^{13}C NMR** ($CDCl_3$, 100 MHz): δ 147.84, 136.80, 132.40, 132.33, 131.36, 130.13, 129.04, 118.24, 113.43, 52.58, -1.02 ppm. **FTIR**: 553.0, 611.2, 631.0, 654.3, 687.2, 708.2, 722.8, 752.2, 839.0, 1006.7, 1047.8, 1114.4, 1154.8, 1192.4, 1247.5, 1356.3, 1437.4, 1488.5, 2233.2, 2959.9, 3086.9 cm^{-1}.

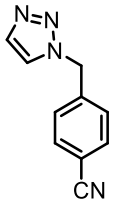

4-((1*H*-1,2,3-Triazol-1-yl)methyl)benzonitrile 35c. TBAF (1 M in THF, 2.14 eq., 4.40 mL, 4.40 mmol) was added dropwise at 0 °C to a solution of silane **45** (1.00 eq., 527 mg, 2.06 mmol) in THF (4 mL). The reaction mixture was stirred ON at RT and quenched with sat. NH_4Cl. CH_2Cl_2 was added and the organic layer was washed with water (3 ×) and dried over $MgSO_4$. The solvent was evaporated under reduced pressure and the crude product was purified by column chromatography (Cyclohexane / EtOAc, 80:10 to 30:70) to yield *triazole* **35c** as a white powder (301 mg, 79%). **MP**: 87 °C. **^{1}H NMR** ($CDCl_3$, 400 MHz): 7.77 (s, 1H), 7.72 – 7.64 (m, 2H), 7.55 (s, 1H), 7.39 – 7.30 (m, 2H), 5.64 (s, 2H) ppm.**^{13}C NMR** ($CDCl_3$, 100 MHz): 140.05, 134.78, 133.03, 128.44, 123.73, 118.24, 112.95, 53.34 ppm. **FTIR:** 535.0, 555.0, 584.2, 595.7, 635.5, 684.2, 702.2, 724.0, 766.2, 814.9, 863.8, 953.4, 1029.8, 1093.0, 1120.1, 1259.3, 1293.5, 1374.1, 1441.8, 1462.8, 1488.0, 1507.0, 1610.9, 2229.9, 3117.8 cm^{-1}. The data are consistent with the literature values.[253]

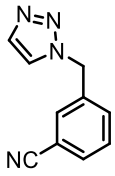

3-((1*H*-1,2,3-Triazol-1-yl)methyl)benzonitrile 35d. TBAF (1 M in THF, 1.50 eq., 4.50 mL, 4.50 mmol) was added dropwise at 0 °C to a solution of silane **46** (1.00 eq., 757 mg, 2.95 mmol) in THF (6 mL). The reaction mixture was stirred ON at RT and quenched with sat. NH_4Cl. CH_2Cl_2 was added and the organic phase was washed with water (3 ×) and dried over $MgSO_4$. The solvent was evaporated under reduced pressure and he crude product was purified by column chromatography (CH_2Cl_2 / EtOAc, 80:20) to yield *triazole* **35d** as a white powder (431 mg, 79%). **MP**: 90 °C. **^{1}H NMR** ($CDCl_3$, 400 MHz): δ 7.75 (s, 1H), 7.66 – 7.61 (m, 1H), 7.58 (s, 1H), 7.56 – 7.46 (m, 3H), 5.62 (s, 2H). **^{13}C NMR** ($CDCl_3$, 100 MHz): 136.54, 134.72, 132.45, 132.21, 131.26, 130.14, 123.72, 118.14, 113.41, 52.97. FTIR: 552.5, 564.3, 604.9, 643.3, 684.2, 696.6, 719.3, 743.3, 797.7, 815.9, 884.3, 916.7, 939.6, 963.1, 1001.2, 1028.3, 1084.2, 1100.6, 1116.3, 1153.6, 1180.3, 1242.7, 1265.8, 1295.6, 1365.3, 1462.7, 1482.9, 1584.8, 1605.2 , 2230.2, 3061.5, 3091.4, 3138.1 cm^{-1}

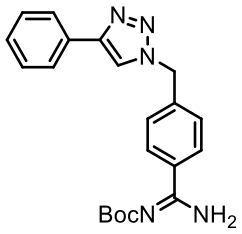

***tert*-Butyl (amino(4-((4-phenyl-1*H*-1,2,3-triazol-1-yl)methyl)phenyl) methylene)carbamate 49**. Protocols adapted from the literature.[168–170] Et_3N (4.00 eq., 1.90 mL, 13.8 mmol) was added to a suspension of nitrile **35a** (1.00 eq., 900 mg, 3.46 mmol) and $NH_2OH \cdot HCl$ (4.00 eq., 961 mg, 13.8 mmol) in EtOH (10 mL). The mixture was stirred at reflux for 3 h. After cooling down to RT, the suspension was poured into water (100 mL). The precipitate was filtered, washed with CH_3OH (1 ×) then Et_2O (1 ×) to yield crude *hydroxyamidine* **47** as a white powder (499 mg ~1.49 mmol) which was used as such for the next reaction. **^{1}H NMR** (DMSO-d_6, 400 MHz): δ 9.65 (s, 1H), 8.65 (s, 1H), 7.87 – 7.80 (m, 2H), 7.70 – 7.65 (m, 2H), 7.47 – 7.40 (m, 2H), 7.36 – 7.29 (m, 3H), 5.81 (s, 2H), 5.66 (s, 2H) ppm.

The residue was dissolved in AcOH (10 mL) and Ac_2O (4.00 eq., 563 µL, 5.96 mmol) was added to the solution. The mixture was stirred for at RT for 2 h. The precipitate was filtered, washed with CH_3OH (1 ×) then Et_2O (1 ×) to yield crude *acetoxyamidine* **48** as a white crust, which was used as such in the next reaction (420 mg, ~1.25 mmol). **^{1}H NMR** (DMSO-d_6, 400 MHz): δ 8.66 (s, 1H), 7.85 (d, J = 7.3 Hz, 2H), 7.72 (d, J = 8.2 Hz, 2H), 7.52 – 7.26 (m, 5H), 6.81 (br, 2H), 5.70 (s, 2H), 2.12 (s, 3H) ppm.

Acetoxyamidine **48** (420 mg, 1.25 mmol) reacted according to general procedure J to afford crude *amidinium acetate* **34 ·AcOH** as a white powder, which was used as such in the next reaction (372 mg, ~1.10 mmol). **^{1}H NMR** (DMSO-d_6, 400 MHz): δ 8.69 (s, 2H), 7.84 (d, *J* = 7.3 Hz, 2H), 7.79 (d, *J* = 8.0 Hz, 2H), 7.52 (d, *J* = 8.0 Hz, 2H), 7.45 (t, *J* = 7.7 Hz, 2H), 7.37 – 7.30 (m, 1H), 5.77 (s, 3H), 1.79 (s, 3H) ppm.

Finally, the residue was dissolved in CH_3OH (25 mL) and $(Boc)_2O$ (1.50 eq., 361 mg, 1.65 mmol) and Et_3N (1.50 eq., 230 µL, 1.65 mmol) were added. The reaction mixture was stirred for 3 h at 40 °C. The solvent was evaporated under reduced pressure and the crude product was purified by column chromatography (CH_2Cl_2 / CH_3OH**,** 100:0 to 98:2) to yield *Boc-protected amidine* **49** as a white powder (378 mg, 29% over 4 steps). **MP**: 134 °C (decomposition). **^{1}H NMR** (DMSO-d_6, 400 MHz): δ 8.99 (br, 2H), 8.67 (s, 1H), 7.95 (d, *J* = 8.3 Hz, 2H), 7.88 – 7.82 (m, 2H), 7.48 – 7.39 (m, 4H), 7.38 – 7.29 (m, 1H), 5.73 (s, 2H), 1.43 (s, 9H) ppm. **^{13}C NMR** (CD_3OD, 400 MHz): δ 167.06, 164.38, 148.48, 138.50, 135.67, 130.38, 128.99, 128.45, 128.21, 128.13, 125.80, 119.80, 79.97, 53.76, 28.29 ppm.

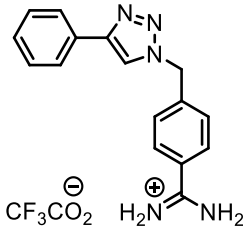

Amino(4-((4-phenyl-1H-1,2,3-triazol-1-yl)methyl)phenyl) methaniminium trifluoroacetate 34a · TFA. Boc-protected amidine **49** (100 mg, 0.26 mmol) reacted according to general procedure G to yield *amidinium salt* **34a · TFA** (103 mg, quant.) as a white snowy powder. **MP**: 210 °C (decomposition). **^{1}H NMR** (DMSO-d_6, 400 MHz): δ 9.30 (br, 2H), 9.07 (br, 2H), 8.71 (s, 1H), 7.88 – 7.77 (m, 4H), 7.56 (d, *J* = 8.2 Hz, 2H), 7.45 (t, *J* = 7.7 Hz, 2H), 7.34 (t, *J* = 7.5 Hz, 1H), 5.79 (s, 2H) ppm. **FTIR**: 658.6, 691.9, 725.5, 765.7, 796.2, 838.8, 915.1, 978.3, 1019.1, 1044.1, 1080.1, 1139.6, 1184.9, 1373.9, 1437.8, 1493.1, 1543.7, 1617.1, 1666.9, 3092.0, 3311.9 cm^{-1}. **HRMS**: m/z calcd for $[M]^+$ 278.1400, found 278.1401.

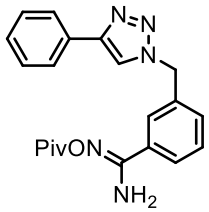

(3-((4-Phenyl-1*H*-1,2,3-triazol-1-yl)methyl)-*N*-(pivaloyloxy)benzimidamide 50b. Nitrile **35b** (337 mg, 1.29 mmol) reacted according to general procedure I. The crude product was purified by column chromatography (CH_2Cl_2 / CH_3OH**,** 99:1 to 95:5) to yield *acyloxyamidine* **50b** as a white snowy powder (183 mg, 38%). **MP**: 148 °C. **^{1}H NMR** (CD_3OD, 400 MHz): δ 8.40 (s, 1H), 7.90 – 7.80 (m, 3H), 7.80 – 7.73 (m, 1H), 7.60 – 7.48 (m, 2H), 7.48 – 7.41 (m, 2H), 7.40 – 7.31 (m, 1H), 5.71 (s, 2H), 1.36 (s, 9H) ppm. **^{13}C NMR** (CD_3OD, 125 MHz): δ 177.71, 159.15, 149.27, 137.19, 133.69, 131.67, 131.59, 130.41, 129.96, 129.37, 128.49, 128.36, 126.68, 122.34, 54.73, 39.91, 27.72 ppm. **FTIR:** 607.5, 635.2, 688.7, 708.7, 744.8, 764.5, 813.3, 881.7, 899.1, 912.4, 928.6, 975.1, 1032.6 1081.9, 1140.1, 1278.1, 1368.0, 1399.4, 1459.6, 1478.1, 1590.8, 1618.9, 1736.0, 2974.9, 3350.4, 3482.8 cm^{-1}.

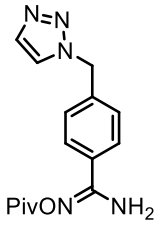

(4-((1*H*-1,2,3-Triazol-1-yl)methyl)-*N*-(pivaloyloxy)benzimidamide 50c. Nitrile **35c** (145 mg, 0.79 mmol) reacted according to general procedure I. The crude product was purified by column chromatography (cyclohexane / EtOAc, 50:50 to 0:100) to yield *acyloxyamidine* **50c** as a white powder (98 mg, 41%). **MP:** 185 °C. **^{1}H NMR** ($CDCl_3$, 400 MHz): δ 8.05 (d, *J* = 1.0 Hz, 1H), 7.82 – 7.73 (m, 3H), 7.45 – 7.37 (m, 2H), 5.72 (s, 2H), 4.92 (s, 3H), 1.35 (s, 9H) ppm. **^{13}C NMR** ($CDCl_3$, 100 MHz): 177.71, 159.07, 139.66, 134.77, 133.06, 129.15, 128.88, 126.05, 54.23, 39.93, 27.71 ppm. **FTIR**: 611.6, 630.9, 685.8, 712.1, 723.2, 761.7, 804.0, 825.0, 864.1, 888.3, 928.3, 1029.0, 1083.7, 1142.7, 1275.1, 1312.0, 1366.6, 1406.7, 1464.7, 1476.0, 1522.1, 1560.6, 1583.3, 1614.2, 1735.0, 3099.3, 3375.5, 3503.7 cm^{-1}.

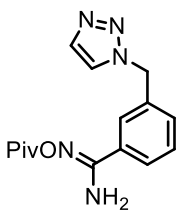

(3-((1*H*-1,2,3-Triazol-1-yl)methyl)-*N'*-(pivaloyloxy)benzimidamide 50d. Nitrile **35d** (132 mg, 0.71 mmol) reacted according to the general procedure I. The crude product was purified by column chromatography (cyclohexane / EtOAc, 50:50 to 0:100) to yield *acyloxyamidine* **50d** as a white powder (125 mg, 58%). **MP:** 130 °C. **^{1}H NMR** ($CDCl_3$, 400 MHz): δ 7.68 (s, 2H), 7.67 – 7.63 (m, 1H),

7.53 (s, 1H), 7.38 (t, *J* = 7.7 Hz, 1H), 7.33 – 7.28 (m, 1H), 5.54 (s, 2H), 5.16 (br, 2H), 1.32 (s, 9H) ppm.**^{13}C NMR** ($CDCl_3$, 100 MHz): 175.07, 156.20, 135.60, 134.47, 132.27, 130.53, 129.65, 127.04, 126.67, 123.75, 53.59, 39.07, 27.61 ppm. **FTIR**: 600.0, 647.0, 710.9, 759.7, 825.1, 880.1, 925.2, 962.3, 1031.0, 1139.1, 1214.0, 1276.1, 1349.2, 1398.9, 1437.8, 1477.2 1589.6, 1618.6, 1735.5, 3100.9, 3352.8, 3483.9 cm^{-1}.

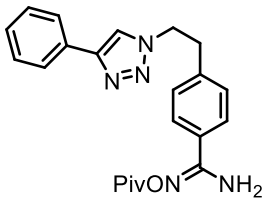

4-(2-(4-Phenyl-1H-1,2,3-triazol-1-yl)ethyl)-*N*'-(pivaloyloxy) benzimidamide 50e. Et_3N (4.00 eq., 720 µL, 5.17 mmol) was added to a suspension of nitrile **35e** (1.00 eq., 357 mg, 1.30 mmol) and $NH_2OH \cdot HCl$ (4.00 eq., 360 mg, 5.17 mmol) in EtOH (5 mL). The mixture was stirred at reflux for 2 h. After cooling down to RT, EtOAc was added and the organic phase was washed with water (3 ×) and brine (1 ×), and dried over $MgSO_4$. The solvent was evaporated under reduced pressure and the solid residue was triturated in CH_2Cl_2 and filtered to yield the intermediate *hydroxyamidine* as a white powder (300 mg, 75%). **^{1}H NMR** (DMSO-d_6, 400 MHz): δ 9.58 (s, 1H), 8.55 (s, 1H), 7.80 (d, *J* = 8.2 Hz, 3H), 7.58 (d, *J* = 8.1 Hz, 2H), 7.44 (t, *J* = 7.6 Hz, 2H), 7.32 (t, *J* = 7.7 Hz, 1H), 7.22 (d, *J* = 8.1 Hz, 2H), 5.77 (br, 2H), 4.67 (t, *J* = 7.2 Hz, 2H), 3.24 (t, *J* = 7.2 Hz, 2H) ppm.

PivCl (1.00 eq., 80 µL, 0.61 mmol) was added to a solution of the previously synthesized hydroxyamidine (1.00 eq., 187 mg, 0.61 mmol) and Et_3N (1.00 eq., 90 µL, 0.61 mmol) in CH_2Cl_2 (10 mL). The mixture was stirred 1 h at RT. The solvent was evaporated under reduced pressure and the crude product was purified by column chromatography (CH_2Cl_2 / CH_3OH, 100:0 to 94:6) to yield *acyloxyamidine* **50e** as a white powder (130 mg, 54%, 41% over 2 steps). **MP**: 192 °C (decomposition). **^{1}H NMR** (DMSO-d_6, 500 MHz): δ 8.56 (s 1H), 7.88 – 7.74 (m, 2H), 7.69 – 7.54 (m, 2H), 7.49 – 7.39 (m, 2H), 7.37 – 7.24 (m, 3H), 6.55 (br, 2H), 4.69 (t, *J* = 7.6 Hz), 3.28 (t, *J* = 7.7 Hz), 1.24 (s, 9H) ppm. **^{13}C NMR** (DMSO-d_6, 125 MHz): δ 174.57, 156.18, 146.19, 140.16, 130.81, 130.17, 128.94, 128.69, 127.83, 126.90, 125.10, 121.35, 50.35, 38.35, 35.27, 27.18 ppm. **FTIR**: 689.4, 709.1, 732.3, 764.1, 818.4, 833.3, 858.0, 892.3, 931.2, 973.9, 1028.8, 1051.2, 1080.1, 1135.7, 1194.5, 1275.3, 1400.4, 1466.1, 1519.5, 1558.0, 1586.4, 1619.0, 1739.2, 3367.5, 3488.1 cm^{-1}.

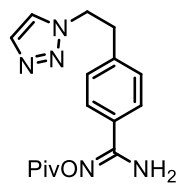

4-(2-(1*H*-1,2,3-Triazol-1-yl)ethyl)-*N'*-(pivaloyloxy)benzimidamide 50f. Nitrile **35f** (67 mg, 0.34 mmol) reacted according to general procedure I. The crude product was purified by column chromatography (cyclohexane / AcOEt 50:50 to 0:100) to yield *acyloxyamidine* **50f** as a white powder (49 mg, 46%)**. MP**: 175 °C (decomposition). **^{1}H NMR** ($CDCl_3$, 400 MHz): δ 7.64 – 7.58 (m, 3H), 7.24 (s, 1H), 7.14 – 7.06 (m, 2H), 5.03 (br, 2H), 4.62 (t, *J* = 6.9 Hz, 2H), 3.25 (t, *J* = 6.9 Hz, 2H), 1.33 (s, 9H) ppm. **^{13}C NMR**

($CDCl_3$, 100 MHz): δ 175.01, 156.40, 140.31, 133.73, 130.27, 129.16, 127.32, 124.00, 51.27, 39.08, 36.67, 27.64 ppm. **FTIR**: 619.6, 694.6, 731.8, 763.8, 802.0, 841.1, 881.5, 928.0, 1023.1, 1034.7, 1085.0, 1116.8, 1150.7, 1277.1, 1408.5, 1441.9, 1475.0, 1526.5, 1557.9, 1583.3, 1614.7, 1730.2, 3099.5, 3383.5, 3507.1 cm^{-1}.

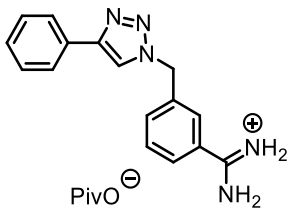

Amino(3-((4-phenyl-1*H*-1,2,3-triazol-1-yl)methyl)phenyl) methaniminium pivalate 34b · PivOH. Acyloxyamidine **50b** (100 mg, 0.26 mmol) reacted according to general procedure J to yield *amidinium pivalate* **34b · PivOH.** as a white powder (101 mg, quant.) **MP**: 242 °C (decomposition) **^{1}H NMR** (DMSO-d_6, 400 MHz): δ 8.68 (s, 1H), 7.92 – 7.80 (m, 3H), 7.79 – 7.69 (m, 1H), 7.67 – 7.55 (m, 2H), 7.50 – 7.39 (m, 2H), 7.40 – 7.28 (m, 1H), 5.73 (s, 2H), 1.04 (s, 9H) ppm. **^{13}C NMR** (DMSO-d_6, 100 MHz): δ 183.58, 165.74, 146.73, 136.53, 132.17, 131.15, 130.62, 129.41, 128.89, 127.93, 127.32, 127.22, 125.19, 121.70, 52.59, 38.52, 28.36 ppm. **FTIR**: 622.0, 692.5, 711.9, 742.2, 763.8, 816.9, 884.8, 913.9, 974.8, 1027.3, 1048.4, 1077.0, 1136.7, 1194.7, 1222.2, 1354.8, 1366.9, 1407.4, 1463.6, 1478.8, 1505.4, 1531.5, 1567.5, 1612.5, 2953.8 cm^{-1}. **HRMS**: m/z calcd for $[M]^+$ 278.1400, found 278.1408.

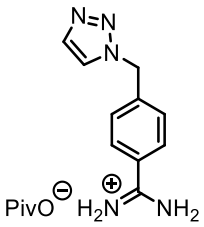

((4-((1*H*-1,2,3-Triazol-1-yl)methyl)phenyl)(amino)methaniminium pivalate 34c · PivOH. Acyloxyamidine **50c** (80 mg, 0.27 mmol) reacted according to general procedure J to yield *amidinium pivalate* **34c · PivOH** as a white powder (81 mg, quant.). **MP**: 236 °C (decomposition). **^{1}H NMR** (CD_3OD, 400 MHz): δ 8.12 (d, *J* = 1.0 Hz, 1H), 7.86 – 7.80 (m, 3H), 7.57 – 7.52 (m, 2H), 5.81 (s, 2H), 4.96 (br, 4H), 1.17 (s, 9H). **^{13}C NMR** (CD_3OD, 125 MHz): δ 187.65, 168.13, 143.16, 134.88, 130.01, 129.7347, 129.54, 126.33, 53.90, 40.78, 28.82. **FTIR:** 630.7, 692.9, 712.2, 741.9, 763.8, 802.0, 886.4, 974.9, 1026.2, 1048.8, 1075.8, 1143.8, 1221.9, 1355.6, 1408.2, 1478.7, 1504.9, 1619.2, 2955.6 cm^{-1}. **HRMS**: m/z calcd for $[M]^+$ 202.1087, found 202.1106.

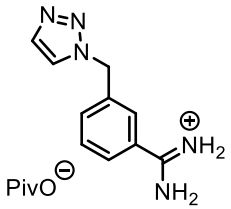

(3-((1H-1,2,3-Triazol-1-yl)methyl)phenyl)(amino)methaniminium pivalate 34d · PivOH. Acyloxyamidine **50d** (107 mg, 0.35 mmol) reacted according to general procedure J to yield *amidinium pivalate* **34d · PivOH.** as a white powder (107 mg, quant.). **MP**: 236 °C (decomposition). **^{1}H NMR** (DMSO-d_6, 400 MHz): δ 8.25 (s, 1H), 7.81 – 7.75 (m, 2H), 7.75 – 7.68 (m, 1H), 7.61 – 7.51 (m, 2H), 5.71 (s, 2H), 1.03 (s, 9H). **^{13}C NMR** (DMSO-d_6, 100 MHz): δ 183.69, 165.87, 136.79, 133.67, 132.06, 130.99, 129.35, 127.25, 127.12, 125.16, 52.14, 38.55, 28.41. **FTIR**: 558.1, 590.3, 622.0, 647.3, 698.2, 711.8, 733.4, 798.7, 885.1, 1029.4, 1073.4, 1109.1, 1141.0, 1214.7, 1266.8, 1355.3, 1366.5, 1406.8, 1478.2, 1501.2, 1533.0, 1564.4, 1615.9, 2955.2 cm^{-1}. **HRMS**: m/z calcd for $[M]^+$ 202.1087, found 202.1090.

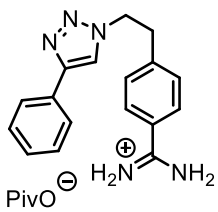

Amino(4-(2-(4-phenyl-1H-1,2,3-triazol-1-yl)ethyl)phenyl) methaniminium pivalate 34e · PivOH. Acyloxyamidine **50e** (80 mg, 0.20 mmol) reacted according to general procedure J to yield *amidinium pivalate* **34e · PivOH.** as a white powder (80 mg, quant.). **MP**: 227 °C (decomposition). **^{1}H NMR** (CD_3OD, 125 MHz): δ 8.23 (s, 1H), 7.78 – 7.73 (m, 2H), 7.73 – 7.68 (m, 2H), 7.44 – 7.38 (m, 4H), 7.33 – 7.27 (m, 1H), 4.78 (t, *J* = 7.0 Hz, 2H), 3.42 (t, *J* = 7.0 Hz, 2H), 1.13 (s, 9H) ppm. **^{13}C NMR** (CD_3OD, 125 MHz): δ 187.75, 168.25, 148.84, 145.73, 131.60, 130.94, 129.98, 129.41, 129.19, 128.38, 126.59, 122.33, 52.00, 40.81, 37.00, 28.86 ppm. **HRMS**: m/z calcd for $[M]^+$ 293.1509, found 293.1512.

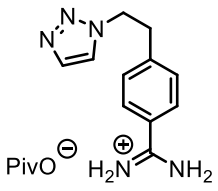

(4-(2-(1*H*-1,2,3-Triazol-1-yl)ethyl)phenyl)(amino)methaniminium pivalate 34f · PivOH. Acyloxyamidine **50f** (40 mg, 0.13 mmol) reacted according to general procedure J to yield *amidinium pivalate* **34f · PivOH** as a white powder (41 mg, quant.). **MP**: 236 °C (decomposition). **^{1}H NMR** (DMSO-d_6, 400 MHz): δ 8.08 (s, 1H), 7.73 – 7.64 (m, 3H), 7.42 – 7.36 (m, 2H), 4.70 (*t*, J = 7.1 Hz, 2H), 3.28 (*t*, J = 7.1 Hz, 2H), 1.03 (s, 9H) ppm. **^{13}C NMR** (DMSO-d_6, 100 MHz): δ 183.72, 165.72, 143.09, 133.18, 129.13, 128.28, 127.50, 124.67, 49.67, 38.55, 35.31, 28.44 ppm. **HRMS**: m/z calcd for $[M]^+$ 216.1244, found 216.1272.

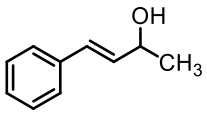

4-Phenylbut-3-en-2-ol 58. Protocol adapted from the literature.[172] A solution of α,β-unsaturated ketone **59** (1.00 eq., 3.061 mmol, 448 mg) in THF (3mL) was added to a solution of $NaBH_4$ (4.00 eq., 12.1 mmol, 456 mg) in THF (36 mL). The reaction mixture was stirred at RT for 30 min. Water was added and the aqueous phase was extracted with Et_2O (3 ×). The combined organic phases were washed with brine and dried over $MgSO_4$. The solvent was evaporated under reduced pressure and the crude product was purified by column chromatography (cyclohexane / AcOEt 80:20) to yield *allylic alcohol* **58** as a colorless oil. (426 mg, 94%) **MP**: 45 °C. **^{1}H NMR** ($CDCl_3$, 400 MHz): δ 7.40 – 7.36 (m, 2H), 7.35 – 7.29 (m, 2H), 7.27 – 7.21 (m, 1H), 6.57 (d, *J* = 16,0 Hz, 1H), 6.27 (dd, J^1=15.9 Hz, J^2=6.4 Hz, 1H,), 4.53–4.46 (m, 1H), 1.68 (s, 1H), 1.38 (d, *J* = 6.4 Hz, 3H) ppm. **^{13}C NMR** ($CDCl_3$, 100 MHz): δ 136.83, 133.69, 129.52, 128.73, 127.79, 126.60, 69.12, 23.57 ppm. **FTIR**: 521.7, 547.9, 603.2, 692.1, 746.7, 824.5, 854.9, 875.5, 941.2, 965.3, 1027.9, 1056.8, 1140.5, 1240.3, 1330.6, 1367.5, 1404.1, 1448.1, 1493.2, 1597.5, 1804.4, 2867.6, 2972.1, 3025.5, 3320.3 cm^{-1}. The data are consistent with the literature values.[172]

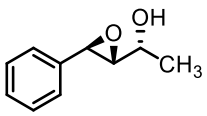

(*R*)-1-((2*R*,3*R*)-3-Phenyloxiran-2-yl)ethan-1-ol 60. Protocol adapted from the literature.[173] (-)-DET (1.20 eq., 4.86 mmol, 830 µL) was added to a solution of $Ti(OiPr)_4$ (1.00 eq., 4.05 mmol, 1.20 mL) in CH_2Cl_2 (15 mL). The reaction

mixture was stirred at -20 °C for 10 min. *t*BuOOH (5.5 M in decane, 0.4 eq. 1.62 mmol, 300 µL) was then added. The reaction mixture was further stirred at -20 °C for 5 h and then allowed to warm to RT. A 2.5 mol/kg NaOH solution in brine (10 mL) was added dropwise. The aqueous phase was extracted with CH_2Cl_2 (3 ×). The combined organic layers were dried over $MgSO_4$ and the solvent was evaporated under reduced pressure. The crude product was purified by column chromatography (cyclohexane / AcOEt 100:0 to 80:20) to yield *epoxy alcohol* **60** as a colorless oil (280 mg, 42%). **^{1}H NMR** ($CDCl_3$, 400 MHz): 7.38 – 7.28 (m, 5H), 4.16 – 4.09 (m, 1H), 3.96 (d, *J* = 2.3 Hz, 1H), 3.10 (dd, J_1 = 5.0 Hz, J_2 = 2.4 Hz), 2.01 (s, 1H), 1.32 (d, *J* = 6.4 HZ, 3H) ppm. **^{13}C NMR** ($CDCl_3$, 100 MHz): 136.85, 128.48, 128.23, 125.66, 65.58, 64.77, 54.60, 18.68 ppm. ***α***: 27.2° (0.80, CH_2Cl_2). **FTIR**: 645.6, 696.5, 746.9, 790.5, 837.4, 864.3, 877.3, 918.9, 945.2, 1021.3, 1060.4, 1073.9, 1107.5, 1145.4, 1177.8, 1209.6, 1244.0, 1287.2, 1309.8, 1338.3, 1368.4, 1407.0, 1433.5, 1453.8, 1496.3, 1606.0, 2871.6, 2932.3, 2975.0, 3457.6 cm^{-1}. The data are consistent with the literatures values.[256]

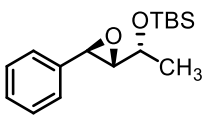

tert*-Butyldimethyl((*R*)-1-((2*S*,3*R*)-3-phenyloxiran-2-yl)ethoxy)silane 57**. Protocol adapted from the literature.[176] TBSCl (2.00 eq., 12.7 mmol, 1.91 g) was added to a solution of alcohol **60** (1.00 eq., 6.34 mmol, 1.05 g) and imidazole (3.00 eq., 19.0 mmol, 1.29 g) in DMF (15 mL). The reaction was stirred ON at RT. Sat. NH_4Cl was added and the aqueous phase was extracted with Et_2O (3 ×). The combined organic layers were washed with brine (5 ×) and dried over $MgSO_4$. The solvent was evaporated under reduced pressure and the crude product was purified by column chromatography (cyclohexane / AcOEt 99:1) to yield *silyl ether* **57** as a colorless oil. (1.73 g, 92%). **^{1}H NMR** ($CDCl_3$, 400 MHz): 7.36 – 7.27 (m, 5H), 3.92 – 3.86 (m, 1H), 3.82 (d, *J* = 2.1 Hz, 1H), 2.92 (dd, J_1 = 4.1 Hz, J_2 =2.1, 1H), 1.28 (d, *J* = 6.4 Hz, 3H), 0.90 (s, 9H), 0.10 (s, 3H), 0.08 (s, 3H) ppm. **^{13}C NMR** ($CDCl_3$, 100 MHz): 137.70, 128.57, 128.13, 125.73, 67.70, 66.21, 56.20, 25.94, 21.03, -4.49, -4.66 ppm. ***α: 28.2° (0.30, CH_2Cl_2). **FTIR**: 617.1, 666.4, 696.5, 751.9, 776.1, 810.2, 831.9, 885.2, 905.7, 925.9, 967.7, 995.5, 1038.9, 1095.9, 1149.4, 1250.7, 1333.3, 1360.9, 1372.2, 1462.5, 1471.6, 1498.1, 1605.9, 2856.4, 2885.1, 2928.7, 2954.5 cm^{-1}. The data are consistent with the literature values.[176]

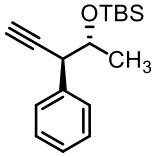

***tert*-Butyldimethyl(((2*R*,3*R*)-3-phenylpent-4-yn-2-yl)oxy)silane 55**. Protocol adapted from the literature.[178] $Al(CH_3)_3$ (2 M in toluene, 2.00 eq., 1.08 mmol, 539 µL) was added dropwise to a solution of 4-bromo-2,6-di-*tert*-butylphenol (4.00 eq., 2.16 mmol, 615 mg) in degassed CH_2Cl_2 (50 mL). The reaction mixture was stirred at RT for 1 h, then was cooled down to -78 °C. A solution of epoxide **57** (1.00 eq., 0.54 mmol, 150 mg) in degassed CH_2Cl_2 (2 mL) was added dropwise. The solution was stirred at -78 °C for 3 h. 2 M HCl was added (10 mL) and sat. $NaHCO_3$ was then added until pH 7. The aqueous phase was extracted

with CH_2Cl_2 (3 ×), and the combined organic layers were dried over $MgSO_4$. The solvent was evaporated under reduced pressure to yield crude *aldehyde* **56** and the residue was dissolved in THF (5 mL). In parallel, metallic Na (4.00 eq., 2.16 mmol, 50 mg) was slowly added to CH_3OH (1 ml). The mixture was stirred for 30 min then cooled down to -78 °C. The solution of crude aldehyde **56** was added dropwise at -78 °C. The reaction was stirred at that temperature for 30 min, was allowed to warm up to RT, and was then stirred further for 3 h. Water was added, and the aqueous phase was extracted with MTBE (3 ×). The combined organic layers were dried over $MgSO_4$. The solvent was evaporated under reduced pressure and the crude product was purified by column chromatography (cyclohexane / toluene 9:1) to yield alkyne **55** as a colorless oil (85 mg, 58% over 2 steps). **^{1}H NMR** ($CDCl_3$, 400 MHz): 7.38 – 7.22 (m, 5H), 4.01 – 4.07 (m, 1H), 3.68 (dd, J_1 = 4.8 Hz, J_2 = 2.5 Hz, 1H), 2.26 (d, J_1 = 2.5 Hz, 1H), 1.13 (d, J = 6.2 Hz, 3H), 0.86 (s, 9H), 0.03 (s, 3H), -0.12 (s, 3H) ppm. **^{13}C NMR** (acetone-d_6, 100 MHz): 138.87, 128.96, 127.93, 126.88, 83.43, 72.85, 71.92, 46.04, 25.40, 21.11, 17.76, -5.40, -5.84 ppm. ***α***: -16.0° (0.10, CH_2Cl_2). **FTIR:** 702.1, 777.3, 834.8, 892.4, 986.1, 1091.6, 1129.8, 1220.0, 1359.1, 1419.1, 1711.4, 2929.1 cm^{-1}.

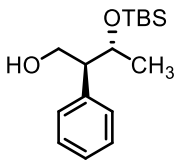

(2*S*,3*R*)-3-((*tert*-Butyldimethylsilyl)oxy)-2-phenylbutan-1-ol 66. Protocol adapted from the literature.[176] $Al(CH_3)_3$ (2 M in toluene, 2.00 eq., 1.08 mmol, 539 µL) was added dropwise to a solution of 4-bromo-2,6-di-*tert*-butylphenol (4.00 eq., 2.16 mmol, 615 mg) in degassed CH_2Cl_2 (50 mL). The reaction mixture was stirred at RT for 1 h, then was cooled down at -78 °C. A solution of epoxide **57** in degassed CH_2Cl_2 was added dropwise. The solution is stirred at -78 °C for 3 h. 2 M HCl was added (10 mL) and sat. $NaHCO_3$ was then added until pH 7. The aqueous phase was extracted with CH_2Cl_2 (3 ×), and the combined organic layers were dried over $MgSO_4$. The solvent was evaporated under reduced pressure to yield crude *aldehyde* **56**. The residue was dissolved in CH_3OH and the solution was cooled down to 0 °C. $NaBH_4$ (1.00 eq., 0.54 mmol, 20 mg) was added and the reaction mixture was stirred at 0 °C for 20 min. Sat. NaCl was added and the aqueous phase was extracted with Et_2O (3 ×). The combined organic layers were dried over $MgSO_4$. The solvent was evaporated under reduced pressure and the residue was purified by column chromatography (cyclohexane / AcOEt 85:15) to yield *alcohol* **66** as a pale-yellow oil. (114 mg, 76% over 2 steps). **^{1}H NMR** ($CDCl_3$, 400 MHz): 7.32 – 7.18 (m, 5H), 4.15 – 4.08 (m, 1H), 4.06 (dd, J_1 = 10.8 Hz, J_2 = 6.9 Hz, 1H), 3.81 (dd, J_1 = 11.0 Hz, J_2 = 5.3 Hz), 2.79 – 2.74 (m, 1H), 1.07 (d, J = 6.0, 3H), 0.91 (s, 9H), 0.09 (s, 3H), 0.08 (s, 3H) ppm. **^{13}C NMR** ($CDCl_3$, 100 MHz): 140.97, 128.46, 127.83, 126.87, 73.36, 65.82, 56.10, 29.96, 25.75, 17.94, -4.21 -5.07 ppm. ***α***: -21.5° (0.20, CH_2Cl_2). **FTIR**: 534.0, 565.6, 616.2, 667.0, 700.4, 775.8, 808.9, 835.2, 866.3, 885.8, 938.6, 984.7, 1023.3, 1057.7, 1087.8, 1135.6,

1232.6, 1249.9, 1308.0, 1361.6, 1391.1, 1416.6, 1470.9, 1602.0, 1740.9, 2857.0, 2928.2, 2955.2, 3636.3 cm^{-1}.

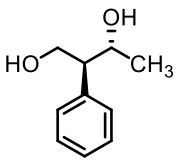

(2*S*,3*R*)-2-Phenylbutane-1,3-diol 67. TBAF (1 M in THF, 12.0 eq., 4.92 mmol, 4.92 mL) was added at 0 °C to a solution of alcohol **16** (1.00 eq., 0.41 mmol, 114 mg) in THF (5 mL). The reaction mixture was stirred at 0 °C for 30 min. Sat. NH_4Cl was added and the aqueous phase was extracted with Et_2O (3 ×). The combined organic layers were dried over $MgSO_4$. The solvent was evaporated under reduced pressure and the crude product was purified by column chromatography (CH_2Cl_2 / CH_3OH 99:1) to yield *diol* **67** as a pale-yellow oil (37 mg, 55%). **^{1}H NMR** ($CDCl_3$, 400 MHz): 7.33 – 7.14 (m, 5H), 4.25 – 4.18 (m, 1H), 4.10 (dd, J_1 = 11.0 Hz, J_2 = 8.6 Hz), 3.90 (dd, J_1 = 11.0 Hz, J_2 = 4.6 Hz), 2.77 (ddd, J_1 = 13.3 Hz, J_2 = 8.7 Hz, J_3 = 4.6 Hz, 1H), 2.65 (br, 1H), 1.06 (d, J_1 = 6.2 Hz, 3H) ppm. **^{13}C NMR** ($CDCl_3$, 100 MHz): 140.06, 128.86, 128.24, 127.16, 73.04, 67.41, 55.31, 22.82 ppm. ***α***: 3.8° (0.13, CH_2Cl_2).

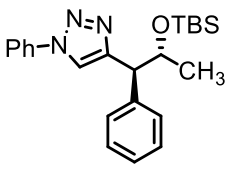

4-((1*S*,2*R*)-2-((*tert*-Butyldimethylsilyl)oxy)-1-phenylpropyl)-1-phenyl-1*H*-1,2,3-triazole 69. PhN_3 (85% in cyclohexane, 3.00 eq., 0.42 mmol, 59 mg) reacted with alkyne **55** (1.00 eq., 0.14 mmol, 38 mg) according to general procedure C. The crude product was purified by column chromatography (cyclohexane / AcOEt 90:10) to yield *triazole* **69** as a yellow oil (45 mg, 82 %). **^{1}H NMR** ($CDCl_3$, 400 MHz): 8.02 (s, 1H), 7.54 – 7.50 (m, 2H), 7.44 – 7.36 (m, 3H), 7.30 – 7.16 (m, 3H), 5.50 – 4.40 (m, 1H), 4.20 (d, J = 5.7, 1H), 1.15 (d, J = 6.2 Hz, 3H), 0.79 (s, 9H), -0.04 (s, 3H), -0.33 (s, 3H) ppm. **^{13}C NMR** (acetone-d_6, 100 MHz): 148.36, 141.19, 137.43, 129.75, 129.14, 128.91, 128.38, 125.39, 120.84, 120.54, 72.37, 51.93, 25.90, 22.92, 18.01, -4.47, -5.41 ppm. ***α***: 46.1° (0.26, CH_2Cl_2).

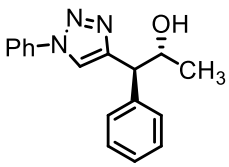

(1*S*,2*R*)-1-Phenyl-1-(1-phenyl-1*H*-1,2,3-triazol-4-yl)propan-2-ol 53. TBAF (1 M in THF, 12.0 eq., 1.67 mmol, 1.67 mL) was added at 0 °C to a solution of silyl ether **69** (1.00 eq., 0.41 mmol, 55 mg) in THF (5 mL). The reaction mixture was stirred at 0 °C for 1 h. Sat. NH_4Cl was added and the aqueous phase was extracted with Et_2O (3 ×). The combined organic layers were dried over $MgSO_4$. The solvent was evaporated under reduced pressure and the crude product was purified by column chromatography to yield *alcohol* **53** as a white solid (31 mg, 79%). **^{1}H NMR** ($CDCl_3$, 400 MHz): δ 7.67 – 7.66 (m, 2H), 7.58 (s, 1H), 7.50 – 7.47 (m, 2H), 7.43 – 7.40 (m, 1H), 7.35 – 7.32 (m 2H), 7.29 – 7.26 (m, 3H), 4.54 – 4.49 (m, 1H), 4.02 (d, J = 6.9 Hz, 1H), 1.13 (d, J = 6.3 Hz, 3H) ppm. **^{13}C NMR** (acetone-d_6, 100 MHz): δ 150.88, 140.76, 136.99, 129.82, 129.23, 128.95, 128.65, 127.35, 120.86, 120.58, 71.31, 51.59, 21.17 ppm. ***α***: -18.0° (0.30, CH_2Cl_2).

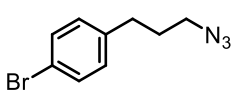

1-(3-Azidopropyl)-4-bromobenzene 75b. Protocol adapted from the literature.[187] MsCl (1.60 mL, 20.8 mmol, 1.50 eq.) was added dropwise at 0 °C to a solution of 3-(4-bromophenyl)propan-1-ol **79** (3.00 g, 13.9 mmol) and Et_3N (5.80 mL, 42.0 mmol, 3.00 eq.) in CH_2Cl_2 (80 ml). The mixture was stirred 2 h at RT. Sat. NH_4Cl was added. The organic layer was separated, washed with NH_4Cl (3 ×), dried over $MgSO_4$, and concentrated under reduced pressure to yield the crude mesylate as a colorless oil which was used in the next reaction without further purification. NaN_3 (1.08 g, 16.7 mmol, 1.2 eq.) was added to a solution of the freshly synthesized mesylate in DMF (40 mL). The suspension was stirred ON at 80 °C. EtOAc was added and the mixture was washed with saturated NaCl (3 ×), water (1 ×), dried over $MgSO_4$ and concentrated under reduced pressure. The crude yellow oil was filtered over silica with CH_2Cl_2 to yield *azide* **75b** as a colorless oil (3.14 g, 94%). **^{1}H NMR** ($CDCl_3$, 400 MHz): δ 7.41 (d, *J* = 8.4 Hz, 2H), 7.06 (d, *J* = 8.4 Hz, 2H), 3.28 (t, *J* = 6.8 Hz, 2H), 2.66 (t, *J* = 7.6, 2H), 1.88 (quint., *J* = 6.5 Hz, 2H) ppm. **^{13}C NMR** ($CDCl_3$, 100 MHz): δ 139.93, 131.73, 130.34, 120.07, 50.62, 32.30, 30.41 ppm. **FTIR**: 601.4, 641.5, 710.6, 757.2, 793.5, 830.0, 921.4, 1010.6, 1071.5, 1103.7, 1174.6, 1252.6, 1277.3, 1346.3, 1404.3, 1451.0, 1487.7, 1591.8, 1724.6, 1898.7, 2092.0, 2865.7, 2943.5 cm^{-1}. The data are consistent with the literature values.[257]

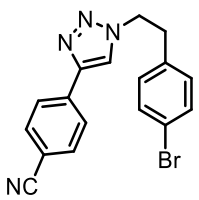

4-(1-(4-Bromophenethyl)-1*H*-1,2,3-triazol-4-yl)benzonitrile 74a. Azide **43** (1.25 eq., 380 mg, 1.68 mmol) reacted with acetylene **76** (1.00 eq., 170 mg, 1.34 mmol) according to general procedure C. The crude product was purified by column chromatography (cyclohexane / AcOEt 90:10 to 50:50) to yield *triazole* **74a** as a yellow powder (314 mg, 67%). **^{1}H NMR** ($CDCl_3$, 400 MHz): δ 7.88 (d, *J* = 6.4 Hz, 2H), 7.70 (d, *J* = 7.2 Hz, 2H), 7.57 (s, 1H), 7.42 (d, *J* = 6.8 Hz, 2H), 6.99 (d, *J* = 7.2 Hz, 2H), 4.64 (t, *J* = 5.4 Hz, 2H), 3.24 (t, *J* = 5.8 Hz, 2H) ppm. **^{13}C NMR** ($CDCl_3$, 100 MHz): δ 146.33, 136.30, 135.42, 133.32, 132.62, 130.98, 126.63, 121.84, 121.60, 119.32, 112.12, 52.20, 36.63 ppm. **FTIR**: 576.7, 599.5, 623.4, 663.6, 707.1, 743.6, 806.0, 832.4, 975.8, 1012.2, 1045.7, 1071.6, 1098.8, 1180.9, 1230.2, 1369.3, 1405.1, 1457.0, 1488.9, 1614.8, 2227.5, 2926.0, 3103.0 cm^{-1}.

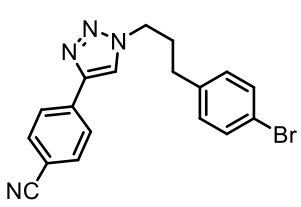

4-(1-(3-(4-Bromophenyl)propyl)-1*H*-1,2,3-triazol-4-yl)benzonitrile 74b. Azide **75b** (1.00 eq., 305 mg, 1.27 mmol) reacted with acetylene **76** (1.00 eq., 162 mg, 1.27 mmol) according to general procedure C. The crude product was purified by column chromatography (cyclohexane / AcOEt 90:10 to 50:50) to yield *triazole* **74b** as a yellow powder (322 mg, 69%). **MP**: 110 °C. **^{1}H NMR** ($CDCl_3$, 400 MHz): δ 7.92 (d, *J* = 8.4 Hz, 2H), 7.82 (s, 1H), 7.69 (d, *J* = 7.6 Hz, 2H), 7.40 (d, *J* = 7.6 Hz Hz, 2H), 7.05 (d, *J* = 7.6 Hz, 2H), 4.41 (t, *J* = 7.0 Hz, 2H), 2.65 (t, *J* = 7.6 Hz, 2H), 2.28 (quint., *J* = 7.2 Hz, 2H) ppm. **^{13}C NMR** ($CDCl_3$, 100 MHz): δ 145.10, 138.98, 135.06, 132.83,

131.82, 130.28, 126.14, 120.87, 120.35, 118.86, 111.57, 49.73, 32.00, 31.51 ppm. **FTIR**: 454.4, 466.2, 486.6, 504.0, 548.0, 639.7, 651.3, 682.2, 706.9, 774.3, 812.3, 839.3, 850.9, 970.0, 1008.4, 1030.5, 1056.2, 1067.4, 1075.4, 1100.3, 1137.4, 1173.7, 1216.9, 1230.2, 1259.5, 1321.6, 1349.6, 1403.9, 1438.9, 1457.0, 1484.8, 1554.7, 1611.0, 2229.7, 2926.7 , 3129.1 cm^{-1}.

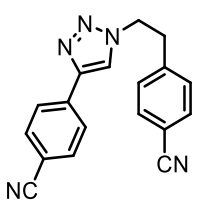

4-(1-(4-Cyanophenethyl)-1*H*-1,2,3-triazol-4-yl) benzonitrile 73a. Bromide **74a** (285 mg, 0.81 mmol) reacted according to general procedure H. The crude product was purified by column chromatography (cyclohexane / AcOEt 80:20 to 20:80) to yield *nitrile* **73a** as a white powder (89 mg, 37% yield). **MP**: 183 °C. **^{1}H NMR** ($CDCl_3$, 400 MHz): δ 7.88 (d, *J* = 6.8, 2H), 7.70 (d, *J* = 7.2, 2H), 7.59 (m, 3H), 7.42 (d, *J* = 6.8, 2H), 7.24 (d, *J* = 6.4, 2H), 4.68 (t, *J* = 5.8, 2H), 3.38 (t, *J* = 5.8, 2H). **^{13}C NMR** ($CDCl_3$, 100 MHz): δ 142.32, 134.78, 132.93, 132.84, 129.67, 126.20, 121.05, 118.81, 118.57, 111.86, 111.62, 51.27, 36.71 ppm. **FTIR**: 555.8, 601.0, 660.1 704.2, 734.6, 761.0, 826.8, 973.7, 1026.3, 1044.5, 1078.0, 1108.5, 1178.5, 1233.7,1455.9, 1491.6, 1506.3, 1608.3, 2225.3, 2853.6, 2923.8, 3098.6 cm^{-1}.

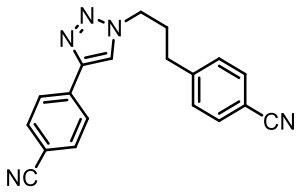

4-(3-(4-(4-Cyanophenyl)-1*H*-1,2,3-triazol-1-yl)propyl)benzonitrile 73b. Bromide **74b** (305 mg, 0.83 mmol) reacted according to general procedure H. The crude product was purified by column chromatography (cyclohexane / AcOEt 80:20 to 20:80) to yield *nitrile* **73b** as an orange powder (156 mg, 60% yield). **MP**: 198 °C. **^{1}H NMR** ($CDCl_3$, 500 MHz): δ 7.91 (d, *J* = 6.4 Hz, 2H), 7.85 (s, 1H), 7.68 (d, *J* = 6.8 Hz, 2H), 7.56 (d, *J* = 6.8 Hz, 2H), 7.29 (d, *J* = 6.8 Hz, 2H), 4.43 (t, *J* = 5.6 Hz, 2H), 2.74 (t, *J* = 6.2 Hz, 2H), 2.31 (quint., *J* = 7.9 Hz, 2H) ppm. **^{13}C NMR** ($CDCl_3$, 125 MHz): δ 146.19, 145.70, 134.94, 132.85, 132.54, 129.38, 126.13, 120.87, 118.88, 118.84, 49.64, 32.67, 31.26 ppm. **FTIR**: 460.7, 479.3, 545.8, 557.6, 662.1, 706.9, 733.7, 759.4, 781.8, 808.6, 834.4, 866.2, 908.2, 976.8, 1020.7, 1043.9, 1056.2, 1084.0, 1107.9, 1178.0, 1194.1, 1221.9, 1296.8, 1348.2, 1424.4, 1459.6, 1492.7, 1505.6, 1566.6, 1606.7, 1672.1, 2224.5, 2893.1, 2957.9, 3092.9 cm^{-1}.

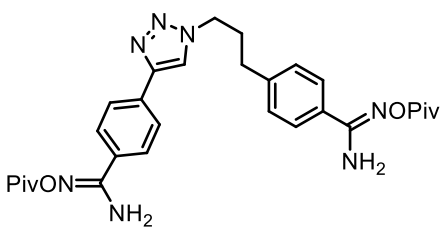

***N'*-(pivaloyloxy)-4-(3-(4-(4-(*N'*-(pivaloyloxy) carbamimidoyl)phenyl)-1*H*-1,2,3-triazol-1-yl)propyl) benzimidamide 82b.** Nitrile **73b** (120 mg, 0.38 mmol) reacted according to general procedure I, by using 2.00 eq. of Et_3N and PivCl in the second step instead of 1.00 eq. each. The crude product was purified by column chromatography (CH_2Cl_2 / CH_3OH, 100:0 to 95:5) to yield *pivaloxyamidine* **82b** as a white powder (119 mg, 57 % yield). **MP**: 181 °C (decomposition). **^{1}H NMR** (CD_3OD, 500 MHz): δ 8.73 (s, 1H), 7.93 (d, *J* = 9.0 Hz, 2H), 7.79 (d, *J* = 9.0 Hz, 2H),

7.65 (d, *J* = 8.0 Hz, 2H), 7.32 (d, *J* = 8.0 Hz, 2H), 4.44 (t, *J* = 6.8 Hz, 2H), 2.67 (t, *J* = 7.8 Hz, 2H), 2.18 (quint., *J* = 7.0 Hz, 2H), 1.26 (s, 9H), 1.24 (s, 9H) ppm. **^{13}C NMR** (CD_3OD, 125 MHz): δ 175.11, 156.82, 156.52, 146.23, 143.84, 133.28, 132.98, 131.49, 130.19, 128.87, 127.93, 127.45, 125.41, 122.49, 49.62, 38.89, 32.21, 31.55, 27.70 ppm. **FTIR**: 641.7, 687.9, 723.4, 761.8, 806.2, 836.9, 891.0, 1056.8, 1066.1, 1075.6, 1138.9, 1228.9, 1241.7, 1250.2, 1393.9, 1405.7, 1450.7, 1498.8, 1604.4, 1736.7, 2104.9, 2229.3, 2901.1, 2972.2, 2987.7, 3230.7, 3359.0, 3484.0, 3675.1 cm^{-1}.

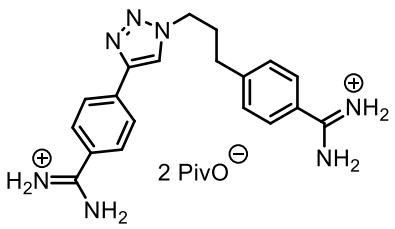

Amino(4-(3-(4-(4-(amino(iminio)methyl)phenyl)-1*H*-1,2,3-triazol-1-yl)propyl)phenyl)methaniminium pivalate 72b · 2PivOH. Pivaloxyamidine **82b** (59 mg, 0.11 mmol) reacted according to general procedure J to yield *amidinium pivalate* **72b · 2PivOH** as a white powder (59 mg, quant.). **MP**: 223 °C (decomposition). **^{1}H NMR** (CD_3OD, 500 MHz): δ 8.54 (s, 1H), 8.06 (d, *J* = 6.4 Hz, 2H), 7.90 (d, *J* = 6.8 Hz, 2H), 7.74 (d, *J* = 6.4 Hz, 2H), 7.48 (d, *J* = 7.2 Hz, 2H), 4.54 (t, *J* = 5.4 Hz, 2H), 2.82 (t, *J* = 6.4 Hz, 2H), 2.38 (quint., *J* = 5.8 Hz, 2H), 1.14 (s, 18H) ppm. **^{13}C NMR** (CD_3OD, 125 MHz): δ 187.83, 168.20, 163.02, 148.95, 147.16, 137.21, 130.56, 129.71, 129.19, 129.06, 127.68, 127.11, 123.75, 50.93, 40.72, 33.48, 32.33, 28.77 ppm. **FTIR**: 634.2, 678.6, 711.1, 753.2, 800.7, 883.0, 1027.8, 1056.7, 1066.0, 1075.3, 1227.0, 1241.5, 1250.1, 1368.1, 1383.0, 1394.1, 1406.3, 1453.6, 1478.6, 1616.9, 1933.3, 2901.0, 2972.0, 2987.4, 3675.0 cm^{-1}. **HRMS**: m/z calcd for $[M]^{2+}$ 174.6007, found 174.6012.

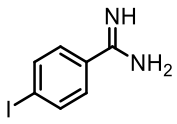

4-Iodobenzimidamide 98a. 4-Iodobenzonitrile **97a** (2.29 g, 10.0 mmol) reacted according to general procedure K with 1.05 eq. of LiHMDS and ON at RT to yield *amidine* **9a** as a crystalline yellow powder (1.48 g, 60%). **MP**: 191 °C (decomposition). **^{1}H NMR** (DMSO-d_6, 400 MHz): δ 7.76 (d, *J* = 8.0 Hz, 2H), 7.56 (d, *J* = 8.4 Hz, 2H), 6.49 (br, 3H) ppm. **^{13}C NMR** (DMSO-d_6, 100 MHz): δ 161.63, 136.82, 135.81, 128.71, 96.73 ppm. **FTIR**: 556.1, 578.4, 586.8, 600.4, 625.9, 635.3, 667.0, 730.3, 758.2, 827.2, 1003.3, 1057.8, 1095.9, 1134.7, 1183.9, 1274.9, 1384.9, 1427.9, 1483.4, 1550.0, 1584.0, 1643.0, 3037.7, 3322.6, 3463.6 cm^{-1}.

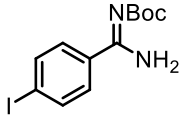

***tert*-Butyl (amino(4-iodophenyl)methylene)carbamate 103a.** Amidine **98a** (7.45 g, 30.3 mmol) reacted according to general procedure L to yield *Boc-protected amidine* **103a** as a yellow powder (10.4 g, quant.). **MP**: 120 °C (slow decomposition). **^{1}H NMR** ($CDCl_3$, 400 MHz): δ 9.47 (br, 1H), 7.66 (d, *J* = 8.4 Hz, 2H), 7.48 (d, *J* = 8.4 Hz, 2H), 6.81 (br, 1H), 1.51 (s, 9H) ppm. **^{13}C NMR** ($CDCl_3$, 100 MHz): δ 166.99, 164.24, 137.80, 134.47, 128.83, 99.05, 79.94, 28.27 ppm. **FTIR**: 617.9, 669.7, 730.6, 808.3, 826.5, 837.1,

882.5, 949.8, 978.7, 1004.6, 1059.8, 1101.0, 1120.1, 1141.9, 1159.4, 1254.7, 1275.8, 1306.5, 1365.8, 1389.2, 1473.7, 1511.0, 1563.5, 1589.2, 1611.0, 1662.9, 3167.5, 3340.5 cm^{-1}.

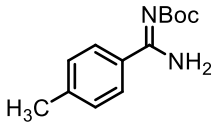

***tert*-Butyl (amino(*p*-tolyl)methylene)carbamate 103b.** 4-Methyl benzamidinium chloride (3.41 g, 20 mmol) reacted according to general procedure L, with the difference that 1.5 M K_2CO_3 (0.50 eq.) was also added at the beginning of the reaction, to yield *Boc-protected amidine* **103b** as an off-white powder (4.45 g, 95%). **MP**: 136 °C (decomposition). **^{1}H NMR** ($CDCl_3$, 400 MHz): δ 9.52 (br, 1H), 7.71 (d, *J* = 8.0 Hz, 2H), 7.16 (d, *J* = 7.6 Hz, 2H), 6.60 (br, 1H), 2.35 (s, 3H), 1.52 (s, 9H) ppm. **^{13}C NMR** ($CDCl_3$, 100 MHz): δ 167.68, 164.58, 142.51, 132.11, 129.31, 127.27, 79.56, 28.30, 21.52 ppm. **FTIR**: 567.0, 622.1, 739.3, 814.2, 835.0, 885.1, 981.0, 1039.3, 1141.6, 1165.2, 1251.4, 1276.3, 1365.0, 1390.3, 1492.9, 1527.6, 1573.9, 1611.4, 1659.3, 2971.2, 3170.5, 3338.0 cm^{-1}.

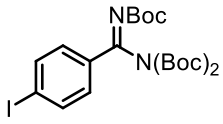

***tert*-Butyl (*tert*-butoxycarbonyl)(((*tert*-butoxycarbonyl)imino)(4-iodophenyl)methyl)carbamate 104a.** Boc-protected amidine **103a** (9.54 g, 27.5 mmol) reacted according to general procedure M to yield *tris-Boc-protected amidine* **104a** as a yellow powder (12.9 g, 86%). **MP**: 131 °C. **^{1}H NMR** ($CDCl_3$, 400 MHz): δ 7.74 (d, *J* = 8.8 Hz, 2H), 7.50 (d, *J* = 8.0 Hz, 2H), 1.49 (s, 9H), 1.33 (s, 18H) ppm. **^{13}C NMR** ($CDCl_3$, 100 MHz): δ 158.11, 150.72,148.24, 137.89, 133.50, 129.59, 99.54, 84.33, 83.11, 28.02, 27.70 ppm. **FTIR**: 571.0, 600.7, 737.9, 774.5, 793.6, 833.5, 851.5, 872.6, 948.9, 988.3, 1008.7, 1039.8, 1061.3, 1114.9, 1140.7, 1246.9, 1273.9, 1296.1, 1367.3, 1395.2, 1458.2, 1562.4, 1586.2, 1664.9, 1732.9, 1797.8, 2978.9 cm^{-1}.

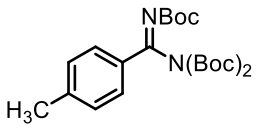

***tert*-Butyl (*tert*-butoxycarbonyl)(((*tert*-butoxycarbonyl)imino)(*p*-tolyl)methyl)carbamate 104b.** Boc-protected amidine **103b** (3.50 g, 14.9 mmol) reacted according to the general procedure M to yield *tris-Boc-protected amidine* **104b** as an off-white powder (4.97 g, 77%). **MP**: 141 °C. **^{1}H NMR** ($CDCl_3$, 400 MHz): δ 7.69 (d, *J* = 8.0 Hz, 2H), 7.19 (d, *J* = 8.0 Hz, 2H), 2.38 (s, 3H), 1.50 (s, 9H), 1.33 (s, 18H) ppm. **^{13}C NMR** ($CDCl_3$, 125 MHz): δ 158.60, 151.48, 148.67, 142.90, 131.18, 129.37, 128.30, 88.99, 82.73, 28.10, 27.75, 21.65 ppm. **FTIR**: 589.9, 641.7, 689.0, 726.3, 775.0, 846.2, 885.7, 927.6, 948.7, 988.0, 1105.9, 1139.5, 1156.8, 1250.9, 1268.4, 1310.4, 1393.9, 1458.6, 1574.6, 1611.5, 1648.5, 1719.4, 1791.6, 2978.1 cm^{-1}.

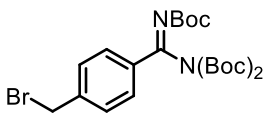

***tert*-Butyl ((4-(bromomethyl)phenyl)((*tert*-butoxycarbonyl)imino)methyl)(*tert*-butoxycarbonyl)carbamate 105.** Protocol adapted from the literature.[206] NBS (1.00 eq., 2.23 g, 7.40 mmol) was added to a solution of toluyl derivative **104b** (1.00 eq., 3.23 g, 7.40 mmol) and of AIBN (0.10 eq., 121 mg, 0.74 mmol)

in $CHCl_3$ (25 mL). The solution was stirred at reflux for 6 h. After cooling down, the solution was washed with water (3 ×). The organic layer was separated, dried over $MgSO_4$, and concentrated under reduced pressure. The crude product was purified by column chromatography (cyclohexane / EtOAc, from 100:0 to 95:5) to yield *benzyl bromide* **105** as off-white flakes (3.43 g, 90%). **MP**: 104 °C (decomposition). **^{1}H NMR** ($CDCl_3$, 400 MHz): δ 7.74 (d, *J* = 8.0 Hz, 2H), 7.40 (d, *J* = 8.0, 2H) 4.46 (s, 2H), 1.48 (s, 9H), 1.31 (s, 18H) ppm. **^{13}C NMR** ($CDCl_3$, 125 MHz): δ 158.22, 150.81, 148.40, 141.94, 133.90, 129.24, 128.58, 84.55, 82.95, 32.17, 28.00, 27.66 ppm. **FTIR**: 557.3, 574.1, 606.9, 640.8, 688.8, 717.0, 741.2, 771.4, 783.6, 846.9, 878.4, 947.4, 986.1, 1036.0, 1095.7, 1139.3, 1248.1, 1266.4, 1280.0, 1367.8, 1394.5, 1457.7, 1477.7, 1573.5, 1611.5, 1648.6, 1728.8, 1792.1, 2982.8 cm^{-1}.

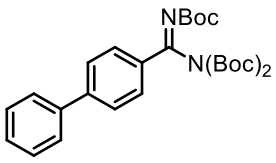

***tert*-Butyl ([1,1'-biphenyl]-4-yl((*tert*-butoxycarbonyl)imino)methyl) (*tert*-butoxycarbonyl)carbamate 106.** Protocol adapted from the literature.[207] Aryl iodide **104a** (1.00 eq., 200 mg, 0.37 mmol) was added to a suspension of $[Pd_2dba_3] \cdot CHCl_3$ (0.05 eq., 19 mg, 0.02 mmol), $P(tBu)_3 \cdot HBF_4$ (0.10 eq., 12 mg, 0.04 mmol), KF (3.30 eq., 71 mg, 1.22 mmol) and phenylboronic acid (1.10 eq., 50 mg, 0.41 mmol) in THF (3 mL). The solution was degassed and stirred for 6 h at RT. Et_2O was added and the mixture was filtered over Celite. The solvent was evaporated under reduced pressure and the crude product was purified by column chromatography (cyclohexane / EtOAc, 100:0 to 90:10) to yield *biphenyl* **106** as a white powder (132 mg, 71%). **MP**: 186 °C (decomposition). **^{1}H NMR** ($CDCl_3$, 500 MHz): δ 7.85 (d, *J* = 5.2 Hz, 2H), 7.47 (d, *J* = 6.0 Hz, 2H). 6.98 – 6.92 (m, 1H), 6.92 – 6.85 (m, 2H), 6.84 – 6.77 (m, 1H). 5.64 (s, 1H), 5.18 (s, 2H), 1.53 (s, 9H), 1.36 (s, 18H) ppm. **^{13}C NMR** ($CDCl_3$, 125 MHz): δ 158.98, 151.65, 149.10, 145.34, 140.24, 133.25, 129.66, 129.29, 128.77, 127.72, 127.66, 84.67, 83.40, 28.58, 28.24 ppm. **FTIR:** 648.6, 691.3, 701.0, 736.0, 776.2, 799.6, 846.0, 856.6, 882.1, 950.8, 990.5, 1006.9, 1036.7, 1105.1, 1138.5, 1153.6, 1244.8, 1268.4, 1314.9, 1368.2, 1393.3, 1455.6, 1474.0, 1560.0, 1604.8, 1645.0, 1724.2, 1792.6, 2934.9, 2979.8 cm^{-1}.

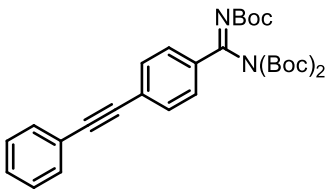

***tert*-Butyl (*tert*-butoxycarbonyl(((*tert*-butoxycarbonyl)imino) (4-(phenylethynyl)phenyl)methyl)carbamate 107**. Protocol adapted from the literature.[188] A solution of aryl iodide **104a** (1.00 eq., 200 mg, 0.37 mmol), $[Pd(PPh_3)_2Cl_2]$ (0.10 eq., 28 mg, 0.04 mmol) and CuI (0.20 eq., 15 mg, 0.08 mmol) in DIPA (2 mL) was degassed and phenylacetylene (1.20 eq., 50 µL, 0.44 mmol) was then added. The reaction mixture was stirred ON at RT. EtOAc was added and the organic layer was washed with sat. NH_4Cl (3 ×) and water (3 ×), and dried over $MgSO_4$. The solvent was evaporated under reduced pressure and the crude product was purified by column

chromatography (cyclohexane / EtOAc, 100:0 to 90:10) to yield *acetylene* **107** as an off-white powder. (169 mg, 88%). **MP**: 130 °C. **^{1}H NMR** ($CDCl_3$, 500 MHz): δ 7.83 (m, 2H), 7.60-7.52 (m, 4H), 7.38-7.33 (m, 3H), 1.54 (s, 9H), 1.37 (s, 18H). **^{13}C NMR** ($CDCl_3$, 125 MHz): δ 158.80, 151.35, 148.90, 133.96, 132.27, 129.36, 129.02, 128.67, 127.80, 123.21, 93.13, 89.17, 84.81, 83.58, 28.57, 28.22. **FTIR**: 559.5, 575.7, 694.7, 723.8, 764.1, 773.3, 790.5, 853.3, 877.7, 926.2, 947.5, 989.5, 1037.8, 1094.9, 1133.6, 1144.6, 1246.4, 1268.3 1308.5, , 1394.2, 1408.2, 1455.4, 1474.3, 1556.7, 1605.7, 1649.8, 1726.2, 1798.4, 2220.6, 2974.3 cm^{-1}.

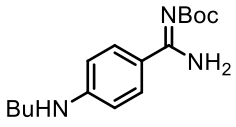

***tert*-Butyl (*tert*-butoxycarbonyl)(((*tert*-butoxycarbonyl)imino)(4-(butylamino)phenyl)methyl)carbamate 108.** Protocol adapted from the literature.[208] *t*BuOH (1.40 eq., 130 µL, 1.40 mmol) was added to a suspension of NaH (90% pure, 1.28 eq., 34 mg, 1.28 mmol) in DME (2 mL). The reaction mixture was stirred for 1 h at RT. Aryl iodide **104a** (1.00 eq., 546 mg, 1.00 mmol), DavePhos (0.15 eq., 59 mg, 0.15 mmol), and $[Pd_2dba_3] \cdot CHCl_3$ (0.05 eq., 46 mg, 0.05 mmol) were then added. The solution was degassed and butylamine (1.20 eq., 120 µL, 1.20 mmol) was added. The reaction was stirred ON at RT. EtOAc was added and the mixture was filtered over Celite. The solvent was evaporated under reduced pressure and the crude product was purified by column chromatography (cyclohexane / EtOAc, 100:0 to 50:50) to yield *aniline* **108** as a brownish powder (166 mg, 57%). **MP**: 131 °C **^{1}H NMR** ($CDCl_3$, 400 MHz): δ 10.12 (br, 2H), 7.75 (d, *J* = 7.6 Hz, 2H), 7.19 (d, *J* = 7.2 Hz, 2H), 4.95 (br, 1H), 3.41 – 3.19 (m, 2H), 1.55 – 1.30 (m, 13H), 0.87 (m, 3H). **^{13}C NMR** ($CDCl_3$, 125 MHz): **FTIR**: 557.5, 577.4, 607.7, 623.2, 635.1, 687.2, 722.0, 742.8, 781.4, 806.3, 826.8, 867.7, 948.7, 972.8, 1003.7, 1014.7, 1041.1, 1060.4, 1115.5, 1131.6, 1178.6, 1247.4, 1276.8, 1338.7, 1387.2, 1461.7, 1484.0, 1537.3, 1570.3, 1619.8, 1658.9, 2869.7, 2927.8, 2955.5, 3082.8, 3239.0 cm^{-1}.

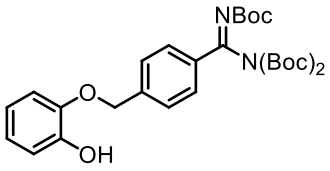

***tert*-Butyl (*tert*-butoxycarbonyl)(((*tert*-butoxycarbonyl)imino) (4-((2-hydroxyphenoxy)methyl)phenyl)methyl)carbamate 109.** Protocol adapted from the literature. Solid NaOH (1.10 eq., 44 mg, 1.10 mmol) was added to a solution of pyrocatechol (5.00 eq., 550 mg, 5.00 mmol) in CH_3OH (3 mL). The reaction mixture was stirred for 15 min at RT. Benzyl bromide **105** (1.00 eq., 513 mg, 1.00 mmol) was then added. The solution was refluxed for 2 h. After cooling down, CH_2Cl_2 was added and the mixture was washed with water (5 ×). The organic phase was separated and and dried over $MgSO_4$. The solvent was evaporated under reduced pressure and the crude product was purified by column chromatography (cyclohexane / EtOAc, 100:0 to 50:50) to yield *ether* **109** as an off-white powder. (416 mg, 77%). **MP**: 150 °C (decomposition). **^{1}H NMR** ($CDCl_3$, 500 MHz): δ 7.85 (d, *J* = 5.2 Hz, 2H), 7.47 (*d*, *J* = 6.0 Hz, 2H). 6.98 – 6.92 (m, 1H), 6.92

– 6.85 (m, 2H), 6.84 – 6.77 (m, 1H). 5.64 (s, 1H), 5.18 (s, 2H), 1.53 (s, 9H), 1.36 (s, 18H). **^{13}C NMR** ($CDCl_3$, 125 MHz): δ 158.84, 151.41, 149.01, 146.51, 145.99, 141.27, 134.47, 129.13, 128.05, 122.79, 120.74, 115.58, 113.06, 84.77, 83.55, 71.00, 28.57, 28.23. **FTIR**: 565.8, 577.3, 641.4, 688.4, 731.2, 772.5, 795.1, 849.0, 878.6, 905.8, 946.8, 983.5, 1044.4, 1105.9, 1136.3, 1152.4, 1241.0, 1367.9, 1393.5, 1455.0, 1503.6, 1610.8, 1654.3, 1722.6, 1790.2, 2978.3, 3495.9 cm^{-1}.

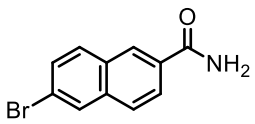

6-Bromo-2-naphthamide 118. Protocol adapted from the literature.[210] $(COCl)_2$ (1.5 eq., 4.10 mL, 48.0 mmol) was added dropwise at 0 °C to a suspension of 6-bromo-2-naphthoic acid **117** (1.00 eq., 8.00 g, 32.0 mmol) and DMF (0.10 eq. 240 µL, 3.20 mmol) in CH_2Cl_2 (250 mL)The mixture was stirred 1 h at 0 °C and then 2 h at RT, until the solution became clear. The solution was evaporated under reduced pressure and the dry residue was dissolved in CH_2Cl_2 (250 mL). NH_3 was bubbled into the solution for 5 minutes, resulting in a white precipate. EtOAc was then added until dissolution of the solid and the solution was washed with saturated $NaHCO_3$ (3 ×), brine (1 ×), dried over $MgSO_4$, and concentrated under reduced pressure. The crude product was recrystallized from EtOH, yielding a first crop of *amide* **118** as a white crystalline powder (4.51 g, 56%). After evaporation of the filtrate, the recrystallization was performed again to yield a second crop (830 mg, 10%, 66% total yield). **MP**: 219 °C. **^{1}H NMR** (DMSO-d_6, 500 MHz): δ 8.50 (s, 1H), 8.28 (d, J = 1.6 Hz, 1H), 8.17 (br, 1H), 8.02 – 7.96 (m, 3H), 7.71 (dd, J_1 = 8.8 Hz, J_2 = 2.0 Hz, 2H), 7.54 (br, 1H) ppm. **^{13}C NMR** (DMSO-d_6, 125 MHz): δ 168.17, 135.79, 132.78, 131.61, 131.25, 130.22, 130.09, 128.38, 127.60, 126.09, 121.44 ppm. **FTIR**: 470.8, 520.8, 541.2, 626.3, 732.5, 764.0, 807.1, 880.9, 901.1, 954.5, 1062.5, 1126.3, 1182.0, 1266.8, 1344.2, 1390.8, 1406.5, 1463.0, 1496.2, 1563.7, 1613.7, 1651.2, 3165.9, 3355.5 cm^{-1}. The data are consistent with the literature values.[258]

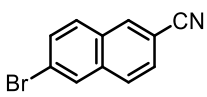

6-Bromo-2-naphthonitrile 116. Protocol adapted from the literature.[210] TFAA (1.10 eq., 2.70 mL, 19.6 mmol) was added dropwise at 0 °C to a suspension of 6-bromo-2-naphtamide **118** (1.00 eq., 4.45 g, 17.8 mmol) and pyridine (2.90 mL, 35.6 mmol, 2.00 eq.) in 1,4-dioxane (22 mL). The mixture was stirred for 16 h at RT. Additional portions of TFAA (740 µl, 5.3 mmol, 0.30 eq.) and of pyridine (860 µl, 10.7 mmol, 0.60 eq.) were added to drive the reaction to completion. After 1 h, AcOEt was added and the solution was washed with 1 M HCl (3 ×), sat. $NaHCO_3$ (3 ×), dried over $MgSO_4$, and concentrated under reduced pressure. The crude product was filtered over silica with CH_2Cl_2 to yield *nitrile* **116** as a white powder (2.53 g, 61% yield). **MP**: 156 °C. **^{1}H NMR** ($CDCl_3$, 400 MHz): δ 8.21 (s, 1H), 8.07 (s, 1H), 7.84 (d, J = 8.4 Hz, 1H), 7.77 (d, J = 8.8 Hz, 1H), 7.70 – 7.63 (m, 2H) ppm. **^{13}C NMR** ($CDCl_3$, 100 MHz): δ 135.67, 134.18, 131.43, 130.84, 130.38, 130.06, 128.43, 127.66, 123.74, 119.00, 110.05 ppm. **FTIR**: 453.8,

471.8, 513.5, 559.3, 646.0, 700.9, 810.1, 876.6, 891.0, 958.1, 1060.3, 1129.4, 1159.8, 1188.3, 1244.1, 1267.9, 1331.1, 1352.3, 1378.0, 1458.8, 1489.8, 1582.5, 1622.2, 1688.8, 2221.3, 2987.8 cm^{-1}. The data are consistent with the literature values.[259]

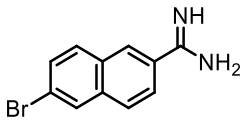

6-Bromo-2-naphthimidamide 119. 6-Bromo-2-naphthonitrile **116** (1.75 g, 7.50 mmol) reacted according to general procedure K with 2.50 eq. of LiHMDS and at reflux for 2 h to yield *amidine* **119** as a crystalline yellow powder (1.67 g, 89% yield). **MP**: 192 °C. **^{1}H NMR** (DMSO-d_6, 500 MHz): δ 8.34 (s, 1H), 8.24 (s, 1H), 8.00 – 7.98 (m, 1H), 7.94 – 7.91 (m, 2H), 7.67 (dd, J_1 = 2.0 Hz, J_2 = 9.0 Hz, 1H), 6.60 (br, 2H) ppm. **^{13}C NMR** (DMSO-d_6, 100 MHz): δ 162.18, 134.67, 134.29, 130.87, 130.76, 129.47, 129.44, 126.76, 125.95, 125.73, 120.12 ppm. **FTIR**: 474.0, 489.9, 522.9, 535.8, 605.0, 618.8, 640.1, 714.0, 722.2, 740.0, 768.1, 807.8, 839.1, 884.3, 901.0, 951.1, 961.1, 1059.9, 1082.3, 1137.6, 1165.9, 1175.9, 1188.2, 1242.2, 1347.4, 1419.3, 1462.0, 1492.1, 1555.2, 1578.6, 1621.5, 1638.8, 1765.7, 1919.1, 2987.8, 3332.7, 3354.0, 3463.6 cm^{-1}.

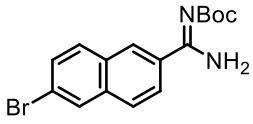

***tert*-Butyl (amino(6-bromonaphthalen-2-yl)methylene)carbamate 120.** 6-Bromo-2-naphthimidamide **119** (1.63 g, 6.54 mmol) reacted according to general procedure L to yield *Boc-protected amidine* **120** as a yellow powder (2.11 g, 92%). **MP**: 78°C (decomposition). **^{1}H NMR** ($CDCl_3$, 400 MHz): δ 9.66 (br, 1H), 8.32 (s, 1H), 7.96 (s, 1H), 7.83 (dd, J_1 = 8.8 Hz, J_2 = 1.6 Hz), 7.73 – 7.67 (m, 2H), 7.57 (dd, J_1 = 8.8 Hz, J_2 = 1.6 Hz), 6.64 (br, 1H), 1.54 (s, 9H) ppm. **^{13}C NMR** ($CDCl_3$, 100 MHz): δ 167.48, 164.38, 136.37, 132.95, 131.49, 131.06, 130.83, 130.36, 128.52, 128.06, 125.16, 122.71, 80.62, 28.77 ppm. **FTIR**: 472.1, 496.1, 624.1, 639.6, 707.4, 760.0, 803.9, 868.8, 902.3, 953.2, 983.7, 1063.0, 1110.6, 1149.3, 1238.0, 1252.9, 1275.7, 1365.2, 1391.0, 1454.0, 1487.3, 1517.4, 1607.3, 1660.9, 2975.9, 3345.5 cm^{-1}.

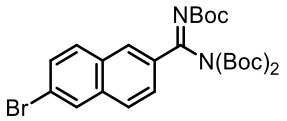

***tert*-Butyl ((6-bromonaphthalen-2-yl)((tert-butoxycarbonyl)imino) methyl)(tert-butoxycarbonyl)carbamate 115.** Boc-protected amidine **120** (2.05 g, 5.87 mmol) reacted according to general procedure M to yield *tris-Boc-protected amidine* **115** as a yellow powder (2.37 g, 74% yield). **MP**: 149 °C (decomposition). **^{1}H NMR** ($CDCl_3$, 400 MHz): δ 8.22 (s, 1H), 8.02 – 7.96 (m, 2H), 7.77 (d, J = 6.8 Hz, 1H), 7.73 (d, J = 6.4 Hz, 1H), 7.58 (d, J = 7.2 Hz, 1H), 1.53 (s, 9H), 1.32 (s, 18H) ppm. **^{13}C NMR** ($CDCl_3$, 125 MHz): δ 158.31, 151.03, 148.52, 136.01, 131.82, 131.11, 130.58, 130.45, 130.00, 128.90, 127.63, 125.53, 122.58, 84.30, 83.07, 28.06, 27.69 ppm. **FTIR**: 556.6, 572.0, 608.6, 629.8, 657.7, 703.7, 719.9, 749.1, 772.8, 793.4, 815.4, 844.0, 880.2, 908.0, 935.2, 1003.4, 1036.0, 1064.0, 1100.1, 1123.9, 1149.7, 1248.4, 1265.4, 1304.8, 1333.7, 1368.7, 1392.9, 1463.0, 1589.9, 1620.8, 1651.5, 1728.0, 1797.6, 2936.0, 2983.1 cm^{-1}.

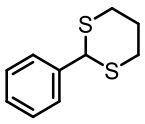

2-Phenyl-1,3-dithiane 136. Protocol adapted from the literature.[214] I_2 (0.10 eq., 1.50 mmol, 380 mg) was added portionwise to a solution of benzaldehyde 1**37** (1.00 eq., 15.0 mmol, 1.50 mL) and 1,3-propanedithiol (1.10 eq., 16.5 mmol, 1.70 mL) in CH_2Cl_2 (50 mL). The reaction mixture was stirred for 2 h at RT. Sat. $Na_2S_2O_3$ was added. The organic phase was washed with 1 M NaOH (3 ×), separated and dried over $MgSO_4$. The solvent was evaporated under reduced pressure and the crude product was recrystallized in iPrOH to yield *dithiane* **136** as colorless plates (2.91 g, quant.) **MP**: 70 °C **^{1}H NMR** ($CDCl_3$, 400 MHz): δ 7.50 – 7.44 (m, 2H), 7.38 – 7.25 (m, 2H), 5.17 (s, 1H), 3.11 – 3.00 (m, 2H), 2.94 – 2.85 (m, 2H), 2.21 – 2.09 (m, 1H), 2.00 – 1.84 (m, 1H) ppm. **^{13}C NMR** ($CDCl_3$, 100 MHz): δ 139.64, 129.24, 128.93, 128.27, 51.99, 32.61, 25.63 ppm. **FTIR**: 556.6, 565.8, 594.0, 674.7, 695.2, 723.4, 790.8, 831.1, 882.6, 909.1, 1004.5, 1025.7, 1072.0, 1114.7, 1170.7, 1249.0, 1274.8, 1296.3, 1411.1, 1422.5, 1450.5, 1482.0, 1495.7, 1582.7, 1955.7, 2891.4, 2948.9 cm^{-1}. The data are consistent with the literature values.[260]

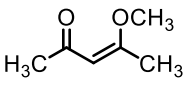

4-Methoxypent-3-en-2-one 149. Protocol adapted from the literature.[229] A solution of 2,4-methoxypentanedione **150** (1.00 eq., 51.0 mmol, 5.10 mL,), $HC(OCH_3)_3$ (1.00 eq., 51.0 mmol, 6.50 mL), and PTSA · H_2O (0.011 eq., 0.57 mmol, 0.108 g) in MeOH (12.5 mL) was stirred at 55 °C during 7.5 h. The mixture was cooled down to RT and the solvent was evaporated under reduced pressure. The residue was purified by vacuum distillation (50-55°C, 5 mbar) to yield *enol ether* **149** as a colorless oil. (3.41g, 59%). **^{1}H NMR** ($CDCl_3$, 400 MHz): δ 5.46 (s, 1H), 3.64 (s, 3H), 2.28 (s, 3H), 2.17 (s, 3H) ppm. **^{13}C NMR** ($CDCl_3$, 100 MHz): δ 197.13, 172.95, 99.44, 55.54, 32.17, 19.76 ppm. **FTIR**: 617.5, 689.9, 803.5, 818.0, 881.7, 924.1, 958.5, 1019.9, 1063.9, 1162.7, 1223.2, 1273.3, 1355.6, 1395.6, 1439.0, 1577.5, 1678.4, 1724.9, 2220.3, 2942.7 cm^{-1}. The data are consistent with the literature values.[229]

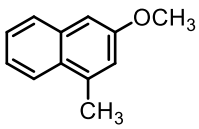

3-Methoxy-1-methylnaphthalene 146. Protocol adapted from the literature.[230] *t*BuOH (2.00 eq., 8.76 mmol, 0.83 mL) was added dropwise at RT to a suspension of $NaNH_2$ (7.33 eq., 32.1 mmol, 1.25 g) in THF (10.5 mL). The resulting mixture was heated up to 40 °C and stirred for 1 h. A solution of compound **149** (2.00 eq., 1.00 g, 8.76 mmol) in THF (7 mL) was added dropwise at 40 °C. The mixture was further stirred at 40°C for 1.5 h. A solution of bromobenzene (1.00 eq., 0.46 mL, 4.38 mmol) in THF (3.5 mL) was added dropwise and the mixture was heated up to 55°C, stirred for 5 h, and allowed to cool down ON to RT. The mixture was poured in ice, and the resulting solution was acidified with HCl 1M to pH 1 and extracted with EtOAc (3 ×). The organic layers were combined, and the solvent was evaporated under under reduced pressure. The residue was dissolved in acetone (7 mL) and concd HCl (0.3 mL) was added. The mixture was stirred at RT for 15 min. EtOAc was added, and the organic layer

was washed with brine (3 ×) and dried over Na_2SO_4. The solvent was evaporated under reduced pressure and the crude product was purified by column chromatography (cyclohexane / toluene 95:5) to yield *naphthol ether* **147** as an off-white solid (750 mg, 53 %). **MP**: 48 °C. **^{1}H NMR** ($CDCl_3$, 400 MHz): δ 7.91 (d, 1H, *J* = 8.2 Hz), 7.74 (d, 1H, *J* = 8.0 Hz), 7.45 (m, 2H), 7.38 (m, 2H), 3.91 (s, 3H), 2.66 (s, 3H) ppm . **^{13}C NMR** ($CDCl_3$, 100 MHz): δ 157.25, 136.28, 134.84, 128.59, 127.46, 126.01, 124.20, 119.36, 103.96, 55.24, 19.35 ppm. **FTIR**: 571.3, 647.8, 746.1, 769.4, 829.1, 857.9, 945.0, 1022.1, 1034.5, 1054.1, 1133.8, 1154.8, 1166.8, 1196.8, 1219.4, 1230.4, 1279.7, 1347.3, 1405.9, 1449.6, 1470.5, 1508.7, 1583.7, 1600.9, 1622.0, 2962.6 cm^{-1}. The data are consistent with the literature values.[261]

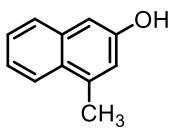

4-Methylnaphthalen-2-ol 161. Protocol adapted from the literature.[230] A solution of BCl_3 (1.0 M in CH_2Cl_2, 1.33 eq., 1.55 mmol, 1.8 mL) was added dropwise at -84 °C to a solution of naphthol ether **146** (1.00 eq., 1.16 mmol, 203 mg) and TBAI (1.54 eq., 1.79 mmol, 475 mg) in CH_2Cl_2 (9 mL). After 5 min, the solution was allowed to warm to 0°C and stirred for 2 hours. The reaction was quenched with water and the aqueous phase was extracted with CH_2Cl_2 (3 ×). The organic layers were combined and dried over Na_2SO_4. The solvent was evaporated under reduced pressure and the crude product was purified by column chromatography (cyclohexane / EtOAC 90:10 to 70:30) to yield *naphthol* **161** as a brownish powder (178 mg, 97%). **MP**: 63 °C. **^{1}H NMR** ($CDCl_3$, 400 MHz): δ 7.92 (d, *J* = 8.6 Hz, 1H), 7.69 (d, *J* = 8.02 Hz, 1H), 7.45 (m, 1H), 7.38 (m, 1H), 7.02 (d, *J* = 2.3 Hz, 1H), 6.97 (s, 1H), 4.96 (br, 1H), 2.69 (s, 3H) ppm. **^{13}C NMR** ($CDCl_3$, 100 MHz): δ 152.88, 136.97, 134.82, 128.42, 127.60, 126.55, 124.21, 123.57, 118.38, 107.76, 19.44 ppm. The data are consistent with the literature values.[262] **FTIR**: 605.0, 643.9, 686.3, 744.0, 769.2, 833.0, 853.3, 877.0, 950.9, 967.2, 998.9, 1043.9, 1132.0, 1151.7, 1166.0, 1202.8, 1231.3, 1273.3, 1349.2, 1374.9, 1438.7, 1461.9, 1510.4, 1584.9, 1601.1, 1620.8, 1704.3, 2921.1, 3217.6 cm^{-1}.

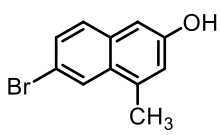

6-Bromo-4-methylnaphthalen-2-ol 145. Br_2 (2.00 eq., 6.32 mmol, 320 µL) in AcOH (1 mL) was added dropwise to solution of naphthol **161** (1.00 eq., 3.16 mmol, 500 mg) in AcOH (5 mL) and water (0.5 mL). The mixture was heated up to 70 °C and was stirred for 3 h. Tin was added (1.35 eq, 4.22 mmol, 501 mg) was added. Th reaction mixture was further stirred at 70 °C for 3H and was allowed to cool down to RT. the mixture was filtered on Celite and the precipitate was washed with EtOAc. The filtrate was then washed with sat. $NaHCO_3$ (5 ×) and dried over Na_2SO_4. The solvent was evaporated under reduced pressure and the crude product was purified by column chromatography (cyclohexane / EtOAC 90:10 to 60:40) to yield *bromonaphthol* **145** as a yellow oil (458 mg, 61%). **^{1}H NMR** ($CDCl_3$, 400

MHz): δ 8.03 (d, *J* = 1.83 Hz, 1H), 7.54 (d, *J* = 8.7 Hz, 1H), 7.49 (dd, 1H, J_1 = 8.7 Hz, J_2 = 1.83 Hz,), 6.97 (m, 2H) , 4,86 (br, 1H), 2,61 (s, 3H) ppm. **^{13}C NMR** ($CDCl_3$, 100 MHz): δ 153.16, 136.22, 133.42, 129.63, 129.57, 128.72, 126.63, 119.51, 117.27, 107.78, 19.73 ppm.

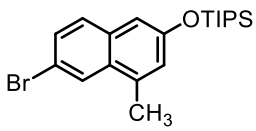

((6-Bromo-4-methylnaphthalen-2-yl)oxy)triisopropylsilane 145a. TIPSCl (1.00 eq., 1.27 mmol, 244 mg) was added dropwise at 0°C to a solution of naphthol **145** (1.00 eq., 1.27 mmol, 300 mg) and imidazole (1.10 eq., 1.39 mmol, 95 mg) in DMF (1.5 mL). The solution was allowed to warm up to RT and stirred for 4 h. Et_2O was added, and the organic layer was with brine (3 ×) and dried over $MgSO_4$. The solvent was evaporated under reduced pressure and the crude product was purified by column chromatography (cyclohexane) to yield *silyl ether* **145a** as a pale-yellow oil (432 mg, 87 %). **^{1}H NMR** ($CDCl_3$, 400 MHz): δ 8.03 (d, *J* = 1.8 Hz, 1H), 7.54 (d, *J* = 8.7 Hz, 1H), 7.47 (dd, J_1 = 8.7 Hz, J_2 = 1.8 Hz, 1H), 7.02 (d, *J* = 2.1, 1H), 6.99 (d, *J* = 1.4 Hz, 1H), 1.38 – 1.25 (m, 3H), 1.12 (d, *J* = 7.33 Hz, 18H) ppm. **^{13}C NMR** ($CDCl_3$, 100 MHz): δ 153.92, 135.51, 133.57, 129.76, 129.28, 126.57, 123.87, 117.38, 112.65, 19.37, 18.12, 12.88 ppm. **FTIR**: 648.0, 660.0, 683.5, 747.9, 797.0, 833.3, 859.8, 883.3, 919.4, 979.5, 996.8, 1013.7, 1073.1, 1140.6, 1164.1, 1211.3, 1226.9, 1281.1, 1325.0, 1364.2, 1383.4, 1407.0, 1463.8, 1489.8, 1590.4, 1618.8, 2865.7, 2891.8, 2943.7 cm^{-1}.

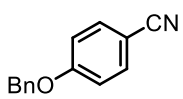

4-(Benzyloxy)benzonitrile 174. Protocol adapted from the literature.[238] 4-Cyanophenol **171** (1.00 eq., 26.3 mmol, 3.14 g) was added portionwise at 0 °C to a suspension of NaH (60% in paraffin oil, 1.00 eq., 26.3 mmol, 1.07 g) in DMF (60 mL). After 5 min, BnBr (1.00 eq., 26.3 mmol, 3.20 mL) was added dropwise at 0 °C. The solution was heated up to 60 °C and stirred for 1.75 h. The reaction mixture was then poured in water. The precipitate was collected and recrystallized in methanol to yield *ether* **174** as a white powder (4.87 g, 84%). **MP**: 93 °C. **^{1}H NMR** ($CDCl_3$, 400 MHz): 7.59 (d, *J* = 8.4 Hz, 2H), 7.45 – 7.30 (m, 5H), 7.02 (d, *J* = 8.4 Hz, 2H), 5.12 (s, 2H) ppm. **^{13}C NMR** ($CDCl_3$, 125 MHz): δ 162.09, 135.82, 134.21, 128.96, 128.56, 127.64, 119.35, 115.73, 104.41, 77.16, 70.41 ppm. **FTIR**: 647.6, 695.6, 734.2, 835.6, 854.5, 906.1, 1026.9, 1037.5, 1077.8, 1114.8, 1170.2, 1260.9, 1300.7, 1315.9, 1386.0, 1420.0, 1452.3, 1461.9, 1498.0, 1508.4, 1572.5, 1604.2, 1659.3, 1908.9, 2221.1, 2919.9, 3058.0, 3393.1 cm^{-1}. The data are consistent with the literature values.[263]

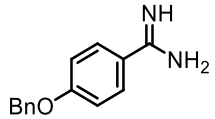

4-(Benzyloxy)benzimidamide 175. Nitrile **174** (23.3 mmol, 4.87 g) reacted according to general procedure K with 1.20 eq. of LiHMDS and at reflux ON to yield *amidine* **175** as white needles (4.17 g, 79% yield). **MP**: 160 °C. **^{1}H NMR** (DMSO-d_6, 500 MHz): δ 7.74 (d, *J* = 8.4 Hz, 2H), 7.48 – 7.29 (m, 5H), 7.26 (br, 3H), 7.04 (d, *J* = 8.4 Hz, 2H) ppm. **^{13}C NMR** (DMSO-d_6, 125 MHz): 164.75, 162.61, 136.29, 130.16, 128.52, 128.08, 127.80, 119.68, 115.15, 69.61 ppm. **FTIR**: 628.7, 644.0, 699.9, 732.9, 762.6, 836.7, 862.2,

921.4, 992.3, 1009.9, 1139.2, 1189.1, 1264.2, 1310.2, 1380.2, 1453.5, 1485.5, 1608.6, 1676.5, 3093.9, 3294.8 cm^{-1}.

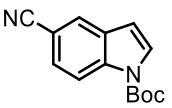

***tert*-Butyl 5-cyano-1*H*-indole-1-carboxylate 181.** Protocol adapted from the literature.[241] $(Boc)_2O$ (1.10 eq, 38.7 mmol, 8.45 g) was added in a solution of 5-cyanoindole **173** (1.00 eq, 35.2 mmol, 5.00 g) and DMAP (0.02 eq, 0.70 mmol, 86 mg) in CH_2Cl_2 (25 mL). The mixture was stirred at RT for 45 min. The solution was then washed with 1 M HCl (3 ×) and was dried over Na_2SO_4. The solvent evaporated under reduced pressure. The residue was dissolved in CH_3OH, and water was added until complete precipitation of a brown solid. The powder was filtered, washed with water, and dissolved in EtOAc. The organic layer was dried over Na_2SO_4 the solvent was evaporated under reduced pressure to yield *protected indole* **181** as a brown powder (6.33 g, 74 %). **MP:** 126 °C. **^{1}H NMR** ($CDCl_3$, 400 MHz): δ 8.25 (d, J = 8.4 Hz, 1H), 7.90 (s, 1H), 7.70 (d, J = 3.6 Hz, 1H), 7.55 (dd, J_1 = 8.5 Hz, J_2 = 1.8 Hz, 1H), 6.63 (d, J = 3.2 Hz, 1H), 1.68 (s, 9H) ppm. **^{13}C NMR** ($CDCl_3$, 125 MHz): δ 149.16, 137.19, 130.63, 128.20, 127.44, 125.91, 119.91, 116.13, 107.06, 106.20, 85.05, 28.24 ppm. **FTIR**: 562.4, 575.1, 622.9, 636.9, 726.8, 752.4, 763.8, 797.6, 814.7, 832.2, 850.9, 870.6, 886.1, 1019.0, 1040.2, 1082.8, 1122.1, 1136.7, 1158.8, 1189.0, 1214.9, 1257.8, 1282.3, 1334.0, 1348.0, 1363.3, 1459.2, 1539.3, 1608.7, 1740.0, 2220.6, 2979.4 cm^{-1}. The data are consistent with the literature values.[241]

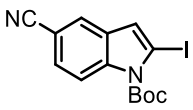

***tert*-Butyl 5-cyano-2-iodo-1*H*-indole-1-carboxylate 172**. Protocol adapted from the literature.[242] BuLi (2.38 M in hexanes, 1.25 eq., 5.14 mmol, 2.16 mL) was added to a solution of DIPA (1.35 eq, 5.48 mmol, 780 µL) in THF. The mixture was stirred at RT for 15 min and was then added dropwise at -84 °C to a solution of protected indole **181** (1.00 eq, 4.13 mmol, 1.00 g) in THF (12 mL). The reaction mixture was stirred at -84°C for 1 h and a solution of I_2 (1.12 eq, 4.65 mmol, 1.18 g) in THF (10 mL) was added dropwise. The reaction mixture was allowed to warm to RT and was further stirred for 45 min. After addition of sat. $Na_2S_2O_3$, the mixture was filtered, and the aqueous phase was extracted with EtOAc (3 ×). The combined organic layers were dried over Na_2SO_4 and the solvent was evaporated under reduced pressure. The crude product was purified by filtration over silica with cyclohexane / EtOAc 9:1 to yield *indoyl iodide* **172** as a pale-yellow oil , which turned into an off-white solid after trituration in pentane (1.23 g, 81%). **MP**: 99 °C. **^{1}H NMR** ($CDCl_3$, 400 MHz): δ 8.19 (d, J = 8.4 Hz, 1H), 7.80 (d, J = 1.6 Hz, 1H), 7.48 (dd, J_1 = 5.0 Hz, J_2 = 1.8 Hz), 7.05 (s, 1H), 1.71 (s, 9H) ppm. **^{13}C NMR** ($CDCl_3$, 100 MHz): δ 149.09, 137.12, 130.55, 128.15, 127.34, 125.83, 119.84, 116.06, 106.99, 106.11, 84.99, 28.17 ppm. **FTIR**: 622.6, 637.9, 648.1, 725.8, 755.6, 766.3, 809.6, 843.0, 870.9, 885.8, 898.4, 944.5, 1030.8, 1046.3, 1083.3, 1127.6, 1150.3, 1189.9, 1211.2, 1256.2,

1280.2, 1315.4, 1348.1, 1366.0, 1394.8, 1448.2, 1514.7, 1571.7, 1608.8, 1731.2, 1736.5, 1890.5, 2226.7, 2981.0, 3112.2 cm^{-1}. The data are consistent with the literature values.[242]

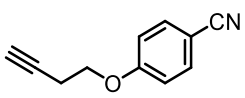

4-(But-3-yn-1-yloxy)benzonitrile 180. Protocol adapted from the literature.[243] A solution of DIAD (2.00 eq, 8.39 mmol, 1.65 mL) in THF (1.5 mL) was added dropwise at 0 °C to a solution of but-3-yn-1-ol **169** (1.10 eq, 4.62 mmol, 0.345 mL), 4-cyanophenol **171** (1.00 eq, 4.19 mmol, 0.500 g), Et_3N (1.00 eq, 4.19 mmol, 0.600 mL) and PPh_3 (2.00 eq, 8.39 mmol, 2.20 g) in THF (15 mL). The solution was allowed to warm to RT and was stirred ON. The solvent was evaporated under reduced pressure. TBME (5 mL) was added and the mixture was stirred for 1 h. The precipitate was filtered and the filtrate was collected. The solvent was evaporated under reduced pressure and the crude product was purified by column chromatography (cyclohexane / AcOEt, 90:10 to 85:15) to yield *ether* **180** as a yellow powder (239 mg, 32 %). **MP**: 72 °C. **^{1}H NMR** ($CDCl_3$, 400 MHz): δ 7.62 – 7.57 (m, 2H), 7.00 – 6.94 (m, 2H), 4.14 (t, J = 6.9 Hz, 2H), 2.72 (td, J_1 = 6.9 Hz, J_2 = 2.7 Hz, 2H), 2.06 (t, J = 2.9 Hz, 1H) ppm. **^{13}C NMR** ($CDCl_3$, 125 MHz): δ 161.79, 134.13, 119.18, 115.38, 104.50, 79.84, 70.43, 66.32, 19.49 ppm. **FTIR**: 689.3, 773.4, 808.5, 832.1, 853.4, 894.6, 962.3, 1026.5, 1039.2, 1092.3, 1146.6, 1176.3, 1254.5, 1295.7, 1336.9, 1376.0, 1391.3, 1419.7, 1470.4, 1508.2, 1575.5, 1604.8, 1731.8, 1767.7, 1804.5, 2223.8, 2947.9, 2983.8, 3252.1 cm^{-1}. The data are consistent with the literature values.[264]

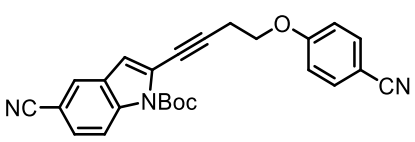

***tert*-Butyl 5-cyano-2-(4-(4-cyanophenoxy)but-1-yn-1-yl)-1*H*-indole-1-carboxylate 179**. A solution of alkyne **180** (1.20 eq, 2.28 mmol, 390 mg) in degassed DIPA (3 mL) was slowly added to a solution of indole **172** (1.00 eq, 1.90 mmol, 700 mg), $[Pd(PPh_3)_2Cl_2]$ (0.10 eq, 0.190 mmol, 133 mg) and CuI (0.20 eq, 0.380 mmol, 72 mg) in degassed DIPA (6 mL) The mixture was stirred at RT for 2h. EtOAc was added and the mixture was filtered over Celite, washed with sat. NH_4Cl (3 ×) and dried over Na_2SO_4. The solvent was evaporated under reduced pressure and the crude product was purified by column chromatography (cyclohexane / AcOEt, 80:20 to 60:40) to yield *internal alkyne* **179** as a beige powder (730 mg, 93%). **MP**: 136 °C. **^{1}H NMR** ($CDCl_3$, 400 MHz): δ 8.22 (d, J = 8.8 Hz, 1H), 7.83 (s, 1H), 7.64 – 7.58 (m, 2H), 7.55 (dd, J_1 = 8.6 Hz, J_2 = 1.8 Hz, 1H), 7.02 – 6.96 (m, 2H), 6.87 (s, 1H), 4.25 (t, J = 6.8 Hz, 2H), 3.03 (t, J = 6.8 Hz, 2H), 1.69 (s, 9H) ppm. **^{13}C NMR** ($CDCl_3$, 100 MHz): δ 161.78, 148.93, 137.73, 134.20, 128.66, 128.24, 125.39, 123.00, 119.36, 119.16, 116.57, 115.41, 115.30, 106.78, 104.68, 93.08, 85.47, 74.29, 66.08, 28.27, 21.04 ppm. **FTIR**: 614.0, 643.6, 663.2, 706.4, 720.0, 766.4, 813.7, 838.5, 881.8, 970.9, 1023.0, 1036.0, 1116.0, 1129.6, 1144.6, 1158.3, 1175.2, 1225.2, 1251.1, 1280.3, 1336.3, 1355.9, 1372.5, 1394.6, 1415.9, 1465.0, 1508.1, 1551.4, 1574.4, 1603.2, 1724.6, 2219.7, 2986.2 cm^{-1}.

7.4. FXIIf Inhibition Assay

Stock solution of the tested molecules were prepared at 50 mM in DMSO and stored at -20°C, protected from light. For the assay, these stock solutions were diluted at the desired concentration with DMSO.

The kinetic buffer was made up of 30 mM HEPES, 150 mM NaCl and 0.005% Triton-X-100, adjusted at pH 7.4 with 1 M NaOH. 6 µL of tested compound at the desired concentration in DMSO (or DMSO alone), 10 µL of human FXIIf (290 nM), and 164 µL of kinetic buffer were mixed for 5 s and incubated for 10 min at 37 °C. 20 µL of 2.5 mM S-2302 were then injected in each well to start the reaction. The release of *para*-nitroaniline was recorded for 3.5 min at 405 nm. Between each absorbance read, the plate is shaken for 1 s.

For the treatment of activity data generated during screening, SoftMax Pro 7.0.3 was used to extract the slope of the kinetic reaction between 15 s and 200 s and to transform it in inhibition percentage using the following equation: inhibition

$$\text{inhibition (\%)} = \left(1 - \frac{v_i}{v_0}\right) \cdot 100$$

where v_i and v_0 are the reactions rates with inhibitor and with vehicle alone, respectively.

7.5. Molecular Docking Studies

Schrödinger Maestro 2019-2 software package was used. The Chemical structure for the docking were optimized and energetically minimized via OPLS3 force field algorithm implemented in the LigPrep module of Schrödinger suite. The Epik tool was used to predict the ionization states of the ligands at pH 7 ± 2 and to generate tautomers. Salts were then removed and all stereoisomers were generated. The prepared 3D structures were saved as Maestro format.

The X-ray crystal structure of FXIIf complexed with benzamidine was imported from the RCSB Protein Data Bank. PrepWiz module included in Schrödinger suite performed the protein preparation. The protein was first preprocessed to assign the bond orders. Water molecules implicated in less than three H bonds with the protein were deleted. The ligands were docked using GLIDE v8.3 docking with the extra precision (XP) mode.

Bibliography

[1] O. D. Ratnoff, J. E. Colopy, *J. Clin. Invest.* **1955**, *34*, 602–613.

[2] O. D. Ratnoff, R. J. Busse, R. P. Sheon, *N. Engl. J. Med.* **1968**, *279*, 760–761.

[3] A. J. Gale, *Toxicol. Pathol.* **2011**, *39*, 273–280.

[4] J. E. Freedman, J. Loscalzo, in *Harrison's Princ. Intern. Med.*, McGraw-Hill Education, New York, **2015**, pp. 740–745.

[5] M. Koupenova, B. E. Kehrel, H. A. Corkrey, J. E. Freedman, *Eur. Heart J.* **2017**, *38*, 785–791.

[6] G. F. Michaud, W. G. Stevenson, in *Harrison's Princ. Intern. Med.*, McGraw-Hill Education, New York, **2015**, pp. 1476–1489.

[7] T. Watson, E. Shantsila, G. Y. Lip, *Lancet* **2009**, *373*, 155–166.

[8] F. Violi, D. Pastori, P. Pignatelli, *J. Atr. Fibrillation* **2014**, *7*, 71–76.

[9] A. Brandes, M. D. Smit, B. O. Nguyen, M. Rienstra, I. C. Van Gelder, *Arrhythmia Electrophysiol. Rev.* **2018**, *7*, 118–127.

[10] R. Ferrandis, J. Castillo, J. de Andrés, C. Gomar, A. Gómez-Luque, F. Hidalgo, J. V. Llau, P. Sierra, L. M. Torres, *Thromb. Haemost.* **2013**, *110*, 515–522.

[11] C. Becattini, G. Agnelli, *Blood* **2020**, *135*, 305–316.

[12] C. Kearon, S. R. Kahn, *Blood* **2020**, *135*, 317–325.

[13] I. H. Jaffer, I. H. Fredenburgh, J. Hirsh, J. I. Weitz, *J. Thromb. Haemost.* **2015**, *13*, S72–S81.

[14] C. Maas, C. Oschatz, T. Renné, *Semin. Thromb. Hemost.* **2011**, *37*, 375–381.

[15] I. H. Jaffer, J. I. Weitz, *Acta Biomater.* **2019**, *94*, 2–10.

[16] C. Wall, J. Moore, J. Thachil, *J. Intensive Care Soc.* **2016**, *17*, 160–167.

[17] N. C. Chan, J. I. Weitz, J. W. Eikelboom, *Arterioscler. Thromb. Vasc. Biol.* **2017**, *37*, 743–745.

[18] *Drug Ther. Bull.* **2017**, *55*, 129–132.

[19] W. B. Gibler, *Crit. Pathw. Cardiol.* **2019**, *18*, 150–166.

[20] J. I. Weitz, N. C. Chan, *Blood* **2020**, *135*, 351–359.

[21] S. Palta, R. Saroa, A. Palta, *Indian J. Anaesth.* **2014**, *58*, 515–523.

[22] J. Erlich, G. C. N. Parry, C. Fearns, M. Muller, P. Carmeliet, T. Luther, N. Mackman, *Proc. Natl. Acad. Sci. U. S. A.* **1999**, *96*, 8138–8143.

[23] J. C. Fredenburgh, P. L. Gross, J. I. Weitz, *Blood* **2017**, *129*, 147–154.

[24] H. U. Pauer, T. Renné, B. Hemmerlein, T. Legler, S. Fritzlar, I. Adham, W. Müller-Esterl, G. Emons, U. Sancken, W. Engel, et al., *Thromb. Haemost.* **2004**, *92*, 503–508.

[25] M. L. Van Montfoort, J. C. M. Meijers, *Hematology* **2014**, *2014*, 60–65.

[26] J. Hirsh, S. S. Anand, J. L. Halperin, V. Fuster, *Arterioscler. Thromb. Vasc. Biol.* **2001**, *21*, 1094–1096.

[27] J. I. Weitz, in *Harrison's Princ. Intern. Med.*, McGraw-Hill Education, New York, **2015**, pp. 745–760.

[28] G. Gatti, B. Casu, G. K. Hamer, A. S. Perlin, *Macromolecules* **1979**, *12*, 1001–1007.

[29] P. Dowd, S. W. Ham, S. Naganathan, R. Hershline, *Annu. Rev. Nutr.* **1995**, *15*, 419–440.

[30] R. De Caterina, S. Husted, L. Wallentin, F. Andreotti, H. Arnesen, F. Bachmann, C. Baigent, K. Huber, J. Jespersen, S. D. Kristensen, et al., *Thromb. Haemost.* **2013**, *110*, 1087–1107.

[31] N. C. Chan, J. W. Eikelboom, J. I. Weitz, *Circ. Res.* **2016**, *118*, 1409–1424.

[32] E. Altiok, N. Marx, *Dtsch. Arztebl. Int.* **2018**, *115*, 776–783.

[33] M. V. Huisman, F. A. Klok, *Eur. Hear. Journal, Suppl.* **2018**, *20*, E12–E15.

[34] H. Rasche, *Eur. Hear. Journal, Suppl.* **2001**, *3*, 3–7.

[35] R. W. Colman, *J. Exp. Med.* **2006**, *203*, 493–495.

[36] J. W. Yau, P. Liao, J. C. Fredenburgh, A. R. Stafford, A. S. Revenko, B. P. Monia, J. I. Weitz, *Blood* **2014**, *123*, 2102–2108.

[37] M. Larsson, V. Rayzman, M. W. Nolte, K. F. Nickel, J. Björkqvist, A. Jämsä, M. P. Hardy, M. Fries, S. Schmidbauer, P. Hedenqvist, et al., *Sci .Transl. Med.* **2014**, *6*, 222ra17.

[38] J. W. Yau, A. R. Stafford, P. Liao, J. C. Fredenburgh, R. Roberts, J. L. Brash, J. I. Weitz, *Acta Biomater.* **2012**, *8*, 4092–4100.

[39] A. Matafonov, P. Y. Leung, A. E. Gailani, S. L. Grach, C. Puy, Q. Cheng, M. F. Sun, O. J. T. McCarty, E. I. Tucker, H. Kataoka, et al., *Blood* **2014**, *123*, 1739–1746.

[40] M. Wallisch, C. U. Lorentz, H. H. S. Lakshmanan, J. Johnson, M. R. Carris, C. Puy, D. Gailani, M. T. Hinds, O. J. T. McCarty, A. Gruber, et al., *Res. Pract. Thromb. Haemost.* **2020**, *4*, 205–216.

[41] T. Renné, M. Pozgajová, S. Grüner, K. Schuh, H. U. Pauer, P. Burfeind, D. Gailani, B. Nieswandt, *J. Exp. Med.* **2005**, *202*, 271–281.

[42] Q. Cheng, E. I. Tucker, M. S. Pine, A. Matafonov, M. Sun, T. C. White-adams, S. a Smith, S. R. Hanson, O. J. T. Mccarty, T. Renne, et al., *Blood* **2010**, *116*, 3981–3989.

[43] C. Kleinschnitz, G. Stoll, M. Bendszus, K. Schuh, H. U. Pauer, P. Burfeind, C. Renné, D. Gailani, B. Nieswandt, T. Renné, *J. Exp. Med.* **2006**, *203*, 513–518.

[44] A. S. Revenko, D. Gao, J. R. Crosby, G. Bhattacharjee, C. Zhao, C. May, D. Gailani, B. P. Monia, A. R. MacLeod, *Blood* **2011**, *118*, 5302–5311.

[45] Y. Xu, T. Q. Cai, G. Castriota, Y. Zhou, L. Hoos, N. Jochnowitz, C. Loewrigkeit, J. A. Cook, A. Wickham, J. M. Metzger, et al., *Thromb. Haemost.* **2013**, *111*, 694–704.

[46] F. Zito, G. D. O. Lowe, A. Rumley, A. D. McMahon, S. E. Humphries, *Atherosclerosis* **2002**, *165*, 153–158.

[47] W.-M. Halbmayer, A. Haushofer, J. Radek, R. Schön, M. Deutsch, M. Fischer, *Coron. Artery Dis.* **1994**, *5*, 451–454.

[48] M. J. Gallimore, S. L. Harris, D. W. Jones, M. Winter, *Thromb. Res.* **2004**, *114*, 91–96.

[49] I. Tirado, J. M. Soria, J. Mateo, A. Oliver, J. C. Souto, A. Santamaria, R. Felices, M. Borrell, J. Fontcuberta, *Thromb. Haemost.* **2004**, *91*, 899–904.

[50] A. Santamaría, J. Mateo, I. Tirado, A. Oliver, R. Belvís, J. Martí-Fábregas, R. Felices, J. M. Soria, J. C. Souto, J. Fontcuberta, *Stroke* **2004**, *35*, 1795–1799.

[51] R. Von Kanel, W. A. Wuillemin, M. Furlan, B. Lammle, *Blood Coagul. Fibrinolysis* **1992**, *3*, 555–561.

[52] T. Koster, F. R. Rosendaal, E. Briet, J. P. Vandenbroucke, *Br. J. Haematol.* **1994**, *87*, 422–424.

[53] M. Schloesser, S. Zeerleder, G. Lutze, W. M. Halbmayer, S. Hofferbert, B. Hinney, H. Koestering, B. Lämmle, G. Pindur, K. Thies, et al., *Blood* **1997**, *90*, 3967–3977.

[54] S. Zeerleder, M. Schloesser, M. Redondo, W. A. Wuillemin, W. Engel, M. Furlan, B. Lämmle, *Thromb. Haemost.* **1999**, *82*, 1240–1246.

[55] B. Siegerink, F. R. Rosendaal, A. Algra, *J. Thromb. Haemost.* **2014**, *12*, 606–613.

[56] G. Endler, C. Mannhalter, H. Sunder-Plassmann, W. Lalouschek, S. Kapiotis, M. Exner, N. Jordanova, S. Meier, F. Kunze, O. Wagner, et al., *Br. J. Haematol.* **2001**, *115*, 1007–1009.

[57] G. Endler, C. Marsik, B. Jilma, T. Schickbauer, P. Quehenberger, C. Mannhalter, *J. Thromb. Haemost.* **2007**, *5*, 1143–1148.

[58] A. Girolami, S. Ferrari, E. Cosi, M. L. Randi, *Blood Cells, Mol. Dis.* **2019**, *77*, 8–11.

[59] A. Girolami, S. Ferrari, E. Cosi, B. Girolami, M. L. Randi, *J. Thromb. Thrombolysis* **2019**, *47*, 481–485.

[60] M. L. van Montfoort, J. C. M. Meijers, *Thromb. Haemost.* **2013**, *110*, 223–232.

[61] J. I. Weitz, J. Fredenburgh, *Front. Med.* **2017**, *4*, 19.

[62] E. Kenne, T. Renné, *Drug Discov. Today* **2014**, *19*, 1459–1464.

[63] D. Gailani, *Hematology* **2014**, *2014*, 52–59.

[64] B. F. Tillman, A. Gruber, O. J. T. McCarty, D. Gailani, *Blood Rev.* **2018**, *32*, 433–448.

[65] D. Gailani, T. Renné, *J. Thromb. Haemost.* **2007**, *5*, 1106–1112.

[66] I. Ivanov, A. Matafonov, D. Gailani, *Curr. Opin. Hematol.* **2017**, *24*, 411–418.

[67] S. de Maat, C. Maas, *J. Thromb. Haemost.* **2016**, *14*, 1498–1506.

[68] A. H. Schmaier, *Thromb. Res.* **2014**, *133*, S41–S44.

[69] L. J, S. Madar Z, *J. Clin. Toxicol.* **2012**, *02*, 10–12.

[70] T. Renné, A. H. Schmaier, K. F. Nickel, M. Blombäck, C. Maas, *Blood* **2012**, *120*, 4296–4303.

[71] K. F. Nickel, A. T. Long, T. A. Fuchs, L. M. Butler, T. Renné, *Arter. Thromb. Vasc. Biol.* **2016**, *37*, 13–20.

[72] J. Liu, J. Qin, A. Borodovsky, T. Racie, A. Castoreno, M. Schlegel, M. A. Maier, T. Zimmerman, K. Fitzgerald, J. Butler, et al., *RNA* **2019**, *25*, 255–263.

[73] H. Cao, M. Biondo, H. Lioe, S. Busfield, V. Rayzman, B. Nieswandt, K. Bork, L. C. Harrison, P. Auyeung, H. Farkas, et al., *J. Allergy Clin. Immunol.* **2018**, *142*, 1355–1358.

[74] P. Taylor, "BioCryst says oral drug works for HAE attacks," can be found under https://www.fiercebiotech.com/biotech/biocryst-says-oral-drug-works-for-hae-attacks, **2018**.

[75] J. Gever, "FDA Approves 6th Drug for HAE," can be found under https://www.medpagetoday.com/rheumatology/generalrheumatology/74729, **2018**.

[76] S. Thomas, A. Caplan, *JAMA - J. Am. Med. Assoc.* **2019**, *321*, 833–834.

[77] V. Raghunathan, J. Zilberman-Rudenko, S. R. Olson, F. Lupu, O. J. T. McCarty, J. J. Shatzel, *Res. Pract. Thromb. Haemost.* **2019**, *3*, 331–339.

[78] I. Stroo, S. Zeerleder, C. Ding, B. M. Luken, J. J. T. H. Roelofs, O. J. De Boer, J. C. M. Meijers, F. J. Castellino, C. Van 'T Veer, T. Van Der Poll, *Thromb. Haemost.* **2017**, *117*, 1601–1614.

[79] E. I. Tucker, N. G. Verbout, P. Y. Leung, S. Hurst, O. J. T. McCarty, D. Gailani, A.

Gruber, *Blood* **2012**, *119*, 4762–4768.

[80] R. Silasi, R. S. Keshari, C. Lupu, W. J. Van Rensburg, H. Chaaban, G. Regmi, A. Shamanaev, J. J. Shatzel, C. Puy, C. U. Lorentz, et al., *Blood Adv.* **2019**, *3*, 658–669.

[81] T. Iwaki, D. Cruz-Topete, F. J. Castellino, *J. Thromb. Haemost.* **2008**, *6*, 1993–1995.

[82] R. A. Pixley, R. De La Cadena, J. D. Page, N. Kaufman, E. G. Wyshock, A. Chang, F. B. Taylor, R. W. Colman, *J. Clin. Invest.* **1993**, *91*, 61–68.

[83] D. Zamolodchikov, Z. L. Chen, B. A. Conti, T. Renné, S. Stricklan, *Proc. Natl. Acad. Sci. U. S. A.* **2015**, *112*, 4068–4073.

[84] D. Zamolodchikov, T. Renné, S. Strickland, *J. Thromb. Haemost.* **2016**, *14*, 995–1007.

[85] Z. L. Chen, A. S. Revenko, P. Singh, A. R. MacLeod, E. H. Norris, S. Strickland, *Blood* **2017**, *129*, 2547–2556.

[86] M. Filippi, A. Bar-Or, F. Piehl, P. Preziosa, A. Solari, S. Vukusic, M. A. Rocca, *Nat. Rev. Dis. Prim.* **2018**, *4*, 1–27.

[87] K. Göbel, S. Pankratz, C. M. Asaridou, A. M. Herrmann, S. Bittner, M. Merker, T. Ruck, S. Glumm, F. Langhauser, P. Kraft, et al., *Nat. Commun.* **2016**, *7*, DOI 10.1038/ncomms11626.

[88] N. Ziliotto, M. Baroni, S. Straudi, F. Manfredini, R. Mari, E. Menegatti, R. Voltan, P. Secchiero, P. Zamboni, N. Basaglia, et al., *Front. Neurol.* **2018**, *9*, 1–8.

[89] L. Hedstrom, *Chem. Rev.* **2002**, *102*, 4501–4523.

[90] D. E. Cool, C. J. S. Edgell, G. V. Louie, M. J. Zoller, G. D. Brayer, R. T. MacGillivray, *J. Biol. Chem.* **1985**, *260*, 13666–13676.

[91] E. Stavrou, A. H. Schmaier, *Thromb. Res.* **2010**, *125*, 210–215.

[92] H. Weidmann, L. Heikaus, A. T. Long, C. Naudin, H. Schlüter, T. Renné, *Biochim. Biophys. Acta - Mol. Cell Res.* **2017**, *1864*, 2118–2127.

[93] A. R. Kornblihtt, K. Umezawa, K. Vibe-Pedersen, F. E. Baralle, *EMBO J.* **1985**, *4*, 1755–1759.

[94] R. Pankov, K. M. Yamada, *J. Cell Sci.* **2002**, *115*, 3861–3863.

[95] R. M. Cooke, A. J. Wilkinson, M. Baron, A. Pastore, M. J. Tappin, I. D. Campbell, H. Gregory, B. Sheard, *Nature* **1987**, *327*, 339–341.

[96] X. Li, A. M. Bokman, M. Llinás, R. A. G. Smith, C. M. Dobson, *J. Mol. Biol.* **1994**, *235*, 1548–1559.

[97] D. Pennica, W. E. Holmes, W. J. Kohr, R. N. Harkins, G. A. Vehar, C. A. Ward, W. F. Bennett, E. Yelverton, P. H. Seeburg, H. L. Heyneker, et al., *Nature* **1983**, *301*, 214–221.

[98] D. X. Beringer, L. M. J. Kroon-Batenburg, *Acta Crystallogr. Sect. F Struct. Biol. Cryst. Commun.* **2013**, *69*, 94–102.

[99] C. C. Clark, Z. L. M. Hofman, W. Sanrattana, L. Den Braven, S. De Maat, C. Maas, *Thromb. Haemost.* **2020**, *120*, 400–411.

[100] F. Citarella, G. Fedele, D. Roem, A. Fantoni, C. E. Hack, *Blood* **1998**, *92*, 4198–4206.

[101] F. Citarella, H. Te Velthuis, M. Helmer-Citterich, C. E. Hack, *Thromb. Haemost.* **2000**, *84*, 1057–1065.

[102] F. Citarella, D. M. Ravon, B. Pascucci, A. Felici, A. Fantoni, C. E. Hack, *Eur. J. Biochem.* **1996**, *238*, 240–249.

[103] R. A. Pixley, R. W. Colman, *Adv. Exp. Med. Biol.* **1989**, *247 A*, 473–476.

[104] Z. L. M. Hofman, C. C. Clark, W. Sanrattana, A. Nosairi, N. M. J. Parr, M. Živkovic, K. Krause, N. A. Mahnke, J. Scheffel, C. Erik Hack, et al., *J. Biol. Chem.* **2020**, *295*, 363–374.

[105] J. Scheffel, N. A. Mahnke, Z. L. M. Hofman, S. de Maat, J. Wu, H. Bonnekoh, R. J. Pengelly, S. Ennis, J. W. Holloway, M. Kirchner, et al., *Nat. Commun.* **2020**, *11*, DOI 10.1038/s41467-019-13984-8.

[106] A. Dementiev, A. Silva, C. Yee, Z. Li, M. T. Flavin, H. Sham, J. R. Partridge, *Blood Adv.* **2018**, *2*, 549–558.

[107] M. Pathak, R. Manna, C. Li, B. G. Kaira, B. K. Hamad, B. D. Belviso, C. R. Bonturi, I. Dreveny, P. M. Fischer, L. V. Dekker, et al., *Acta Crystallogr. Sect. D Struct. Biol.* **2019**, *75*, 578–591.

[108] M. Worm, E. C. Köhler, R. Panda, A. Long, L. M. Butler, E. X. Stavrou, K. F. Nickel, T. A. Fuchs, T. Renné, *Ann. Transl. Med.* **2015**, *3*, 5–9.

[109] P. Y. Leung, S. Hurst, M. A. Berny-Lang, N. G. Verbout, D. Gailani, E. I. Tucker, R. K. Wang, O. J. T. McCarty, A. Gruber, *Transl. Stroke Res.* **2012**, *3*, 381–389.

[110] C. U. Lorentz, N. G. Verbout, Z. Cao, L. Liu, M. T. Hinds, O. J. T. McCarty, I. Ivanov, E. I. Tucker, D. Gailani, A. Gruber, *Blood Adv.* **2018**, *2*, 85–88.

[111] C. U. Lorentz, N. G. Verbout, M. Wallisch, M. W. Hagen, J. J. Shatzel, S. R. Olson, C. Puy, M. T. Hinds, O. J. T. McCarty, D. Gailani, et al., *Arterioscler. Thromb. Vasc. Biol.* **2019**, *39*, 799–809.

[112] Y. Decrem, G. Rath, V. Blasioli, P. Cauchie, S. Robert, J. Beaufays, J. M. Frère, O. Feron, J. M. Dogné, C. Dessy, et al., *J. Exp. Med.* **2009**, *206*, 2381–2395.

[113] V. Pireaux, J. Tassignon, S. Demoulin, S. Derochette, N. Borenstein, A. Ente, L. Fiette, J. Douxfils, P. Lancellotti, M. Guyaux, et al., *J. Am. Coll. Cardiol.* **2019**, *74*, 2178–2189.

[114] Bioxodes, *Bioxodes Obtains Authorization to Launch Phase I Trial of Its Antithrombotic Drug, Ir-CPI, in Healthy Male Volunteers*, Press Release, **2019**.

[115] I. T. N. Campos, R. Amino, C. A. M. Sampaio, E. A. Auerswald, T. Friedrich, H. G. Lemaire, S. Schenkman, A. S. Tanaka, *Insect Biochem. Mol. Biol.* **2002**, *32*, 991–997.

[116] I. Hagedorn, S. Schmidbauer, I. Pleines, C. Kleinschnitz, U. Kronthaler, G. Stoll, G. Dickneite, B. Nieswandt, *Circulation* **2010**, *121*, 1510–1517.

[117] V. N. Kolyadko, S. V. Lushchekina, T. A. Vuimo, S. S. Surov, R. A. Ovsepyan, V. A. Korneeva, I. I. Vorobiev, N. A. Orlova, L. Minakhin, K. Kuznedelov, et al., *PLoS One* **2015**, *10*, 1–24.

[118] I. Chen, H. L. Mitchell, *Phytochemistry* **1973**, *12*, 327–330.

[119] K. M. Hansson, S. Nielsen, M. Elg, J. Deinum, *J. Thromb. Haemost.* **2014**, *12*, 1678–1686.

[120] Y. Dargaud, R. Luddington, T. P. Baglin, *J. Thromb. Haemost.* **2006**, *4*, 1160–1161.

[121] J. F. Hernandez, J. Gagnon, L. Chiche, T. M. Nguyen, J. P. Andrieu, A. Heitz, T. T. Hong, T. T. C. Pham, D. Le Nguyen, *Biochemistry* **2000**, *39*, 5722–5730.

[122] S. J. De Veer, M. W. Kan, D. J. Craik, *Chem. Rev.* **2019**, *119*, 12375–12421.

[123] J. E. Swedberg, T. Mahatmanto, H. Abdul Ghani, S. J. De Veer, C. I. Schroeder, J. M. Harris, D. J. Craik, *J. Med. Chem.* **2016**, *59*, 7287–7292.

[124] M. E. McGrath, S. A. Gillmor, R. J. Fletterick, *Protein Sci.* **1995**, *4*, 141–148.

[125] J. L. Seymour, R. N. Lindquist, M. S. Dennis, R. A. Lazarus, B. Moffat, D. Yansura, D. Reilly, M. E. Wessinger, *Biochemistry* **1994**, *33*, 3949–3958.

[126] J. S. Ulmer, R. N. Lindquist, M. S. Dennis, R. A. Lazarus, *FEBS Lett.* **1995**, *365*, 159–163.

[127] A. A. Stoop, C. S. Craik, *Nat. Biotechnol.* **2003**, *21*, 1063–1068.

[128] J. K. Watts, D. R. Corey, *J. Pathol.* **2012**, *226*, 365–379.

[129] T. Adachi, Y. Nakamura, *Molecules* **2019**, *24*, DOI 10.3390/molecules24234229.

[130] R. S. Woodruff, Y. Xu, J. Layzer, W. Wu, M. L. Ogletree, B. A. Sullenger, *J. Thromb. Haemost.* **2013**, *11*, 1364–1373.

[131] G. Tans, T. Janssen-Claessen, J. Rosing, J. H. Griffin, *Eur. J. Biochem.* **1987**, *164*, 637–642.

[132] S. Robert, C. Bertolla, B. Masereel, J. M. Dogné, L. Pochet, *J. Med. Chem.* **2008**, *51*, 3077–3080.

[133] V. Baeriswyl, S. Calzavarini, C. Gerschheimer, P. Diderich, A. Angelillo-Scherrer, C. Heinis, *J. Med. Chem.* **2013**, *56*, 3742–3746.

[134] V. Baeriswyl, S. Calzavarini, S. Chen, A. Zorzi, L. Bologna, A. Angelillo-scherrer, C. Heinis, *ACS Chem. Biol.* **2015**, *10*, 1861–1870.

[135] S. J. Middendorp, J. Wilbs, C. Quarroz, S. Calzavarini, A. Angelillo-Scherrer, C. Heinis, *J. Med. Chem.* **2017**, *60*, 1151–1158.

[136] A. Zorzi, S. J. Middendorp, J. Wilbs, K. Deyle, C. Heinis, *Nat. Commun.* **2017**, *8*, 1–9.

[137] J. Wilbs, X. Kong, S. J. Middendorp, R. Prince, A. Cooke, C. T. Demarest, M. M. Abdelhafez, K. Roberts, N. Umei, P. Gonschorek, et al., *Nat. Commun.* **2020**, *11*, 3890.

[138] J. J. F. Chen, D. P. Visco, *Eur. J. Med. Chem.* **2017**, *140*, 31–41.

[139] M. Korff, L. Imberg, J. M. Will, N. Bückreiß, S. A. Kalinina, B. M. Wenzel, G. A. Kastner, C. G. Daniliuc, M. Barth, R. A. Ovsepyan, et al., *J. Med. Chem.* **2020**, DOI 10.1021/acs.jmedchem.0c01635.

[140] L. Pochet, C. Doucet, G. Dive, J. Wouters, B. Masereel, M. Reboud-Ravaux, B. Pirotte, *Bioorganic Med. Chem.* **2000**, *8*, 1489–1501.

[141] P. Kraft, T. Schwarz, L. Pochet, G. Stoll, C. Kleinschnitz, *Exp. Transl. Stroke Med.* **2010**, *2*, 2–7.

[142] C. Bouckaert, S. Serra, G. Rondelet, E. Dolušić, J. Wouters, J. M. Dogné, R. Frédérick, L. Pochet, *Eur. J. Med. Chem.* **2016**, *110*, 181–194.

[143] C. Bouckaert, S. Zhu, J. W. P. Govers-Riemslag, M. Depoorter, S. L. Diamond, L. Pochet, *Thromb. Res.* **2017**, *157*, 126–133.

[144] T. J. Tucker, S. F. Brady, W. C. Lumma, S. D. Lewis, S. J. Gardell, A. M. Naylor-Olsen, Y. Yan, J. T. Sisko, K. J. Stauffer, B. J. Lucas, et al., *J. Med. Chem.* **1998**, *41*, 3210–3219.

[145] Y. N. Imai, Y. Inoue, I. Nakanishi, K. Kitaura, *Protein Sci.* **2008**, *17*, 1129–1137.

[146] H. Philippou, R. Foster, C. Fishwick, C. Revill, I. Yule, R. Taylor, A. Naylor, P. S. Fallon, S. Crosby, A. Hopkins, et al., *FACTOR XIIa INHIBITORS*, **2019**, WO2019211585A1.

[147] R. P. Rozek, *Adv. Econ. Bus.* **2013**, *1*, 258–269.

[148] E. A. Blackstone, J. P. Fuhr, *Am. Heal. Drug Benefits* **2013**, *6*, 469–477.

[149] J. P. Wolfe, J. Ahman, J. P. Sadighi, R. A. Singer, S. L. Buchwald, *Tetrahedron Lett.* **1997**, *38*, 6367–6370.

[150] M. D. Tzirakis, B. Breiten, M. Ebert, M. T. Beels, I. Biaggio, F. Diederich, *Chem. - A Eur. J.* **2013**, *2013*, 12693–12704.

[151] V. Tona, A. De La Torre, M. Padmanaban, S. Ruider, L. González, N. Maulide, *J. Am.*

Chem. Soc. **2016**, *138*, 8348–8351.

[152] C. Girard, E. Onen, M. Aufort, S. Beauvière, E. Samson, J. Herscovici, *Org. Lett.* **2004**, *8*, 1689–1692.

[153] Z. Guo, A. Cammidge, D. C. Horwell, *Synth. Commun.* **2000**, *30*, 2933–2943.

[154] K. Narise, K. Okuda, Y. Enomoto, T. Hirayama, H. Nagasawa, *Drug Des. Devel. Ther.* **2014**, *8*, 701–717.

[155] P. G. M. Wuts, T. W. Greene, *Greene's Protective Groups in Organic Synthesis (Fourth Edition)*, John Wiley & Sons, Hoboken, **2007**.

[156] J. Cornish, K. E. Callon, C. Q. X. Lin, C. L. Xiao, T. B. Mulvey, G. J. S. Cooper, I. R. Reid, *Am. J. Physiol. - Endocrinol. Metab.* **1999**, *277*, 779–783.

[157] H. Miel, S. Rault, *Tetrahedron Lett.* **1997**, *38*, 7865–7866.

[158] A. V. Hill, *J. Physiol.* **1910**, *40*, iv–vii.

[159] M. I. Stefan, N. Le Novère, *PLoS Comput. Biol.* **2013**, *9*, 2–7.

[160] B. K. Shoichet, *J. Med. Chem.* **2006**, *49*, 7274–7277.

[161] J. W. Thuring, H. Li, N. A. Porter, *Biochemistry* **2002**, *41*, 2002–2013.

[162] *Glide, Version 6.7*, Schrödinger, LLC, New York, **2015**.

[163] R. A. Friesner, J. L. Banks, R. B. Murphy, T. A. Halgren, J. J. Klicic, D. T. Mainz, M. P. Repasky, E. H. Knoll, M. Shelley, J. K. Perry, et al., *J. Med. Chem.* **2004**, *47*, 1739–1749.

[164] T. A. Halgren, R. B. Murphy, R. A. Friesner, H. S. Beard, L. L. Frye, W. T. Pollard, J. L. Banks, *J. Med. Chem.* **2004**, *47*, 1750–1759.

[165] R. A. Friesner, R. B. Murphy, M. P. Repasky, L. L. Frye, J. R. Greenwood, T. A. Halgren, P. C. Sanschagrin, D. T. Mainz, *J. Med. Chem.* **2006**, *49*, 6177–6196.

[166] S. A. Weissman, D. Zewge, C. Chen, *J. Org. Chem.* **2005**, *70*, 1508–1510.

[167] D. C. Lenstra, P. E. Lenting, J. Mecinović, *Green Chem.* **2018**, *20*, 4418–4422.

[168] D. G. Batt, G. C. Houghton, W. F. Daneker, P. K. Jadhav, *J. Org. Chem.* **2000**, *65*, 8100–8104.

[169] B. D. Judkins, D. G. Allen, T. A. Cook, B. Evans, T. E. Sardharwala, *Synth. Commun.* **1996**, *26*, 4351–4367.

[170] K. Mizusawa, Y. Ishida, Y. Takaoka, M. Miyagawa, S. Tsukiji, I. Hamachi, *J. Am. Chem. Soc.* **2010**, *132*, 7291–7293.

[171] S. Moniot, M. Forgione, A. Lucidi, G. S. Hailu, A. Nebbioso, V. Carafa, F. Baratta, L. Altucci, N. Giacché, D. Passeri, et al., *J. Med. Chem.* **2017**, *60*, 2344–2360.

[172] W. Gładkowski, A. Skrobiszewski, M. Mazur, M. Siepka, A. Pawlak, B. Obmińska-Mrukowicz, A. Białońska, D. Poradowski, A. Drynda, M. Urbaniak, *Tetrahedron* **2013**, *69*, 10414–10423.

[173] P. Radha Krishna, D. V. Ramana, *J. Org. Chem.* **2012**, *77*, 674–679.

[174] Y. Gao, J. M. Klunder, R. M. Hanson, H. Masamune, S. Y. Ko, K. B. Sharpless, *J. Am. Chem. Soc.* **1987**, *109*, 5765–5780.

[175] A. B. Charette, M. C. Lacasse, *Org. Lett.* **2002**, *4*, 3351–3353.

[176] K. Maruoka, T. Ooi, S. Nagahara, H. Yamamoto, *Tetrahedron* **1991**, *47*, 6983–6998.

[177] A. Fürstner, L. C. Bouchez, J. Funel, V. Liepins, F. Porøe, R. Gilmour, F. Beaufils, D. Laurich, M. Tamiya, *Angew. Chem. Int. Ed.* **2007**, *46*, 9265–9270.

[178] T. Nagano, J. Pospíšil, G. Chollet, S. Schulthoff, V. Hickmann, E. Moulin, J. Herrmann, R.

Müller, A. Fürstner, *Chem. - A Eur. J.* **2009**, *15*, 9697–9706.

[179] C. Davoine, C. Bouckaert, M. Fillet, L. Pochet, *Eur. J. Med. Chem.* **2020**, *208*, 112753.

[180] C. Davoine, M. Fillet, L. Pochet, *Manuscr. Prep.* **2020**.

[181] W. Yorke, *Trans. R. Soc. Trop. Med. Hyg.* **1940**, *33*, 463–476.

[182] M. Sands, M. A. Kron, R. B. Brown, *Rev. Infect. Dis.* **1985**, *7*, 625–634.

[183] T. Aoyama, Y. Ino, M. Ozeki, M. Oda, T. Sato, Y. Koshiyama, S. Suzuki, M. Fujita, *Jpn. J. Pharmacol.* **1984**, *35*, 203–227.

[184] K. Okajima, M. Uchiba, K. Murakami, *Cardiovasc. Drug Rev.* **1995**, *13*, 51–65.

[185] J. Y. Choi, Y. J. Kang, H. M. Jang, H. Y. Jung, J. H. Cho, S. H. Park, Y. L. Kim, C. D. Kim, *Med. (United States)* **2015**, *94*, 1–7.

[186] T. Akizawa, S. Koshikawa, K. Ota, M. Kazama, N. Mimura, Y. Hirasawa, *Nephron* **1993**, *64*, 376–381.

[187] K. Oukoloff, N. Coquelle, M. Bartolini, M. Naldi, R. Le Guevel, S. Bach, B. Josselin, S. Ruchaud, M. Catto, L. Pisani, et al., *Eur. J. Med. Chem.* **2019**, *168*, 58–77.

[188] J. Tasseroul, M. M. Lorenzo-Garcia, J. Dosso, F. Simon, S. Velari, A. De Vita, P. Tecilla, D. Bonifazi, *J. Org. Chem.* **2020**, *85*, 3454–3464.

[189] M. R. Wiley, L. C. Weir, S. Briggs, N. A. Bryan, J. Buben, C. Campbell, N. Y. Chirgadze, R. C. Conrad, T. J. Craft, J. V. Ficorilli, et al., *J. Med. Chem.* **2000**, *43*, 883–899.

[190] M. A. Ismail, R. Brun, J. D. Easterbrook, F. A. Tanious, W. D. Wilson, D. W. Boykin, *J. Med. Chem.* **2003**, *46*, 4761–4769.

[191] A. J. Kennedy, T. P. Mathews, Y. Kharel, S. D. Field, M. L. Moyer, J. E. East, J. D. Houck, K. R. Lynch, T. L. MacDonald, *J. Med. Chem.* **2011**, *54*, 3524–3548.

[192] R. Simonsson, G. Stenhagen, C. Ericsson, C. S. Elmore, *J. Label. Compd. Radiopharm.* **2013**, *56*, 334–337.

[193] M. N. C. Soeiro, K. Werbovetz, D. W. Boykin, W. D. Wilson, M. Z. Wang, A. Hemphill, *Parasitology* **2013**, *140*, 929–951.

[194] P. V. Solanki, S. B. Uppelli, R. B. Patil, P. A. Dhokrat, S. R. Bembalkar, V. T. Mathad, *ACS Omega* **2018**, *3*, 5744–5753.

[195] A. Pinner, F. Klein, *Berichte der Dtsch. Chem. Gesellschaft* **1877**, *10*, 1889–1897.

[196] P. J. Dunn, in *Compr. Org. Funct. Gr. Transform. II*, Elsevier Science, **2005**, pp. 655–699.

[197] R. T. Boeré, R. T. Oakley, R. W. Reed, *J. Organomet. Chem.* **1987**, *331*, 161–167.

[198] R. E. Bolton, S. J. Coote, H. Finch, A. Lowdon, N. Pegg, M. V. Vinader, *Tetrahedron Lett.* **1995**, *36*, 4471–4474.

[199] C. L. Kusturin, L. S. Liebeskind, W. L. Neumann, *Org. Lett.* **2002**, *4*, 983–985.

[200] J. Wang, F. Lu, Q. Ren, H. Sun, Z. Xu, R. Lan, Y. Liu, D. Ward, J. Quan, T. Ye, et al., *Cancer Res.* **2011**, *71*, 7238–7249.

[201] D. G. Brown, J. Boström, *J. Med. Chem.* **2016**, *59*, 4443–4458.

[202] S. Aharonovich, M. Kapon, M. Botoshanski, M. S. Eisen, *Organometallics* **2008**, *27*, 1869–1877.

[203] A. Lisovskii, M. Botoshansky, M. S. Eisen, *J. Chem. Soc. Dalt. Trans.* **2001**, 1692–1698.

[204] E. A. C. Brussee, A. Meetsma, B. Hessen, J. H. Teuben, *Chem. Commun.* **2000**, *082*, 497–498.

[205] B. Hu, A. L. Vavere, K. D. Neumann, B. L. Shulkin, S. G. DiMagno, S. E. Snyder, *ACS*

Chem. Neurosci. **2015**, *6*, 1870–1879.

[206] C. Djerassi, *Chem. Rev.* **1948**, *43*, 271–317.

[207] M. R. Netherton, G. C. Fu, *Org. Lett.* **2001**, *3*, 4295–4298.

[208] D. W. Old, J. P. Wolfe, S. L. Buchwald, *J. Am. Chem. Soc.* **1998**, *120*, 9722–9723.

[209] N. Asao, T. Nogami, K. Takahashi, Y. Yamamoto, *J. Am. Chem. Soc.* **2002**, *124*, 764–765.

[210] M. D. Wendt, T. W. Rockway, A. Geyer, W. McClellan, M. Weitzberg, X. Zhao, R. Mantei, V. L. Nienaber, K. Stewart, V. Klinghofer, et al., *J. Med. Chem.* **2004**, *47*, 303–324.

[211] M. Kawatsura, J. F. Hartwig, *J. Am. Chem. Soc.* **1999**, *121*, 1473–1478.

[212] J. M. Fox, X. Huang, A. Chieffi, S. L. Buchwald, *J. Am. Chem. Soc.* **2000**, *122*, 1360–1370.

[213] M. S. Viciu, R. F. Germaneau, S. P. Nolan, *Org. Lett.* **2002**, *4*, 4053–4055.

[214] H. Firouzabadi, N. Iranpoor, H. Hazarkhani, *J. Org. Chem.* **2001**, *66*, 7527–7529.

[215] J. Faragó, A. Kotschy, *Synthesis (Stuttg).* **2009**, 85–90.

[216] A. Garcia, L. Castedo, D. Domínguez, *Tetrahedron* **1995**, *51*, 8585–8598.

[217] A. B. Sánchez Maya, C. Pérez-Melero, N. Salvador, R. Peláez, E. Caballero, M. Medarde, *Bioorganic Med. Chem.* **2005**, *13*, 2097–2107.

[218] C. M. Sun, L. G. Lin, H. J. Yu, C. Y. Cheng, Y. C. Tsai, C. W. Chu, Y. H. Din, Y. P. Chau, M. J. Don, *Bioorganic Med. Chem. Lett.* **2007**, *17*, 1078–1081.

[219] G. Sudhakar, K. Satish, *Chem. - A Eur. J.* **2015**, *21*, 6475–6480.

[220] K. Nozawa-Kumada, S. Ito, K. Noguchi, M. Shigeno, Y. Kondo, *Chem. Commun.* **2019**, *55*, 12968–12971.

[221] M. D. Weingarten, J. Skudlarek, J. A. Sikorski, *Preparation of 1,2-Bis(Substituted-Phenyl) -2-Propen-1-Ones That Inhibit Expression of Vascular Cell Adhesion Molecule-1 as Anti-Inflammatories*, **2006**, WO 2006004903.

[222] M. Jaye, N. Duverger, G. Searfoss, A. Minnich, *Therapeutic Uses of PPAR Mediators as ABC-1 Expression Modulators, and Preparation Thereof*, **2001**, WO 2001066098.

[223] H. P. Lin, N. Ibrahim, O. Provot, M. Alami, A. Hamze, *RSC Adv.* **2018**, *8*, 11536–11542.

[224] N. Marion, R. S. Ramón, S. P. Nolan, *J. Am. Chem. Soc.* **2009**, *131*, 448–449.

[225] M. Karle, W. Knecht, Y. Xue, *Bioorganic Med. Chem. Lett.* **2012**, *22*, 4839–4843.

[226] M. Nazaré, D. W. Will, H. Matter, H. Schreuder, K. Ritter, M. Urmann, M. Essrich, A. Bauer, M. Wagner, J. Czech, et al., *J. Med. Chem.* **2005**, *48*, 4511–4525.

[227] A. Mayweg, S. Roever, M. G. Rudolph, Crystal Structure of Factor VIIa in Complex with 1-(1-Aminoisoquinolin-6-Yl)-3-Benzylurea, **2017**.

[228] X. Fradera, B. Kazemier, E. Carswell, A. Cooke, A. Oubrie, W. Hamilton, M. Dempster, S. Krapp, S. Nagel, A. Jestel, *Acta Crystallogr. Sect. F Struct. Biol. Cryst. Commun.* **2012**, *68*, 404–408.

[229] G. A. Kraus, M. E. Krolski, J. Sy, *Org. Synth.* **1989**, *67*, 202.

[230] J. Thomas, X. Liu, E. Y.-S. Lin, G. Z. Zheng, B. Ma, R. D. Caldwell, K. M. Guckian, G. Kumaravel, A. G. Taveras, *Bicyclic Aryl Sphingosine 1-Phosphate Analogs*, **2011**, WO/2011/017561.

[231] J. J. Brunet, M. Essiz, P. Caubere, *Tetrahedron Lett.* **1974**, *15*, 871–874.

[232] P. G. Sammes, T. W. Wallace, *J. Chem. Soc. Perkin Trans. 1* **1975**, 1377.

[233] P. Caubere, *Acc. Chem. Res.* **1974**, *7*, 301–308.

[234] C. F. Koelsch, *Org. Synth.* **1940**, *20*, 18.

[235] T. Schareina, R. Jackstell, T. Schulz, A. Zapf, A. Cotté, M. Gotta, M. Beller, *Adv. Synth. Catal.* **2009**, *351*, 643–648.

[236] P. Anbarasan, T. Schareina, M. Beller, *Chem. Soc. Rev.* **2011**, *40*, 5049–5067.

[237] D. T. Cohen, S. L. Buchwald, *Org. Lett.* **2015**, *17*, 202–205.

[238] L. Lebreton, O. Curet, S. Gueddari, F. Mazouz, S. Bernard, C. Burstein, R. Milcent, *J. Med. Chem.* **1995**, *38*, 4786–4792.

[239] H. -J Knölker, T. Braxmeier, G. Schlechtingen, *Angew. Chemie Int. Ed. English* **1995**, *34*, 2497–2500.

[240] Y. N. Huang, Y. L. Li, J. Li, J. Deng, *J. Org. Chem.* **2016**, *81*, 4645–4653.

[241] E. Vazquez, I. W. Davies, J. F. Payack, *J. Org. Chem.* **2002**, *67*, 7551–7552.

[242] F. A. Romero, S. R. Magnuson, R. Pastor, V. H.-W. Tsui, J. Murray, T. Crawford, D. J. Burdick, B. K. Albrecht, A. Cote, A. M. Taylor, et al., *Heterocyclic Compds. as Inhibitors of Bromodomain CBP and EP300 and Their Preparation*, **2016**, WO 2016055028.

[243] T. W. Johnson, P. F. Richardson, S. Bailey, A. Brooun, B. J. Burke, M. R. Collins, J. J. Cui, J. G. Deal, Y. L. Deng, D. Dinh, et al., *J. Med. Chem.* **2014**, *57*, 4720–4744.

[244] A. K. Ghosh, S. Gemma, in *Struct. Des. Drugs Other Bioact. Mol.*, Wiley-VCH Verlag GmbH & Co. KGaA, Weinheim, Germany, **2015**, pp. 67–112.

[245] T. Brandl, U. Maier, M. Hoffmann, S. Scheuerer, A. T. Joergensen, A. Pautsch, S. Breitfelder, M. Grauert, C. Hoenke, K. Erb, et al., *Preparation of Dihydrothiazoloquinazolines as PI-3 Kinase Inhibitors*, **2007**, WO 2007115929.

[246] E. Oueis, M. Jaspars, N. J. Westwood, J. H. Naismith, *Angew. Chemie - Int. Ed.* **2016**, *55*, 5842–5845.

[247] J. C. Vantourout, R. P. Law, A. Isidro-llobet, S. J. Atkinson, A. J. B. Watson, *J. Am. Chem. Soc.* **2016**, *81*, 3942–3950.

[248] C. Shu, Y. Wang, B. Zhou, X. Li, Y. Ping, X. Lu, L. Ye, *J. Am. Chem. Soc.* **2015**, *137*, 9567–9570.

[249] S. Sharma, K. C. Basavaraju, A. K. Singh, D. P. Kim, *Org. Lett.* **2014**, *16*, 3974–3977.

[250] S. H. Kang, T. Y. Tai, T. H. Fang, *Curr. Appl. Phys.* **2010**, *10*, 625–630.

[251] M. E. Jung, S. Ouk, D. Yoo, C. L. Sawyers, C. Chen, C. Tran, J. Wongvipat, *J. Med. Chem.* **2010**, *53*, 2779–2796.

[252] K. M. Bonger, S. Hoogendoorn, C. J. Van Koppen, C. M. Timmers, H. S. Overkleeft, G. A. Van Der Marel, *ChemMedChem* **2009**, *4*, 2098–2102.

[253] H. Hu, A. Ohno, T. Sato, T. Mase, Y. Uozumi, Y. M. A. Yamada, *Org. Process Res. Dev.* **2019**, *23*, 493–498.

[254] A. Xie, X. Xu, J. Li, B. Wang, W. Dong, *Asian J. Org. Chem.* **2014**, *3*, 1278–1283.

[255] F. Sebest, J. J. Dunsford, M. Adams, J. Pivot, P. D. Newman, S. Díez-González, *ChemCatChem* **2018**, *10*, 2041–2045.

[256] Y. C. Liu, Z. L. Wu, *Chem. Commun.* **2016**, *52*, 1158–1161.

[257] C. Travelli, S. Aprile, R. Rahimian, A. A. Grolla, F. Rogati, M. Bertolotti, F. Malagnino, R. Di Paola, D. Impellizzeri, R. Fusco, et al., *J. Med. Chem.* **2017**, *60*, 1768–1792.

[258] M. I. Sánchez, J. Martínez-Costas, J. L. Mascareñas, M. E. Vázquez, *ACS Chem. Biol.*

2014, *9*, 2742–2747.

[259] J. Ossowski, T. Wächter, L. Silies, M. Kind, A. Noworolska, F. Blobner, D. Gnatek, J. Rysz, M. Bolte, P. Feulner, et al., *ACS Nano* **2015**, *9*, 4508–4526.

[260] R. B. Kothapalli, R. Niddana, R. Balamurugan, *Org. Lett.* **2014**, *16*, 1278–1281.

[261] G. Baccolini, G. Bartoli, M. Bosco, R. Dalpozzo, *J. Chem. Soc. Perkin Trans. 2* **1984**, 363.

[262] Y. Dai, X. Feng, H. Liu, H. Jiang, M. Bao, *J. Org. Chem.* **2011**, *76*, 10068–10077.

[263] J. T. Reeves, C. A. Malapit, F. G. Buono, K. P. Sidhu, M. A. Marsini, C. A. Sader, K. R. Fandrick, C. A. Busacca, C. H. Senanayake, *J. Am. Chem. Soc.* **2015**, *137*, 9481–9488.

[264] H. Li, Z. Xia, S. Chen, K. Koya, M. Ono, L. Sun, *Org. Process Res. Dev.* **2007**, *11*, 246–250.